

NAVFAC
Naval Facilities Engineering Command

ENGINEERING SERVICE CENTER
Port Hueneme, California 93043-4370

TECHNICAL REPORT
TR-2291-ENV

**DETAILED HYDRAULIC ASSESSMENT USING A
HIGH-RESOLUTION PIEZOCONE COUPLED
TO THE GEOVIS**

ESTCP PROJECT: CU-0421

by

Mark Kram, PhD, NAVFAC ESC

Gary Robbins, PhD, University of Connecticut

Jessica Chau, University of Connecticut

Amvrossios Bagtzoglou, PhD, University of Connecticut

Daniel Eng, U.S. Army ERDC

Norm Jones, PhD, Brigham Young University

April 2008

REPORT DOCUMENTATION PAGE

*Form Approved
OMB No. 0704-0811*

The public reporting burden for this collection of information is estimated to average 1 hour per response, including the time for reviewing instructions, searching existing data sources, gathering and maintaining the data needed, and completing and reviewing the collection of information. Send comments regarding this burden estimate or any other aspect of this collection of information, including suggestions for reducing the burden to Department of Defense, Washington Headquarters Services, Directorate for Information Operations and Reports (0704-0188), 1215 Jefferson Davis Highway, Suite 1204, Arlington, VA 22202-4302. Respondents should be aware that notwithstanding any other provision of law, no person shall be subject to any penalty for failing to comply with a collection of information, if it does not display a currently valid OMB control number.

PLEASE DO NOT RETURN YOUR FORM TO THE ABOVE ADDRESS.

1. REPORT DATE (DD-MM-YYYY) 15-April-2008		2. REPORT TYPE Technical Report		3. DATES COVERED (From - To) 19-May-2003 to 15-April-2008	
4. TITLE AND SUBTITLE DETAILED HYDRAULIC ASSESSMENT USING A HIGH-RESOLUTION PIEZOCONE COUPLED TO THE GEOVIS				5a. CONTRACT NUMBER N47408-04-C-7514	
				5b. GRANT NUMBER	
				5c. PROGRAM ELEMENT NUMBER	
6. AUTHOR(S) Mark Kram, PhD, NAVFAC ESC Gary Robbins, PhD, University of Connecticut Jessica Chau, University of Connecticut Amvrossios Bagtzoglou, PhD, University of Connecticut Daniel Eng, U.S. Army ERDC Norm Jones, PhD, Brigham Young University				5d. PROJECT NUMBER ESTCP ER-0421	
				5e. TASK NUMBER	
				5f. WORK UNIT NUMBER	
7. PERFORMING ORGANIZATION NAME(S) AND ADDRESSES Naval Facilities Engineering Service Center 1100 23 rd Ave. Port Hueneme, CA 93043				8. PERFORMING ORGANIZATION REPORT NUMBER TR-2291-ENV	
9. SPONSORING/MONITORING AGENCY NAME(S) AND ADDRESS(ES) Environmental Security Technology Certification Program 901 North Stuart Street, Suite 303 Arlington, VA 22203				10. SPONSOR/MONITORS ACRONYM(S) ESTCP	
				11. SPONSOR/MONITOR'S REPORT NUMBER(S)	
12. DISTRIBUTION/AVAILABILITY STATEMENT Approved for public release; distribution is unlimited					
13. SUPPLEMENTARY NOTES					
14. ABSTRACT The objective of this effort was to conduct a full-scale demonstration of the use of the high-resolution piezocone and GeoVIS to determine direction and rate of ground water flow in three dimensions. The following items were demonstrated: <ol style="list-style-type: none"> 1) Use of the high-resolution piezocone for determining soil type, head values, and hydraulic conductivity as a function of depth; 2) Use of the GeoVIS for determining effective porosity in aquifers; 3) How field parameters can be readily integrated into transport models and three-dimensional distributions of seepage velocity and contaminant flux. <p>While the GeoVIS did not provide effective porosity values within the anticipated range, the high-resolution piezocone and resulting models fall within the quantitative tolerances set forth in this demonstration. Therefore, the sensor probe approach to determining hydrogeologic characteristics is deemed appropriate for the demonstration site characteristics. When compared to conventional approaches comprised of clustered well installations, aquifer tests, sample analyses, and three-dimensional and cross-sectional interpolations, cost savings for flux distribution determination using the high-resolution piezocone coupled with a membrane interface probe system exceeds 60 percent.</p>					
15. SUBJECT TERMS Piezocone, GeoVIS, hydraulic conductivity, flux, seepage velocity, transport model, remediation, groundwater					
16. SECURITY CLASSIFICATION OF:			17. LIMITATION OF ABSTRACT	18. NUMBER OF PAGES	19a. NAME OF RESPONSIBLE PERSON
a. REPORT	b. ABSTRACT	c. THIS PAGE			Dr. Mark Kram
U	U	U		99	19b. TELEPHONE NUMBER (include area code) 805-982-2669

**DETAILED HYDRAULIC ASSESSMENT USING A
HIGH-RESOLUTION PIEZOCONE COUPLED
TO THE GEOVIS**

ESTCP PROJECT: CU-0421

FINAL REPORT

Prepared for:

ENVIRONMENTAL SECURITY TECHNOLOGY CERTIFICATION PROGRAM



Prepared by:

Naval Facilities Engineering Service Center
Code 413
Port Hueneme, California

April, 2008

TABLE OF CONTENTS

	Page
Acknowledgements	vii
Executive Summary	1
1. Introduction	
1.1 Background	5
1.2 Objectives of the Demonstration	8
1.3 Regulatory Drivers	10
1.4 Stakeholder/End-User Issues	10
2. Technology Description	
2.1 Technology Development and Application	11
2.2 Previous Testing of the Technology	26
2.3 Factors Affecting Cost and Performance	29
2.4 Advantages and Limitations of the Technology	30
3. Demonstration Design	
3.1 Performance Objectives	35
3.2 Selecting Test Site(s)	37
3.3 Test Site Description	38
3.4 Pre-Demonstration Testing and Analysis	42
3.5 Testing and Evaluation Plan	47
3.5.1 Demonstration Installation and Start-Up	47
3.5.2 Period of Operation	48
3.5.3 Amount /Treatment Rate of Material to be Treated	48
3.5.4 Residuals Handling	49
3.5.5 Operating Parameters for the Technology	49
3.5.6 Experimental Design	50
3.5.7 Sampling Plan	54
3.5.8 Demobilization	58
3.6 Selection of Analytical/Testing Methods	58
3.7 Selection of Analytical/Testing Laboratory	59
4. Performance Assessment	
4.1 Performance Criteria	60
4.2 Performance Confirmation Methods	61
4.3 Data Analysis, Interpretation and Evaluation	63
4.3.1 Comparison of K Values	63
4.3.2 Comparison of Head Values	66
4.3.3 Tracer Test Results	66
4.3.4 Modeling Results	66
5. Cost Assessment	79

5.1 Cost Reporting	79
5.2 Cost Analysis	80
6. Implementation Issues	86
6.1 Environmental Checklist	86
6.2 Other Regulatory Issues	87
6.3 Lessons Learned	90
6.4 End-User Issues	92
7. References	95
8. Points of Contact	98

FIGURES

Figure 2-1. High-Resolution Piezocone	12
Figure 2-2. Estimates of Ground Water Table	14
Figure 2-3. Pressure Dissipation Curve	14
Figure 2-4. Hydrostatic Pressure Profile	15
Figure 2-5. Parez and Fauriel (1988) Relationship Between K and t50	16
Figure 2-6. Upgraded Piezocone Test Output Example for a Single Push	18
Figure 2-7. Schematic of GeoVIS Soil Video Imaging System Probe	19
Figure 2-8. Soil Porosity Estimates using GeoVIS Digital Video Microscope Conversion	20
Figure 2-9. Transport Conceptualization Based on Flux (after Enfield, 2002)	23
Figure 2-10. GeoVIS and API Porosity Comparisons	27
Figure 2-11. Piezocone Potentiometric Surface Determination	28
Figure 2-12. Hydraulic Conductivity based on Soil Type (after Robertson and Campanella, 1989)	34
Figure 3-1. Site Map Depicting Location of Demonstration Test Facility Relative to NETTS MTBE Plume	39
Figure 3-2. Selected Port Hueneme NETTS Site	41
Figure 3-3. Site Soil Type and Well Design Logs	42
Figure 3-4. Contours of the Differential Electric Resistivity in the Silty Sand Formation (10.5-12.0 ft bgs) between the Date of Survey and February 28, 2005	43
Figure 3-5. Test Site Configuration	44
Figure 3-6. Concentration Versus Flux Distribution Using GMS	45
Figure 3-7. Well Cluster and Push Configurations	55
Figure 4-1. Comparison of all K Values	64
Figure 4-2. Comparison of all K Values, Log Transformed	64
Figure 4-3. Hydraulic Conductivity Distributions	65
Figure 4-4. Relative Frequency of K Values	65
Figure 4-5. Three-Dimensional Head Distributions for High-Resolution Piezocone and Well Clusters	67
Figure 4-6. Head Comparisons, Middle Zone	68
Figure 4-7. Well and High-Resolution Piezocone Derived Velocity Distributions	69

Figure 4-8. Tracer Concentrations at the Depth of the Injection Well for Various Scenarios and Three Timesteps	72
Figure 4-9. Flux distributions for Various Scenarios and Three Timesteps	73
Figure 4-10. Breakthrough Curves for Cluster 5, Middle Depth	74
Figure 4-11. Breakthrough Curves for Cluster 6, Middle Depth	75
Figure 4-12. Breakthrough Curves for Cluster 6, Middle Depth	75
Figure 5-1. Per Site Cost Savings for High-Resolution Piezocone Flux Approach Relative to Well Flux Approaches for Three Depths	82
Figure 5-2. Anticipated Early DoD Annual Savings by High-Resolution Piezocone Flux Approaches	85
Figure 5-3. Anticipated Five-Year DoD Savings by High-Resolution Piezocone Flux Approaches	85

TABLES

Table 2-1. Estimated Effective Soil Porosity Conversion Chart Based on Soil Type	21
Table 3-1. Performance Objectives	36
Table 3-2. Data Quality Objectives	54
Table 4-1. Performance Criteria and Level of Success	60
Table 4-2. Expected Performance and Performance Confirmation Methods	62
Table 4-3. Data Sources for Inputs to Modeled Scenarios	70
Table 4-4. Results of Inter-Model Comparison	76
Table 4-5. Performance Summary	77
Table 5-1. Cost Reporting for High-Resolution Piezocone Component	79
Table 5-2. Itemized Cost Assumptions	81
Table 5-3. Per Site Cost Comparison between High-Resolution Piezocone and MIP Flux Distribution Approach and Conventional Monitoring Well Flux Distribution Approach	82
Table 5-4. Itemized Well Removal Cost Assumptions	84
Table 8-1. Points of Contact	98

APPENDICES

Appendix A: Analytical Methods Supporting the Experimental Design	
Appendix B: Analytical Methods Supporting the Sampling Plan	
Appendix C: Quality Assurance Project Plan (QAPP)	
Appendix D: Health and Safety Plan (HASP)	
Appendix E: Geophysical Test Report	
Appendix F: Comparison of Hydraulic Conductivity and Head Values	
Appendix G: Rhodamine WT Tracer Test	
Appendix H: GMS Guidance - Velocity and Mass Flux Calculators	
Appendix I: Development and Testing of Groundwater Flow and Tracer Transport Models	
Appendix J: High-Resolution Piezocone Standard Operating Procedure	
Appendix K: Well Logs	
Appendix L: High-Resolution Piezocone Push Logs	

KEY ACRONYMS

ASTM	American Society of Testing and Materials
BGS	Below Ground Surface
CFR	Code of Federal Regulations
CPT	Cone Penetrometer Testing
DoD	Department of Defense
DOE	Department of Energy
DP	Direct Push
EPA	Environmental Protection Agency
ERDC	Army Corps Engineering Research and Development Center
ESTCP	Environmental Security Testing and Certification Program
GMS	Groundwater Modeling Software
HASP	Health and Safety Plan
IDW	Industrial Derived Waste
ITRC	Interstate Technology and Regulatory Council
LTM	Long Term Monitoring
MNA	Monitored Natural Attenuation
NBVC	Naval Base Ventura Complex
NETTS	National Environmental Technology Test Site
NFESC	Naval Facilities Engineering Service Center
QAPP	Quality Assurance Project Plan
QC	Quality Control
RITS	Remediation Innovative Technology Seminar
RSD	Relative Standard Deviation
SCAPS	Site Characterization and Analysis Penetrometer System
TAC	Technical Advisory Committee
USEPA	United States Environmental Protection Agency
WinOCPT	Windows Optical Cone Penetrometer Testing

ACKNOWLEDGEMENTS

The authors would like to express their gratitude to the members of the ESTCP review committees, and current and past team members from the Army, Navy, University of Wyoming and University of Connecticut. In particular, we would like to thank Dale Lorenzana of General Dynamics, Tim Shields (R. Brady and Associates), Kenda Neal (NFESC), Dr. Renduo Zhang (U. Wyoming), Meredith Metcalf (U. Conn.), Jessica Chau (U.Conn.), and Lanbo Liu (U.Conn.), as their field, data management and modeling efforts proved critical to the success of this project. We would also like to acknowledge the efforts provided by ASTM, ITRC, and other intergovernmental, academic, and private sector participants serving on our Technical Advisory Committee. Their support has been instrumental in helping achieve national recognition and acceptance for the cost-effective technologies demonstrated under the aegis of this ESTCP project.

EXECUTIVE SUMMARY

Department of Defense (DoD) ground water assessment and remediation projects require cost effective methods for determining the direction and rate of ground water and contaminant flow. Monitoring wells have typically been used to estimate these parameters. However, detailed three-dimensional ground water and contaminant flow pathways cannot typically be delineated using monitoring well data. Understanding three-dimensional flow pathways, gradients, and contaminant flux is essential for developing a remedial design, for risk determination, and to evaluate—remediation effectiveness. DoD has hired contractors to install thousands of ground water monitoring wells for their site monitoring and remediation strategies. Since conventional wells are not adequate for determining ground water and contaminant flow pathways in three-dimensions, ineffective remediation, faulty monitoring strategies, poor model predictions and inaccurate risk assessments are common. Methods capable of providing the required level of resolution to evaluate site conditions in three-dimensions include non-conventional multi-level well installation networks, comprehensive soil sampling and laboratory analyses, or the use of tracer tests. These options can be cost-prohibitive, especially at sites where contamination may be aerially extensive or the site has complex hydrogeologic conditions.

This project employs the use of two innovative direct push sensor probes (the high-resolution piezocone and GeoVIS) deployed with a standard cone penetrometer system for the purpose of determining direction and rate of ground water flow in three dimensions. The key to determining direction and rate of flow (or “seepage velocity”) is to understand the distribution of ground water head, gradient (i.e., change in head divided by the distance between measurement points along the direction of flow), soil effective porosity, and soil hydraulic conductivity. When coupled to the distribution of contaminant concentration, a contaminant flux estimate can be derived.

The piezocone and GeoVIS are direct push probes that are part of the cone penetrometer suite of tools. A piezocone (ASTM D5778 and D6067) is a direct push sensor probe consisting of a porous element connected to a customized transducer that converts pore pressure to water level. A high-resolution piezocone (U.S. Patents 6,208,940 and 6,236,941) is a direct push sensor probe capable of generating highly resolved hydraulic head values (plus or minus 1-inch of water level) while simultaneously collecting critical soil type information. The GeoVIS (U.S. Patent 6,115,061) is a Navy/SERDP-developed

video microscope sensor probe capable of yielding real-time soil and contaminant images that can render effective porosity estimates in aquifers.

The objective of this effort was to conduct a full-scale demonstration of the use of the high-resolution piezocone and GeoVIS to determine direction and rate of ground water flow in three dimensions. Upon successful demonstration, the technology will be transferred to government partners and industry service providers. The following items were demonstrated:

- 4) Use of the high-resolution piezocone for determining soil type, head values, and hydraulic conductivity as a function of depth;
- 5) Use of the GeoVIS for determining effective porosity in aquifers;
- 6) How field parameters can be readily integrated into transport models and three-dimensional distributions of seepage velocity and contaminant flux.

Unfortunately, conventional monitoring wells only yield a single weighted average head value, which typically constrains the flow analysis to two dimensions. In comparison, the high-resolution piezocone is capable of yielding multiple values of hydraulic head in a single sounding, which allows for generation of a three-dimensional depiction of the flow characteristics. The capabilities for transport predictions and elucidation of high contaminant flux zones are significantly increased when data of such high resolution is imported into conceptual and fate and transport models. This has been demonstrated by comparing direct push probe data to data collected using clusters of short screened monitoring wells, and by comparing model outputs based on the two different data collection approaches.

Thirty-nine customized small screen wells (3/4-inch diameter PVC with six-inch prepacked screens) were installed in thirteen clusters, each comprised of three wells set to three specific depths within the anticipated solute travel pathway of the test domain. Each well was designed using the Kram and Farrar method, and in accordance with ASTM D5521, D6724, and D6725. In the Fall of 2005, each well was tested for hydraulic conductivity using the GeoProbe Pneumatic Slug Test Kit, and water level using a water level sounder to characterize the spatial distribution of conductivity and hydraulic head. These well values served as the control parameters for comparison with the cone penetrometer determinations.

Also in the Summer of 2005, GMS was modified to enable users to generate three-dimensional gradient distributions based on the interpolation of probe and well hydraulic head data. In addition, GMS was upgraded to allow for the calculation of the three-dimensional distribution of seepage velocity (using hydraulic conductivity, effective porosity and gradient distributions) and contaminant flux (provided the distribution of solute concentrations are known). All model simulations of seepage velocity, contaminant flux, and projected plume distributions and breakthrough curves were generated using this upgraded version of GMS.

Throughout the project duration, WinOCPT, the SCAPS probe data acquisition and management software package was under continuous modification. A new GUI was produced, a new set of output and data analysis tools derived, and a robust data export function was generated to facilitate GMS modeling requirements. This complex and critical software allows for determination of high-precision head values, determination of hydraulic conductivity using three distinct methods (e.g., dissipation via the Perez and Fauriel graphical relationships [providing three distinct values of hydraulic conductivity, including max, min, and mean values], dissipation via the Perez and Fauriel algorithm [formula values], and using a lookup chart to convert soil type characterizations to hydraulic conductivity), and determination of effective porosity using two methods (e.g., a lookup chart to convert piezocone soil type to porosity and sophisticated GeoVIS image processing algorithms). This unique piece of software is Windows based, modular, and robust. It has also been integrated with chemical, soil type, and well design modules, as well as probe calibration and quality control modules for seamless Triad-enabled environmental characterization activities.

Field efforts were not continuous and were separated into four main phases. A Pre-Demonstration effort was conducted to determine general lithologic characteristics, well design constraints, and to help orient the configuration of the demonstration facility. Phase I Field Tests (March through August 2005) consisted of well installation and determination of hydraulic conductivity distribution. Phase II Field Tests (June 2006) included deployment of the high-resolution piezocone and GeoVIS. During this deployment, a formal public demonstration was conducted. Participants included demonstration partners, candidate licensees, representatives from the Army and east coast Navy SCAPS teams, DOE, Bureau of Reclamation, regulators, and private sector parties interested in using the technologies at their sites. Phase III Field Tests (July through December 2006) included release and monitoring of a Rhodamine (WT) tracer through

the well cluster domain. Follow-up efforts were comprised of dismantling of selected tracer test monitoring components (January 2007), and technology transfer via incorporation into ITRC Technical Regulatory guides and workshops (Fall 2006), assistance with Army technology incorporation (on-going), and efforts to license the technology to private entities (July 2007).

While technology limitations such as appropriate lithologic requirements exist, the majority of the comparisons between well hydraulic data and high-resolution piezocone data demonstrate that the piezocone can be an effective tool for detailed hydraulic site characterization. More specifically, it was found that the high-resolution piezocone derived hydraulic conductivity values were on average similar to those obtained from monitoring wells. Furthermore, within the limits of resolution for both methods, the piezocone results agreed closely with the monitoring well head values with respect to finding no discernible vertical and minimal horizontal gradients, mean value of the hydraulic head and the degree of variability. Differences between well and high resolution piezocone derived head values were on average less than 0.08 feet (1 inch).

GeoVIS effective porosity values were initially to be compared with API Dean Starks laboratory values derived for soil samples collected adjacent to the probe measurement locations. However, it readily became apparent that the probe images and software were yielding lower values than anticipated for the saturated silty sand soils dominating the strata at the selected field site. Therefore, soil samples were not collected for comparison. In anticipation of this potential challenge, WinOCPT was modified to enable users to estimate porosity based on soil type.

While there are some directional nuances associated with each data set, the general gradients (again, very shallow) and head distributions display similarities, especially within the well cluster domain. This is critical, as the piezocone will typically be deployed with much larger push spacing. Therefore, it is anticipated that by meeting these challenging field conditions, the high-resolution piezocone will be able to readily meet most field application requirements. Furthermore, the level of detail afforded by the high-resolution piezocone is unprecedented.

Comparison of models based on traditional (well-based) measurements and the high-resolution piezocone measurements were indistinguishable in terms of performance for the conditions present at this site. Although none of the model scenarios correctly

predicted observed tracer behavior (primarily due to the instrumentation detection interference caused by turbidity, potential transport logistics related to specific pathways, and low gradient), the models based on conventional well data match very well with the model scenarios based on high-resolution piezocone data. Plume flow directions, concentration distributions, and flux distribution predictions (based on velocity distributions coupled with concentration distribution model predictions) each compared very well and met all project performance goals.

In summary, while the GeoVIS did not provide effective porosity values within the anticipated range, the high-resolution piezocone and resulting models fall within the quantitative tolerances set forth in this demonstration. Therefore, the sensor probe approach to determining hydrogeologic characteristics is deemed appropriate for the demonstration site characteristics. When compared to conventional approaches comprised of clustered well installations, aquifer tests, sample analyses, and three-dimensional and cross-sectional interpolations, cost savings for flux distribution determination using the high-resolution piezocone coupled with a membrane interface probe system exceeds 60 percent and could represent a cost avoidance of approximately \$20M to \$60M over the next five years.

1. Introduction

1.1 Background

Department of Defense (DoD) ground water assessment and remediation projects require cost effective methods for determination of the direction and rate of ground water and contaminant flow. Monitoring wells have typically been used to estimate these parameters. However, detailed three-dimensional ground water and contaminant flow pathways cannot typically be delineated using monitoring well data. Understanding of three-dimensional flow pathways, gradients, and contaminant flux is essential to develop a remedial design, for risk determination, and to evaluate-remediation effectiveness. DoD has hired contractors to install thousands of ground water monitoring wells for their site monitoring and remediation strategies. Since conventional wells are not adequate for determining ground water and contaminant flow pathways in three-dimensions, this can result in ineffective remediation, faulty monitoring strategies, poor model predictions and inaccurate risk assessments. Methods capable of providing the required level of resolution to evaluate site conditions in three-dimensions include non-conventional multi-level well installation networks, comprehensive soil sampling and laboratory analyses, or

the use of tracer tests. These options can be cost-prohibitive, especially at sites where contamination may be aerially extensive or the site has complex hydrogeologic conditions. It is likely that decades and tens of billions of dollars will be required to cleanup DoD sites using standard hydrogeologic assessment methods.

This project employs the use of two innovative direct push sensor probes (the high-resolution piezocone and GeoVIS) deployed with a standard cone penetrometer system for the purpose of determining direction and rate of ground water flow in three dimensions. The key to determining direction and rate of flow (or “seepage velocity”) is to understand the distribution of ground water head, gradient (i.e., change in head divided by the distance between measurement points along the direction of flow), soil porosity, and soil hydraulic conductivity. When coupled to the distribution of contaminant concentration, a contaminant flux estimate can be derived.

Saturated flow velocity, or *seepage velocity* (v), is estimated using the following relationship:

$$v = \frac{K i}{\rho} \quad (\text{length/time})$$

where: K = hydraulic conductivity
 i = hydraulic gradient
 ρ = effective porosity

Contaminant *flux* (F) is estimated using the following relationship:

$$F = v [X]$$

(mass/length²-time; mg/m²-s) where: v = seepage velocity (length/time; m/s)
 $[X]$ = concentration of solute
(mass/volume; mg/m³)

The piezocone and GeoVIS are direct push probes that are part of the cone penetrometer suite of tools. A piezocone (ASTM D5778 and D6067) is a direct push sensor probe consisting of a porous element connected to a customized transducer that converts pore pressure to water level. A high-resolution piezocone (U.S. Patents 6,208,940 and 6,236,941) is a direct push sensor probe capable of generating highly resolved hydraulic head values (plus or minus 1-inch of water level) while simultaneously collecting critical soil type information. The GeoVIS (U.S. Patent 6,115,061) is a Navy/SERDP-developed

video microscope sensor probe capable of yielding real-time soil and contaminant images that can render effective porosity estimates in aquifers.

The DoD Site Characterization and Analysis Penetrometer System (SCAPS) is a direct-push platform used for advancing hydrological and chemical sensor probes and samplers into the subsurface. Probe data is managed through an integrated system of data acquisition and processing software. Through this effort, high-resolution piezocone and GeoVIS data acquisition functions were streamlined for rapid data processing. The sensor probe data was exported to Groundwater Modeling Software (GMS) for conceptualization, statistical rendering and graphical representations of the three-dimensional distribution of seepage velocity. GMS was modified specifically for this project to allow conversion of head values to gradient, thus opening the way for determination of seepage velocity and flux distributions in three dimensions. Furthermore, this highly-resolved conceptual hydrogeologic model can now be available for fate and transport modeling, risk assessment, and remediation design and optimization applications using simulation and predictive modules within the GMS platform.

This technology will be extremely useful during the Remedial Action Optimization (RAO) and Long-Term Monitoring (LTM) phases of a project. For instance, using this approach to determine the contaminant flux distribution will enable Remedial Project Managers (RPMs) to prioritize and target areas for soil removal, in situ remediation, and hydraulic containment. The models generated through implementation of this technology can be used to evaluate competing remedial action designs. For LTM applications, understanding direction of flow, rate of flow, flux distribution, soil type distribution, and plume configuration are critical for establishing a monitoring network and for generating time series analyses appropriate for demonstrating plume attenuation (Kram and Goetz, 1999). This technology will allow for generation of a high-resolution conceptual model, proper placement and design of monitoring wells, and for generation of input to models for projecting timeframes for remediation and exposure point concentration in the vicinity of potential receptors.

When compared to conventional hydrologic assessment approaches, these innovative probes allows for three-dimensional flow determination, significantly reduce the time and costs associated with hydrogeologic assessment, and will lead to improvements to remediation approaches and risk assessment. This concept represents a groundbreaking

development with potential applications at hundreds of government installations and private sector properties requiring ground water restoration.

The philosophy of minimally invasive methods embodied by direct push approaches represents a major SERDP and ESTCP success story. For example, the SCAPS laser-induced fluorescence (LIF) technology for petroleum hydrocarbons (commercialized as the Rapid Optical Screening Tool) has been applied at hundreds of fuel-contaminated sites. DoD urgently requires a direct push method (or combination of methods) that can rapidly and definitively quantify, interpolate, graphically represent, and model hydrogeologic characteristics that are essential for understanding migration patterns and reducing the impacts of contaminant releases. This ESTCP project, which builds upon the original SCAPS vision of continuous data logging as a function of depth below ground surface, will bring such a method to fruition.

1.2 Objectives of the Demonstration

The objective of this effort was to conduct a full-scale demonstration of the use of two innovative direct push sensor systems, the high-resolution piezocone and GeoVIS, to determine direction and rate of ground water flow in three dimensions. Upon successful demonstration, the technology will be transferred to government partners and industry service providers. The following items were demonstrated:

- 1) Use of the high-resolution piezocone for determining soil type, head values, and hydraulic conductivity as a function of depth;
- 2) Use of the GeoVIS for determining effective porosity in aquifers;
- 3) How field parameters can be readily integrated into transport models and three-dimensional distributions of seepage velocity and contaminant flux.

Generation of three-dimensional flow conceptual and numerical models based on highly resolved field data without the need for well installation or sample collection represents a significant advantage over conventional site characterization approaches. Several direct-push sensor probes are capable of yielding classification logs with a resolution of less than a few inches in the vertical orientation. For instance, the GeoVIS can provide effective porosity values for a microscopic image focused on an area 200mm by 250mm. In addition, monitoring wells are typically used for measuring hydraulic head, which is required to determine gradient, direction, and rate of ground water and contaminant transport. Unfortunately, conventional long-screen monitoring wells only yield a single weighted average head value, which constrains the flow analysis to two dimensions. In

comparison, the high-resolution piezocone is capable of yielding multiple values of hydraulic head in a single sounding, which allows for generation of a three-dimensional depiction of the flow characteristics. The capabilities for transport predictions and elucidation of high contaminant flux zones are significantly increased when data of such high resolution is imported into conceptual and fate and transport models. This has been demonstrated by comparing direct push probe data to data collected using clusters of short screened monitoring wells, and by comparing model outputs based on the two different data collection approaches.

The project field components were implemented in three phases. During Phase I, clustered wells were installed in appropriate locations. Pneumatic and non-pneumatic slug tests were conducted to determine the spatial hydraulic conductivity distribution. Phase II field tests consisted of high-resolution piezocone and GeoVIS deployment in selected side-by-side locations adjacent to the clustered wells to determine the three-dimensional distribution of hydraulic head and effective porosity. Since GeoVIS effective porosity values can be challenging to resolve in silty sands, high-resolution piezocone porosity values based on soil type classification lookup charts were also derived. Modeling was used to simulate the migration of a tracer through the well cluster network. Simulations provided a means to compare data derived from the piezocone pushes with that from the well clusters in an integrated manner. Phase III field efforts consisted of a tracer test within the well cluster network to provide concentration data for modeling. Hydraulic conductivity values derived from well slug tests and soil type estimates were used in a sensitivity analysis to determine the level of velocity variability associated with each approach, and the ramifications with respect to contaminant migration assessed. Hydraulic conductivity estimates derived from high-resolution piezocone measurements were also incorporated into this analysis. Appendix E summarizes field work associated with the development of the test site well clusters. It includes the results of a time series geophysical study to determine the direction of ground water flow and calculations for the design of the tracer study. Appendix F summarizes the hydraulic conductivity and hydraulic head test results. Appendix G summarizes the results of the tracer study.

While the selected site is within the domain of a Methyl Tertiary Butyl Ether (MTBE) solute plume, this technology can be used at any contaminant site amenable to direct-push applications (e.g., unconsolidated medium to fine grained subsurface materials). The Port Hueneme National Environmental Technology Test Site (NETTS) is an ideal

location for performing the comparison studies and demonstration, as the soils consist of penetrable soils and a shallow water table. In addition, hundreds of direct push wells and instrumented probes have been advanced at the facility. Infrastructure for supporting field logistics is excellent, the soil subsurface environment is well characterized, and several team members have worked on NETTS projects in the past and are therefore familiar with logistics and staging requirements. In fact, an ideal site, formerly used by EPA researchers to evaluate wellhead treatment technologies, was used that consists of proper dimensions, orientation and infrastructure for conducting this demonstration effort.

1.3 Regulatory Drivers

There are numerous specific federal, state, and local regulations that require understanding of direction and rate of ground water flow for all ground water contaminated sites. On a related note, results from this effort were incorporated into an Interstate Technology Regulatory Cooperative (ITRC) Technical Regulatory guide workshop focusing on the use of direct push wells for long-term monitoring. Furthermore, the ITRC Site Characterization and Monitoring group expressed an interest in using this effort as a case study for the generation of a new Technical Regulatory Guidance document on contaminant flux monitoring.

1.4 Stakeholder/End-User Issues

Remediation of contaminated sites has proven to be costly and often challenging, particularly for recalcitrant contaminants (e.g., halogenated solvents) under complex hydrogeologic conditions. Furthermore, regulators have recently become more amenable to risk-based and monitored natural attenuation remediation approaches, provided the characterization data supports claims of contaminant attenuation tendencies or low risk. These claims cannot be verified without adequate understanding of site-specific ground water and contaminant flow conditions. Furthermore, contaminant flux is gaining more attention by regulators as a key consideration when evaluating contaminant risk, natural attenuation and remediation performance. Regulators, who typically use guidelines based on contaminant concentration, are beginning to recognize that flux is perhaps more indicative of potential risk, and that understanding contaminant flux distribution is essential for prioritization and optimization of remedial logistics. For instance, an immobile organic contaminant residing in a highly sorptive clay zone can pose relatively little risk to the environment, regardless of the concentration, provided the hydraulic conditions reflect low advective flux and opportunities for dispersive/diffusive fluxes are

minimal. Determination of the spatial variability and heterogeneity of hydraulic properties as they relate to flux distribution is the key to proper site contaminant assessment. Recent regulatory emphasis on the Triad Approach, which strives to perform cost-effective field investigations based on dynamic work plans aimed at characterizing the hydrogeologic and chemical aspects of a site using innovative near real-time detection and data processing applications, exemplifies the current trend towards making better decisions that depend on highly resolved field data.

This report documents the performance of a suite of direct push sensor technologies that are designed to assess critical site-specific hydrogeologic factors. Successful implementation of this effort offers the stakeholder and end-users with cost and performance data on a novel approach for characterizing ground water and transport properties in three-dimensions. Furthermore, the models resulting from this effort and approach should assist stakeholders and end-users with remediation design and optimization projects.

2. Technology Description

2.1 Technology Development and Application

A piezocone is a direct push sensor probe consisting of a porous element connected to a customized transducer that converts pore pressure to water level (Figure 2-1). The porous element is filled with viscous oil that is in contact with the transducer, which is located inside the probe housing. As the probe is advanced through the soil, water pressures are transferred through the oil filled porous element directly to the transducer. The signal is recorded and converted to hydraulic head estimations through correlations between recorded signal and hydrostatic pressure. Since the environment is disturbed when the probe is advanced, dissipation of the pressure while the probe is held in place yields critical information related to hydraulic conductivity. The piezocone is also capable of generating soil type estimates based on measurements of vertical resistance to force and sleeve friction, or based on pore pressure and vertical resistance to force.

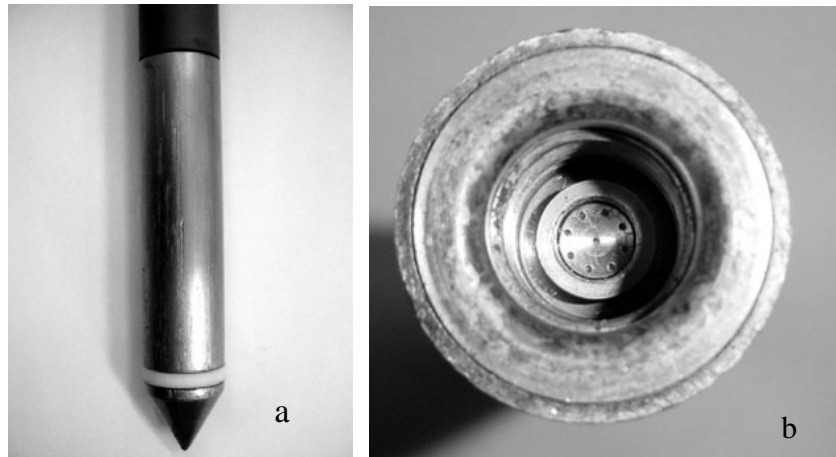


Figure 2-1. High-Resolution Piezocone. The profile image (a) displays the probe tip, porous element, and sleeve. Image (b) was taken with the tip and porous element removed. The transducer can readily be seen, as well as the mandrel (inner ring) connecting the tip to the load cell for measuring vertical resistance.

Piezocones have been in use for more than 20 years (ASTM D3441) to evaluate soil properties for construction purposes. In the late 1990s, Dr. Kram modified a standard piezocone to offer SCAPS customers detailed hydrologic assessment services for environmental applications. This high-resolution piezocone (U.S. Patents 6,208,940 and 6,236,941) is capable of generating highly resolved hydraulic head values (plus or minus 1-inch of water level) while simultaneously collecting critical soil type information. Conventional piezocones are only capable of yielding resolution on the order of one to two feet of water level. A customized probe from Vertek was used in combination with a specially designed set of transducers from Kulite, and a high-resolution voltmeter from Hewlett Packard in order to refine the water level measurement capabilities without sacrificing the field operational characteristics. In addition, Mr. James Massey partnered with Dr. Kram to design and develop Piezocone Dissipation Analysis (PDA) software for measuring, displaying, and processing the pressure dissipation data. As a result, the customized probe components and software now allow for high-resolution hydrologic assessment under field conditions. The static head resolution is critical, since many ground water contamination sites are located in areas with relatively low ground water gradients. While regional gradients can be significant, especially in areas of high topographic relief, the high-resolution piezocone allows for the localized hydrologic assessment of relatively small sites in shallow gradient environments, such as point sources (i.e., storage tanks, landfills, fire training areas, etc.) located in coastal plains.

Furthermore, since vertical ground water gradients are prevalent, the current prototype high-resolution piezocone is capable of determining three-dimensional direction and gradient of ground water flow at practical scales. This innovative measurement device has led to significant hydrologic assessment capabilities that, until recently, were only achievable using costly multi-level monitoring points that required appropriate design and placement. In general, when an RPM selects locations for multi-level well installation, decisions are made without access to subsurface stratigraphic or hydrologic information, often leading to incorrect assessment strategies. This innovative probe now allows project managers to make comprehensive hydrologic assessments without the need for committing to well and multi-level monitoring locations, except for post-assessment monitoring applications. When post-assessment monitoring points are deemed necessary, design and placement locations can be made with a thorough understanding of the subsurface strata and hydrologic details. In fact, Dr. Kram and Mr. Jeff Farrar developed a method for converting penetrometer soil type classifications to ASTM recommended well design specifications (U.S. Patent Number 6,317,694), enabling practitioners to design and install monitoring networks following hydraulic and chemical assessment activities within a single deployment.

The piezocone measures soil resistance to penetration and dynamic pore water pressure while being advanced into the ground. Hydrogeologic information, such as depth to ground water (static pressure), aquifer connectivity, and permeability (hydraulic conductivity based on pressure dissipation or soil classification) can be derived from the piezocone pore pressure measurements. Continuous tracking of dynamic pressure, barometric pressure, soil type, and temperature occur while the probe is advanced. A water saturated zone is identified by a positive pore pressure. To define the potentiometric surface of an aquifer, the probe is advanced to specified depths beneath the water table, and the pressure is allowed to dissipate to a final equilibrium pressure representing hydrostatic conditions (Figures 2-2 and 2-3). Final hydrostatic pressures are generated for several depths at a single location, leading to a hydrostatic pressure profile for the push (Figure 2-4). The software allows for extrapolation of the hydrostatic pore pressure profile back to the depth of zero pressure, corresponding to the depth to water table, or potentiometric surface. When corrected for elevation following a survey, this value is converted to water table elevation relative to mean sea level. Final pressures can be used to develop three-dimensional models. In addition, the hydrostatic pore pressure profile can be used to determine whether a fine layer is confining.

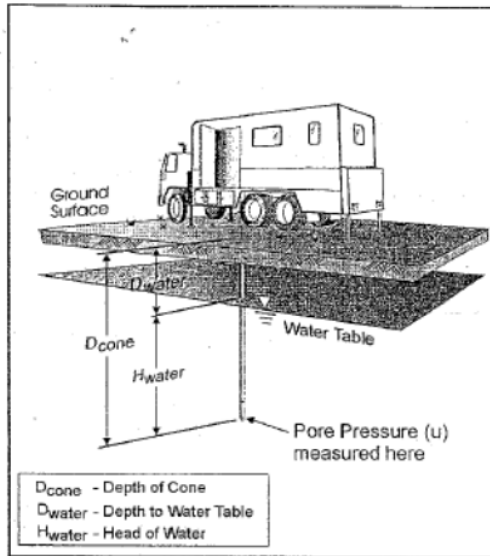


Figure 2-2. Estimates of Ground Water Table. Dissipated pore pressure at the depth of cone (D_{cone}) reflects head of water (H_{water}). The depth to water table (D_{water}) therefore equals D_{cone} minus H_{water} .

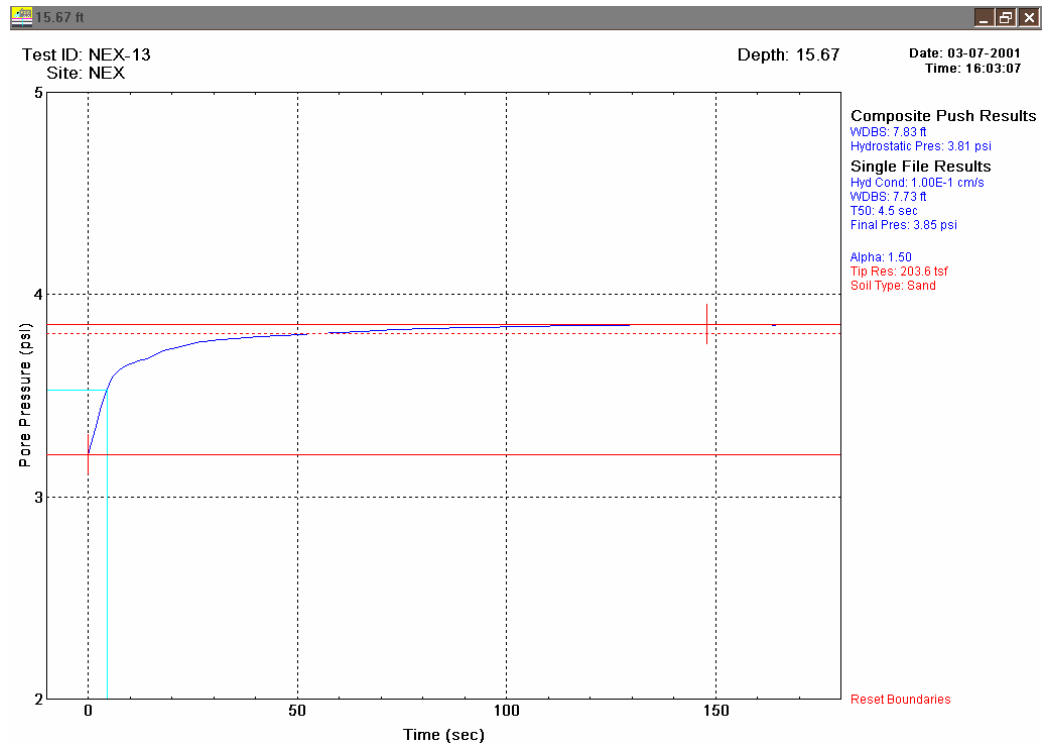


Figure 2-3. Pressure Dissipation Curve. The final pressure (D_{cone}), time for dissipation, and hydraulic conductivity can all be estimated using the dissipation curve.

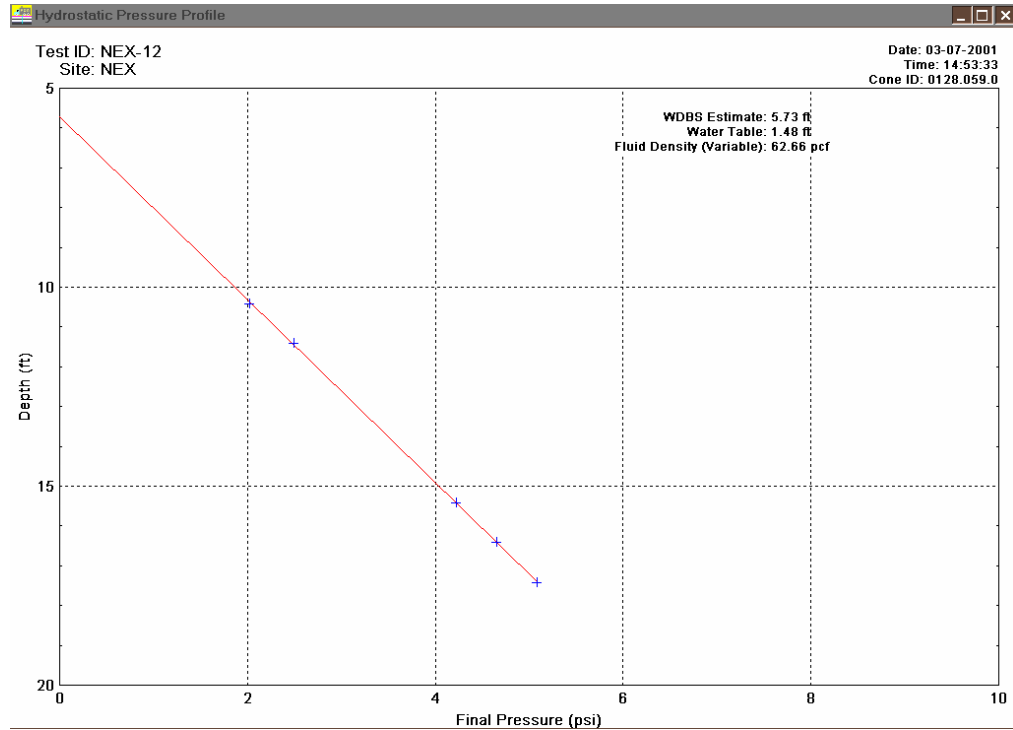


Figure 2-4. Hydrostatic Pressure Profile. Water table depth is obtained by extrapolation to zero final pressure. Head values (e.g., final pressures) can be used for three-dimensional models.

In the past, operation of the high-resolution piezocone required use of the customized PDA data acquisition and processing software, as well as software for interfacing with a high-resolution voltmeter and a reference barometer. Dissipation data collection, water table elevation determination, and hydraulic conductivity estimation based on either soil type or dissipation have recently been automated within WinOCPT. In addition, a graphical user interface (GUI) allows the user to adjust the default values interpreted from the dissipation curve, allowing for improvements to the hydrostatic pressure profile and automatic calculation updates. The output consists of dissipation curves, hydrostatic pressure profiles, and hydraulic conductivity profiles for each push. Hydraulic conductivity can be estimated using several approaches. The first approach utilizes a correlation based on soil type, which is determined using the load cell (e.g., resistance to force and sleeve friction) and pore pressure readings (Campanella and Robertson, 1989; ASTM). This option can render an order of magnitude level of resolution for hydraulic

conductivity. A second option is more resolved, and utilizes the dissipation data in an approach that is very similar to a slug test. This second option utilizes the Parez and Fauriel (1988) relationship between the t_{50} (time required for 50 percent pressure dissipation) and hydraulic conductivity (Figure 2-5). Note that this leads to a range of K values, a maximum, minimum, mean and calculated K values, and that coarse-grained materials can be assessed for K using piezocone dissipation data. All of these options are available within the current version of WinOCPT.

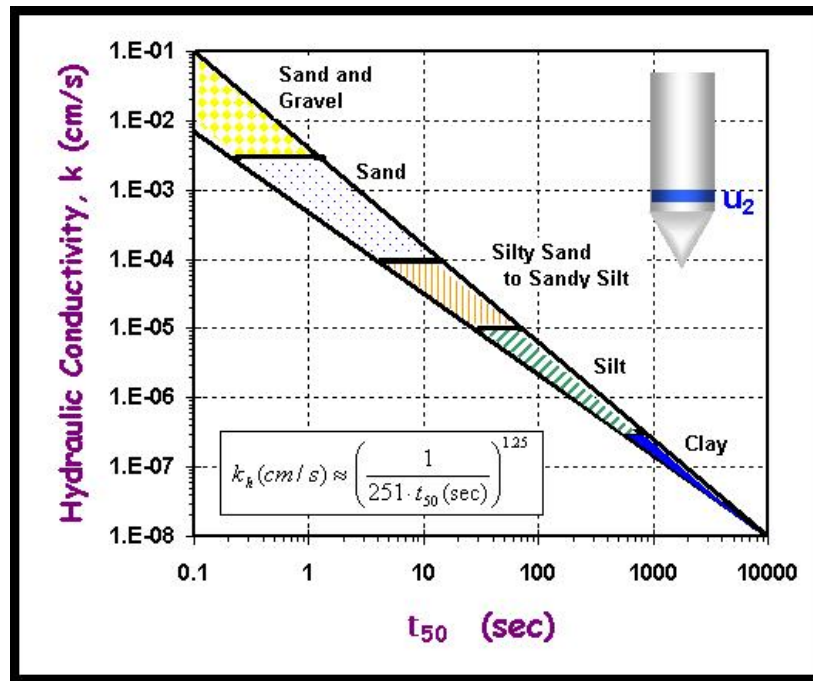


Figure 2-5. Parez and Fauriel (1988) Relationship Between K and t_{50} .

Off-the-shelf piezocones are not capable of providing the type of resolution required to perform detailed hydraulic characterization. To meet the rigorous environmental demands, a high-resolution system was generated by augmenting a commercially available system with customized components and software (U.S. Patents 6,208,940 and 6,236,941). For instance, the transducer was modified to be able to offer water pressure measurements with less than an inch of total error. This customized sensor was designed to be able to withstand burst pressures over 500psi with no hysteresis. Temperature and barometric pressures are also accounted for. Furthermore, the data collection rate has been modified to allow for rapid tracking of dissipation tests, which allows for hydraulic conductivity estimates in highly permeable strata.

Since the prototype high-resolution piezocone was developed by modification of an off-the-shelf probe, the system did not interface with WinOCPT (the SCAPS data acquisition and reporting system). Project developments included increasing the depth of resolution capabilities, upgrading the software so that it becomes a single macro within the WinOCPT platform, use of a more current analog-to-digital card to remove the high resolution voltmeter requirement, incorporating soil type relationships for K and effective porosity, and modification of the current hydraulic conductivity algorithm to accommodate for recent observations related to dissipation in coarse-grained materials.

Figure 2-6 displays one available WinOCPT version of the upgraded piezocone output for a single push with five dissipation tests. Beginning with the left portion of the graphic, a soil type classification log, hydraulic conductivity log (based on Robertson and Campanella lookup chart), hydraulic conductivity at specific depths (based on Parez and Fauriel pressure dissipation relationships), and a log of effective porosity estimates (based on soil type lookup chart) are displayed in columns with depths listed along the y-axes. The dissipation curves for specific depths tests were conducted are displayed along the lower right portion of the graphic. Final pressures and hydraulic conductivity values are derived from this dissipation test summary. The hydraulic pressure profile is presented in the upper right graph, along with calculated water depth below surface and corrected water table depth (relative to sea level). All hydraulic data is available for modeling via GMS.

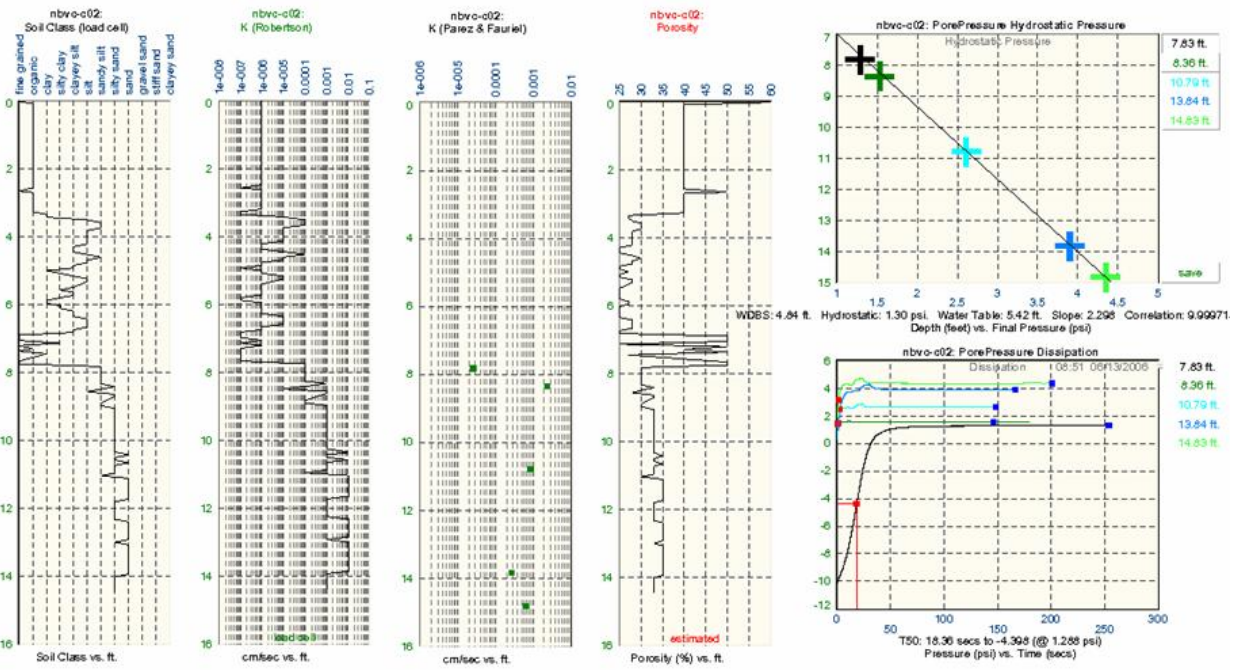


Figure 2-6. Upgraded Piezocone Test Output Example for a Single Push.

The GeoVIS (U.S. Patent 6,115,061) is a Navy/SERDP-developed video microscope sensor probe capable of yielding real-time soil and contaminant images that can render effective porosity estimates. Specifically, the methods are based upon the digital enhancement of recognizable pore spaces contained within the captured images and calculating the relative areas of these features in each image. Standard laboratory methods require 6-inch long samples, whereas the GeoVIS can provide field estimates of effective porosity on the millimeter scale. Details of the GeoVIS video imaging system have been described previously by Lieberman, 1997, and Lieberman and Knowles, 1998. A schematic of the camera probe is shown in Figure 2-7. Soil in contact with the probe is imaged through a sapphire window using a miniature CCD color camera coupled to a zoom lens system. The lens system provides magnification and focusing of the imaged area. A mirror positioned at a 45-degree angle to the axis of the optics system is used to redirect light from the soil surface into the lens system. Illumination is provided by an array of four white light-emitting diodes (LEDs) located in the probe. The window is positioned approximately 75 cm from the tip of the probe and the outside diameter of the probe is 5-cm at the window. Continuous video is saved to a recordable CD and is collected at a rate of 30 frames per second, at a push rate of approximately 4 inches per minute. The resulting photomicrographs represent an area of soil approximately 3.0 mm

wide by 2.0 mm high, with a calibration box within the image that is 2.5 mm wide by 2.0 mm high. At these dimensions, approximately 8 unique (non-overlapping) photomicrographs can be collected per inch of soil or approximately 96 unique images per foot of video push. All soil photomicrographs are collected using a frame capture device and are saved as uncompressed bitmaps to minimize color distortions produced by file compression processing.

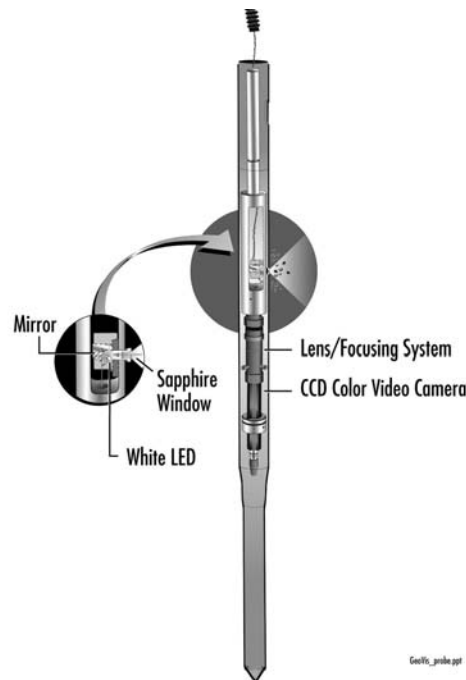


Figure 2-7. Schematic of GeoVIS Soil Video Imaging System Probe.

All photomicrographs collected to date are slightly underlit. Without correcting for the lighting effects, image processing will not extract the pore space pixels consistently across the image. Soil video CCD cameras record reflected and refracted light only, and only color and color intensity information are collected. The colors for each pixel of the photomicrograph are stored as various intensities of three color channels: red, green, and blue (RGB). Data for each pixel of the photos is stored using 24 memory bits, with 8 bits each for the red, green, and blue (RGB) color bands. Up to 256 values for each of the RGB color bands or channels can be stored for each pixel, and combining the three colors can result in one of 16 million possible colors for a pixel. A value of 256 for each of the RGB channels would result in pure white and a value of 0 for each would result in pure black. Gray colors result between white and black when all the RGB values are the same

value. To accentuate the pore space edges and evenly distribute the color intensities of the matrix and pore space across the whole image, a high pass frequency filter (Fast Fourier Transform filter) is used on all the photomicrographs (Figure 2-8). After the high pass or FFT filter, a “thresholding” function is used to convert the pore space pixels to pure black (0 color intensity) and the grain or matrix pixels pure white (255 color intensity). Based upon observations of the pore spaces, average reflectance values from the push images, and calibration to collected soil samples, a threshold color intensity of 130 (51%) has been determined to yield the best results to date. After “thresholding”, counts of black versus white pixels are used to calculate the surface area of grains versus pore area of the photomicrograph, reported as percent. For all the images, this is conducted for objects within the calibrated and focused white square visible in the photomicrographs.

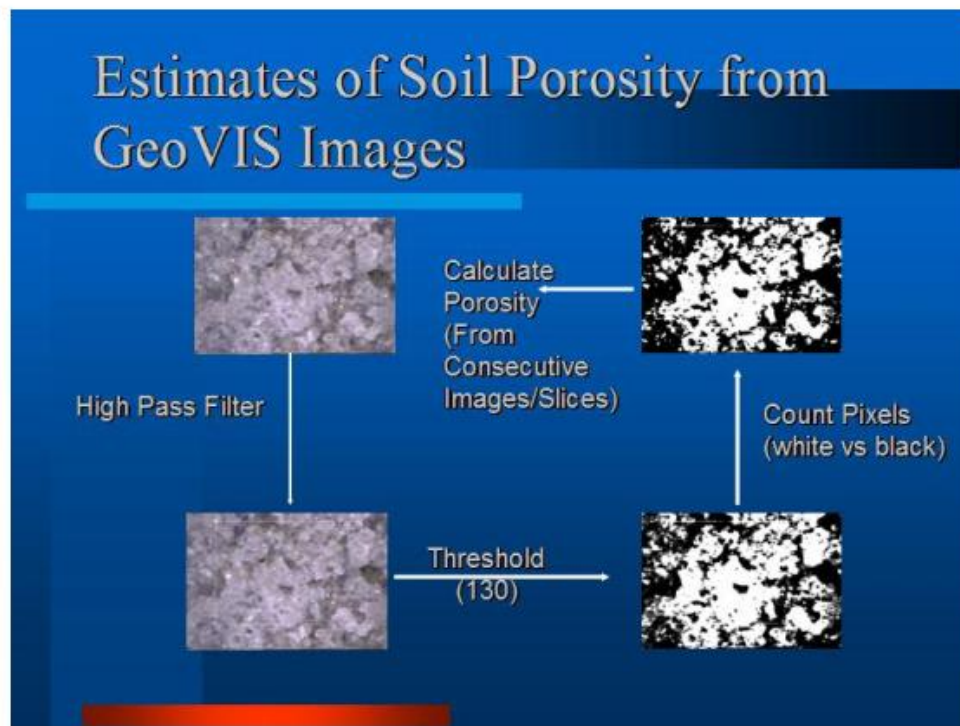


Figure 2-8. Soil Porosity Estimates Using GeoVIS Digital Video Microscope Conversion.

To obtain effective porosity estimates, defined as the ratio (in percent) of the volume of interconnected pore space to the total sample volume, the pore edges and area are enhanced through the use of a high pass filter image, converting colors to either black or white using a binary threshold, and then pixels are counted to obtain porosity values. A method of consecutive images (slices) is used to quantify the total imaged volume and total percent of interconnected pore space (Sinfield *et al.*, 2004). If a sufficient number of compositional determinations of two-dimensional slices are conducted on a three dimensional volume, then a reliable estimate of the composition of the volume can be determined. In geology, this is analogous to determining petrologic classifications by conducting point counts on stained hand specimens of plutonic rocks, or point counts on petrographic thin sections. For porosity, the pore spaces and pore areas are clearly visible and quantifiable within the two-dimensional photomicrographs, which represent one slice through the 3-dimensional soil volume. Multiple photomicrographs and rendering of the same soil volume will yield the porosity of the soil. Although not the focus of this effort, the same technique can be used to derive estimates of NAPL saturation in source zones (Sinfield *et al.*, 2004), and can even be used to assist with liquefaction assessment (Ferritto, 1997).

Improvements to the current system included automation of digital processing functions such as photomicrograph filtering, pixel counting, and method of slices imaging techniques. While the GeoVIS photomicrographs are currently generated and digitally displayed using WinOCPT, generation of logs of effective porosity are also now possible. In addition, files exported to GMS now include vertical effective porosity profiles and can be converted to three-dimensional distributions of effective porosity estimates. Since effective porosity values derived from GeoVIS are not always accurate below the water table (e.g., for silty sands), a relationship to convert soil type classification to estimates of porosity (Table 2-1) was incorporated into the WinOCPT platform, effectively allowing for all hydraulic parameters related to seepage velocity to be collected using only the piezocone. The relationship between soil type and effective porosity is based on a survey of expert opinion from key industry leaders.

Table 2-1. Estimated Effective Soil Porosity Conversion Chart Based on Soil Type.

Zone	Soil Behavior Type	Percent Effective Porosity
1	Sensitive Fine Grained	60
2	Organic Material	50

3	Clay	40
4	Silty Clay to Clay	27
5	Clayey Silt to Silty Clay	25
6	Sandy Silt to Clayey Silt	25
7	Silty Sand to Sandy Silt	28
8	Sand to Silty Sand	30
9	Sand	33
10	Gravelly Sand to Sand	35
11	Very Stiff Fine Grained (Overconsolidated or Cemented)	15
12	Sand to Clayey Sand (Overconsolidated or Cemented)	20

Porosity and head measurements are essential for determining the true rate of ground water and contaminant flow. Since these parameters can be measured at multiple depths beneath the ground water using these two penetrometer devices, a detailed three-dimensional flow assessment can now be possible. The coupling of high-resolution hydraulic assessment probe data with concentration data allows for contaminant flux estimates. This data can be used for development of site-specific monitored natural attenuation (MNA) models, remediation design specifications, remedial action optimization/long-term monitoring (RAO/LTM) approaches, and evaluation of spatial heterogeneities. When these values are coupled to the distribution of hydraulic conductivity, significant increases in the understanding of fate and transport become possible (Figure 2-9). Note that high concentration does not always indicate high risk. Data processing via Ground Water Modeling Software (GMS) allows for conversion from conceptual to fate and transport and remediation models.

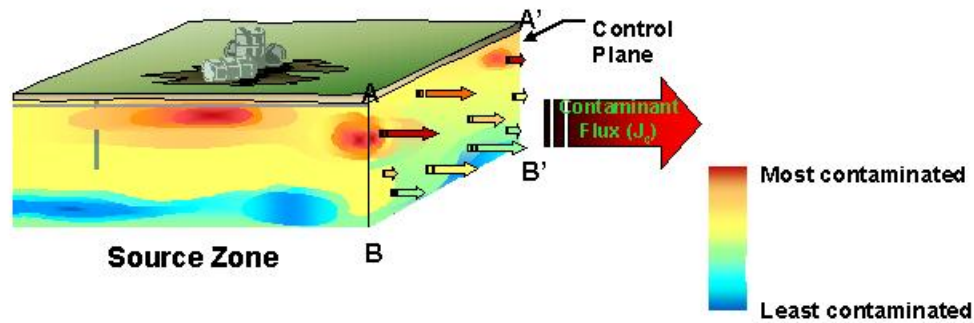


Figure 2-9. Transport Conceptualization Based on Flux (after Enfield, 2002).

GMS was modified as part of this project to allow for the determination of estimated distributions of seepage velocity and contaminant flux. More specifically, head values from high-resolution final dissipation pressures were interpolated and converted to hydraulic gradient through a recently developed gradient builder. This critical function effectively converts scalar head into three-dimensional distributions of gradient. By determining the distribution of hydraulic conductivity (from the piezocone dissipation tests or soil type conversions) and effective porosity (from either the GeoVIS image processing results or piezocone soil type conversions), GMS can now be used to determine three dimensional seepage velocity distributions through the recently developed velocity builder. The velocity builder solves Darcy's relationship for seepage velocity within the measured and interpolated domain. Using a similar concept, provided concentration distributions are determined by analysis of water samples or through a sensor based direct push probe (e.g., membrane interface probe coupled to a detector), three-dimensional flux distribution can be determined and visualized using the GMS flux builder by multiplying seepage velocity and concentration at each element or node within the model domain.

To study contamination problems at field scales, we considered spatial variability and heterogeneity of soils and hydraulic properties. Appropriately treating our hydraulic data was a critical component of this effort, as spatial interpolation of limited measured data will be required for three-dimensional assessment. Geostatistical methods offer unique ways to describe the spatial continuity of soil properties, and provide a more accurate estimation method than the classical regression techniques (Myers and Journel, 1990; Rouhani and Myers, 1990). Using well-established geostatistical methods such as kriging, we generated continuous data layers of soil properties at desired locations for model inputs. Based on geostatistical analyses, team members determined the accuracy of the estimated hydraulic properties at unsampled locations, and assessed simulation errors of transport processes related to uncertainties of these soil hydraulic properties. A key characteristic associated with kriging is that it allows for documentation of the assumptions used in the geostatistical approach. This is critical, as the fabric of spatial associations, particularly hydrologic associations such as flow direction, can be integrated into the interpolation algorithms. Another key advantage of the geostatistical method is that it allows for an extensive use of all available information to improve estimations of soil hydraulic properties at unsampled locations. For instance, by constraining our hydraulic property interpolations based on our soil type data assessment (e.g., via cokriging or pseudo-cokriging), we can significantly improve the estimation accuracy of the soil hydraulic properties. Cokriging was not within the scope of this project. However, data sets have been generated that are amenable to these higher level interpolative approaches. Geostatistical methods can also be used to design optimal sampling strategies to minimize sampling costs and maximize sampling accuracy. Although not conducted as part of this demonstration, once probe data has been collected, additional interpolation analyses (e.g., Markov chain transitional probabilities, Kalman analyses, etc.) can be applied through GIS and other spatial statistical platforms.

While preliminary demonstration of these applications had been achieved, software development was required to upgrade the WinOCPT data acquisition and processing capabilities, and to create a seamless interface with GIS. In addition, validation through comparison of this approach to conventional alternatives (e.g., well installation, soil tests and ground water monitoring) was needed for end-user and regulatory acceptance.

While the current focus of this project was to generate the key hydrogeologic components of flux, measurement of concentration was not a primary component of this demonstration. This is not to say that during implementation concentration was not

modeled, measured and incorporated into the flux distribution renderings. However, with one exception, the GeoVIS and piezocone are not currently capable of generating concentration data. The primary exception to this would be when NAPL is identified using the GeoVIS. During the demonstration, the team estimated flux distributions through simulation of a tracer test.

An optimum protocol for using these tools to generate contaminant flux to provide contaminant mass balances, evaluate remedial performance, and predict trends in natural attenuation would include the incorporation of a contaminant concentration measurement tool deployed adjacent to the hydrologic probe pushes. In practice, this could include deployment of the hydrologic probes under demonstration as well as a probe for measuring concentration. Several direct push options currently exist. The Membrane Interface Probe (coupled to either a Gas Chromatograph or Ion Trap Mass Spectrometer) is capable of yielding reproducible organic concentration data, as is the Halogen Specific Detector (XSD) probe, which can be used to measure halogenated solute concentrations. In practice, it could be best to use these concentration probes in a screening mode, then install monitoring well clusters in optimal zones for evaluating remedial performance or long-term trends in natural attenuation, as dynamic concentration tracking is required for remediation monitoring. Once the original model is generated, these sentry wells can be used to conduct long-term monitoring of concentration and head, which could be superimposed onto the original rendering of K and effective porosity to generate successive flux iterations. Probe push and well locations would be selected with specific goals in mind. For instance, when evaluating remedial performance or natural attenuation, data shall be collected from zones upgradient of the release, within the plume, downgradient, and cross gradient of the plume. Mass balances may be more difficult to perform, as spatial and temporal heterogeneities can be challenging to overcome without a large investment of time and cost, and could be subject to the shortcomings of integration algorithms used in the interpolation. As always, spatial configuration (i.e., number and spatial distribution) of the push locations and monitoring wells is critical, as this directly impacts the accuracy and predictive capabilities of the resulting model. Although additional research will be required, technical augmentation of this approach can potentially be achieved through coupling probe data to geophysical and tomographic applications to constrain the interpolations with respect to hydraulic conductivity distributions. In practice, high-resolution piezocone data can be used to effectively “anchor” and constrain geophysical data, whereby correlations can be used to

attribute hydraulic values to the geophysical observations in locations between piezocone pushes. This information can then be incorporated into the distributions of seepage velocity and flux using the GMS platform.

In summary, to place probe deployment and related activities into proper context, an optimum protocol would consist of the following steps:

- Advance the hydraulic probes and generate a three-dimensional distribution of seepage velocity;
- Advance a chemical screening probe to generate a three-dimensional distribution of concentration;
- Merge the concentration and seepage velocity data to generate a preliminary three-dimensional distribution of contaminant flux via the new GMS functions;
- Identify optimal locations for long-term monitoring, and install short-screened well clusters into these specific zones;
- At specified increments, sample these wells, measure head values, and reiterate the contaminant distribution and fate and transport models;
- Use the models for trend analyses (e.g., remediation performance evaluation, MNA, etc.) and predictive applications (e.g., time of remediation at a point of compliance, capture zone analyses, remedial optimization, etc.).

2.2 Previous Testing of the Technology

All of the sensor technologies have undergone the appropriate field-testing to prove they are rugged enough and sufficiently mature to go to the demonstration validation stage. For instance, the Navy has deployed the GeoVIS video camera at many sites, and offers this service to other DoD and DOE counterparts. The GeoVIS has been successfully used to view soils and NAPLs in real time, and to help determine appropriate remediation design constraints at high-visibility sites. Preliminary GeoVIS porosity estimates have been within 1 to 5 percent of standard grab sample laboratory results using standard API methods (Figure 2-10). In addition, recent image enhancement developments have allowed for the determination of percent NAPL saturation, which compare well with industry standard methods, but with significantly higher vertical resolution capabilities.

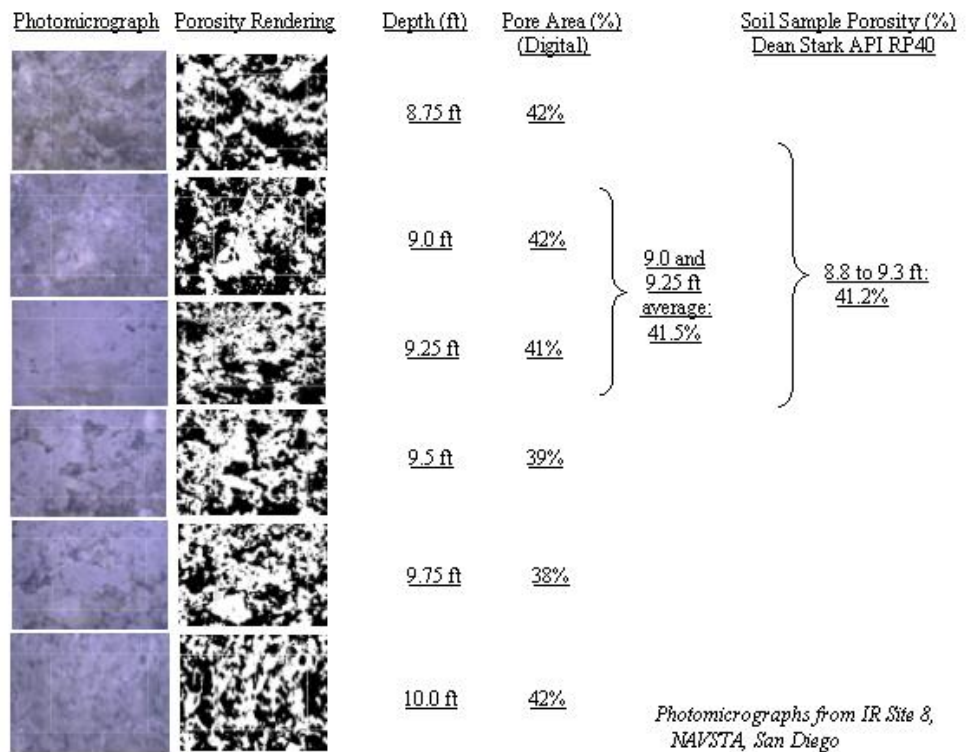


Figure 2-10. GeoVIS and API Porosity Comparisons. Digital porosity values derived from images at specific depths compare well to API porosity values derived from tests conducted on 6-inch soil cores (from Sinfield *et al.*, 2004).

The standard piezocone is an off-the-shelf item that has been used for several decades. Project members were able to use the high-resolution piezocone to successfully determine the ground water migration pathway at the leading edge of the MTBE plume located at the Port Hueneme National Environmental Technology Test Site (NETTS). In the process, they identified a hydraulic sink and artesian conditions (high head at depth relative to shallow depths within the same water bearing zone) corresponding to a broken sewer line and an adjacent pump station that were influencing ground water flow in the region (Figure 2-11). These findings resulted in an expedited and cost-effective leak repair effort, and helped define design constraints for the current plume containment system. During this Port Hueneme deployment, 1.5-inches of water level precision were achievable. Since that time, increased precision (down to below 1.0-inch of total error)

resulted from hardware and software changes to the probe and system, allowing for three-dimensional hydraulic gradient determination in non-pumping situations.

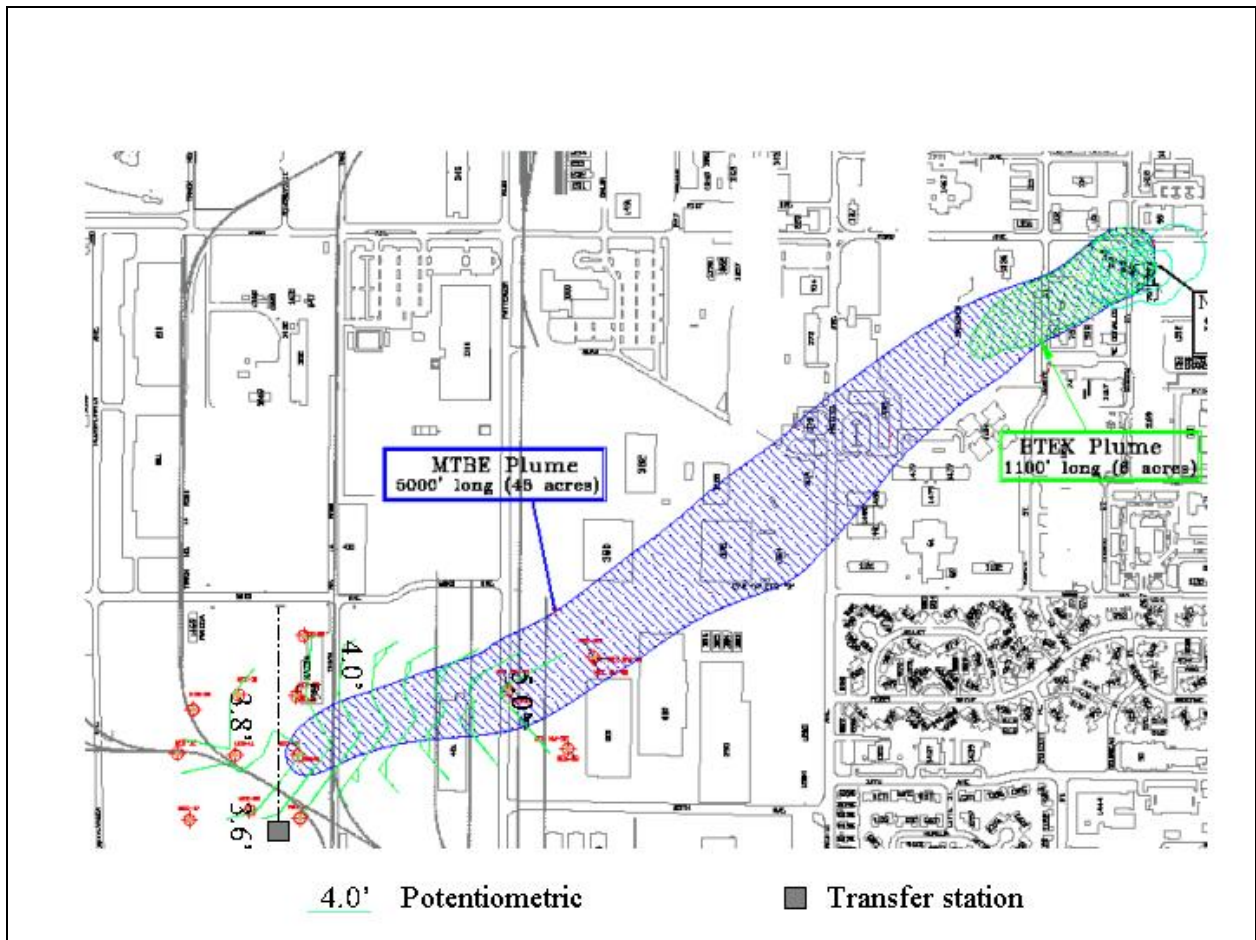


Figure 2-11. Piezocone Potentiometric Surface Determination. Note the ground water low identified adjacent to a sewer line (dashed line near transfer station) in the southwest portion of the map. Background map from NETTS, 2003.

Previous field efforts reflected the need for the following items for process streamlining and production oriented field efforts:

- Ability to determine and display GeoVIS effective porosity values in a more efficient log form (software alteration);
- Ability to collect, display, and manage high-resolution piezocone data in a more robust and efficient manner using WinOCPT (software alteration), and with higher precision (hardware upgrade);
- Ability to convert piezocone soil type classification to hydraulic conductivity and effective porosity estimates (software alteration);

- Ability to convert piezocone head values to three-dimensional gradient (software alteration);
- Ability to solve for seepage velocity and contaminant flux distributions using piezocone and GeoVIS data exported to GMS (software alteration);
- Comprehensive comparison between conventional well data and high resolution piezocone data (field efforts along with model development and statistical analyses).

2.3 Factors Affecting Cost and Performance

The cost and performance of direct push in situ sensors are subject to factors related to site specific conditions, as are conventional site characterization methods. Specific geological conditions (e.g., the presence of cobbles or bedrock) may impede or limit the ability to push sensor probes into the ground. At present, GeoVIS effective porosity estimates can be generated for granular silty sand, sand, and gravelly sand soils. For finer materials, silts and clays tend to press against the probe window, inhibiting the ability to directly observe pore spaces between silt and clay particles. For these finer zones, soil type classification was determined using the piezocone load cells. Porosity estimation is now possible by utilizing a correlation between piezocone derived soil type and porosity integrated with WinOCPT. Similarly, when collecting water table or head data, it is most effective to use the high-resolution piezocone in silty sand to gravelly soils, as pressure dissipation in finer soils requires more waiting time. Therefore, to expedite field activities and reduce costs, dissipation tests were conducted in coarse-grained soils wherever possible. For depths where piezocone dissipation and GeoVIS data is not collected, but soil type information is determined, we utilized published relationships for estimating hydraulic conductivity (e.g., Robertson and Campanella, 1989) and porosity (Rawls *et al.*, 1982; and Carsel and Parrish, 1988), and hydrogeologic correlations between CPT soil behavior type and hydraulic conductivity and porosity to develop our models.

A chemical tracer test using Rhodamine (WT) was employed as an attempt to validate the predictions of the probe- and well-based hydraulic models. Permits for tracer release and monitoring were obtained and required significant time and expense. In addition, installation of a multi-level, short screen well cluster network was required for the comparisons. Prior to installation of the well network, a salt tracer was released and tracked using time-lapsed resistivity to help determine the groundwater flow direction and appropriate orientation of the well clusters. Each monitoring well required

customization, which was based on the Kram and Farrar method to convert penetrometer soil type classifications to ASTM recommended filter pack and screen slot size. While this approach saved significant amounts of time and money, it was recognized that not all of the ASTM recommended well construction materials are commercially available in prepack configurations. Therefore, wells were customized by purchasing ASTM recommended filter pack gradation materials from one vendor, custom cut slotted polyvinyl chloride pipe from another vendor, then shipping them to a vendor marketing prepack direct push well materials for customization, fabrication and delivery.

Other factors affecting cost and performance during typical deployments include the following:

- Seasonal considerations – During non-rainy times of the year, potentiometric surface fluctuation can be less dramatic, so the rate of high-resolution piezocone data collection is not as critical. However, if the potentiometric surface is rapidly changing, a piezocone survey should be completed within a very short time period to enable data to be compiled as a complete visualization or model. Similar considerations arise when encountering pumping and tidal impacts;
- Surveying zero elevation push initiation points – The group derived a protocol for georeferencing surveyed push initiation points that included pre-pushing with a blank rod, placing tape across the vacated hole upon retraction, zeroing the piezocone and GeoVIS push initiation routine as it just touched the tape, then later surveying the same zero location using conventional survey equipment.

2.4 Advantages and Limitations of the Technology

The primary advantage of direct push based sensor technologies is that they provide information in real-time while the site investigation is ongoing. Real-time information facilitates optimization and modification of sampling plans without waiting days or weeks for results from the laboratory, and helps eliminate the need for iterative sampling efforts and remobilization that are often required to fill data gaps. Direct push sensor systems generally provide much higher vertical spatial resolution of soil stratigraphy in less time relative to conventional sampling strategies. The high vertical spatial resolution permits accurate identification of soil boundaries needed for modeling and interpretation of hydraulic tests. Although continuous coring approaches provide comparable data, loss of soil material during core recovery can complicate stratigraphic interpretation. Continuous coring is also typically time-consuming.

Generating a hydraulic head distribution using the high-resolution piezocone is preferable to using conventional monitoring wells for many reasons. Monitoring wells are typically installed in soils without adequate knowledge of the subsurface hydrogeologic characteristics. Since zones of relatively high hydraulic conductivity often dictate ground water and contaminant transport, knowledge of soil characteristics (e.g., soil type and distribution) can greatly impact the selected location and therefore the usefulness and performance of the monitoring well. However, wells are typically installed and designed without giving proper consideration to this very important observation, resulting in less than optimal siting and performance. Furthermore, hydraulic conductivity weighted averaging is often associated with observed solute concentrations and hydraulic heads within long-screened (e.g., greater than 5 feet) wells. The point measurements afforded by the piezocone allow for much better head resolution, and therefore allow for much better characterization of the conditions in the natural formation just beyond the well “skin” (e.g., sand pack). For instance, long-screen monitoring well hydraulic and chemical data averaging does not allow for measurement of subtle transport variabilities such as vertical flow, aquifer connectivity, and reliable transport model predictions.

Determining effective porosity using the GeoVIS image processing approach avoids the need for sample collection and laboratory analyses. Furthermore, point measurements of porosity are much more accurate and reliable than measurements obtained using the API Dean Starks Method, which renders a single value for a 6-inch sample. Issues related to sample heterogeneity and representativeness can be avoided by using GeoVIS.

Dovetailing the probe hydrogeologic data with conceptual and transport models represents a significant achievement. Minimizing the level of manual data import requirements will help streamline the data assessment process. When properly applied, this approach can expedite the generation of remediation design options. Once deployed, far fewer wells will be required for understanding ground water and contaminant flow, leading to significant DoD cost savings due to fewer monitoring requirements (e.g., wells, samples, laboratory analyses, aquifer tests, etc.) and greater accuracy and usefulness of transport simulations for the hundreds of LTM and RAO sites. The detailed spatial information afforded by the probes can then be used as a guide for collection of discrete water quality samples or for selecting long-term monitoring well locations. Since contaminant fluxes can vary significantly across a site, whenever possible, it is recommended that contaminant concentration also be used to optimize well locations. The GeoVIS and high-resolution piezocone data allow one to make better informed

sampling and remediation decisions (e.g., how many samples, where to locate them, where to install and screen long-term monitoring wells) in a straightforward and cost-effective manner, eliminating the costly and ineffective “trial-and-error” mentality that conventional assessment approaches are currently based on.

Generation of distributions of hydraulic data and resulting seepage velocity and flux using the direct push probe applications demonstrated within the scope of this project each rely on geostatistical interpolative approaches. Geostatistical applications are limited by data density and assumptions incorporated into the selected interpolation algorithms. While geostatistical approaches do have limitations, estimates of uncertainty are possible, as are capabilities for tracking and reporting statistical progeny. The hydraulic probe and interpolative approach has not yet been directly compared to other innovative contaminant flux distribution methods. However, in terms of implementation, the probe-based approach can be relatively easier to use, as flux can be determined in a single deployment before leaving the field. In addition, alternative flux based approaches typically require installation of dedicated monitoring wells. Most of the alternative flux based assessment approaches are implemented in a transect orientation orthogonal to the direction of ground water flow. The probe based approach can also incorporate a transect orientation. For instance, the high-resolution piezocone can be coupled with a membrane interface probe to develop transects of mass flux. However, multiple transects are recommended, as interpolation of head values are required to obtain gradient distribution through the GMS gradient builder, and a single transect of pushes may not yield appropriate head value distributions for gradient derivation.

Since they are separate probes, it is not possible to collect high-resolution piezocone data from the same location that the GeoVIS sensor push is advanced. Spatial heterogeneity can lead to potential soil variability between the locations probed. For consistency, piezocone pushes and GeoVIS pushes were advanced no more than 18-inches apart and no closer than 12-inches to each other or to well clusters. In addition, all pushes were backfilled with sand to minimize potential impacts on the final tracer test caused by high pressure grouting.

It is recognized that this technology can only be performed at sites amenable to penetration using a cone penetrometer. At present, GeoVIS effective porosity measurements can be generated for granular sandy and gravelly sand soils. For finer materials under liquefiable conditions, silts and clays tend to press against the probe

window, inhibiting the ability to directly observe pore spaces between silt and clay particles. For this reason, a soil type conversion for porosity estimation was incorporated into the piezocone to allow for data collection regardless of soil type. Similarly, when collecting water table or head data, it is most effective to use the high-resolution piezocone in silty sand to gravelly soils, as pressure dissipation in finer soils requires more waiting time. For this project, preliminary piezocone pushes were advanced around the perimeter of the test domain to identify candidate coarse-grained strata for relatively rapid dissipation tests and corresponding well screen depth ranges.

Parez and Fauriel (1988) have derived a relationship between 50 percent dissipation (t_{50}) and hydraulic conductivity (Figure 2-5). For each depth where a dissipation test is completed, a range of K values can be reported as maximum, minimum, and mean. Mean K values are presented in log form using the recently upgraded WinOCPT data management package. Alternatively, when a dissipation test does not exist for a specific zone, operators can utilize a look-up chart to convert CPT soil behavior type to hydraulic conductivity estimates, which are also displayed in log form. The benefits of this approach include the fact that a soil type classification can be generated for each inch of penetration for each push, and the fact that this relationship has already been incorporated into an early version of Piezocone Dissipation Analysis (PDA). However, these estimates are only reliable within an order of magnitude. For depths where piezocone dissipation and GeoVIS data are not collected, but soil type information will be determined, we utilized published relationships for estimating hydraulic conductivity (e.g., Robertson and Campanella, 1989 [Figure 2-12] and porosity (Rawls *et al.*, 1982; and Carsel and Parrish, 1988), and hydrogeologic correlations between soil type and hydraulic conductivity and porosity to develop our model.

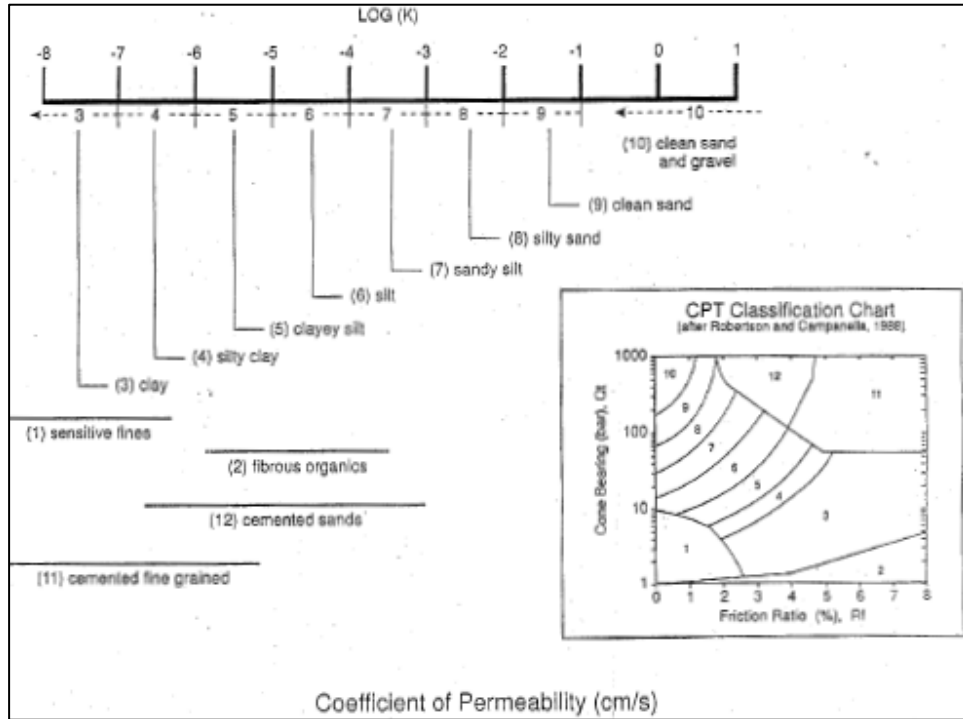


Figure 2-12. Hydraulic Conductivity based on Soil Type (after Robertson and Campanella, 1989).

With respect to potential impacts of oily or viscous waste materials smearing during camera deployment, the SCAPS laser induced fluorescence (LIF) probe uses the same type of sapphire window as the GeoVIS. Except for a few occurrences in the vadose zone and capillary fringe, no smearing of oily or viscous materials has been observed in the thousands of SCAPS LIF pushes and in any of the GeoVIS pushes conducted to-date. For example, LIF pushes display a very specific vertical hiatus in fluorescence signals corresponding to “clean” strata beneath contaminated zones. Therefore, smearing does not appear to be a problem with direct push probes.

The GMS software required modification to allow for the development of a gradient builder, seepage velocity field, flux distribution, and three-dimensional visualizations of the probe-derived hydraulic parameters (Appendix H). To generate three-dimensional hydraulic gradient vector values from scalar head value distributions, a finite difference solution was derived. Control over hydraulic isotropy is afforded the user, so the resulting models can be tailored to match observations and site specific assumptions. The seepage velocity can now be derived from interpolated hydraulic conductivity, hydraulic

gradient, and effective porosity values, whereby Darcy solutions are estimated at each node within the site model domain. This probe-derived velocity field can then be used in Modflow to establish ground water transport simulations. Once the solute concentration distribution has been determined (using interpolated values from other probes or samples from wells), a mass flux calculator (also recently added to the GMS capabilities through this effort) can be employed to multiply the seepage velocity distribution data set by the concentration distribution data set to create a data set representing the mass flux distribution. These changes represent significant achievements, as probe data can now be converted to highly resolved three-dimensional hydraulic and flux distributions (when concentrations are known) that were previously not available to field practitioners. Limitations stem from the fact that the models are based on interpolation of probe data. Improvements could include coupling the probe data with geophysical information to better estimate the distribution of hydraulic parameters (e.g., hydraulic conductivity) in areas not sampled or probed. In this instance, the probe data could serve to constrain the interpretations of geophysical observations, effectively leading to superior interpolations based on field data. However, coupling geophysical techniques with the piezocone was not within the scope of this project.

3. Demonstration Design

3.1 Performance Objectives

Successful implementation of this project included meeting several key objectives. While the overall objective was to generate superior high-resolution three-dimensional models using data derived from penetrometer tools integrated with comprehensive statistical and modeling software, several probe-specific objectives were also achieved. Performance objectives for this demonstration/validation are listed in Table 3-1. It should be noted that solute concentration was not measured using the hydraulic assessment demonstration probes. Flux estimates require solute concentration measurement when implementing this approach. For derivation of a flux domain using a purely direct-push approach, ground water sampling or chemical sensing probes are required in addition to the hydraulic assessment probes. During the performance evaluation phase of this project, a tracer was released and tracked in an attempt to obtain concentration data required for estimating flux distributions. Due to complications associated with the tracer test, model performance objectives were refocused to determine how well piezocone based model projections compare with well based model projections.

Table 3-1. Performance Objectives

Type of Performance Objective	Primary Performance Criteria	Expected Performance (Metric)
Qualitative	1. Ability to generate superior conceptual and fate and transport models	Improved capability for identifying zones of high seepage velocity, and conceptualization of distribution of key hydrogeologic attributes
	2. Capability to resolve small spatial scale variations in contaminant flux	Improved capability for localizing small scale spatial variations in ground water flow when coupled to solute concentration
	3. Ease of use	Operator acceptance
Quantitative	1. Determine the high-resolution piezocone accuracy relative to the short screen control wells for determining head values, flow direction, hydraulic gradients, and hydraulic conductivity	Uncertainty of the probe values versus multi-level ground water monitoring approaches shall be low (e.g., head values within one inch [0.08 ft]; hydraulic conductivity within one order of magnitude)
	2. Determine the GeoVIS accuracy for determining effective porosity	Uncertainty of the probe values versus lab analyses shall be low (e.g., within 30%)

	3. Determine accuracy of resulting model for solute transport predictions	Uncertainty levels of the data layers for hydraulic head, effective porosity, soil type, and velocity distributions shall be low (e.g., low variance based on kriging and other geostatistical analyses). Breakthrough predictions for probe derived models and well derived models shall compare favorably to each other [e.g., comparable breakthrough curves, and probe based model efficiency accounts for more than 15% of the variance associated with well based models])
	4. Time required for characterizing and hydraulically delineating contaminant sites	Reduction in time required for delineating hydraulic properties controlling contaminant transport, remedial design, and monitoring and restoration optimization alternatives

3.2 Selecting Test Site(s)

The ideal test site for this project is one that consists of penetrable soils, a shallow water table, climate amenable to year-long field activities, and infrastructure for supporting field logistics.

Several practical and logistical factors were considered when selecting the test site. These include the following criteria:

- The US Department of Defense (DoD) agreed to allow access to the site for the demonstration.
- The site is accessible to the direct push vehicle.
- The soil types at the site consist of unconsolidated sediments of native sands, silts, clays, and gravel. These soil types are suitable for CPT pushing and present appropriate matrices for the sensor technologies to be evaluated in this demonstration/validation.
- The site has successfully undergone regulatory scrutiny in the past, and all regulatory challenges have been met.
- The site consists of adequate protection from vehicle traffic.

Available site baseline data established that wells can be installed, direct-push sensors can be deployed, soil samples can be collected, and ground water monitoring can be accomplished. It is highly probable that the combined data from the suite of sensor probes will provide a level of certainty far greater than has been possible heretofore. Owing to the importance and complexity of the problem, project team members consulted with industry and academic experts to assist with site selection, data interpretation, and performance criteria for the new characterization technologies against traditional site characterization approaches. Furthermore, team members have received significant interest from outside parties hoping to be able to conduct hydraulic conductivity and flux analyses using alternative techniques that would be complementary to the approaches demonstrated under the aegis of this effort. If approved, this could increase the available site-specific database and could lead to an innovative hybrid approach that is superior to any alternative currently available within the commercial and research domains.

3.3 Test Site Description

The NETTS is located in Port Hueneme, California, at the Naval Base Ventura County (NBVC) Port Hueneme Site. The NETTS was established for advanced petroleum based contaminant characterization and remediation technology demonstrations. According to site personnel, gasoline was released from underground storage tanks (USTs) and fuel distribution lines associated with the NEX Gasoline Station between September 1984 and

March 1985 (Kram *et al.*, 2001). Based on NEX Gasoline Station inventory records, approximately 4,000 gallons of leaded gasoline and 6,800 gallons of premium unleaded gasoline (for a total of 10,800 gallons) containing the additive methyl tertiary-butyl ether (MTBE) were released from product delivery lines into the subsurface. A large source zone and associated dissolved contaminant plume have resulted in MTBE concentrations of concern in the shallow, unconfined sand and silt aquifer. The dissolved MTBE plume extends 45 acres, more than 4,575 feet from the release site. The plume is, for the most part, under open hardstands (parade ground, parking lots, and storage areas). On-going remediation and containment efforts are comprised of biobarriers placed in strategic locations downgradient of the release, mid-plume, and along the plume's leading edge. The demonstration site is located within the MTBE plume just upgradient from the leading edge (Figure 3-1).

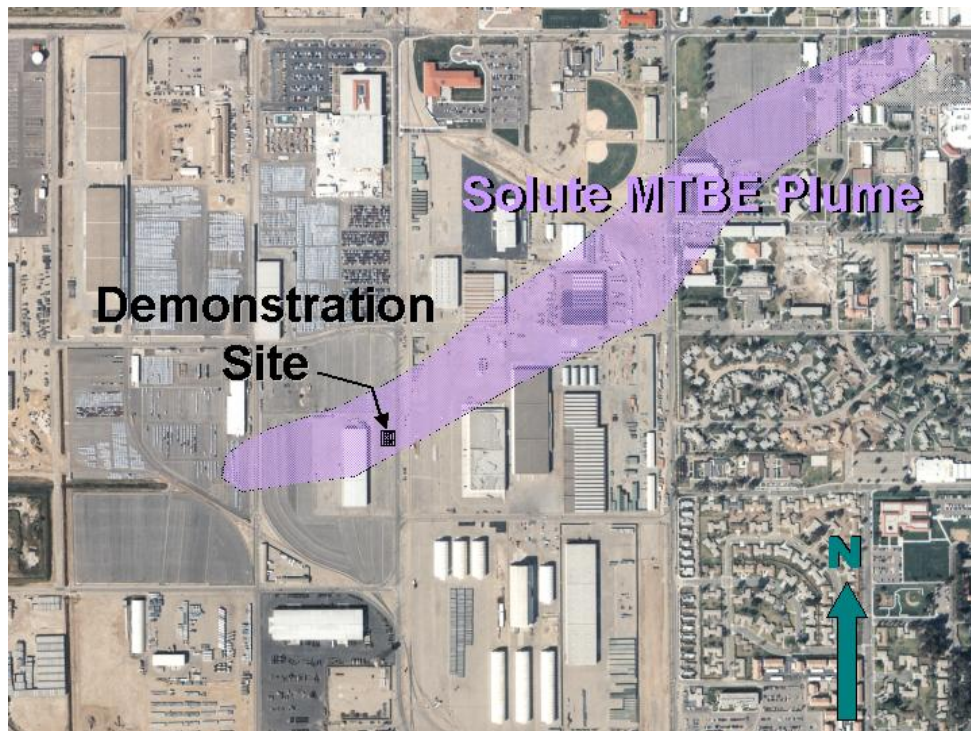


Figure 3-1. Site Map Depicting Location of Demonstration Test Facility Relative to NETTS MTBE Plume. Background image from NETTS, 2003.

Port Hueneme is bordered by the Pacific Ocean to the west and by the Cities of Oxnard and Port Hueneme in Ventura County towards the north and east. The Naval Facilities Engineering Service Center (NFESC), a tenant command on NBVC, manages NETTS sites for both *in-situ* and *ex-situ* characterization and remedial technology

demonstrations. Technology demonstrations are performed by various federal government, academia, and private industry groups. Furthermore, all investigations conducted at the facility benefit from oversight provided by the NETTS Advisory Committee.

The Port Hueneme NETTS is an ideal location for the demonstration, as the soils consist of penetrable fine to medium grained soils, a shallow water table, and the selected site meets all the criteria described in 3.2. Infrastructure for supporting field logistics is excellent, the soil subsurface environment is well characterized, and several team members have worked on NETTS projects in the past and are therefore familiar with logistics and staging requirements. In addition, hundreds of direct push wells and instrumented probes have been advanced at the facility. In fact, the selected site was formerly used by EPA researchers to evaluate wellhead treatment technologies. It consists of proper dimensions, orientation and infrastructure for conducting this demonstration effort (Figure 3-2). Clustered wells and push locations were oriented to accommodate for local water flow direction determined prior to installations. Flow direction was determined using preliminary bounding monitoring wells as well as a CaCl_2 tracer test coupled with a time-lapsed resistivity survey. Tracer injection was implemented using a well consisting of a custom designed 5-foot fully submerged screen interval located a few feet upgradient from the candidate well cluster locations. The secure site is equipped with power, water storage tanks, a storage shed, and fencing amenable to heavy equipment ingress/egress.

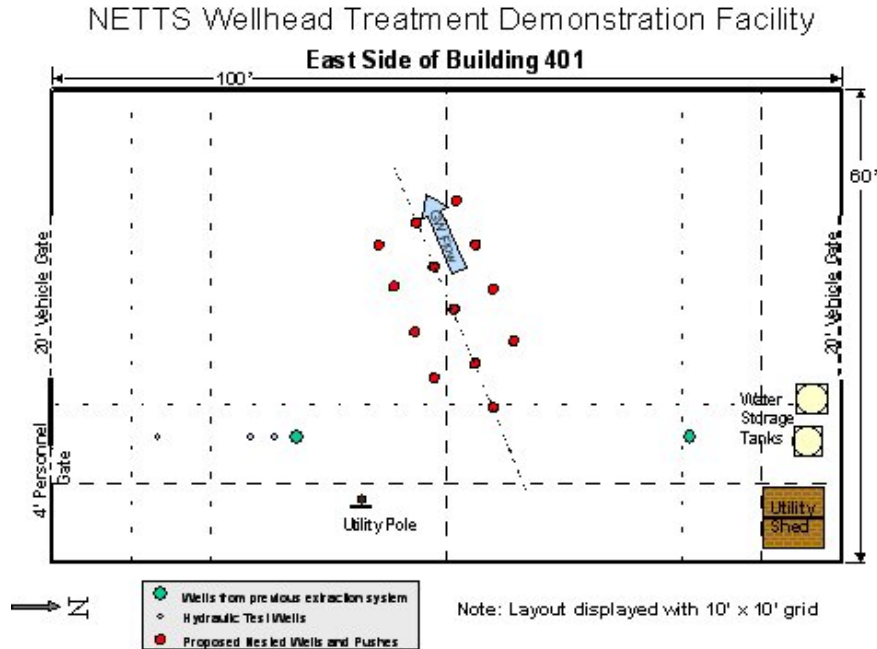


Figure 3-2. Selected Port Hueneme NETTS Site (Formerly used by USEPA to evaluate wellhead treatment technologies).

The “semi-perched” aquifer zone consists of fluvial-deltaic sediments approximately 25 feet (4.6 m) thick in the vicinity of the site. The uppermost silty sands grade into more clean sands and medium to coarse sand at depths ranging from approximately 6.0 to 25 feet (1.8 to 4.6 m) below ground surface (bgs), depending upon the location within the plume footprint (Figure 3-3). The unconfined water table ranges from 5 to 8 feet (1.5 to 2.4 m) bgs, depending on the location along the plume, the distance from the coastline, and the most recent climatic conditions. The saturated aquifer thickness ranges from approximately 15 to 20 feet (4.6 to 6.1 m). Mean hydraulic conductivity in the most permeable downgradient areas evaluated before the project began ranged from 6.3×10^{-4} to 6.4×10^{-2} cm/s, and tended to be higher in the deeper portions of the aquifer where the sand units are relatively more coarse (Kram *et al.*, 2001). Prior to project commencement, the average linear ground water velocity observed in the unconfined aquifer ranged from approximately 0.5 to 1.5 feet (0.15 to 0.46 m) per day towards the west-southwest. Lower values were observed within the site footprint, primarily due to the low hydraulic gradient.

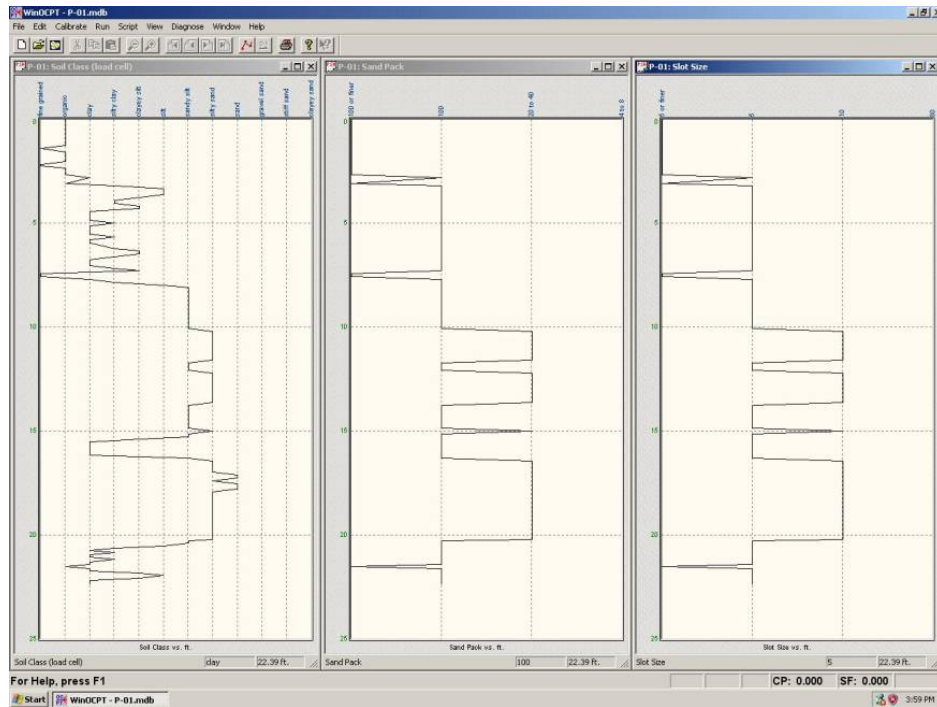


Figure 3-3. Site Soil Type and Well Design Logs. This direct-push log was generated approximately 5 feet upgradient of the demonstration site footprint and was used to design the upgradient monitoring well and the test domain well clusters.

3.4 Pre-Demonstration Testing and Analysis

Project team members, the Navy PWC San Diego SCAPS group, and NFESC personnel conducted pre-demonstration activities. These activities included advancing three initial cone penetrometer pushes around and within the footprint of the test facility in November 2004 to determine general lithologic characteristics and specific well design criteria for future well installations (Figure 3-3) based on the Kram and Farrar well design method (U.S. Patent Number 6,317,694). Three direct push wells were installed adjacent to the cone penetrometer pushes around the perimeter of the test facility to determine localized ground water flow directions using spatial interpolation of the head data. It became apparent that the low hydraulic gradient could not be accurately discerned by the three wells. The orientation of the centerline of the clusters was determined based on a preliminary potentiometric assessment as well as a CaCl_2 tracer and time-lapsed resistivity survey (Appendix E). In the Summer of 2005, two additional direct-push monitoring wells were installed approximately fifty feet downgradient of the test domain

boundary wells, as it became apparent that the gradient within the test cell was very low and could not be accurately determined for modeling using test cell data. For the initial tracer test, resistivity probes were deployed to track a 50-gallon slug of salt tracer (CaCl_2 at approximately 215,000 mg/l) released from an upgradient well over a six-week period (Figure 3-4). This information was used to help orient the configuration of test facility wells and pushes, with the primary goal of establishing a distribution of multi-level monitoring points and probe pushes parallel to the localized gradient as depicted in Figure 3-5.

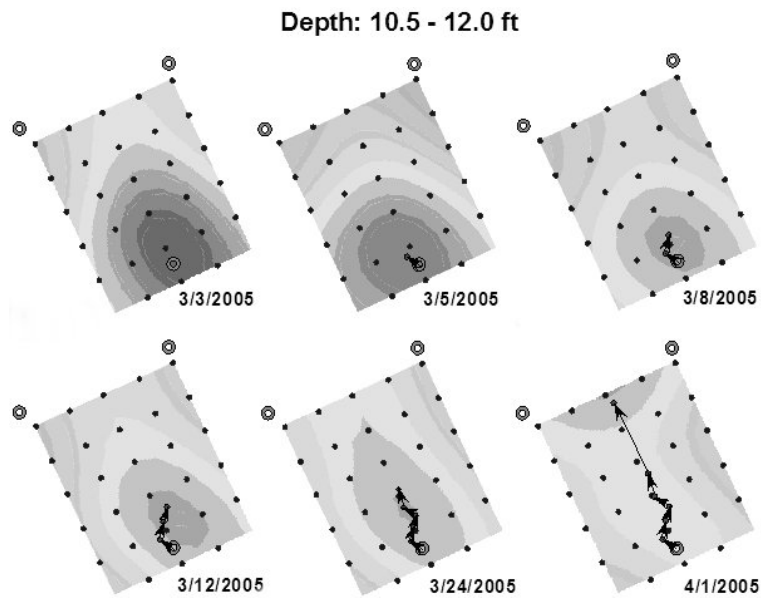


Figure 3-4. Contours of the Differential Electric Resistivity in the Silty Sand Formation (10.5-12.0 ft bgs) Between the Date of Survey (marked for each contour) and February 28, 2005. Dots represent electrodes and rings represent monitoring wells. Arrows represent flow azimuth for time increment. Dark shade depicts conductivity increase (resistivity decrease) and light shade indicates conductivity decrease and resistivity increase.

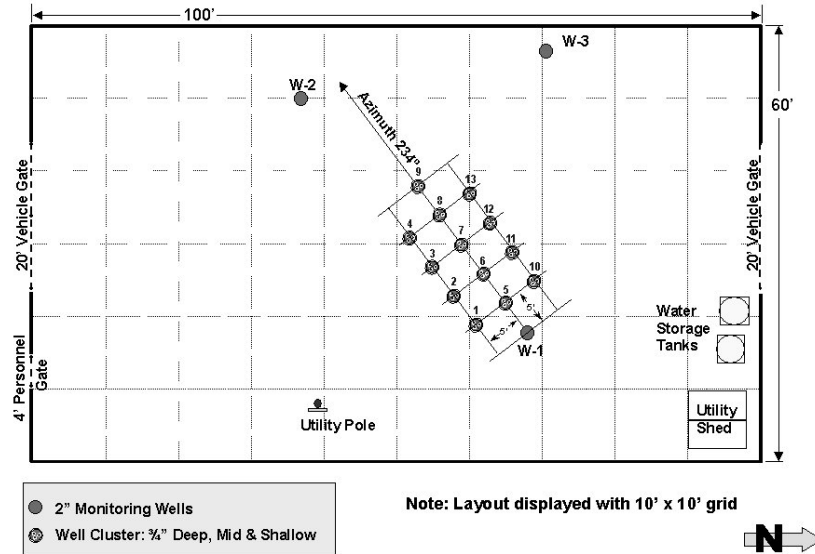


Figure 3-5. Test Site Configuration. W1 represents the upgradient injection well, while the numbered dots represent the well and push clusters.

As mentioned above, because of the size of the test cell and low hydraulic gradient, well data did not permit accurate determination of the direction of ground water flow. To aid in determining flow direction and rate, and to assure that the second tracer effort (e.g., release of a Rhodamine WT dye following probe pushes and modeling efforts) would proceed with the tracer migrating within the well cluster domain, the time series resistivity survey was performed to track the migration of a saline tracer injected into well W-1. Figure 3-4 illustrates contours of the differential resistivity at 10.5 to 12.0 feet bgs for six specific dates following the salt tracer release. Note that the flow rate appears relatively low for the early part of the survey just downgradient of the release, and then becomes significantly higher in the later phase and further downgradient. This is consistent with the penetrometer push profiles from locations adjacent to the three initial wells (W1, W2, and W3), which indicated that soils in the 10.5 to 12.0 feet bgs range were more permeable in the areas adjacent to W2 and W3. The resistivity survey revealed a mean azimuth of tracer migration of approximately 234 degrees, which was used as reference for orienting the well clusters. It is interesting to note that water levels observed in the three initial wells (W1, W2, and W3) displayed a mean flow azimuth of 287 degrees, with a range of 225 to 311 and standard deviation of 32 degrees based on measurements taken during the time period of the salt tracer test.

Thirty-nine customized small screen wells (3/4-inch diameter PVC with six-inch preppacked screens) were installed in thirteen clusters, each comprised of three wells set to

three specific depths within the anticipated solute travel pathway of the test domain. Each well was designed using the Kram and Farrar method, and in accordance with ASTM D5521, D6724, and D6725. In the Fall of 2005, each well was tested for hydraulic conductivity using the GeoProbe Pneumatic Slug Test Kit, and water level using a water level sounder to characterize the spatial distribution of conductivity and hydraulic head (Appendix F). These well values serve as the control parameters for comparison with the cone penetrometer determinations.

Also in the Summer of 2005, GMS was modified to enable users to generate three-dimensional gradient distributions based on the interpolation of probe and well hydraulic head data. In addition, GMS was upgraded to allow for the calculation of the three-dimensional distribution of seepage velocity (using hydraulic conductivity, effective porosity and gradient distributions) and contaminant flux (provided the distribution of solute concentrations are known). All model simulations of seepage velocity, contaminant flux, and projected plume distributions and breakthrough curves were generated using this upgraded version of GMS. A one-day training workshop was held in San Diego to provide the users with experience conducting the new data management and simulation tasks. In addition, a guidance document was added to the GMS training documentation for future users (Appendix H). Shortly following the GMS upgrades, the system was tested at a selected site at North Island to generate concentration versus flux distributions (Figure 3-6).

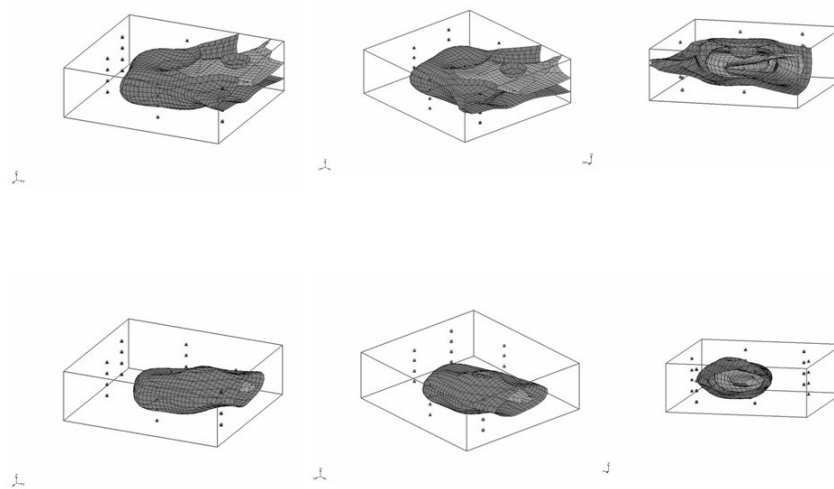


Figure 3-6. Concentration Versus Flux Distribution Using GMS. Concentration (displayed in the top row) and flux (represented in the bottom row)

distributions are rotated to facilitate conceptualization. Concentration outer isosurface represents 1ppm benzene. Flux outer isosurface represents 1 mg/m²-s.

Throughout the project duration, WinOCPT, the SCAPS probe data acquisition and management software package, was under continuous modification. A new GUI was produced, a new set of output and data analysis tools derived, and a robust data export function was generated to facilitate GMS modeling requirements. This complex and critical software allows for determination of high-precision head values, determination of hydraulic conductivity using three distinct methods (e.g., dissipation via the Parez and Fauriel graphical relationships [providing three distinct values of hydraulic conductivity, including max, min, and mean values], dissipation via the Parez and Fauriel algorithm [formula values], and using a lookup chart to convert soil type characterizations to hydraulic conductivity), and estimation of effective porosity using two methods (e.g., a lookup chart to convert piezocone soil type to porosity and sophisticated GeoVIS image processing algorithms). This unique piece of software is Windows based, modular, and extremely robust. It has also been integrated with chemical, soil type, and well design modules, as well as probe calibration and quality control modules for seamless Triad-enabled environmental characterization activities. An example of the graphical output available to the users is presented in Figure 2-6.

In February 2006 the team was deployed to the site, where multiple pre-demo high-resolution piezocone pushes were advanced adjacent to boundary monitoring wells around and downgradient of the test plot domain. A 1.5-inch water level precision was achieved, as evidenced by multiple pushes adjacent to each other which were surveyed via GPS and traditional location and elevation methods. However, the demonstration was postponed for the following reasons:

- 1) The target precision level of 1.0-inches of total error was not yet reached;
- 2) A few additional software issues remained to ensure that the exported data package was accurate for GMS processing; and
- 3) The GeoVIS light source was not bright enough for accurate effective porosity determination.

To address these concerns, precision improvements were achieved through software improvements (e.g., incorporation of a more stringent quality control protocol, prompted

by software user interface, establishing file and graphic format default settings and templates, etc.) and by resetting the GeoVIS illumination and lens components.

3.5 Testing and Evaluation Plan

3.5.1 Demonstration Installation and Start-Up

The SCAPS truck mounted CPT platform is a stand-alone, roll-on, roll-off unit requiring no outside utilities during operation. No special structures, either temporary or permanent are required for operation. All power is supplied from an onboard generator and is regulated through an uninterruptible power supply with a bank of batteries. An external electrical power input is also available. A hydraulic system, integrated into the truck, provides the force required to insert the probe into the ground. Compressed air powers the grout pump and grout mixing systems. Water, from an onboard tank, is consumed during decontamination and grouting. Waste decontamination water is accumulated on an onboard holding tank. A local source of water is required for refilling the onboard tanks. Another consumable is grout. These items may be acquired locally or carried along in the SCAPS support vehicles. Decontamination rinsate water is transferred to DOT rated 208-liter (55 gallon) drums and handled as potentially hazardous waste. Operations yield approximately half a drum or less of rinsate waste each day. Wastewater disposal is coordinated with NETTS personnel and handled locally after results of sampling are obtained.

The demonstration facility consists of a fenced area protecting electric power, water storage tanks, a storage shed, and several previously installed monitoring wells. Prior to initiation of field efforts, key project representatives conducted a walk-through to determine whether alterations were required to accommodate for test equipment ingress/egress, facility footprint, well configuration, and general operational requirements. No site alterations were required. During several phases of the demonstration, a survey reference station was deployed to allow for accurate latitude, longitude, and elevation of key activities, hardware and related demonstration elements.

Preliminary piezocone pushes were advanced to assist with future well design and installation efforts. In addition, three background wells were installed (design based on piezocone observations and the Kram and Farrar approach) to help determine site hydraulic gradient and flow direction so that well clusters were placed in appropriate orientations. When it was observed that the gradient was too shallow to discern flow

direction based on the observation wells, a salt tracer was released and tracked via time-lapsed resistivity to assist with siting the control well clusters (Appendix E).

The NFESC program manager communicated regularly with the demonstration participants and advisory committee members to coordinate all field activities associated with this demonstration and to resolve any logistical, technical, or quality assurance issues that may arise as the demonstration progresses. The successful implementation of the demonstration required detailed coordination and constant communication among all demonstration participants. NFESC coordinated the acquisition and availability of all equipment needed for fieldwork associated with this demonstration as well as all permitting logistics in conjunction with PWC San Diego, University of Connecticut, University of Wyoming, USAERCDC, NETTS Port Hueneme, and local facility personnel.

3.5.2 Period of Operation

Field efforts were not continuous, as they were separated into four main phases. A Pre-Demonstration effort was conducted to determine general lithologic characteristics, well design constraints, and to help orient the configuration of the demonstration facility. Phase I Field Tests (March through August 2005) consisted of well installation and determination of hydraulic conductivity distribution. Phase II Field Tests (June 2006) included deployment of the high-resolution piezocone and GeoVIS. During this deployment, a formal public demonstration was conducted. Participants included demonstration partners, candidate licensees, representatives from the Army and east coast Navy SCAPS teams, DOE, Bureau of Reclamation, Bureau of Reclamation, regulators, and private sector parties interested in using the technologies at their sites. Phase III Field Tests (July through December 2006) included release and monitoring of a Rhodamine (WT) tracer through the well cluster domain. Follow-up efforts were comprised of dismantling of selected tracer test monitoring components (January 2007), and technology transfer via incorporation into ITRC Technical Regulatory guides and workshops (Fall 2006), assistance with Army technology incorporation (on-going), and efforts to license the technology to private entities (completed July 2007).

3.5.3 Amount /Treatment Rate of Material to be Treated

Since this is not a remediation project, no in-situ contaminant materials were treated. A minor amount of industrial derived waste (less than one drum of liquid wastes) were generated by the use of the probes, while 16 drums of waste water and one drum of solid

wastes were generated by the installation, development and testing of the monitoring well network. Facility personnel handled and managed all derived wastes.

3.5.4. Residuals Handling

Unlike conventional drilling and sampling methods, direct push sensor technologies do not bring significant quantities of soil or water to the surface. However, for this project, some components generated residuals that required attention. Phase I field efforts, which included direct push well installation and development lead to waste water generation (16 drums) and minimal solid waste (one drum). The primary residual consisted of pumped ground water that was collected in 55-gallon drums, which were labeled accordingly, and disposed of appropriately through coordination with facility personnel. Phase II field efforts, which consisted of high-resolution piezocone and GeoVIS deployment, lead to minimal liquid waste generation (less than one drum of decontamination water). The closed-loop probe cleaning waste was transferred to a 55-gallon drum located on the tailgate of the SCAPS vehicle. The drum was labeled and disposed of appropriately through coordination with facility personnel. Phase III field efforts consisted of a tracer test. Minimal liquid residuals were generated (less than one drum), as there was minimal pumping to avoid impacting the tracer test results. Post-demonstration monitoring will be required to meet the permit requirements associated with release of the salt and Rh(WT) tracers. Purge water generated will be collected in 55-gallon drums, which will be labeled and disposed of appropriately.

3.5.5 Operating Parameters for the Technology

The technologies demonstrated as part of this effort were designed to be deployed from a direct push sensor platform. The high-resolution piezocone was pushed continuously in a dynamic mode at a rate of approximately 0.5-2.0 cm/sec. During probe advancement, dynamic pore pressure and soil type (based on cone friction and vertical resistance) was continuously monitored. When a candidate depth was selected, the high-resolution piezocone push was temporarily stopped while a dissipation test was conducted. Following completion of the dissipation test, the push was again deployed in a dynamic mode until another target depth was selected for a dissipation test. This continued until all the dissipation tests had been completed for a specific push. The GeoVIS soil video imaging system was advanced continuously at a rate of 10 cm/min. The standard 20-ton cone penetrometer system normally requires two people in the push room (one rod handler plus one hydraulic system operator). A minimum of one technician is required to manage the high-resolution piezocone and GeoVIS probe data collection activities.

During the demonstration, a field team member serves as field project manager. As such, this person is responsible for field team logistics, assisting with instrumentation issues, evaluating real-time data, generating maps and reports, maintaining field records, generating conceptual site and analytical models, and serving as project supervisor.

3.5.6 Experimental Design

The following items were evaluated in this demonstration:

- 1) Accuracy of piezocone for determining head, vertical hydraulic gradients and hydraulic conductivity values;
- 2) Accuracy of GeoVIS for determining effective porosity;
- 3) Accuracy of the resulting model based on the SCAPS derived data as a solute transport predictor relative to well-derived hydraulic information.

In this context, the term “accuracy” refers to how well the probe values compare to conventional data collection methods.

In order to validate the high-resolution piezocone’s head determination capabilities, thirteen groups of clustered wells (nested to 3 depths) were installed at selected locations in a grid pattern as depicted in Figure 3-5. This configuration was selected based on an iterative sensitivity modeling approach that considered known hydrogeologic parameters measured in nearby wells, predicted tracer dispersion, anticipated field logistics (e.g., tracer concentration requirements, time steps for tracer measurements and flow models), and spatial considerations. The orientation of the centerline of the clusters was determined based on a preliminary potentiometric assessment as well as a CaCl_2 tracer and resistivity effort (Figure 3-4). The piezocone was advanced in a location adjacent to these clustered wells, static head readings were measured at depths corresponding to the well screen mid-points, and piezocone head values were compared to the head values observed in each of the wells. While head differences were anticipated due to well hydraulics and probe configuration factors, a systematic error was anticipated, which allowed investigators to compare slopes and gradient directions of potentiometric surfaces rendered using the clustered values to those derived from the piezocone. The piezocone hydraulic conductivity values derived by pressure dissipation tests were statistically compared to those derived from slug tests. Hydraulic conductivity based on soil type relationships, although not as resolved, was also incorporated into the software, and therefore also incorporated into the comparisons. The hydraulic conductivity and water level comparisons were used to evaluate the accuracy of the pressure dissipation tests, the need for corrections (e.g., for fractional losses) to improve correspondence of

conductivity values between the tests, and to improve pressure dissipation test procedures.

GeoVIS effective porosity values were derived for soils adjacent to the piezocone pushes, at depths corresponding to those where head values are available (from both the clustered wells and the high-resolution piezocone). Soil samples were to be collected from these same depths, and analyzed by the Dean Stark API RP 40 method. However, since preliminary values were lower than anticipated, and personnel responsible for developing and upgrading the GeoVIS for this application did not remain on the project, soil samples were not collected. As an alternative, project leaders insisted that effective porosity be estimated by integrating a soil type lookup chart into WinOCPT to convert soil classifications to estimates of effective porosity. Therefore, the piezocone can now be used to collect all hydraulic data required for deriving three-dimensional seepage velocity variables and distributions.

Following demonstrations of the piezocone and GeoVIS head and effective porosity capabilities, methods for determining seepage velocity were demonstrated. Hydraulic conductivity values were derived using slug tests in the clustered wells, through use of the piezocone dissipation tests at adjacent locations, and by using the Robertson/Campanella relationships (Figure 2-12). Head, effective porosity, and hydraulic conductivity data were imported to GMS to generate values and distributions of seepage velocity. Ground water models depicting seepage velocity distribution were generated and used as the basis for transport models to predict RhodamineWT dye tracer breakthroughs and distributions. Each model was derived using different methods for estimating specific hydrogeologic parameters. For instance, one iteration include head values obtained from the clustered well network, while another was derived using head values obtained from the piezocone pushes and final dissipation values.

Field efforts were conducted in three main phases as described below:

- *Phase I* field efforts consisted of determination of appropriate well field configuration through potentiometric assessment, preliminary tracer (CaCl_2) injection coupled to a resistivity survey, installation of clustered wells, and pneumatic slug tests conducted in clustered wells to determine hydraulic conductivity at specific depths and locations.

- *Phase II* field tests consisted of deploying the high-resolution piezocone and GeoVIS in selected side-by-side locations adjacent to the clustered wells to determine the three-dimensional distribution of hydraulic conductivity, head and effective porosity. Models were used to determine probabilistic realizations of hydraulic head, effective porosity, hydraulic conductivity (derived by pressure dissipation and through soil type correlations), soil type, flowpath, and velocity distribution, each with a calculated level of uncertainty. For comparison, water levels were measured in the well clusters using a water level meter.
- *Phase III* field efforts consisted of conducting a tracer (Rhodamine WT) test within the domain of the test cell to demonstrate the model predictive capabilities based on interpolated probe data. Hydraulic conductivity values derived from slug tests, piezocone dissipation tests, and soil type estimates were used in a sensitivity analysis to determine the level of velocity variability associated with each approach, and the ramifications with respect to contaminant migration assessed. Models were used to determine probabilistic realizations of hydraulic head, effective porosity, hydraulic conductivity (derived by pressure dissipation and through soil type correlations), soil type, flowpath, and velocity distribution. Six separate hydraulic conductivity estimates were used in the analyses. These included: K_{form} (using the Perez and Fauriel equation), K_{mean} (mid-point in the Perez and Fauriel graphical relationship), K_{min} (low point on the Perez and Fauriel graphical relationship), K_{max} (high point on the Perez and Fauriel graphical relationship), K_{lc} (derived from the load cell Robertson and Campanella soil type lookup relationship), and K derived from slug tests. Each set of K values yielded different velocity distribution results, as well as tracer flux distribution and breakthrough predictions.

Transport models were used to predict tracer breakthrough characteristics at observation points within the test cell. Models were developed using a) conventional data exclusively, b) SCAPS data exclusively, and c) a hybrid of conventional (i.e., K from slug tests) and SCAPS data (i.e., effective porosity and head). Comparisons among the predictions were made. This iterative process resulted in a ranking of combined data stream models to help articulate prediction-limiting steps and methods based on project management options such as data collection approach and combinations of data

collection approaches. Since hydraulic conductivity can range over several orders of magnitude, this parameter will have a profound impact on the results. K estimation capabilities of the piezocone were also evaluated through comparison of the Robertson and Campanella soil classification based approach, the Parez and Fauriel relationships, and the measured slug tests.

Although not performed under this project, since an ample number of K values were obtained and the relationships display a spatial fabric we can numerically articulate, it is possible to use co-kriging by associating variogram models of K with soil type distribution data to generate a 3-D interpolated domain of K, including residuals and data progeny. Furthermore, GMS can be used to explore the use of the transition probability/Markov approach to more seriously consider spatial cross-correlations (called “juxtapositional tendencies”). The Markov approach, a method for modeling the distribution of geologic facies as a template for defining the spatial distribution of K, is gaining more acceptance for problems associated with conditional simulations (Carle, et al., 1998). Similarly, one can do the same for the spatial distribution of effective porosity. Head, although spatially distributed, is a dynamic parameter, which therefore has a temporal variability. However, we incorporated head, effective porosity, and K estimates at specific time steps into comprehensive discretized renderings of seepage velocity within the domain of the study. While the tracer test was conducted, several sets of head values were collected using the clustered wells to track gradient stability. To avoid potential climatic impacts to ground water gradient, attempts were made to conduct the tracer test during a relatively static time of the year. Since the gradient was extremely low, large potential predictive errors could result. Therefore, comparisons of head, gradient, and K could be more important than model comparisons. Additional factors, such as fluorescence interference caused by turbidity were considered and addressed during project implementation.

Since they are separate probes, it is not possible to collect high-resolution piezocone data from the same location that the GeoVIS sensor push is advanced. Spatial heterogeneity can lead to potential soil variability between the locations probed. Well screens were very short (e.g., less than one-foot), and sensor data was collected from depths corresponding to the screen mid-points. Furthermore, all pushes were backfilled with sand to minimize potential tracer test impacts caused by high pressure grouting.

In summary, the goal of this effort was to demonstrate the effectiveness of an integrated suite of in-situ sensor probes for rapidly determining hydrogeologic parameters and predicting solute contaminant flow characteristics in the subsurface. Several steps were taken to minimize the potential variability in an effort to generate a meaningful comparison of probe data to more conventional data collection approaches. Furthermore, transport models were generated using multiple data sources in an effort to demonstrate the potential of innovative direct push sensor probe systems, and to determine the most cost effective and accurate combinations of data types and modeling approaches. Table 3-2 displays the data quality objectives.

Table 3-2. Data Quality Objectives

Experiment	Standard Method	Data Quality Objective			
		Evaluation Criteria	Precision	Accuracy	False Positives/False Negatives
High-Resolution Piezocone	Well Head Values	Quantitative	± 0.08 ft Head	Difference between well and piezocone data less than 0.08 ft	N/A
GeoVIS	API Dean Starks Porosity	Quantitative	$\pm 30\%$	Linear correlation $> R^2 = 0.8$	N/A
Hydraulic Conductivity (Dissipation or Soil Type Correlation)	Aquifer Tests	Quantitative	N/A	Difference between well and piezocone data less than one order of magnitude	N/A
Transport Model Based on Probes	Model Based on Samples and Field Measurements or Tracers	Quantitative	N/A	Predicted mean breakthrough times and concentrations within one order of magnitude	N/A

3.5.7 Sampling Plan

In order to validate the high-resolution piezocone's head determination capabilities, thirteen groups of clustered wells (nested to 3 depths) were installed at selected locations in a grid pattern as depicted in Figure 3-5. Figure 3-7 displays the configuration for each of the well and push deployment locations. Each of the thirteen locations depicted in Figure 3-5 consists of clustered well and pushes for piezocone as displayed in Figure 3-7. Since GeoVIS field observations reflected very low effective porosity readings, only six

locations included GeoVIS pushes. The wells were installed using direct push installation and construction methods in accordance with ASTM D6724 and D6725, with depths carefully determined using standard practices with a one-inch vertical resolution.

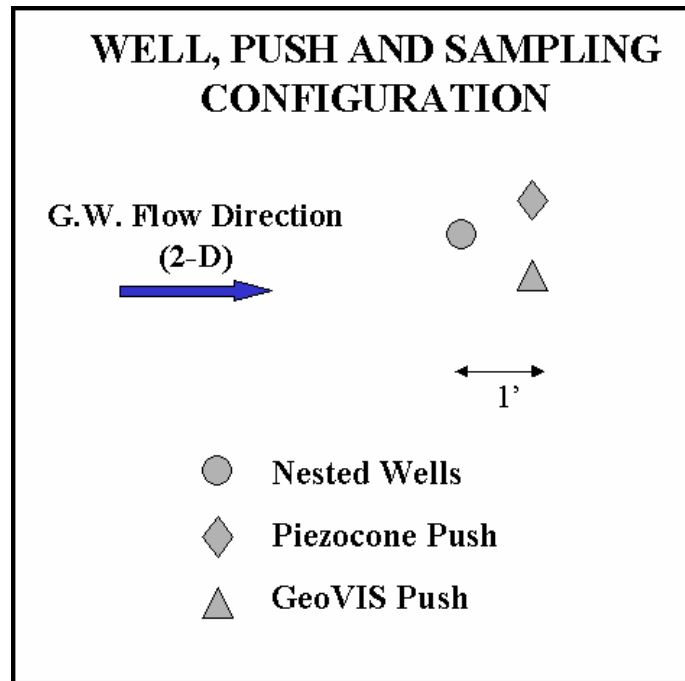


Figure 3-7. Well Cluster and Push Configurations.

Prior to installation of the clustered wells, a few wells were installed along the boundary of the study footprint to help determine the orientation of the clustered well grid within the demonstration domain. Since the observed hydraulic gradient was extremely low in these initial boundary wells, a salt tracer followed by a time lapsed resistivity survey was employed to help orient the test cell. Figure 3-4 illustrates contours of the differential resistivity at 10.5 to 12.0 feet bgs for six specific dates following the salt tracer release. Note that the flow rate appears relatively low for the early part of the survey just downgradient of the release, and then becomes significantly higher in the later phase and further downgradient. This is consistent with the penetrometer push profiles from locations adjacent to the three initial wells (W1, W2, and W3), which indicated that soils in the 10.5 to 12.0 feet bgs range were more permeable in the areas adjacent to W2 and W3. The resistivity survey revealed a mean azimuth of tracer migration of approximately 234 degrees, which was used as reference for orienting the well clusters. It is interesting to note that water levels observed in the three initial wells (W1, W2, and W3) displayed a mean flow azimuth of 287 degrees, with a range of 225 to 311 and standard deviation of

32 degrees. Since gradient was observed to be shallow, additional downgradient wells (W4 and W5) were installed to assist with background water level assessment and establishment of model boundary condition.

The test site well cluster designs were based on preliminary SCAPS soil classification pushes, whereby soil types for depths of interest were converted to well design specification based on the Well Design Specification package devised by Kram and Farrar (US Patent Number 6,317,694). At each cluster location, clustered wells were screened from approximately 8.0 to 8.5 feet bgs (100 sand with 0.006 inch slot prepack), 10.5 to 11.0 feet bgs (20/40 sand with 0.010 inch slot prepack), and 13.5 to 14.0 feet bgs (20/40 sand with 0.010 inch slot prepack). The well depths were chosen to screen three levels within a shallow sandy confined aquifer.

Following well development according to ASTM D5521, aquifer tests were conducted in triplicate on each of the clustered wells using slug tests performed with a modified version of the GW1600 Geoprobe Pneumatic Slug Test Kit. The standard Geoprobe Slug Test Kit consists of a pressure transducer, manifold assembly, data acquisition device and data logger, and software accessories for conducting slug-out tests. Data acquisition rates of up to 38 Hz allow for determination of hydraulic conductivity in highly permeable formations. The test kit has been modified to help improve reproducibility, and to allow for slug-in tests. Based on a previous study nearby, K values in excess of 0.005 cm/s sec were anticipated. Initial pneumatic testing revealed lower than expected K values, rendering the use of the pneumatic system time consuming. To expedite testing, slug-in tests were employed, which entailed injecting at approximately 1L/min of clean water into the well casing using a peristaltic pump to develop an initial head value of about 1 foot. Head dissipation was monitored using the pneumatic slug test kit pressure transducer. All tests were performed in triplicate.

Following well installation and slug tests, the piezocone was advanced in locations adjacent to the clustered wells (e.g., within 12 to 18-inches) and dissipation tests performed at depths corresponding to the well screen mid-points, as well as one shallower depth and one deeper depth. Piezocone head and hydraulic conductivity values were compared to the well head and hydraulic conductivity values. Piezocone soil type data were also collected simultaneously in accordance with ASTM D3441, D5778 and D6067. All sensors, including load cells and pressure and temperature transducers, were calibrated on a frequency consistent with standard practices. For the high-resolution

piezocone, a three-axis pressure calibration curve was required to compensate for both temperature and applied pressure using an apparatus developed by NFESC and SCAPS personnel. Probe calibration was conducted each morning. Depth resolution to greater than one-inch (0.08 feet) was ensured by using a calibrated string pot connected to the push yoke. The depth sensor was calibrated on a daily basis. GeoVIS effective porosity values were derived for soils adjacent to the piezocone pushes (e.g., within 12 to 18-inches) at depths corresponding to those where head and hydraulic conductivity values were available (from both the clustered wells and the high-resolution piezocone).

All field data collection activities were carefully surveyed for longitude and latitude as well as elevation relative to mean sea level using a station tied to a local benchmark. For push locations, protocol for establishing the zero elevation push initiation depths and zero point tracking methods were developed to ensure reference elevations were spatially consistent within the test cell domain. For instance, initiation of each push included advancement of a non-sensor probe to penetrate beyond the asphalt and fill material (approximately 3 feet below grade), retraction of this probe, then placing tape across the open hole. The high-resolution piezocone was then advanced to the depth where the tip just encountered the tape, and then WinOCPT was engaged to set this as the zero point depth for push initiation and commencement of data collection activities.

Following sensor pushes, as the pushrods were retracted, sand slurry was poured into the abandoned push hole. As each pushrod section was retracted, it was cleaned using the on-board steam-cleaning system, which is a closed-loop process that pumps decontamination water to a sealed 55-gallon drum located on the back of the penetrometer vehicle. The top few feet of the push hole was then sealed with bentonite and cement, which was leveled and covered with tape in preparation for a future zero depth survey.

Clustered well water levels were measured using a Solinst water level meter model number 31850, which was resolved to 0.01 feet. During the tracer test, water samples were collected from each well using a low flow, low volume peristaltic pump approach, and analyzed for Rhodamine WT dye tracer concentration using a Turner Design AquaFlor handheld fluorometer. The investigators developed a novel approach for tracer injection and sampling to minimize impact to the tracer plume. The fluorometer was calibrated at least twice per day using pre-mixed fluorescent standards. Samples were collected into in VOA vials, allowed to stand for 24 hours to allow suspended solids to

settle and then aliquots were transferred to cuvettes for analysis. All glassware and plastic material were washed thoroughly with a solution of non- fluorescent detergent (Liquinox™). The material was then rinsed 3 times each with tap water and de-ionized water and allowed to air dry.

Field notebooks were used to track all field activities, including quality control checks and any deviations from original plans in accordance with ASTM D5283. All well construction installations, pneumatic test data and observations, sensor probe push data, sampling observations, and derived wastes were carefully tracked. Hard copies of pneumatic test results and calculations, sensor probe logs, dissipation test calculations, GeoVIS porosity estimates and conceptual modeling results were compiled.

3.5.8 Demobilization

All direct-push sensor and well installation systems rolled onto and off the site in self-contained vehicles. Demobilization primarily involved on-site packing of equipment and return travel of the push vehicle to its home facility. A storage bin located at the site was temporarily used to store field equipment such as pneumatic slug test and ground water sampling equipment. Wastes generated from field activities were handled in accordance with NETTS policies. Facility and NETTS personnel worked together to handle, manage, and treat all derived wastes. The demonstration Principal Investigator coordinated with appropriate personnel to ensure waste handling issues were managed accordingly. All materials were removed following completion of the field activities. The site was formerly used to conduct an EPA wellhead study and is currently surrounded by a fence. The site will eventually be abandoned, with the well network and fencing in place, to allow for future demonstrations at the site. It is anticipated that other SERDP and ESTCP project leaders will hopefully recognize the value of having a facility with such high-resolution data available for future investigations and technology demonstrations.

3.6 Selection of Analytical/Testing Methods

Accuracy of the piezocone for determining head values, flow direction and gradients were determined by measuring the water table elevation in each of the clustered wells in accordance with ASTM D4750. The wells were screened adjacent to the zones where piezocone head values were derived. Extremely low hydraulic gradients were observed in both data sets. Hydraulic conductivity value accuracy based on soil type relationships (e.g., Robertson and Campanella) and dissipation tests were determined using aquifer

tests conducted in accordance with ASTM D4043 and D4044. The slug tests used represent a modification of ASTM D4044.

Furthermore, the team performed the following specific modeling efforts, geostatistical tests, and performance evaluations:

- 1) Generated interpolated data layers of hydraulic head, effective porosity, soil hydraulic conductivity, and calculated velocity distributions, measured and calculated from piezocone derived data;
- 2) Compared velocity distributions derived from measurements of piezocone with velocity distributions derived via conventional methods using multilevel wells;
- 3) Assessed how the field measurements and model assumptions affect transport predictions, such as spatial and temporal distributions of chemicals and flux.

3.7 Selection of Analytical/Testing Laboratory

To assess the performance of the penetrometer probe technologies, the high-resolution piezocone and GeoVIS data were compared to data obtained using conventional water level monitoring and field analytical methods. Since the GeoVIS did not yield effective porosity data of sufficient quality, the Project Manager opted to reduce costs by foregoing soil sample collection and analyses. Therefore, a certified laboratory was not required for confirmatory analytical services to determine soil effective porosity. A certified laboratory was employed for analytical services required to meet long-term tracer monitoring compliance commitments to base facility personnel.

4. Performance Assessment

4.1 Performance Criteria

Primary performance criteria and level of success are presented in Table 4-1.

Table 4-1. Performance Criteria and Level of Success

Performance Criteria	Description	Primary or Secondary	Success Level
Factors Affecting Technology Performance	Includes how hydrogeology (e.g., flow rate, direction, effective porosity, and hydraulic conductivity) will impact measurement resolution, spatial renderings, predictive capabilities, and deployment time requirements. Describe how spatial distribution of pressure head, effective porosity, and soil type will impact observed variabilities and spatial renderings.	Primary	<p>Piezocone: No difference compared to control</p> <p>GeoVIS: Silty sands below water table exhibit lower than anticipated effective porosity values</p>
Versatility	Includes performance under different hydrogeological conditions amenable to direct-push applications	Secondary	<p>Piezocone: No difference compared to control</p> <p>GeoVIS: Silty sands below water table exhibit lower than anticipated effective porosity values</p>
Hazardous Materials	Includes performance under different solute situations	Secondary	No difference compared to control
Process Waste	Includes any waste (and volumes) produced by the technology	Secondary	Less waste compared to control

Reliability	Includes anticipated equipment malfunctions, soil type determination accuracy, sensitivity to changes in soil type	Secondary	Piezocone: No difference compared to control GeoVIS: Silty sands below water table exhibit lower than anticipated effective porosity values
Ease of Use	Includes number of personnel required to operate equipment, skill levels and training of personnel, and amount of data processing/post processing required	Primary	No difference or lower labor and time requirements compared to control
Maintenance	Includes requirements and frequency for required calibration/maintenance and level of training required for maintenance personnel	Secondary	No difference compared to other push probes
Scale-up Constraints	Includes issues related to scale up for full implementation (mostly focused on probe and software transfer to other systems)	Secondary	No difference compared to other push probes

4.2 Performance Confirmation Methods

Performance criteria, metrics, and confirmation methods are presented in **Table 4-2**. Quantitative criteria included technology performance, hazardous materials, ease of use, and long-term performance. Monitoring well cluster sampling, field and laboratory measurements, field experience, and associated statistical methods were used to confirm whether or not the expected performance metrics were met.

Table 4-2. Expected Performance and Performance Confirmation Methods

Performance Criteria	Expected Performance Metric	Performance Confirmation Method
PRIMARY CRITERIA (Performance Objectives -Qualitative)		
N/A		
PRIMARY CRITERIA (Performance Objectives -Quantitative)		
Accuracy of high-resolution piezocone for determining head values, flow direction and gradients	± 0.08 ft head values	Compare to well values, interpolation of well values, 2-D and 3-D model of well values
Accuracy of GeoVIS for determining effective porosity	± 30%	Compare to API Dean Starks porosity values averaged over sample depth range
Hydraulic conductivity (dissipation or soil type correlation)	± 0.5 to 1 order of magnitude	Compare to aquifer tests
Transport model based on probes	Predicted breakthrough times and concentrations within one order of magnitude; probe based model efficiency accounts for more than 15% of the variance associated with well based models	Compare probe model breakthrough predictions to predictions generated using conventional methods
Time required for generation of 3-D conceptual and transport models	At least 50% reduction in time	Compare time requirements for developing model using conventional data management approaches to streamlined WinOCPT data export
SECONDARY PERFORMANCE CRITERIA (Qualitative)		
Reliability	Expect sensors to be robust, with good agreement between GeoVIS and piezocone soil type descriptors	Field records and observations
Ease of Use	Operator experience	Experience from demonstration
Versatility - applicable to different geological conditions - use with different push systems	Yes Yes	Experience from demonstration

Maintenance	Expect reasonable calibration requirements	Experience from demonstration
Process Waste	Expect minimal wastes derived	Field experience/analysis of steam cleaning effluent

4.3 Data Analysis, Interpretation and Evaluation

Probe sensor performance evaluations were based on specific analytical tests. These analyses were used to determine whether a specific performance goal was reached within an established tolerance. The majority of the comparisons between well hydraulic data and high-resolution piezocone data demonstrate that the piezocone can be an effective tool for detailed hydraulic site characterization. GeoVIS effective porosity values were initially to be compared with API Dean Starks laboratory values derived for soil samples collected adjacent to the probe measurement locations. However, it readily became apparent that the probe images and software were yielding lower values than anticipated for the saturated silty sand soils dominating the strata at the selected field site. Therefore, soil samples were not collected for comparison. In anticipation of this potential challenge, WinOCPT was modified to enable users to estimate porosity based on soil type. Additional data analysis, interpretation and evaluation details are provided in the sections below as well as in Appendices F, G, and I.

4.3.1 Comparison of K Values

Appendix F provides a detailed comparison of K values. K values obtained for the test site were found to be about an order of magnitude lower than originally expected. Based on the high resolution SCAPS derived stratigraphy, it appears that the well screens are positioned at depths near the upper or lower boundary of the high K zone depending on the specific location within the cell domain. It was found that the high-resolution piezocone derived hydraulic conductivity values were on average similar to those obtained from monitoring wells. Comparison of arithmetic and geometric mean values (Figures 4-1 and 4-2) show that on average the K_{mean} and K_{lc} values are within about a factor of 2 of the K_{well} values. On average the K_{min} , K_{max} and K_{form} values fall within a factor of 5 or better of the K_{well} values. K values derived from piezocone pushes ranged much more widely than those derived from slug tests conducted in the adjacent monitoring wells. These differences may be attributed to averaging of the hydraulic conductivity values over the well screen versus more depth discrete determinations from the piezocone, which is more sensitive to vertical heterogeneities. Mid-level hydraulic conductivity distribution comparisons are displayed in Figure 4-3. While subtle differences can be seen, the overall agreement appears to be very good. Of particular

note, Figure 4-4 displays histograms for three conductivity distributions, with outlier datapoints above 30 ft/day removed (representing 5 to 10 percent of the data). The distributions are similar, except that the well Ks are more evenly distributed and the piezocone Ks appear to be more log-normally distributed.

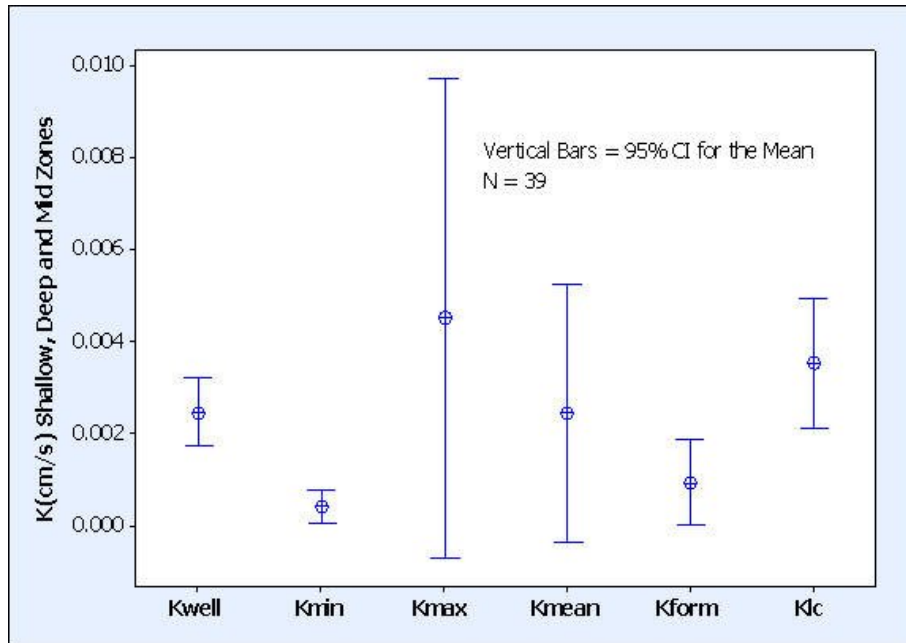


Figure 4-1. Comparison of all K Values. Circles are the arithmetic mean values.

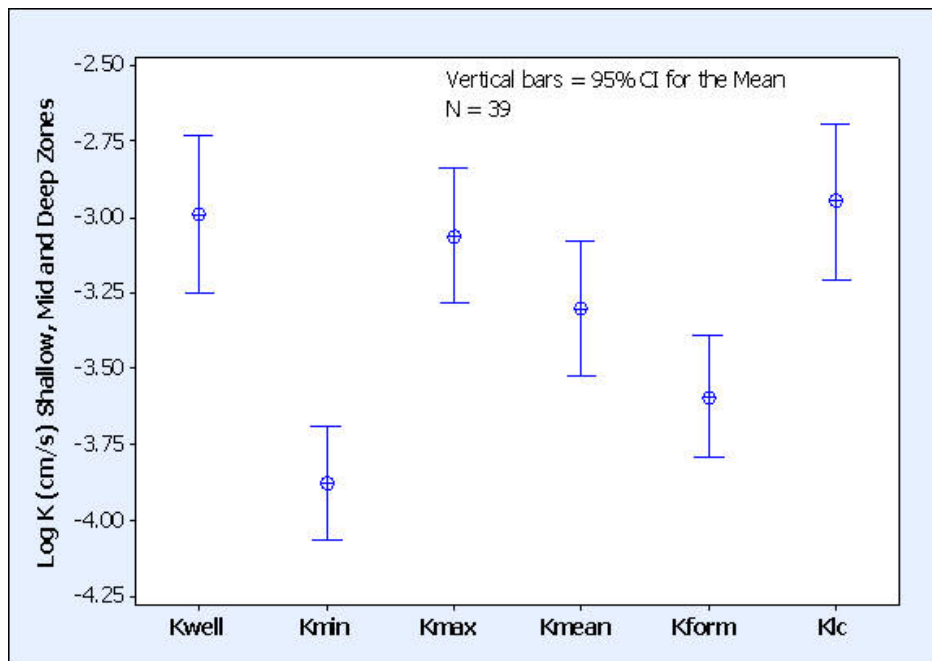


Figure 4-2. Comparison of all K Values, Log Transformed. Circles are the geometric mean values.

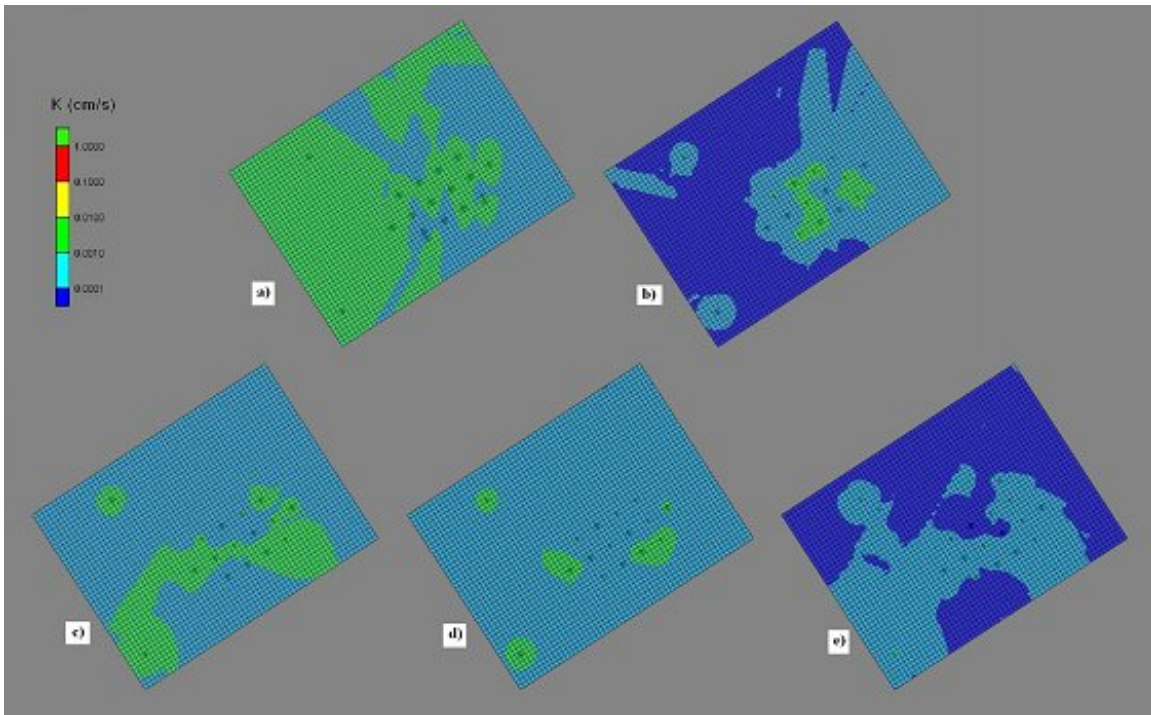


Figure 4-3. Hydraulic Conductivity Distributions for a) K_{well} , b) K_{lookup} , c) K_{max} , d) K_{mean} , and e) K_{min} at 10.75 feet bgs. K values are in cm/s and each contour represents an order of magnitude change in K .

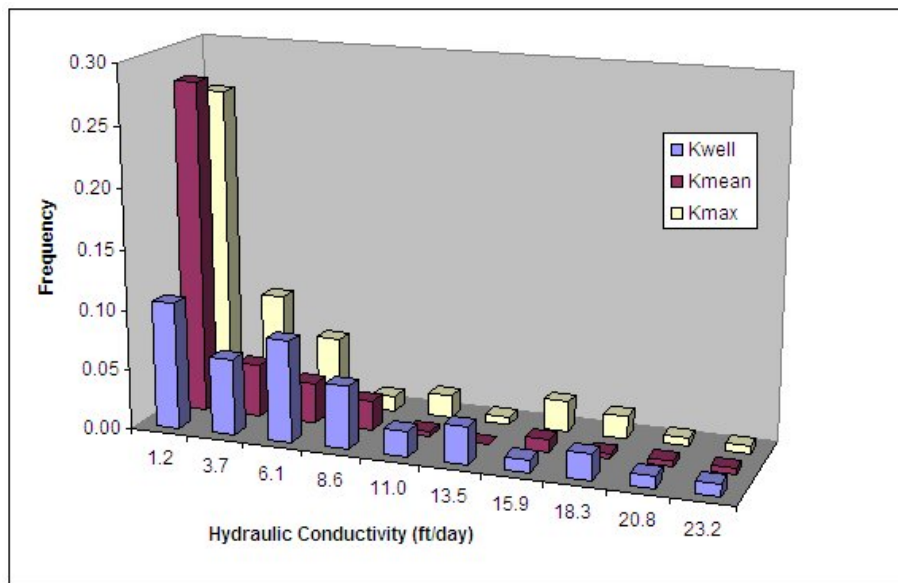


Figure 4-4. Relative Frequency of K Values for Three Conductivity Distributions: K_{well} , K_{mean} , and K_{max} .

4.3.2 Comparison of Head Values

Appendix F provides a detailed comparison of head values. The monitoring well data did not reveal any discernible vertical or horizontal gradients within the test site. Within the limits of resolution for both methods, the piezocone results agreed closely with the monitoring well head values with respect to finding no discernible vertical or horizontal gradients, mean value of the hydraulic head and the degree of variability. Differences between well and high resolution piezocone derived head values were on average less than 0.08 feet (1 inch).

4.3.3 Tracer Test Results

Appendix G summarizes the tracer test project component. There was a lack of definitive tracer observation on-site during the test period. Possible reasons for this outcome are described below. The analytical instrument exhibited false positive interference owing to turbidity, even at very low NTU levels. This could have masked trends in the tracer concentration distribution and breakthrough. It is possible that the rhodamine was diluted during the injection to the point where it became undetectable, especially in light of turbidity interference. Given the low mean velocity, it is possible that the pulse of tracer moved almost in a plug flow fashion, between the wells with very little dispersion. It is possible that the tracer took a higher conductivity path between the depth intervals of the well screens. Given the relatively low hydraulic gradient and the duration of the test, slight water level changes may have resulted in the tracer moving in some direction other than that of the well cluster layout.

The testing demonstrated that the handheld fluorometer was sensitive to turbidity. Given the instrument's relatively low cost, portability, low limit of detection and wide linear range, the fluorometer could potentially have wide usage as a ground water forensic tool. Successful use will necessitate the development of an approach to overcome turbidity interference. If additional tracer studies are to be performed at the Port Hueneme test site, it is suggested that they consist of force gradient testing to circumvent difficulties associated with the low natural gradient. Consideration might also be given to an alternative tracer or the use of higher concentrations of rhodamine coupled with the development of a method to overcome turbidity interference.

4.3.4 Modeling Results

Comparison of models based on traditional (well-based) measurements and the high-resolution piezocone measurements were indistinguishable in terms of performance for

the conditions present at this site (Appendix I). Although none of the model scenarios correctly predicted observed tracer behavior (primarily due to the instrumentation detection interference caused by turbidity, potential transport logistics related to specific pathways, and low gradient), the models based on conventional well data match well with all the model scenarios based on high-resolution piezocone data. Plume flow directions, concentration distributions, and flux distribution predictions (based on velocity distributions coupled with concentration distribution model predictions) each compared very well and met all project performance goals.

Figure 4-5 displays head distributions resulting from both the well clusters and the high-resolution piezocone. Note that the range of head spans only .08 feet for both distributions throughout the 25 foot by 10 foot test cell domain. While there are some directional nuances associated with each data set, the general gradients (again, very shallow) and head distributions display similarities (Figure 4-6), especially within the well cluster domain. This is critical, as the piezocone will typically be deployed with much larger push spacing. Therefore, it is anticipated that by meeting these challenging field conditions, the high-resolution piezocone will be able to readily meet most field application requirements. Furthermore, the level of detail afforded by the high-resolution piezocone is unprecedented.

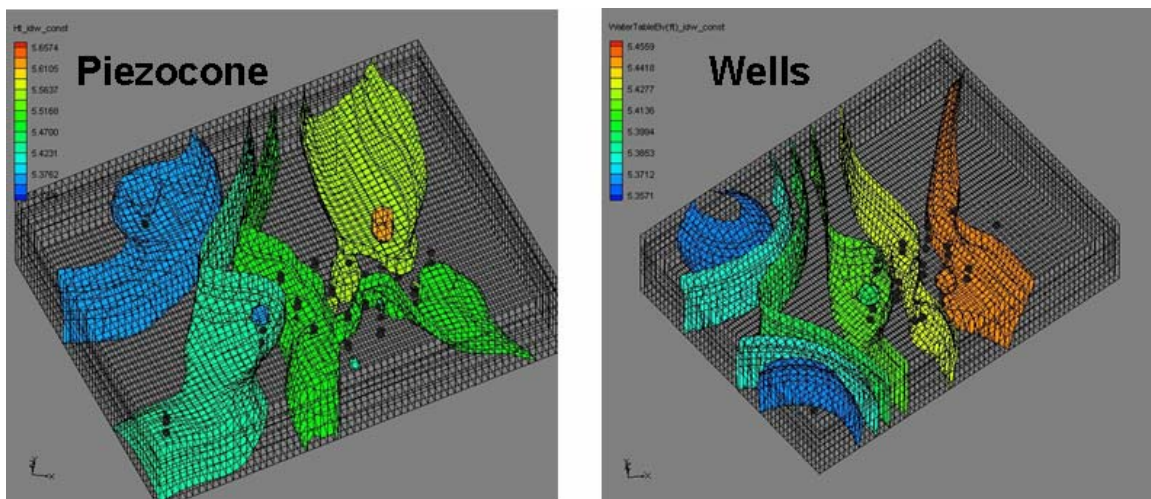


Figure 4-5. Three-Dimensional Head Distributions for High-Resolution Piezocone and Well Clusters.

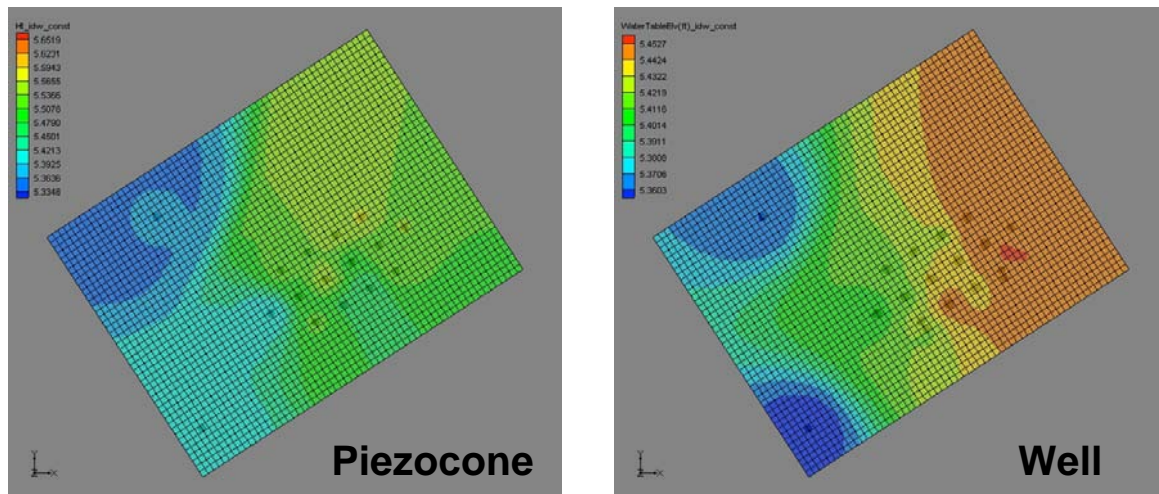


Figure 4-6. Head Comparisons, Middle Zone (10.75 feet bgs).

Gradient determination, critical for modeling efforts, required development of a gradient field based on recent GMS upgrades, which enabled users to convert scalar head values to gradient distributions. When coupled with hydraulic conductivity and effective porosity distributions, the critical gradient builder step allows for determination of seepage velocity distributions through the GMS velocity builder. Figure 4-7 displays velocity distribution comparisons between well data and piezocone (using mean K) data. The “mid” two-dimensional display shows calculated velocity distributions in map view, but at approximately 10.75 feet below grade, while the “1st row” transect is located along the first downgradient row of well clusters and the “centerline” transect extends through the center of the test domain. While differences can be seen, notice the relative similarities in the centerline velocity distributions.

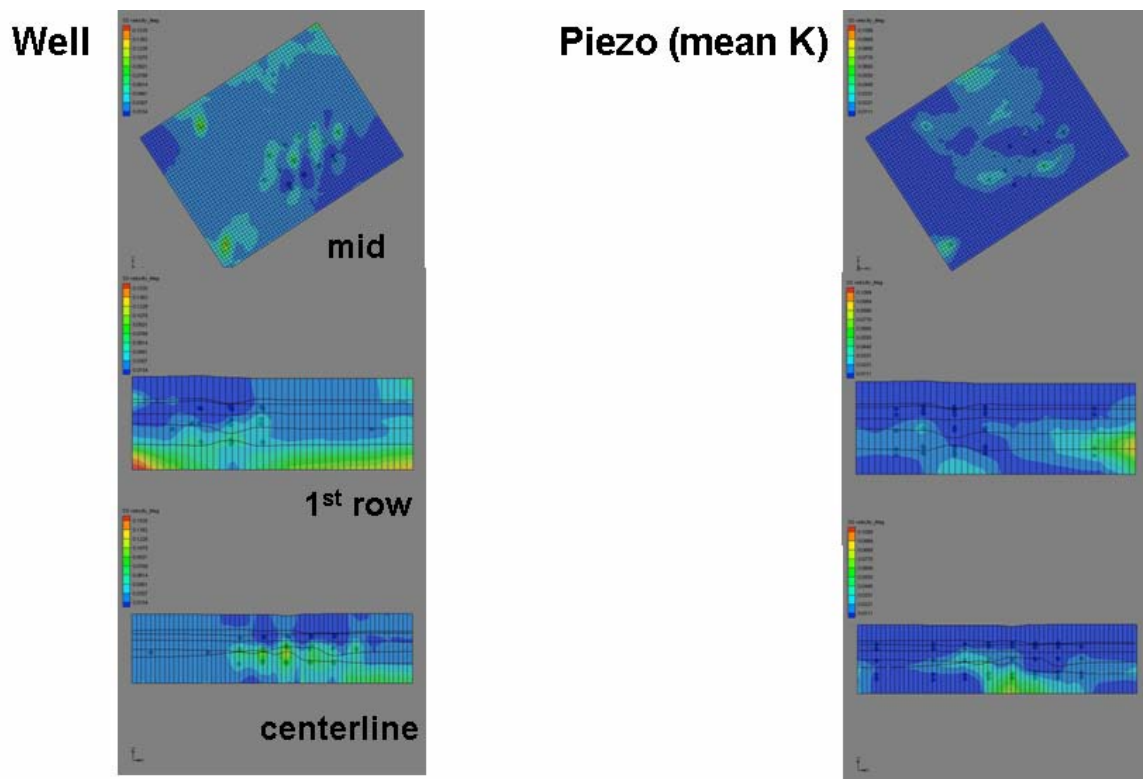


Figure 4-7. Well and High-Resolution Piezocone Derived Velocity Distributions.

Provided concentration distributions are known, GMS now also allows for the determination of flux distributions in three dimensions. To develop concentration distribution predictions, boundary conditions were established through extrapolation of gradient values, and then a Modflow transport model was generated. Once the concentration distributions were determined for specific time steps, flux distributions were developed using the new GMS flux builder tool.

In order to observe the similarities and differences between site characterization data derived from traditional well-derived measurements (i.e., slug tests and water level measurements) vs. SCAPS high-resolution piezocone measurements (i.e., dissipation tests and load cell pressure lookup values), several permutations of the generic flow and transport model were chosen for evaluation. The steady-state head distribution was derived from interpolations of either hand-measured depth-to-water or observations made with the piezocone method. The hydraulic conductivity field was based on either slug test measurements, piezocone dissipation tests (K_{mean} , K_{max} , K_{min}) or load cell pressure lookup

values (K_{lookup}). Porosity was either an average value for the soil type or a lookup value based on load cell pressure. A list of modeled scenarios and data sources is provided in Table 4-3. While every scenario is not thoroughly addressed in this report, the reader is encouraged to review Appendix I for additional details.

Table 4-3. Data Sources for Inputs to Modeled Scenarios.

Scenario	Head	K	Porosity
1	Well	Well	Average
2a	SCAPS	SCAPS K_{mean}	SCAPS
2b	SCAPS	SCAPS K_{min}	SCAPS
2c	SCAPS	SCAPS K_{max}	SCAPS
2d	SCAPS	SCAPS K_{lookup}	SCAPS
3	Well	Well	SCAPS
4a	Well	SCAPS K_{mean}	SCAPS
4b	Well	SCAPS K_{min}	SCAPS
4c	Well	SCAPS K_{max}	SCAPS
4d	Well	SCAPS K_{lookup}	SCAPS
5	Unif. grad.	Average	Average

Two scenarios were selected as “baseline” cases: Scenario 1 used only the traditional well-derived measurements for site characterization, and Scenario 5 used simplified site characterization values (e.g., constant head, gradient, K, and porosity), consistent with the level of detail that would likely be used by an environmental practitioner or consultant. These were selected in order to evaluate the degree to which the piezocone characterization methods produced modeled data that agreed with more traditional measures.

Each scenario was set up as a reiteration of the same GMS flow and transport model configuration. Therefore, the grid and boundary conditions (constant head boundaries) remained constant throughout all scenarios. The initial input of simulated tracer also remained constant. The boundary values of head, initial head distribution, and the K and porosity distributions changed from model to model, depending on the input.

The information obtained from each modeled scenario included 2-D and 3-D images of tracer concentration and flux distribution, as well as predicted tracer concentrations in each well and piezometer. Flux values at every grid cell were also recorded. Fluxes were calculated using concentration values from the transport model and head distributions

interpolated from measurements to eliminate the effects of directionality in the steady-state head distributions as much as possible.

Figure 4-8 shows time series of concentration contours in the middle layer (at the depth of the injection well) for four scenarios: 1 (well-based), 2a (SCAPS K_{mean}), 2d (SCAPS K_{lookup}), and 5 (constant average parameters). Figure 4-9 shows flux isosurfaces for the same scenarios and times. The isosurfaces are generated at fluxes of $30 \mu\text{g}/\text{ft}^2/\text{day}$, which is equivalent to a concentration of 35 ppb moving at the average groundwater velocity at the site (0.03 ft/day).

These two figures address the difference in main flow direction between the well heads and SCAPS heads. As stated above, both flow directions were within approximately 30° of the centerline of the piezometer cluster orientation (234°), but the well heads predict flow slightly to the west of the cluster centerline (Scenario 1), while piezocone heads predict flow slightly to the south (Scenario 2a). In considering the predicted flow directions, it is important to note that there is a significant difference in the reproducibility and zone of influence of the methods used to obtain the hydraulic head data. The well-derived depth-to-water measurements were taken in triplicate with excellent reproducibility (detailed in the accompanying tracer test report). The piezocone dissipation tests, however, were performed once for each depth. Furthermore, the zone of influence of the well measurements is distributed or averaged over a 6-inch screen, while the piezocone dissipation test is essentially a point measurement. Therefore, given the point nature of the piezocone measurement, it is unreasonable to think that the well and piezocone measurements fundamentally disagree on flow direction. It is quite possible that another sampling campaign would generate a very different head distribution with a different flow direction. In our opinion, the fact that there exists a fairly consistent main flow direction demonstrates that the two methods are in good agreement. Nevertheless, the difference does affect the magnitude of the error measures used to evaluate similarity of the models, as described in Appendix I.

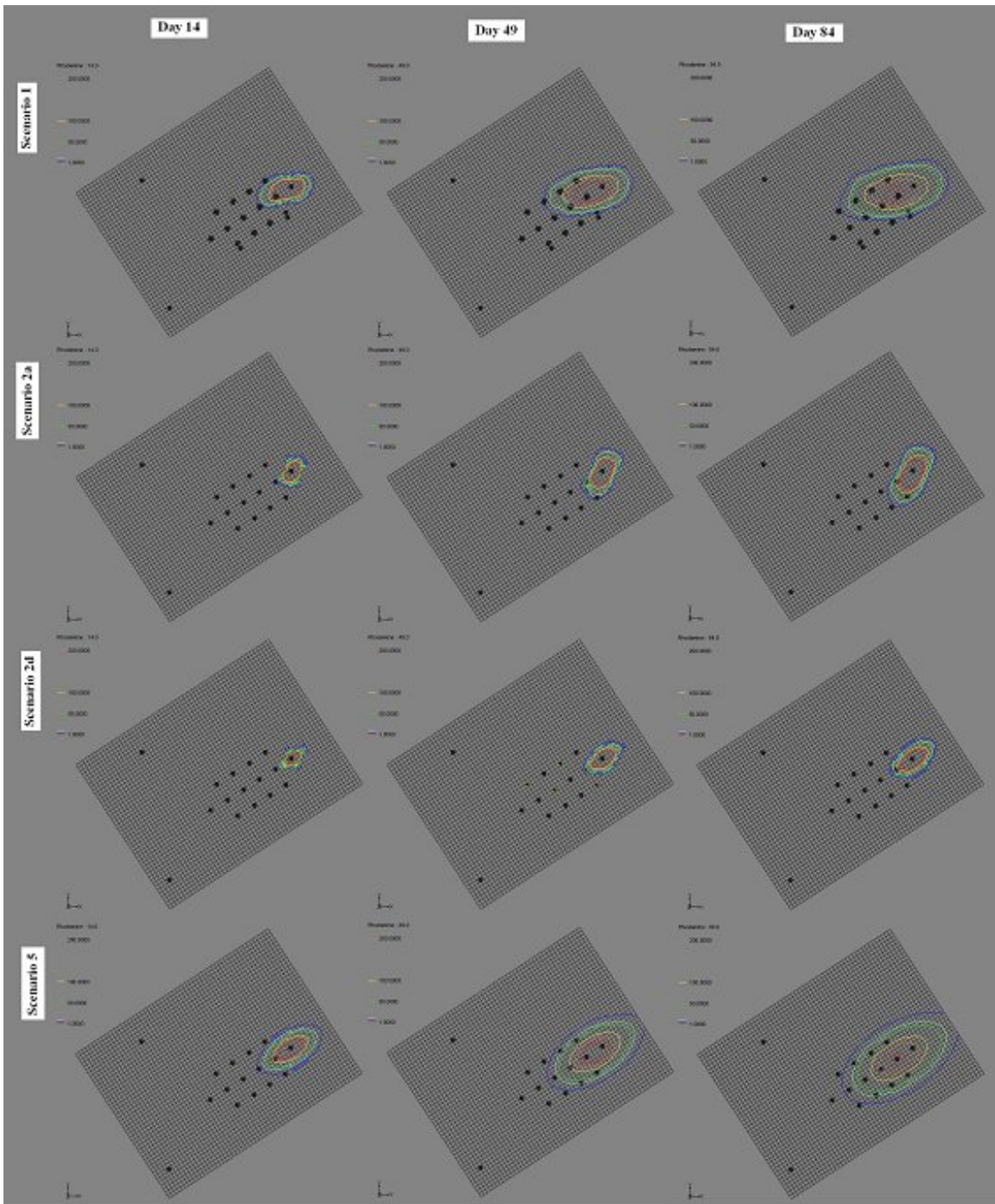


Figure 4-8. Tracer Concentrations at the Depth of the Injection Well for Various Scenarios and Three Timesteps.

Figures 4-10 and 4-11 display predicted tracer breakthrough curves for each scenario at mid-level monitoring wells from clusters 5 and 6, respectively. Cluster 5 is located just downgradient of the tracer release, while cluster 6 is located five feet further downgradient along the centerline of the test cell domain. With only one exception (Scenario 2b with K_{min}), the initial breakthrough predictions for each scenario are relatively close (e.g., within approximately 30 days) to the control scenario. Furthermore, maximum values for the control (approximately 450ppb) and the piezocone K_{mean} scenario (approximately 200ppb and rising) display reasonable agreement given the number of factors considered by each model. Predicted timing of peak concentration breakthrough occurs much earlier (over 100 days sooner) for the control data set relative to the K_{mean} data set. The relationships for cluster 6 are spread farther apart. At least a portion of this spread (including the timing discrepancy for peak concentrations at cluster 5) is due to the slight directional differences for the model predictions. For instance, mid-level cluster 1 (located south of the test cell centerline) data shows peak predicted concentrations much higher for Scenario 2a than for Scenario 1 (**Figure 4-12**).

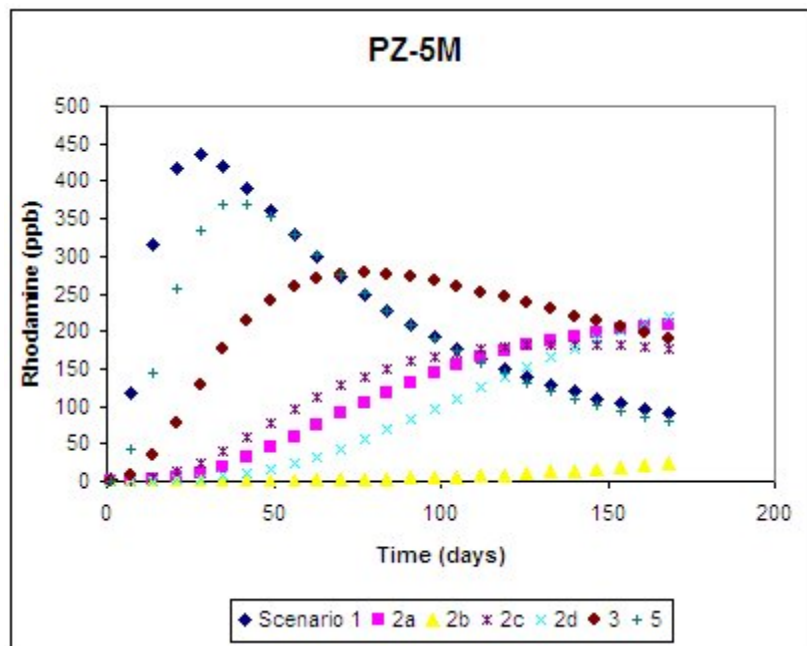


Figure 4-10. Breakthrough Curves for Cluster 5, Middle Depth.

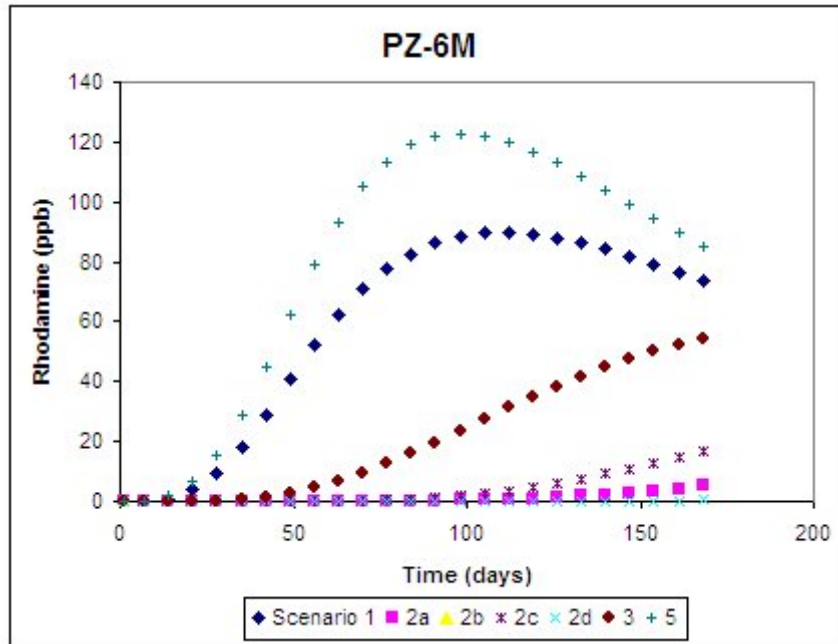


Figure 4-11. Breakthrough Curves for Cluster 6, Middle Depth.

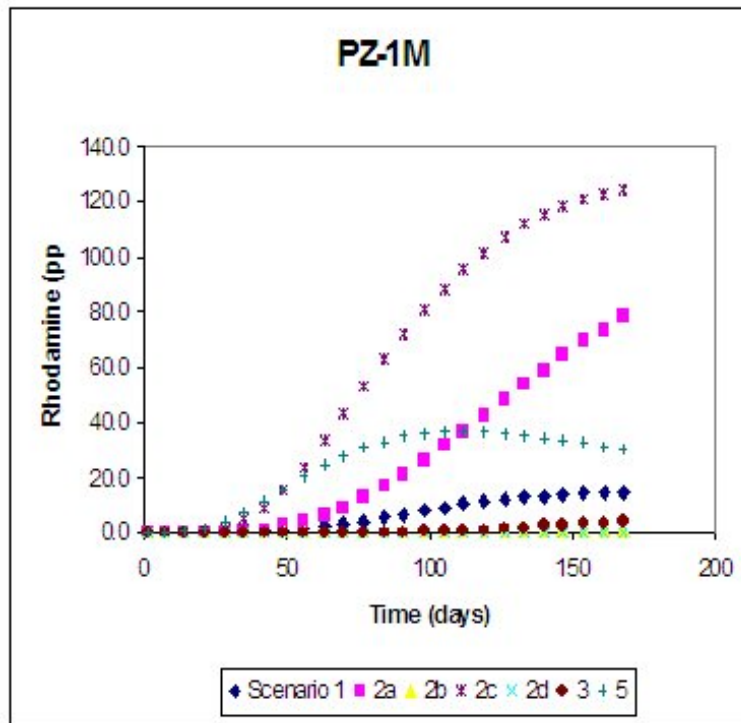


Figure 4-12. Breakthrough Curves for Cluster 1, Middle Depth.

While several quantitative approaches for evaluating error were explored (Appendix I), perhaps the most applicable metric is model efficiency (E) [Nash and Sutcliffe, 1970], given by

$$E = 1 - \frac{\sum_{t=1}^T \sum_{i=1}^n (y_{o,i,t} - y_{m,i,t})^2}{\sum_{t=1}^T \sum_{i=1}^n (y_{o,i,t} - \bar{y}_o)^2},$$

where $\bar{y}_o = \frac{\sum_{t=1}^T \sum_{i=1}^n y_{o,i,t}}{n * T}$ is the average of the observed data. E is analogous (but complementary) to the coefficient of determination in that it indicates what fraction of the observed variance is accounted for by the model under consideration. It has a value of 1 for a perfect model (when $y_{o,i} = y_{m,i}$ for all i), while a value of 0 indicates that the model is no better than assuming $y_{m,i} = \bar{y}_o$ for all i . A negative value indicates that the variance in the model is greater than that of the observed values.

Upon inspection of E , two scenarios stand out as similar to Scenario 1 (Table 4-4). For Scenario 3, which was identical to Scenario 1 except for the porosity distribution, $E = 0.72$, indicating that 28% of the variance in Scenario 1 is due to the effect of porosity. Surprisingly, Scenario 5, which used all average parameters, accounted for 93% of the variance in Scenario 1. Perhaps this is because the parameter values used in Scenario 5 were averages of the well-derived data.

Table 4-4. Results of Inter-Model Comparisons. Well based model is the control.

Scenario	E
2a	0.17
2b	-0.09
2c	0.29
2d	0.04
3	0.72
4a	0.01
4b	-0.09
4c	0.21
4d	-0.09
5	0.93

Aside from the two most similar models, another level of similarity to Scenario 1 was shared by Scenarios 2a, 2c, and 4c. Here the variance in Scenario 1 captured by the other models ranged from 17 to 29 percent. This is a positive result. Given that the gradient was extremely low at the site, and that directional components are subject to high variability in low gradient field conditions, the level of agreement between the piezocone based models and well based models is very good. These scenarios relied on the

piezocone K_{mean} (2a) and K_{max} (2c and 4c) hydraulic conductivity distributions. Figure 4-4 displays histograms for K_{well} with these two K distributions. The distributions are similar, except that the well K s are more evenly distributed and the piezocone K s appear to be more log-normally distributed. Their similarity at the higher end of the distribution is a possible reason for the reasonable match between models that use K_{well} and those that use K_{mean} and K_{max} . Furthermore, the similarity in error measures between Scenarios 2c and 4c shows that head distribution in this case was not as significant a contributor as the K distribution to the modeled concentration. However, as previously mentioned, since head distributions are related to gradient distributions, which in turn dictate flow directions, there is a level of indirect impact exerted by the head values. For instance breakthrough curves at clusters 5 and 6 are impacted by local transport directions. For instance, Scenario 2a reveals a plume front towards the south of cluster 6, with an oblique transport component reflected in the breakthrough curves.

In summary, while the GeoVIS did not provide effective porosity values within the anticipated range, the high-resolution piezocone performance falls within the quantitative tolerances for head estimation, flow direction, gradient, hydraulic conductivity, transport predictions, and time requirements for model development set forth in this demonstration (Table 4-5). Therefore, the sensor probe approach to determining hydrogeologic characteristics is deemed appropriate for the demonstration site characteristics.

Table 4-5. Performance Summary

Performance Criteria	Expected Performance Metric	Results
Accuracy of high-resolution piezocone for determining head values, flow direction and gradients	± 0.08 ft head values	Met Criteria
Accuracy of GeoVIS for determining effective porosity	$\pm 30\%$	Did Not Meet Criteria
Hydraulic conductivity (dissipation or soil type correlation)	± 0.5 to 1 order of magnitude	Met Criteria

Transport model based on probes	Predicted breakthrough times and concentrations within one order of magnitude; probe based model efficiency accounts for more than 15% of the variance associated with well based models	Met Criteria
Time required for generation of 3-D conceptual and transport models	At least 50% reduction in time	Met Criteria

While this demonstration proved to be successful in many respects (e.g., resolution afforded by the high-resolution piezocone, new modeling capabilities through gradient builder, velocity and flux builders, and the good agreement between well based data and piezocone data), additional demonstration efforts could be implemented to increase the level of industry confidence in this innovative approach. A list of potential efforts includes the following:

- Perform piezocone tests in triplicate – This could allow for more traditional statistical treatment of the data comparisons between well and piezocone information, as comparison of the means can be performed;
- Repeat K comparisons at a highly permeable site – The piezocone is capable of estimating K in soils of higher K than those encountered at the Port Hueneme demonstration site;
- Interpolation using data fusion – Markov chain transitional probabilities and co-kriging using soil type data with very high vertical resolution affords additional capabilities for developing K distributions and associated models;
- Forced gradient tracer test – Reiteration of the models (including data fusion simulations) to account for a forced gradient, combined with selection of an appropriate tracer and detector and tracer test design will afford a superior method for comparing model predictions with observations.

Each of these additional efforts will be performed by team members under a new project supported by EPA beginning in late summer of 2007.

5. Cost Assessment

5.1 Cost Reporting

Actual costs to implement the high-resolution piezocone during this demonstration are presented in Table 5-1. A total of eighteen pushes were completed, requiring three field days. Total costs were approximately \$35,600, for a total of approximately \$2000 per push. These numbers do not include costs associated with installing the control well network, preliminary site preparation efforts not associated with the piezocone pushes (e.g., salt tracer tests, permitting and associated analytical costs, initial pushes to design well network, background well installations, etc.), or comprehensive modeling and reporting. Equipment fees are the most expensive cost drivers at approximately \$5,500 per day. In the future, these costs could be much lower, especially once the probe is able to be deployed on smaller push rigs. While this breakdown reveals information about per push costs, since economies of scale will impact anticipated user costs, a more direct comparison between high-resolution piezocone efforts and conventional well installation approaches that address site-specific conditions (e.g., target investigation depths) will be presented below to illustrate cost savings, time savings, and how specific cost drivers and implementation rates impact these critical issues under several scenarios. Additional details are presented in the Cost and Performance Report.

Table 5-1. Cost Reporting for High-Resolution Piezocone Component.

Cost Category	Sub Category	Costs (\$)
FIXED COSTS		
1. CAPITAL COSTS	Mobilization/demobilization	\$1,000
	Planning/Preparation	\$4,000
	Equipment	\$16,500
	Other	\$500
		Sub-Total (\$22,000)
VARIABLE COSTS		
2. OPERATION AND MAINTENANCE	Labor	\$3,500
	Materials/Consumables	\$300
		Sub-Total (\$3,800)
3. OTHER COSTS	Waste Disposal	\$1,200
	Reporting	\$3,000
	Model Preparation	\$5,000
	Per Diem	\$600
		Sub-Total (\$9,800)
TOTAL COSTS		
TOTAL TECHNOLOGY COSTS (\$35,600)		
Throughput Achieved = 18 Pushes		
Unit Cost Per Push (\$1,977.78)		

5.2 Cost Analysis

Costs are based on sensor probe deployment requirements to meet specific characterization objectives. For this example, it is assumed that both the high-resolution piezocone and membrane interface probe (MIP) are used to develop initial flux distributions in three dimensions. For comparable data collection approaches driven by well installation methods, costs considerations include materials (e.g., riser pipe, screens, filter packs, bottom caps, traffic monuments, grout, sealing materials, etc.), depths (which impact hardware and labor costs), rates of installation for each approach (impacting total labor, daily equipment charges, and per diem costs), waste generation, and labor costs (dependent upon installation rates, and survey, logging, development, modeling and reporting requirements). Many of the itemized costs are identical between DP wells and drilled wells. However, differences can arise when target depths, well diameters, and associated material costs are considered.

For this analysis, the following assumptions were used:

- Ten map locations were required for 3D hydraulic and chemical analyses;
- Ten high resolution piezocone pushes and 10 MIP pushes represent the innovative direct push sensor probe approach for determining the 3D flux distribution. Additional efforts include: surveying, waste management, data management, modeling, and reporting;
- Thirty short screened well installations represent the conventional approach for determining the 3D flux distribution throughout the same domain. Thirty clustered wells were used to generate data from three depths per each of 10 map locations. Additional efforts include: surveying, well development, aquifer tests, soil samples, water samples, laboratory efforts (for both porosity and chemistry), waste management, data management, modeling, and reporting.

Table 5-2 presents itemized cost assumptions used in the derivation of the cost comparisons for target depths of 20 feet, 50 feet, and 75 feet below grade. The innovative technology includes deployment of the high-resolution piezocone, the MIP (for concentration distribution), and GMS to determine the three-dimensional distribution of contaminant flux. Baseline technology includes conventional well-based approaches (e.g., installation, sampling, aquifer testing, etc.) required for developing a three-dimensional flux distribution assessment. Several well types are included in the comparison. Specifically, ¾-inch diameter and 2-inch diameter direct-push wells and 2-

inch diameter rotary drilled wells are incorporated into the comparisons to cover both traditional and innovative well installation approaches. For cost comparison purposes, all well screens are assumed to be 5-foot sections, and the examples are based on sets of 30 wells for each deployment set to the target depths specified. Recall that only 10 data collection locations (in map view) are required to cover the same three-dimensional domain, and that well clusters (3 per cluster, for a total of 30 wells) are to be employed. Many of the itemized costs are identical between sensor pushes and wells. However, differences can arise when target depths, well diameters, the MIP versus sampling and analysis, and associated material costs are considered. The most significant differences contributing to direct-push sensor deployment cost savings are due to the rapid deployment and data analysis rates (which impact labor and per diem cost totals) and the low waste generation volume and management requirements.

Table 5-2. Itemized Cost Assumptions. The high-resolution piezocone based approach is compared to the well-based approach to develop a 3D distribution of contaminant flux. Hardware costs are based on quotes from 2007.

Well Installation/Probe Phase	20'			50'			75'		
	Direct-Push Wells 2" and 3/4"	Drilled Wells 2"	HR Piezocone	DP 2" and 3/4"	Drilled 2"	HR Piezocone	DP 2" and 3/4"	Drilled 2"	HR Piezocone
Well Diam	2" (6.1m)	2" (6.1m)	20' (6.1m)	2" and 3/4" (5.0' (15.24m)	2"	50' (15.24m)	2" and 3/4" (7.5' (22.86m)	2"	75' (22.86m)
Max Well Depth	20' (6.1m)	20' (6.1m)	20' (6.1m)	50' (15.24m)	50' (15.24m)	50' (15.24m)	75' (22.86m)	75' (22.86m)	75' (22.86m)
Mobilization (10 wells)	\$1,000	\$1,000	\$1,000	\$1,000	\$1,000	\$1,000	\$1,000	\$1,000	\$1,000
Average No. Installations/Day	15	3	10	5	1	5	3	1	3
Riser Pipe Costs	\$2.51/ft (3/4")	\$2.55/ft	NA	\$2.51/ft (3/4")	\$2.55/ft	NA	\$2.51/ft (3/4")	\$2.55/ft	NA
Screen Costs	\$4.08/ft (3/4")	\$3.65/ft	NA	\$4.08/ft (3/4")	\$3.65/ft	NA	\$4.08/ft (3/4")	\$3.65/ft	NA
Filter Pack Costs	\$15/ft (3/4")	\$2.18/ft	NA	\$15/ft (3/4")	\$2.18/ft	NA	\$15/ft (3/4")	\$2.18/ft	NA
Solid Waste Generation*	0 drums	0.75 drums/well	0 drums	0 drums	1.88 drums/well	0 drums	0 drums	2.82 drums/well	0 drums
Decon Rinseate Generated*	0.2 drum/well (3/4")	1 drum/well	0.2 drum/push	0.5 drum/well (3/4")	2.5 drums/well	0.5 drum/well (3/4")	0.75 drum/well (3/4")	3.75 drums/well	0.75 drum/well (3/4")
Development Water Generated*	20 gal/well (3/4")	45 gal/well	NA	50 gal/well (3/4")	112.5 gal/well	NA	75 gal/well (3/4")	168.75 gal/well	NA
Monument (flush)	\$45 ea. (8" skirt)	\$45 ea. (8" skirt)	NA	\$45 ea. (8" skirt)	\$45 ea. (8" skirt)	NA	\$45 ea. (8" skirt)	\$45 ea. (8" skirt)	NA
Bottom cap	\$7.76 (3/4")	\$8.70	NA	\$7.76/ft (3/4")	\$8.70	NA	\$7.76/ft (3/4")	\$8.70	NA
Labor Rate	\$1000/day	\$1000/day	\$1000/day	\$1000/day	\$1000/day	\$1000/day	\$1000/day	\$1000/day	\$1000/day
Per Diem (\$100pp/day)	\$200/day	\$200/day	\$200/day	\$200/day	\$200/day	\$200/day	\$200/day	\$200/day	\$200/day
# Field Days (30 Wells)	3	10	1	6	30	2	10	30	4
GROUT (per well/push)	\$22	\$22	NA	\$155	\$155	NA	\$235	\$235	\$235
Foam Seal	\$20 (3/4")	NA	NA	\$20 (3/4")	NA	NA	\$20 (3/4")	NA	NA
Survey (30 well/10 push)	\$1,500	\$1,500	\$1,500	\$1,500	\$1,500	\$1,500	\$1,500	\$1,500	\$1,500
Well Log	\$200	\$200	\$0	\$200	\$200	\$0	\$200	\$200	\$0
Well Development	\$250 (3/4") \$500 (2")	\$500	NA	\$500 (3/4") \$1000 (2")	\$1,000	NA	\$700 (3/4") \$1500 (2")	\$1,500	NA
Work Plan	\$4,000	\$4,000	\$4,000	\$4,000	\$4,000	\$4,000	\$4,000	\$4,000	\$4,000
Reporting	\$3,000	\$3,000	\$3,000	\$3,000	\$3,000	\$3,000	\$3,000	\$3,000	\$3,000
Sampling Phase									
<i>Soil Sampling (Porosity)</i>									
Soil Lab (Porosity)	\$50/sample, 30	\$50/sample, 30	NA	\$50/sample, 30	\$50/sample, 30	NA	\$50/sample, 30	\$50/sample, 30	NA
# Field Days	3	10	NA	6	20	NA	10	30	NA
<i>Water Sampling (Chemistry)</i>									
Water Analyses/MIP	\$200/sample, 30	\$200/sample, 30	\$50/sample, 30	\$200/sample, 30	\$200/sample, 30	\$50/sample, 30	\$200/sample, 30	\$200/sample, 30	\$50/sample, 30
Per Diem (\$100pp/day)	\$200/day	\$200/day	\$200/day	\$200/day	\$200/day	\$200/day	\$200/day	\$200/day	\$200/day
# Field Days	3	3	3	4	4	4	6	6	6
Reporting	\$1,500	\$1,500	\$1,500	\$1,500	\$1,500	\$1,500	\$1,500	\$1,500	\$1,500
<i>Aquifer Tests</i>									
Labor Rate	\$1000/day	\$1000/day	NA	\$1000/day	\$1000/day	NA	\$1000/day	\$1000/day	NA
Per Diem (\$100pp/day)	\$200/day	\$200/day	NA	\$200/day	\$200/day	NA	\$200/day	\$200/day	NA
# Field Days	10 (30 wells)	10 (30 wells)	NA	10 (30 wells)	10 (30 wells)	NA	10 (30 wells)	10 (30 wells)	NA
Reporting	\$1,500	\$1,500	\$1,500	\$1,500	\$1,500	\$1,500	\$1,500	\$1,500	\$1,500
<i>Modeling</i>									
Velocity/Flux Modeling Results	\$20,000	\$20,000	\$5,000	\$20,000	\$20,000	\$5,000	\$20,000	\$20,000	\$5,000
Summary Report	\$10,000	\$10,000	\$5,000	\$10,000	\$10,000	\$5,000	\$10,000	\$10,000	\$5,000

Conservative cost savings for a single site are illustrated in Table 5-3. Three specific investigation depths (e.g., 20 feet, 50 feet, and 75 feet) were included to illustrate the relative increases in costs for various site configurations. Two types of direct-push well diameters were included in the comparison (e.g., 3/4-inch and 2-inch diameter), as was the more traditional drilled well approach. Other considerations included costs for work

plans, materials, labor, waste generation, per diem, well development, reporting, and production rates (also a cost driver based on associated labor requirements). Costs range from approximately \$37K for the piezocone approach to 20 feet bgs to approximately \$308K for the drilled well approach to 75 feet bgs. Total savings range from approximately \$76K to approximately \$243K per application (Figure 5-1), while percent savings range from approximately 62 to 81 percent per application. Highest percentage savings can be realized when compared to conventional drilled well approaches, as these tend to require significantly more time to install than DP wells. Users must consider that success will depend upon the soil lithology and resistance to hydraulic or hammer installation techniques for both the sensor probe and DP well approaches.

Table 5-3. Per Site Cost Comparison between High-Resolution Piezocone and MIP Flux Distribution Approach and Conventional Monitoring Well Flux Distribution Approach. Costs are presented for each approach at specific characterization depths (ft), as are percent savings realized by using the piezocone approach relative to the well approaches.

Total Depth	Direct-Push Wells		Drilled Wells	HR Piezocone	HRP Savings		HRP Savings Drilled Wells
	3/4"	2"			3/4" DP	2" DP	
20	\$113,051	\$127,589	\$153,300	\$37,200	67.1%	70.8%	75.7%
50	\$136,110	\$162,084	\$243,191	\$45,800	66.4%	71.7%	81.2%
75	\$169,942	\$208,096	\$307,893	\$64,450	62.1%	69.0%	79.1%

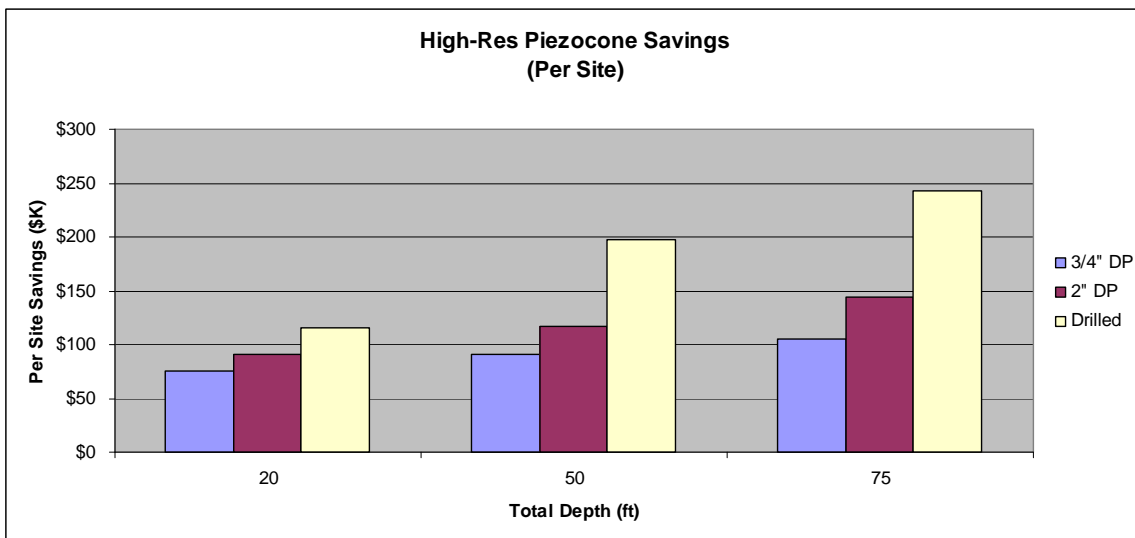


Figure 5-1. Per Site Cost Savings for High-Resolution Piezocone Flux Approach Relative to Well Flux Approaches for Three Depths.

Major cost drivers include depth of characterization, rate of data collection, and duration of field activities. These drivers are interconnected. For instance, when one increases the target characterization depth from 20 to 50 feet, drilled well approach costs increase from approximately \$153K to \$308K (an increase of approximately 100 percent), while the sensor probe approach costs increase from approximately \$37K to \$46K (an increase of approximately 25 percent). Obviously, as the target depth increases, more field time is required, and therefore additional labor and per diem and funding is needed to complete the project tasks. Since rate of data collection will dictate the labor requirements for specific project goals, approaches that can be implemented more rapidly (e.g., sensor probe based approaches) stand to save money in a manner proportional to the relative data collection rate differential. Modeling for the various data collection approaches can also be a driving cost factor, as recent alterations to GMS were tailored to handle the high-resolution piezocone data stream. However, once mainstream users become more familiar with the recent changes, conventional data can also be modeled through this package, albeit with less time efficiency.

When accounting for the total DoD savings realized through the use of the high-resolution piezocone approach for determining flux distribution versus the well-based approaches, several assumptions were used. Since it will require some time before the technology is widely used, it was assumed that 20 sites will be serviced per year early in the transitional cycle, and that 250 sites (5 per state) would be evaluated over a 5 year period. The authors recognize that this value is not correct, and that it is perhaps overly conservative (e.g., actual number could be much higher depending on the success of the transfer of the technology to the private sector).

When considering Life-Cycle costs, since the assumption is that a single sampling round is utilized for the well network, wells will require removal some time in the future. This is not the case for the push probe sensor approach as treated in this comparison. Although not considered here, well rehabilitation would be required for long term monitoring applications. Sampling and monitoring costs for DP and drilled wells should be very similar regardless of well depths. As can be seen in Table 5-4, small differences arise when considering liquid wastes associated with well rehabilitation efforts. Liquid wastes refer to well development water.

Table 5-4. Itemized Well Removal Cost Assumptions. Calculation examples are based on sets of 30 wells for each deployment.

	20'		50'		75'	
	Direct-Push Wells	Drilled Wells	DP	Drilled	DP	Drilled
Labor Rates	\$1000/day	\$1000/day	\$1000/day	\$1000/day	\$1000/day	\$1000/day
Average No.	6	6	6	6	6	6
Labor Days						
Labor (Remove)	6000	6000	6000	6000	6000	6000
Per Diem (Remove)	2800	2800	2800	2800	2800	2800
Grouting	1800	1800	3600	3600	5400	5400
Grout Rig (Mob)	1000	1000	1000	1000	1000	1000
Solid Waste	1500	1500	3000	3000	4500	4500
Liquid Waste*	1600	2400	1600	2400	1600	2400
Reporting	1500	1500	1500	1500	1500	1500
Totals 3/4	\$16,200	-	\$19,500	-	\$22,800	-
Totals 2"	\$17,000	\$17,000	\$20,300	\$20,300	\$23,600	\$23,600

Figure 5-2 displays the total anticipated DoD savings per year assuming only 20 site applications. Cost avoidance estimates range from approximately \$1.5M to close to \$4.9M per year for DoD alone. Figure 5-3 displays the total anticipated DoD savings over a 5-year period assuming 250 site applications. Cost avoidance estimates range from approximately \$19M to close to \$61M for DoD alone. These cost avoidances do not account for savings realized through superior characterization resolution, as the piezocone data is not limited to three depths, and hydraulic information can be collected at a precision equal to every 1 to 2 inches in depth (e.g., when soil type is used to characterize hydraulic conductivity). Furthermore, these cost avoidances do not account for additional savings when life cycle costs associated with well maintenance and removal are considered (Table 5-4).

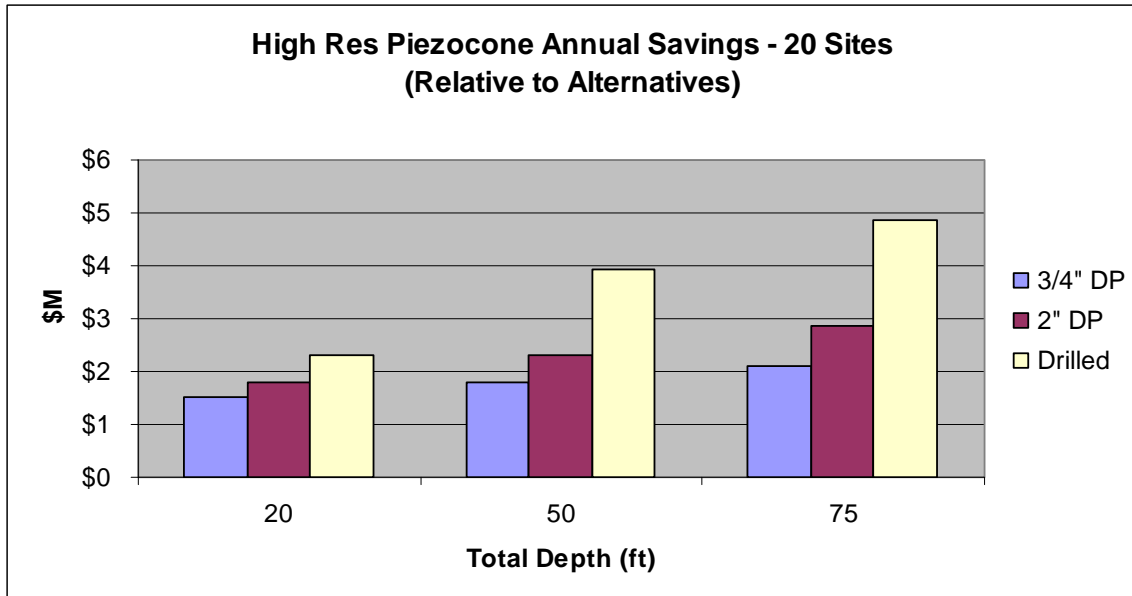


Figure 5-2. Anticipated Early DoD Annual Savings by High-Resolution Piezocone Flux Approaches. Values were derived assuming that 20 sites would be completed per year.

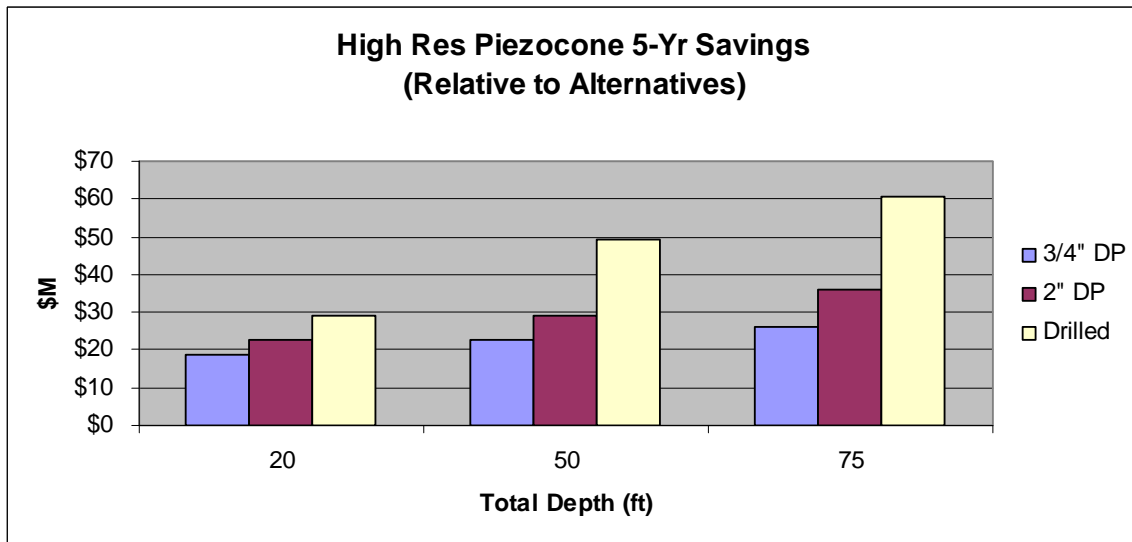


Figure 5-3. Anticipated Five-Year DoD Savings by High-Resolution Piezocone Flux Approaches. Values were derived assuming that 250 sites would be completed over a 5-year period.

6. Implementation Issues

6.1 Environmental Checklist

Based on previous experience with direct push technologies, permitting requirements are expected to vary with individual locality. Some regulators require “drilling permits” and associated fees for direct push investigations. Other regulators do not require permits or payment of fees and only require notification usually via submittal of a test plan. Dr. Kram has successfully received waivers for wells and direct push investigation efforts for this project, and handled all permitting requirements with local regulators and facility personnel. Furthermore, site staging logistics, push location clearance, waste handling, and on-site project coordination were planned in advance through meetings with key facility and field personnel. Tracer test logistics were complicated by permit review application and processing, as well as sampling requirements and associated analytical costs. However, in practice, tracers are not required when deploying these innovative push probes.

When using the high-resolution piezocone, the following recommendations are suggested:

- 1) Probe push locations should be separated by a minimum of 30 feet in areas suspected of shallow gradient;
- 2) The push domain should be a minimum of 100 feet wide by 100 feet across in areas suspected of shallow gradient;
- 3) Push grid configuration should be appropriate for interpolation and three-dimensional statistical and modeling assessment;
- 4) Pressure dissipation tests should be periodically conducted in triplicate to assess reproducibility;
- 5) Once a gradient can be recognized within a domain of interest, it is recommended that piezocone pushes be advanced upgradient and downgradient of the critical area of interest in transect patterns to enable modelers to appropriately set boundary conditions.

For the GeoVIS, we recommend the following considerations:

- 1) Collaboration with Dr. Andrew Ward (DOE) to increase/correct the resolution and image processing capabilities;
- 2) Comparison with Dr. Ward’s system to determine whether a correction factor can be applied to the current GeoVIS effective porosity results;

- 3) Development of a new neural network based on laboratory and field comparisons in saturated soils posing the most significant quantification challenges (e.g., silty sand and finer materials).

Liquid decontamination rinse water wastes will be generated during probe deployment activities. Waste handling permits are typically managed through the county or state regulatory agency. In California, the Regional Water Quality Control Board oversees such activities, and must be contacted to obtain essential waste tracking guidance and essential forms. When on a US military base, the base environmental coordinator typically maintains a base wide permit that can be amended to incorporate waste handling needs. In addition, the facility typically has a staging area for management and logistical support.

6.2 Other Regulatory Issues

Lack of regulatory acceptance by both Federal and State regulatory agencies has traditionally been cited as a major obstacle to implementation of innovative site characterization techniques on DOD sites. ESTCP has previously funded efforts to help establish regulatory acceptance of the SCAPS Laser Induced Fluorescence (LIF) sensor for rapid subsurface detection of petroleum, oil and lubricants and SCAPS Heavy Metal Sensors for mapping subsurface metal contamination. Significant lessons were learned from these efforts. Most notably, there appears to be no single path to gain universal acceptance of new technology by the regulatory community. The LIF sensor for petroleum hydrocarbons was the first major chemical sensor system developed for this SCAPS system. During the early stages of technology transfer of the LIF sensor a common question raised by potential users was: “Is the technology approved by the regulators?” From this question grew the concept that if the LIF technology were “approved” by the regulatory community, then the users would embrace it. The quest for regulatory approval led to a successful multi-year effort to gain regulatory acceptance for the SCAPS LIF sensor technology based on assembling a comprehensive set of field measurements that directly compared the performance of the sensor system with traditional US EPA methods for a variety of contaminants under different hydrogeological conditions. The cornerstone of obtaining as broad an acceptance as possible was the linking of these technical efforts with multi-state and national certification/verification programs such as the US EPA Consortium for Site Characterization Technology “verification” program and “certification” by the California EPA Department of Toxic Substance Control’s Technology Certification Program (Cal

Cert). For the case of the SCAPS nitrogen laser LIF sensor system, these opportunities were subsequently linked to the Western Governors Association, Demonstrating Onsite Innovative Technologies (WGA/DOIT) project. Interest by the WGA/DOIT project subsequently led to the establishment of a SCAPS-LIF Interstate Technology and Regulatory Cooperation (ITRC) workgroup, Technology Specific Task Group (TSTG). Their primary goal was to achieve acceptance by each of the seven TSTG member-states (Utah, Nebraska, New Mexico, Louisiana, New Jersey, Idaho, California) using California Certification (Cal Cert) as the protocol. For the SCAPS nitrogen laser LIF system, these efforts resulted in the successful certification by the Cal Cert Program, verification by the US EPA, and endorsement of the Cal Cert certification by the WGA.

Experience has shown that obtaining regulatory acceptance does not automatically ensure user acceptance. While regulatory acceptance is a desirable goal, the users must be convinced that the new technology will enable them to do their jobs faster, better, and cheaper. Experience from the SCAPS LIF program suggests that user acceptance is built one user at a time. Discussions with both government and commercial LIF service providers indicate that the key to growing the business is to provide a product that meets the customer's needs at a competitive price (personal communications, Tim Shields, R. Brady and Associates, San Diego, California; Racyp Yilmaz, Fugro Geoscience, Inc., Houston, Texas). Satisfied users generate repeat business and tell other potential customers.

Based on lessons learned from the SCAPS LIF sensor technology, it appears that the most effective currently available means to promote acceptance of new direct push technologies is to aggressively market the technology and grow a commercial and government user base for the technology, while simultaneously pursuing ITRC and other regulatory concurrence as well as national consensus (e.g., via ASTM). This approach has proved to be successful for the ESTCP Well Comparison Project (CU-0011) as well. Because of the high turnover in personnel, both the user and regulatory community experiences suggest that a long term and persistent marketing effort is required to establish support for a new technology. In general, a motivated commercial vendor has the capability to rally more marketing savvy (knowledge and experience) for a product or service than does a government technology developer. While the SCAPS LIF ESTCP project focused almost exclusively on gaining acceptance of the technology by regulators, the efforts of the SCAPS metal sensor ESTCP project were directed more towards generating a link with commercial partners that ultimately take the lead for marketing the

technologies to both users and regulators. It is believed that this strategy has the advantage of offering a long-term solution to the difficult problem of nurturing a new technology through its' infancy. Finally, experience from the SCAPS LIF and metals sensor project has shown that users are often slow to accept new methods and technologies due to limited exposure, inadequate technical understanding, and lack of high quality validation data that support developers and/or vendor claims.

Ultimately, acceptance requires technology exposure leading to understanding, as well as comprehensive data validation of the type that is generated in ESTCP demonstrations. Project team members are currently utilizing several available technology transfer vehicles and avenues, including the engagement of top regulatory and industry officials through our Project Advisory Committee activities, presenting to the ITRC SCM task group, including piezocone and GeoVIS descriptions in the ITRC Direct Push Well workshop and presentations, updating appropriate ASTM standards, presenting at the SERDP conference, the Nielsen conference, the GRAC conference, the AEHS conference, and through public demonstrations to commercial and regulatory and academic groups. Perhaps the most significant inroads towards regulatory "acceptance" transpired when Dr. Kram was invited to present to ITRC at their July 19th 2006 SCM meeting. This effort served as stimulus for the addition of new-start ITRC guidance on flux monitoring.

Since the formal public demonstration, the San Diego Navy SCAPS team has arranged for several field deployments of the high-resolution piezocone. In addition, the technology will soon be transferred to the Army SCAPS teams as well as a commercial entity (via license and cooperative agreement).

This demonstration project has satisfied the major objectives set forth at the outset, many of which were designed to promote user acceptance of direct-push probe deployment for high-resolution hydraulic assessment. Successfully met objectives include the following:

- Careful design of a technically rigorous research methodology for comparing the performance of wells to direct-push probes;
- Generation of a consistent data set for conducting such a comparison, using regulatory accepted field protocols;
- Performance of appropriate statistical tests for evaluating the hydraulic performance of high-resolution piezocone using a direct comparison with

conventional nested wells, as well as the development of models for interpolative and predictive applications;

- Augmentation of GMS to allow for depiction of direct-push hydraulic parameter distributions, calculations of seepage velocity, and flux distributions;
- Presentation to ITRC SCM Group (as invited guest speaker);
- Incorporation of technical description into an ITRC Technical Regulatory guidance document and RITS module for the long-term use of direct-push wells;
- Implementation of a well design software package for all wells used in demonstration;
- Presentation at key industry and government conferences including SERDP, the 2006 North American Environmental Field Conference, and the 2006 GRAC Conference on High-Resolution Characterization, with presentations at additional conferences pending;
- Presentations to Navy ARTT members (June, 2007);
- Generation of NAVFAC technology transfer web tool on flux monitoring (<http://coo.battelle.org/MassFluxDS/tool.aspx>);
- Field tours of the sites provided to regulators, UCSB graduate students (some of whom have become regulators), and key industry personnel;
- Active participation with industry and environmental regulatory committees and cooperatives; and
- Transfer of the technology to Army and private sector (in progress).

Future technology transfer vehicles include:

- Advertisement and presentation via ITRC workshop;
- Amendment of an ASTM standard pertaining to the use of direct-push tools for environmental site characterization;
- Release and dissemination of the high-resolution piezocone guide;
- Utilization of DoD technology transfer vehicles such as conferences, RITS, NFESC announcements, and final report dissemination; and
- Continued notification of DoD and industry users and direct-push service providers.

6.3 Lessons Learned

As with all direct-push technologies, the high-resolution piezocone and GeoVIS can only be deployed in unconsolidated soils to depths dictated by local geologic materials and the probe delivery system. As discussed throughout this document, the current GeoVIS

probe does not yet appear to be capable of accurately estimating effective porosity in saturated silty sands. While the high-resolution piezocone soil type data can now be converted to estimates of effective porosity, this is not entirely accurate, as effective porosity is quite different than soil porosity, porosity for a given soil type can range by up to 30 percent, and no tests were conducted to evaluate the level of accuracy. However, since the total relative error potentially introduced by estimating effective porosity is deemed to be low relative to the total relative error potentially introduced by hydraulic conductivity estimates, this level of tolerance for effective porosity estimation via soil type conversion should at least be far superior to using a single value for an entire site (which currently occurs throughout the environmental restoration industry).

During performance of the Rh(WT) tracer test, it appears that total suspended solids (TSS) interfered with the fluorescence readings in a manner that rendered questionable analytical results. Deconvolution of the tracer fluorescence from the turbidity signal proved challenging. In the future, either a better analytical device would be used that is less impaired by TSS, or perhaps an alternative tracer would be employed. Another option could include release of a much higher tracer concentration. The team could probably have released another CaCl_2 tracer and tracked conductivity, chloride or calcium ion in the well network. Alternatively, a forced gradient tracer test could have been easier to conduct, given the extremely low gradient existing at the selected site, and provided the well spacing was appropriate based on dispersion modeling. However, ample time and resources were not available, and proof of the predictive capabilities of the models was considered less critical to the acceptance of the innovative approach than the comparison between high-resolution piezocone and short screened well hydraulic data and predictions.

Spatial heterogeneity can play a significant role in the comparison of innovative and conventional techniques. Since one can not advance the sensor probe in the same location a well is installed, the term “co-located” as used in this context refers to data collection proximities within a few feet of each other in map view, and depths within a few inches of each other. Even within these carefully controlled experiments, spatial heterogeneity among co-located hydraulic conductivity values can vary by orders of magnitude. Since it is impossible to reproduce a push at the same location, this places limitations on the statistical analyses one can conduct, as values can not be evaluated as means with a range and an associated probability distribution function.

When deploying the high-resolution piezocone to develop hydraulic or flux models, it is good practice to establish background conditions by advancing several pushes outside the perimeter of the contaminated domain of interest. Spacing is critical, as it is best to advance these background pushes far enough away from the domain of interest to avoid “edge-effects” caused by interpolations or model aberrations, yet not so far away as to render the data non-relative. A good rule-of-thumb would be to advance the boundary pushes upgradient and downgradient of the domain of interest by a distance ranging between 0.3 and 1.0 times the length or width of the domain of interest (whichever is greater). The more pushes, the greater the confidence one has in the interpolations and models. At least two upgradient and two downgradient pushes are recommended. This is an arbitrary guide, so users are encouraged to try different spatial configurations.

Every time the high-resolution piezocone is deployed, the probe zero depth elevation point (e.g., elevation that the data collection activities begin) must be surveyed. While several options exist, the current practice is to zero the probe when it just touches a piece of tape adhered to the top of the opened pre-push screening hole. Upon retraction of the cone, carefully locate that zero point elevation and survey this to tie the data into an elevation datum (e.g., feet above mean sea level) through WinOCPT. Careful adherence to this procedure is critical, as it allows for all the probe data at a particular site to be incorporated into the models and referenced in a valid spatial context.

6.4 End-User Issues

Two parallel technology transition paths were pursued as part of this effort. One path included transfer of the technology directly to government owned/operated systems. The DoD currently operates 5 cone penetrometer systems (three Army SCAPS systems and 2 Navy SCAPS systems). In addition, the Department of Energy (DOE) and Environmental Protection Agency each operate a CPT system. All five DoD systems are operated on a fee per service basis for work at government facilities. The operators of these systems are motivated to expand the sensing capabilities that they offer because it helps to generate new business. As part of this Dem/Val program these users have been informed of our efforts and invited to attend the field demonstrations so that they can view the technologies in operation in the field. Through our assistance, the Army Tulsa District SCAPS team is in the process of purchasing high-resolution piezocone system components. Furthermore, key government entities are represented on the Project Advisory Committee. Project team members also utilized the technology transfer vehicles available through the Remediation Innovative Technology Seminar, Alternative

Restoration Technology Team, and via alternative ESTCP technology transfer opportunities.

The second technology transfer path included of direct collaboration with key members from the commercial sector. This is being directly facilitated through efforts to commercialize these technologies using CRADA's, licensing of government intellectual property, and through Center for Commercialization of Advanced Technologies (CCAT) efforts. Commercial entities have appointed representatives to our Advisory Committee. Furthermore, SSC-SD currently has a CRADA with Fugro Geosciences Inc. for the technology transfer of the GeoVIS video imaging system. Another commercial partner has recently negotiated a license agreement for the high-resolution piezocone.

On August 31, 2005, a GMS workshop was held to train SCAPS operators, project partners and industry modelers how to integrate high-resolution piezocone and GeoVIS data into the upgraded modeling package. Dr. Norm Jones (BYU) covered data import, processing, and generation of gradient distributions, velocity distributions, and flux distributions, among other items. The guidance is included as Appendix H. A high-resolution piezocone guide (Appendix J) was also prepared and provided to Army and industry technology transfer partners.

Phase II Field Tests (June 2006) included deployment of the high-resolution piezocone and GeoVIS. During this deployment, a formal public demonstration was conducted. Participants included demonstration partners, candidate licensees, representatives from the Army and east coast Navy SCAPS teams, DOE, Bureau of Reclamation, ASTM, universities, regulators, Navy RPMs, and private sector parties interested in using the technologies at their sites.

Future technology transfer plans include:

- Development and dissemination of an ITRC Technical Regulatory guide on flux determination;
- Incorporation of high-resolution piezocone into ASTM D6067, Standard Test Method for Using the Electronic Cone Penetrometer for Environmental Site Characterization;
- Utilization of DoD technology transfer vehicles such as conferences, RITS, NFESC announcements, and final report dissemination;
- Licensing of the high-resolution piezocone to additional private entities;

- Assistance with Army probe integration into their SCAPS program;
- Working with industry leaders to facilitate use of high-resolution data into fate and transport models through development of GUI and mathematical solutions that enable modelers to correctly simulate high-resolution observations and measurements with internal hydraulic boundary conditions;
- Continued notification of DoD and industry users and DP service and materials providers;
- Demonstration and case study presentations at future DoD and industry conferences; and
- Implementation of new EPA-sponsored efforts to demonstrate the capabilities in high permeability soils, perform data fusion modeling, and conduct a new forced gradient tracer test to compare model predictions based on conventional technologies relative to the high-resolution piezocone technology.

7. References

- API, 1998, Recommended Practices for Core Analysis RP40, American Petroleum Institute, Washington, D.C.
- ASTM D3441, Standard Test for Deep, Quasi-Static, Cone and Friction-Cone Penetration Tests of Soil, Annual Book of ASTM Standards, v.04.08.
- ASTM D4043, Standard Guide for Selection of Aquifer-Test Method in Determining Hydraulic Properties by Well Techniques, Annual Book of ASTM Standards, v.04.08.
- ASTM D4044, Test Method (Field Procedure) for Instantaneous Change in Head (Slug Tests) for Determining Hydraulic Properties of Aquifers, Annual Book of ASTM Standards, v.04.08.
- ASTM D4750, Standard Test Method for Determining Subsurface Liquid Levels in a Borehole or Monitoring Well (Observation well), Annual Book of ASTM Standards, v.04.08.
- ASTM D5283, Standard Practice for Generation of Environmental Data Related to Waste Management Activities: Quality Assurance and Quality Control Planning and Implementation, Annual Book of ASTM Standards, v.04.08.
- ASTM D5521, Standard Guide for Development of Ground-Water Monitoring Wells in Granular Aquifers, Annual Book of ASTM Standards, v.04.08.
- ASTM D5778, Standard Test Method for Performing Electronic Friction Cone and Piezocone Penetration Testing of Soils.
- ASTM D6067, Standard Test Method for Using the Electronic Cone Penetrometer for Environmental Site Characterization, Annual Book of ASTM Standards, v.04.08.
- ASTM D6724, Standard Guide for Installation of Direct Push Ground Water Monitoring Wells. Annual Book of ASTM Standards, v.04.08.
- ASTM D6725, Standard Practice for Direct-Push Installation of Prepacked Screen Monitoring Wells in Unconsolidated Aquifers. Annual Book of ASTM Standards, v.04.08.
- Bartlett, S.A., Robbins, G.A., Mandrick, J.D., Barcelona, M.J., McCall, W., and Kram, M.L., 2004, Comparison of Hydraulic Conductivity Determinations in Direct Push and Conventional Wells, Naval Facilities Engineering Service Center Technical Report, TR-2252-ENV, October, 2004, 88pp.

- Butler Jr., J.J., J.M. Healy, G.W. McCall, and S.P. Loheide II, 2002. Hydraulic Tests with Direct-Push Equipment, *Ground Water*, v.40, no. 1, pp.25-36.
- Campanella, R. and P. Robertson, Guidelines for Geotechnical Design using the Cone Penetrometer Test and CPT With Pore Pressure Measurement, Hogentogler & Co., Maryland, 4th edition, 1989.
- Carle, S.F., E.M. Labolle, G.S. Weissman, D. Van Brocklin, and G. E. Fogg, 1998. Conditional Simulation of Hydrofacies Architecture: A Transition Probability/Markov Approach, in Fraser, G.S., and J.M. Davis, 1998, Hydrogeologic Models of Sedimentary Aquifers, Concepts in Hydrogeology and Environmental Geology No. 1, SEPM Special Publication, p.147-170.
- Carsel, R. F., and R. S. Parrish. 1988. Developing Joint Probability Distributions of Soil Water Retention Characteristics. *Water Resources Research*, v.24, p.755-769.
- Enfield, C., 2002. Source Reduction by Flushing, presentation provided for assistance with this proposal.
- ESTCP, 1997. ESTCP Cost and Performance Report: POL Sensor Validation of SCAPS, Environmental Security Technology Certification Program: Arlington, Virginia. 25pp.
- ESTCP, 2001. ESTCP Cost and Performance Report: Tri-Service Site Characterization and Analysis System (SCAPS) Thermal Desorption Sampler for Volatile Organic Compounds, Environmental Security Technology Certification Program: Arlington, VA. 32pp.
- Ferritto, J.M., 1997. NFESC Technical Report TR-2077-SHR, June, 1997.
- Hvorslev, M.J., 1951. Time Lag and Soil Permeability in Ground-Water Observations, U.S. Army Corps of Engineers Waterways Experiment Station, Bulletin no. 36.
- ITRC, 2006. The Use of Direct Push Well Technology for Long-term Environmental Monitoring in Groundwater Investigations, Technical Regulatory Guidance, March, 2006, 71pp.
- Kram, Mark L. and Fred Goetz, 1999. Natural Attenuation General Data User's Guide, Naval Facilities Engineering Command document UG-2035-ENV, February 1999, 35 pp.
- Kram, Mark L., Dale Lorenzana, Joel Michaelson, and Ernest Lory, 2001. Performance Comparison: Direct-Push Wells Versus Drilled Wells, NFESC Technical Report, TR-2120-ENV.

- Kram, Mark L., Gary Robbins, Renduo Zhang, Lanbo Liu, Norm Jones, 2006. Detailed Hydraulic Assessment Using a High-Resolution Piezocone Coupled to the GeoVIS, in Proceedings of the North American Environmental Field Conference, Tampa, FL.
- Kram, Mark L., Gary Robbins, Ross Batzoglou, Jessica Chau, Meridith Metcalf, Norm Jones, 2006. Detailed Hydraulic Assessment Using a High-Resolution Piezocone and 3-D Conceptual Models, in Proceedings of the Groundwater Resources Association Symposium on High Resolution Site Characterization and Monitoring, Long Beach, CA, November 14-15, 2006.
- Lieberman, S.H. and D.S. Knowles, 1998. Cone Penetrometer Deployable In- Situ Video Microscope for Characterizing Sub-Surface Soil Properties. *Field Analytical Chemistry and Technology*, v.2: pp. 127-132.
- Lieberman, S.H., D.S. Knowles, J. Kertesz, P.M. Stang, and D. Mendez, 1997. Cone Penetrometer Deployed In Situ Video Microscope for Characterizing Sub-Surface Soil Properties, *Field Analytical Methods for Hazardous Wastes and Toxic Chemicals*, Air & Waste Management Association, Pittsburgh, PA, pp. 579-587.
- Myers, D.E., and A. Journel, 1990. Variograms with Zonal Anisotropies and Non-Invertible Kriging Matrices, *Mathematical Geology*, v.22, pp. 779-785.
- Nash, J.E. and J.V. Sutcliffe, 1970. River flow forecasting through conceptual models, Part I: A discussion of principles, *J. Hydrol.*, 10, 282-290.
- Parez and Fauriel (1988). "Le piezocone ameliorations apportees a la reconnaissance de sols." *Revue Francaise de Geotech* 44: 13-27
- Rawls, W. J., D. L. Brakensiek, and K. E. Saxton. 1982. Estimating Soil Water Properties, *Transactions, ASAE*, v.25, no.5, p.1316-1320 and 1328.
- Robertson, P.K. and R.G. Campanella, 1989. *Guidelines for Geotechnical Design Using the Cone Penetrometer Test and CPT with Pore Pressure Measurement*, 194pp.
- Rouhani, S. and D.E. Myers, 1990. Problems in Kriging of Spatial-Temporal Geohydrological Data, *Mathematical Geology*, v. 22, pp. 611-623.
- Sinfield, L.D., T. Latas, and W.E. Collins, 2004. Confirmation of CPT Video Microscope Estimates of In-Situ Soil Porosity and NAPL Saturations, *Proceedings of National Defense Industrial Association, 30th Environmental and Energy Symposium & Exhibition*, April 5-8, 2004, San Diego, CA
- Schroeder, J.D., S.R. Booth, and L.K. Trocki, 1991. Cost effectiveness of the Site Characterization and Analysis Penetrometer System, Los Alamos National Laboratory.

U.S. Patent 6,115,061, September, 2000, In Situ Microscope Imaging System for Examining Subsurface Environments, Lieberman, S.H., Knowles, D.S., Martini, L.J.

U.S. Patent 6,208,940, March 27, 2001, Cone Tipped Cylindrical Probe for Use in Groundwater Testing, Kram, Mark L., and Massey, James A.

U.S. Patent 6,236,941, May 22, 2001, Cone Tipped Cylindrical Probe for Use in Groundwater Testing, Kram, Mark L., and Massey, James A.

U.S. Patent 6,317,694, November 13, 2001, Method and Apparatus for Selecting a Sand Pack Mesh for a Filter Pack and a Well Casing Slot Size for a Well, Kram, Mark L., and Farrar, Jeffrey A.

8. Points of Contact

Table 8-1. Points of Contact.

POINT OF CONTACT Name	ORGANIZATION Name Address	Phone/Fax/Email	Role In Project
Dr. Mark L. Kram	NFESC Code 413 1100 23 rd Ave. Port Hueneme, CA 93043	805-982-2669 (voice) 805-982-4304 (fax) mark.kram@navy.mil	Principal Investigator
Dr. Gary Robbins	Department of Geology and Geophysics, University of Connecticut, Storrs, CT, 06269	860-486-2448 (voice) 860-486-1383 (fax) gary.robbs@uconn.edu	Technical Consultant- Modeling/Statistics Field Applications
Dr. Amvrossios C. Bagtzoglou	Department of Civil & Environmental Engineering University of Connecticut, Storrs, CT, 06269	860-486-4017 (voice) 860-486-2298 (fax) acb@engr.uconn.edu	Technical Consultant- Modeling and Statistics

Dan Y. Eng	U.S. Army Engineer Research and Development Center, CEERD-IE- A, Information Technology Laboratory, 3909 Halls Ferry Road, Vicksburg, Ms 39180-6199	601-634-3409 (voice) 634-2747 (fax) Dan.Y.Eng@Erdc.USace.Army.Mil	Army Liaison
------------	--	--	--------------

APPENDIX A:

Analytical Methods Supporting the Experimental Design

The most appropriate ASTM standards are listed below. Complete standards and guides are available at <http://www.astm.org>. The API document is available at http://www.ptslabs.com/Tech_Papers.asp.

- API, 1998, Recommended Practices for Core Analysis RP40 (API Dean Starks), American Petroleum Institute, Washington, D.C.
- ASTM D3441, Standard Test for Deep, Quasi-Static, Cone and Friction-Cone Penetration Tests of Soil, Annual Book of ASTM Standards, v.04.08.
- ASTM D4043, Standard Guide for Selection of Aquifer-Test Method in Determining Hydraulic Properties by Well Techniques, Annual Book of ASTM Standards, v.04.08.
- ASTM D4044, Test Method (Field Procedure) for Instantaneous Change in Head (Slug Tests) for Determining Hydraulic Properties of Aquifers, Annual Book of ASTM Standards, v.04.08.
- ASTM D4750, Standard Test Method for Determining Subsurface Liquid Levels in a Borehole or Monitoring Well (Observation well), Annual Book of ASTM Standards, v.04.08.
- ASTM D5778, Standard Test Method for Performing Electronic Friction Cone and Piezocone Penetration Testing of Soils, Annual Book of ASTM Standards, v.04.08.
- ASTM D6067, Standard Test Method for Using the Electronic Cone Penetrometer for Environmental Site Characterization, Annual Book of ASTM Standards, v.04.08.
- ASTM D6724, Standard Guide for Installation of Direct Push Ground Water Monitoring Wells, Annual Book of ASTM Standards, v.04.08.
- ASTM D6725, Standard Practice for Direct Push Installation of Prepacked Screen Monitoring Wells in Unconsolidated Aquifers, Annual Book of ASTM Standards, v.04.08.

APPENDIX B:

Analytical Methods Supporting the Sampling Plan

The most appropriate ASTM standards are listed below. Complete standards and guides are available at <http://www.astm.org>.

- ASTM D1587, Standard Practice for Thin-Walled Tube Sampling of Soils for Geotechnical Purposes, Annual Book of ASTM Standards, v.04.08.
- ASTM D4448, Standard Guide for Sampling Ground Water Monitoring Wells, Annual Book of ASTM Standards, v.04.08.
- ASTM D5730, Standard Guide for Site Characterization for Environmental Purposes with Emphasis on Soil, Rock, the Vadose Zone, and Ground Water, Annual Book of ASTM Standards, v.04.08.
- ASTM D5778, Standard Test Method for Performing Electronic Friction Cone and Piezocone Penetration Testing of Soils, Annual Book of ASTM Standards, v.04.08.
- ASTM D6001, Standard Guide for Direct-Push Water Sampling for Geoenvironmental Investigations, Annual Book of ASTM Standards, v.04.08.
- ASTM D6067, Standard Test Method for Using the Electronic Cone Penetrometer for Environmental Site Characterization, Annual Book of ASTM Standards, v.04.08.
- ASTM D6282, Standard Guide for Direct-Push Soil Sampling for Environmental Site Characterizations, Annual Book of ASTM Standards, v.04.08.

APPENDIX C:

Quality Assurance Project Plan (QAPP)

The quality assurance (QA) plan for this demonstration specifies procedures that will be used to ensure data quality and integrity. Careful adherence to these procedures will ensure that data generated from the demonstration will meet the desired performance objectives and will provide sound analytical results.

C.1 Purpose and Scope

The primary purpose of this QA plan is to outline steps that will be taken by NFESC, PWC San Diego, SSC-SD, U.S. Army ERDC, University of Connecticut, University of Wyoming, and the confirmatory analytical laboratory to ensure that data resulting from this demonstration are of known quality and that a sufficient number of critical measurements are taken. This section of the demonstration plan addresses the key elements that are required according to guidelines in the US EPA guidance document "A Guidance Manual for the Preparation of Site Characterization Technology Demonstration Plans" (EPA 1995).

C.2 Quality Assurance Responsibilities

The NFESC Program Manager is responsible for coordinating the preparation of the QA plan for this demonstration and for its approval. The NFESC Program Manager, in conjunction with the SSC-SD, PWC San Diego, U.S. Army ERDC, University of Connecticut, and University of Wyoming project teams, will ensure that the QA plan is implemented during all demonstration activities. The NFESC Program Manager, Dr. Mark Kram, will review and approve the QA plan and will provide QA oversight for all demonstration activities.

Data will be collected and analyzed in several ways. Quantitative and qualitative field methods will consist of the direct push sensor technologies (Piezocone and GeoVIS), well installation methods, slug test approaches, and soil sampling activities. An off-site laboratory will be used to conduct porosity measurements using the API Dean Starks analysis. Many individuals will be responsible for sampling and analysis quality assurance/quality control (QA/QC) throughout the demonstration. The primary responsibility for ensuring that sampling activities comply with the requirements of the sampling plan will rest with the NFESC QA manager. QA/QC activities for the two

direct push hydrogeologic sensor technologies will consist of periodic system checks required to assure that the demonstrations provide data of the necessary quality.

QA/QC activities for sample laboratory analyses will be the laboratory QA officer's responsibility. If problems arise or data appear unusual, discrepancies will be documented and corrective actions will be implemented as specified in Sections C4 and C5 of this QA plan. The QA/QC measurements conducted by the confirmatory laboratory will be dictated by the analytical methods being used. QA/QC efforts associated with conceptual and transport modeling efforts will consist of documenting all assumptions and algorithms related to statistical interpolation and model configuration. QA/QC modeling documentation, which will be the responsibility of the University of Wyoming, will be presented in the final report.

C.3 Data Quality Parameters

The data obtained during the demonstration must be of sound quality for conclusions to be drawn regarding the two direct push hydrogeologic sensor technologies. For all measurement and monitoring activities conducted, data quality parameters should be established based on the proposed end uses of the data. Data quality parameters include five indicators of data quality: representativeness, completeness, comparability, accuracy, and precision.

Data generated by the two direct-push sensor technologies will be compared to the data generated from monitoring well piezometric water levels, soil samples, and API Dean Starks porosity laboratory analyses. Furthermore, models generated with direct-push probe sensor data will be compared to models generated with conventional data. Both types of models will be used to generate ground water flow predictions, which will be evaluated by comparison to tracer test observations. High quality, well-documented confirmatory laboratory results and tracer tests are essential for meeting the purpose and objectives of this demonstration. Therefore, the following indicators of data quality will be closely evaluated to determine the performance of the technology when measured against data generated by the confirmatory laboratory and field tracer tests.

3.1 Representativeness. Representativeness refers to the degree to which the data accurately and precisely represent the conditions or characteristics of the parameter represented by the data. In this demonstration, representativeness will be ensured by

executing consistent sample collection and handling procedures, including sample locations, sampling procedures, sample storage, sample packaging, sample shipping, and sample equipment decontamination. Representativeness will also be pursued by applying each method in a manner consistent with stringent guidelines in order to provide the most accurate and precise measurement possible.

The sampling plan was developed to sample soil or measure water levels from as close to the push locations (in map view) as possible. It is well known that variations in contamination levels and hydrogeologic properties can occur over short horizontal distances (less than 1 foot). To minimize spatial error between the soil sample collection locations and the regions sampled by the two direct push sensor probes, the push used for collection of soil samples and wells used for head value measurements will be located within approximately 12 inches of the two probe pushes. The piezocone will be advanced in a location adjacent to the clustered piezometers, at depths corresponding to the piezometer screen mid-points, and head values will be compared to the head values observed in each of the piezometers. Soil samples will be collected from these same depths, and analyzed by the Dean Stark API RP 40 method.

3.2 Completeness. Completeness refers to the amount of data collected from a measurement process compared to the amount that was expected to be obtained. For this demonstration, completeness refers to the proportion of valid, acceptable data generated using each method. The overall completeness objective for data generated during this demonstration is 90 percent.

It is anticipated that less than 100 percent completeness of the two direct-push sensor data and discrete sample analysis results will occur. A broken, cracked or obstructed sapphire window or a problem with the piezocone sampling interface would disqualify the push. Likewise, identification of any broken part of a probe upon retraction would disqualify the push. In addition, a push that was refused due to contact with cobbles, boulders, or a buried obstruction would also be disqualified. A substitute push would be advanced in these cases, generally within 8 inches horizontally of the disqualified push. If slippage greater than 3 inches of the push rod in the hydraulic ram is noted during a push, the data from the push will be disqualified due to excessive depth measurement inaccuracy.

The operating procedure criteria are designed such that the behavior of the two sensor probe technologies is watched closely during a site characterization effort. As a result,

the probe operators tend to fix problems before questionable data are generated. If a sensing probe were to malfunction, however, such as occurs when a sapphire window becomes cracked, the data generated would not be acceptable and the operators would recommend that the probe be repaired prior to its next deployment.

Completeness is defined as follows for all measurements:

$$\%C = 100\% \times (V / T)$$

where: %C = percent completeness

V = number of sample measurements judged valid

T = total number of discrete sample measurements.

3.3 Comparability. Comparability refers to the confidence with which one data set can be compared to another. A primary objective of this demonstration is to evaluate how well the in-situ direct-push sensing technologies perform when compared to conventional analytical methods used by a confirmatory laboratory or piezometers in the vicinity. Additional QC for comparability will be achieved by tracking soil type probe data correlations to probe-derived porosity values, and by adhering to standard methods for sample preparation and instrument operation for all techniques included in the demonstration.

Because an in-situ measurement will be compared with a conventional laboratory measurement, it is not possible to ensure absolute comparability of the two measurement methods. For instance, the API Dean Stark porosity determination method yields a single value for a 6-inch soil core. In comparison, the GeoVIS yields porosity values over a much smaller vertical scale (e.g., less than an inch). It is believed, however, that the proposed approach of pushing the soil stab sampling push in close proximity to the sensor push holes will minimize, but not necessarily eliminate, potential noncomparability issues that result from the sampling process. For instance, several porosity values will be derived over the 6-inches corresponding to the soil sampling depth range. A mean value will be compared to the single API Dean Stark porosity value during the data assessment component of the demonstration.

3.4 Accuracy. Accuracy refers to the degree of agreement of a measurement to the true value. With conventional laboratory-based measurements, the accuracy of the method is a function of both the sampling errors and errors associated with the measurement technique. To evaluate the accuracy of a laboratory method, the conventional approach consists of comparing results obtained from the analysis of quality control samples of known porosity. Errors related to sampling are not addressed.

An inherent challenge with the experimental design is that there is no independent highly resolved measurement of the subsurface porosity or hydraulic head at a specific three-dimensional location. For instance, the conventional porosity values will be derived from tests conducted on a 6-inch core. Similarly, the conventional head values will be derived by measuring water levels in clustered piezometers installed with 3-inch screens. Since it will be necessary to evaluate the accuracy of the probe measurements by comparing probe sensor results with results from conventional methods that may not provide a true value of the subsurface properties, it becomes essential to recognize that there may not be a way to overcome this challenge. However, errors associated with long soil samples or screens will be minimized by collecting and documenting multiple probe values over the depth range of soil samples and head measurements.

3.5 Precision. Precision refers to the reproducibility of measurements of the same characteristic, usually under a given set of conditions. The direct-push sensors' primary utility is for in-situ sensing as the probe is pushed into the subsurface. Since a single measurement is made for each discrete depth, multiple measurements at identical locations are not possible. Therefore, since one cannot collect multiple measurements from discrete locations on the soil, precision assessments on subsurface measurements are not generally possible.

Although there is no approach currently available that can render precision estimates for subsurface sensor measurements, the precision of the method can be estimated using static measurements of probe data while on the surface. The estimate of the method precision will be generated through the use of load cell calibration devices (for soil type precision), GeoVIS porosity estimates using standard soils (for porosity measurement precision), and through the use of pressure calibration devices (for piezocone transducer calibration). This quality control approach should provide a best-case estimate of the precision of each of the probe measurement methods.

Precision for the confirmatory laboratory methods will be evaluated by the QA/QC data generated by the analytical laboratory while adhering to the SOPs for the API Dean Stark method provided in an Addendum once the analytical laboratory has been selected. Precision for the aquifer slug tests will be determined by running each evaluation (e.g., specific slug-in and slug-out tests) in triplicate.

C.4 Calibration Procedures, Quality Control Checks, and Corrective Action

Calibration procedures, method-specific QC requirements, and corrective action associated with nonconformance QC for the direct push sensor technologies and reference methods are described in the following subsections.

4.1 High-Resolution Piezocone calibration. At the start and end of each day, and when abnormal behavior is suspected, a calibration of the piezocone system components is performed. The calibration procedure utilizes a load cell system check, as well as a temperature and barometric system check. The customized transducer is factory calibrated with precision equipment over the appropriate temperature and pressure ranges, and calibration curves and correction factors are incorporated into the probe operational software. Each transducer has a unique temperature calibration curve and associated macro for automated pressure correction. While in the field, extra high-resolution pressure transducers will be available in case of system failure or aberrations are observed.

4.3. GeoVIS Calibration Procedures. At the start and end of each day, and when abnormal behavior is suspected, a GeoVIS porosity calibration step is performed on well-characterized soil samples placed in front of the sapphire window. Another GeoVIS calibration step consists of placing a scale over the viewing window for the camera system to adjust the focus and electronic scales that are imposed on the images during image collection.

4.4 Strain Gauge Calibration. Strain gauge calibration is performed in accordance with ASTM standard D3441. A load cell device and an automated software procedure are used to determine the scale and offset converting strain gauge output in millivolts to tons per square foot, for both the sleeve and cone tip strain gauges. This procedure is required each time a different probe assembly is used or when strain gauge zero checks (performed after each push) differ from zero by more than 1 ton per square foot (TSF) for the sleeve and 10 TSF for the cone tip.

4.5 Performance Evaluation Materials. Performance evaluation (PE) samples will not be used for the field component of this demonstration. The direct-push sensing technologies are dynamic in-situ measurement techniques that are not amenable to performance evaluation checks. The only minor exception would be for soil samples collected and analyzed for porosity using the API Dean Stark method, which will then be compared to the GeoVIS in-situ porosity estimates. However, the depth range over which a porosity value is determined is very different for these two methods, so the evaluation is limited. Furthermore, performance evaluation will not be possible until after laboratory results are compiled and submitted. Therefore, this will not allow for use in a performance audit mode during probe field operations.

4.6 Duplicate Samples. Due to the nature and spatial configuration of in-situ direct-push measurement approaches, duplicate samples and measurements cannot be collected by direct-push sensors. During aquifer testing, slug tests will be conducted in triplicate for each of the parameter sets. For instance, a slug-in test performed with a one-foot hydraulic differential will be conducted three times, and the mean value and standard deviation recorded.

C.5 Demonstration Procedures

The high-resolution piezocone and GeoVIS do not require a warm-up period. No maintenance is required for any of the sensors except in case of equipment failure. Most direct-push sensor components are replaceable in the field within an hour.

The sensor probe operators will verify the completeness of the appropriate data forms, and the completeness and correctness of data acquisition and reduction protocols. The confirmatory laboratory and field project manager will review calculations and inspect laboratory logbooks and data sheets to verify accuracy, completeness, and adherence to the specific analytical method protocols. Calibration and QC data will be examined by the field project manager, sensor probe operators, and the laboratory supervisor.

Laboratory project managers and QA managers will verify that all instrumentation is functioning properly, and that QA objectives for accuracy, completeness, and method detection limits are met.

Analytical outlier data are defined as those QC data lying outside a specific QC objective window for precision and accuracy for a given analytical method. Should QC data be

outside of control limits, the confirmatory laboratory or field team supervisor will investigate the cause of the problem. If the difficulty involves an analytical problem, the sample will be reanalyzed, and the push may be re-advanced in an adjacent location. If the problem can be attributed to the sample matrix, the result will be flagged with a data qualifier. This data qualifier will be included and explained in the final analytical report. A copy of the confirmatory laboratory's Quality Assurance Manual will be included along with the laboratory procedure SOPs in an Addendum once an analytical laboratory is selected for conducting the API Dean Stark porosity estimation method.

5.1 Data Reporting. The following data will be reported:

1. Field data plots from all pushes, including the dynamic cone pressure, pressure dissipation analyses, GeoVIS porosity logs, GeoVIS screen captures, sleeve friction, and soil classification. All push data displaying the raw data collected during the pushes as well as analog and digital video data.
2. Raw and tabulated system check and calibration data.
3. Stab sampling logs indicating soil sample collection information, including sample numbers, depth of samples, location of water table, and other relevant information concerning the collection of the soil samples; chain-of-custody documentation associated with soil samples.
4. Laboratory results for soil porosity measurements, including the standard analytical results and quality control data.

The data for the direct-push sensor probes and the confirmatory analytical laboratory results will be maintained by NFESC, with back-up copies maintained by PWC San Diego. NFESC will provide independent QA oversight for all demonstration activities.

C.6 Calculation of Data Quality Indicators

Data quality indicators will be derived using standard statistical approaches where applicable, and advanced statistical approaches where appropriate. For instance, for porosity measurement indicators, laboratory values will be compared to means of multiple probe estimates collected over the sampling depth range for the soil sample

analyzed in the laboratory. Standard t-tests and analysis of variance will be used to determine the level of comparability, and to identify specific categorical factors potentially contributing to observed variability.

For the modeling component of this demonstration, kriging will be used to interpolate parameter measurements for conceptualization, render three-dimensional representations based on probabilities, document interpolation assumptions through selection of appropriate variogram model estimation parameters, and to determine residuals based on observed variabilities. Furthermore, transport models generated through use of interpolated distribution of hydrogeologic parameters (measured and inferred) will be assessed by comparing tracer breakthrough predictions to field observations using the clustered piezometer network.

All statistical assumptions and results will be presented in the final project report.

C.7 Performance and System Audits

The following audits will be conducted during this demonstration. These audits will help determine whether this demonstration plan is being implemented as intended.

7.1 Performance Audit. Performance evaluation (PE) samples will not be used for this demonstration. The direct-push sensing technologies are dynamic in-situ measurement techniques that are not amenable to performance evaluation checks. PE samples may be used for the laboratory samples.

7.2 On-Site System Audits. On-site system audits for sampling activities, field operations, and laboratories are not a part of the NFESC test plan, but could be carried out at the direction of the ESTCP project manager. On-site system audits and inspections will take place in the field while the demonstration is being conducted, or at the confirmatory laboratory, and results will be formally reported by the auditors to the project manager. Separate audit reports will be completed following the audits and provided to the participating parties through the NFESC project coordinator.

7.3 Contingency Laboratory. A contingency laboratory would be used if the QC data from the reference laboratory indicate a problem with the data quality. A contingency laboratory has not yet been identified.

C.8 Quality Assurance Reports

QA reports provide management with the necessary information to monitor data quality effectively. Proper QA begins with integration into the demonstration plan. The NFESC, PWC San Diego, SSC-SD, US Army, University of Wyoming, and University of Connecticut data quality managers will ensure that QA is an integral component of all phases of this demonstration project, including the technology demonstration plan, field operations, validation sampling, analytical laboratory analysis, and final reporting. Status and audit reports, briefly described below, will be prepared as required as part of this demonstration project.

8.1 Status Reports. The NFESC project manager, in conjunction with PWC San Diego, SSC-SD, US Army, University of Wyoming, and University of Connecticut will prepare written status reports. These reports, which will be submitted to ESTCP by NFESC at required intervals, will discuss project progress, problems and associated corrective actions, and future scheduled activities associated with the demonstration. When problems occur, the project team members will discuss them, estimate the type and degree of impact, and identify the corrective actions to be taken to mitigate the impact, and to prevent their recurrence.

8.2 Audit Reports. As part of this demonstration project, NFESC, PWC San Diego, SSC-SD, US Army, University of Wyoming, and University of Connecticut partners will follow the QA procedures for the direct-push sensor probes and laboratory analyses detailed in this demonstration plan. The analytical laboratory will follow QA procedures that will be detailed in an Addendum to be submitted upon selection of the analytical laboratory. The resulting QA information will be included as part of the technology evaluation report. Independent QA audits are not a part of this test plan, but may be carried out at the direction of the ESTCP project manager. On-site system audits and inspections will take place in the field while the demonstration is being conducted, or at the confirmatory laboratory, and results will be formally reported by the auditors to the project manager. The NFESC project coordinator will forward independent audit reports to PWC San Diego, SSC-SD, US Army, University of Wyoming, University of Connecticut, and the project Advisory Committee for review and appropriate action.

C.9 Data Format

Probe data will be stored electronically on the direct-push vehicle computers, as well as on a dedicated NFESC computer system maintained by the NFESC point of contact. All

field notes will be maintained using field notebooks and scans of specific pages. All laboratory data will be stored as both hard copy and scanned for archiving purposes. All models generated (including input files and statistics) will be stored on a dedicated computer system located at NFESC, as well as at computer systems located at University of Connecticut and University of Wyoming. Unanticipated field and laboratory events, as well as responses to these events will be documented in hard copy as well as electronically. At specific intervals, all electronic data will be backed up onto CD-Rom disks, which will be stored in a dedicated drawer located at NFESC. All hard copies of project materials will also be retained in this drawer.

C.10 Data Storage and Archiving Procedures

Probe data will be stored electronically on the direct-push vehicle computers, as well as on a dedicated NFESC computer system maintained by the NFESC point of contact. All field notes will be maintained using field notebooks and scans of specific pages. All laboratory data will be stored as both hard copy and scanned for archiving purposes. All models generated (including input files and statistics) will be stored on a dedicated computer system located at NFESC, as well as at computer systems located at University of Connecticut and University of Wyoming. Unanticipated field and laboratory events, as well as responses to these events will be documented in hard copy as well as electronically. At specific intervals, all electronic data will be backed up onto CD-Rom disks, which will be stored in a dedicated drawer located at NFESC. All hard raw data documentation, protocols, and reports generated as a result of this demonstration will be retained in a dedicated fireproof drawer located at NFESC. All correspondence and other documents relating to interpretation and evaluation of data will also be archived and retained in this drawer. If at any time key personnel changes occur, a new point of contact for accessing this information will be designated.

**APPENDIX D
HEALTH AND SAFETY PLAN**

SITE CHARACTERIZATION AND ANALYSIS PENETROMETER SYSTEM

***ESTCP CU-0421
DETAILED HYDRAULIC ASSESSMENT USING A HIGH-RESOLUTION PIEZOCONE
COUPLED TO THE GEOVIS***

***Naval Construction Battalion Center Port Hueneme
Port Hueneme, California***

Prepared by:

Jerome W. Fee, Site Health and Safety Officer

Reviewed by:

Christina Graulau, Industrial Hygienist

Code 980, Environmental Department
U.S. Navy Public Works Center

TABLE OF CONTENTS

1. INTRODUCTION	1
1.1 SCOPE AND APPLICATION	1
1.2 SCAPS BACKGROUND	1
1.3 SITE-SPECIFIC APPLICABILITY	1
1.4 SITE BACKGROUND AND HISTORY	1
2. EMERGENCY CONTACT LIST	1
3. KEY PERSONNEL/IDENTIFICATION OF HEALTH & SAFETY PERSONNEL	2
3.1 PERSONNEL LIST	2
3.1.1 <i>SCAPS Project Manager</i>	2
3.1.2 <i>Site Health and Safety Officer</i>	2
3.1.3 <i>All Employees</i>	2
4. TASK/OPERATION SAFETY AND HEALTH ANALYSIS	2
4.1 GENERAL	2
4.1.1 <i>Chemical Hazards</i>	3
4.1.2 <i>Physical Hazards</i>	3
4.2 TASK-BY-TASK RISK ANALYSIS	3
4.2.1 <i>Site reconnaissance and surface geophysical survey</i>	3
4.2.2 <i>Probe Operation</i>	4
4.2.3 <i>Soil and Water Sampling</i>	4
4.2.4 <i>System Calibration</i>	4
4.2.5 <i>Equipment Decontamination</i>	4
5. PERSONNEL TRAINING REQUIREMENTS	5
5.1 GENERAL	5
5.2 TRAINING AND BRIEFING TOPICS	5
5.3 OTHER	5
6. PERSONAL PROTECTIVE EQUIPMENT	6
6.1 PERSONAL PROTECTION LEVEL	6
6.1.1 <i>Level D Protection</i>	6
6.1.2 <i>Level C Protection</i>	6
6.2 LIMITATIONS OF PERSONAL PROTECTIVE EQUIPMENT	7
6.3 WORK MISSION DURATION	7
7. MEDICAL SURVEILLANCE REQUIREMENTS	8
8. FREQUENCY AND TYPES OF AIR MONITORING / SAMPLING	8
8.1 GENERAL	8
8.2 INITIAL AIR MONITORING	8
8.3 PERIODIC AIR MONITORING	8
8.4 ACTION LEVELS	8
8.5 CALIBRATION	9
9. SITE CONTROL MEASURES	9
9.1 GENERAL	9
9.2 SITE MAPS	10
9.3 VISITORS	10
9.4 SITE COMMUNICATIONS PLAN	10
9.4.1 <i>Telephone</i>	10
9.4.2 <i>Visual/Hand Communications</i>	10
9.5 WORK ZONES	10

9.5.1	<i>Exclusion Zone (EZ)</i>	11
9.5.2	<i>Contamination Reduction Zone (CRZ)</i>	11
9.5.3	<i>Support Zone</i>	11
9.5.4	<i>Nearest Medical Assistance</i>	11
9.5.5	<i>Safe Work Practices</i>	11
9.5.6	<i>Avoidance of Excessive Noise Exposure</i>	13
9.5.7	<i>Site Housekeeping</i>	13
9.5.8	<i>SCAPS Deployment</i>	13
10.	DECONTAMINATION	13
10.1	GENERAL.....	13
10.2	SITE-SPECIFIC REQUIREMENTS	13
11.	EMERGENCY RESPONSE / CONTINGENCY PLAN	14
11.1	GENERAL.....	14
11.2	START-UP REQUIREMENTS	14
12.	CONFINED SPACE ENTRY PROCEDURES	14
13.	SPILL CONTAINMENT PROGRAM	14
13.1	GENERAL.....	14
13.2	SPILL RESPONSE EQUIPMENT	15
14.	UPDATES OF HEALTH AND SAFETY PLAN	15

TABLE OF TABLES

TABLE 4-1 OCCUPATIONAL HEALTH GUIDELINES AND TOXICOLOGICAL INFORMATION	(ATTACHMENT E)
TABLE 5-1 PERSONNEL TRAINING REQUIREMENTS	5
TABLE 8-1 ACTION LEVELS	9
TABLE 9-1 HAND SIGNAL DEFINITION	10
TABLE 13-1 SPILL RESPONSE EQUIPMENT	15

LIST OF ATTACHMENTS

- ATTACHMENT A - SITE BACKGROUND AND HISTORY**
- ATTACHMENT B - EMERGENCY CONTACT LIST**
- ATTACHMENT C - MAP TO NEAREST MEDICAL TREATMENT FACILITY**
- ATTACHMENT D - DAILY SITE LOG/COMPLIANCE AGREEMENT FORM.**
- ATTACHMENT E –TABLE 4.1 – OCCUPATIONAL HEALTH GUIDELINES AND TOXICOLOGICAL INFORMATION**

1. INTRODUCTION

1.1 *Scope and Application*

The purpose of this Site-Specific Health and Safety Plan (HASP) is to describe site-specific health and safety requirements for work conducted by Public Works Center San Diego (PWCSO) personnel while operating the Site Characterization and Analysis Penetrometer System (SCAPS). The generic SCAPS HASP was originally developed by the Navy Environmental Health Center (NEHC) for use on the two SCAPS trucks supported by Naval Facilities Engineering Service Center (NFESC), one of which is operated by PWCSO. PWCSO has modified the generic SCAPS HASP to include project-specific information.

This plan is intended to meet requirements of the Occupational Safety and Health Administration's (OSHA) Hazardous Waste Operations and Emergency Response regulation, 29 CFR 1910.120 and applies to all on-site personnel including visitors. All personnel on site, including visitors, will be informed of site emergency response procedures and any potential fire, explosion, health, or safety hazards of on-site activities. This HASP summarizes potential hazards and defines protective measures planned for site activities.

1.2 *SCAPS Background*

SCAPS provides an in-situ investigation of subsurface geophysical features and hydrocarbon contamination. SCAPS is a self-contained truck with enclosed working compartments for personnel to operate the penetrometer probe system and hydrocarbon detection / subsurface characterization data acquisition system. SCAPS performs the investigation by hydraulically pushing the penetrometer probe into the subsurface and collecting data. When the SCAPS push is completed, the penetrometer is withdrawn and decontaminated with a brush / hot steam solution system before entering the truck. SCAPS provides the decontamination water and collects the waste water in a closed system.

SCAPS has the capability to deploy several types of probes including a laser-induced fluorescence (LIF) probe, a piezocone probe, soil and groundwater sampling probes, and a probe that installs small-diameter wells (microwells). Because of the decontamination system under the truck, all equipment is decontaminated prior to being handled by personnel. Potential for exposure to contaminated soil and/or groundwater occurs when soil or water samples are removed from a sampler, or when microwells are sampled.

1.3 *Site-Specific Applicability*

The body of this HASP is written as a generic document in modular form. Site-specific information is provided as supplements and are included as Attachments. The Attachments are located at the end of this HASP. **This HASP shall be considered complete only with the following Attachments:**

- ATTACHMENT A - SITE BACKGROUND AND HISTORY**
- ATTACHMENT B - EMERGENCY CONTACT LIST**
- ATTACHMENT C - MAP TO NEAREST MEDICAL TREATMENT FACILITY**
- ATTACHMENT D - DAILY SITE LOG/COMPLIANCE AGREEMENT FORM.**

1.4 *Site Background and History*

The specific site background and history pertaining to the SCAPS objectives are presented in Attachment A.

2. EMERGENCY CONTACT LIST

An emergency contact list is provided as a site-specific document and is found in Attachment B. A map/description detailing the most direct route to the nearest hospital or medical treatment center is included in Attachment C. The emergency contact list and route map to nearest medical facility shall be conspicuously posted throughout the SCAPS and personnel vehicles.

3. KEY PERSONNEL/IDENTIFICATION OF HEALTH & SAFETY PERSONNEL

3.1 Personnel List

This section describes, in detail, the task descriptions of the Project Manager, Site Health and Safety Officer, and all personnel, as it applies to the health and safety aspects of the SCAPS program.

3.1.1 SCAPS Project Manager

The SCAPS Project Manager is identified on the cover sheet of the HASP as well as in Attachment B, "Emergency Contact List". The SCAPS Project Manager is ultimately responsible for ensuring all site personnel abide by requirements set forth in this plan. The SCAPS Project Manager will oversee and direct field activities.

3.1.2 Site Health and Safety Officer

The SCAPS Project Manager will serve as the Site Health and Safety Officer (SSO). The SCAPS Project Manager/SSO is identified on the cover sheet of this HASP as well as in Attachment B, "Emergency Contact List". In the SCAPS Project Manager's absence, the Site Project Manager will serve as the alternate SSO. The SSO will be responsible for field implementation and will be familiar with health and safety requirements specific to the project. The SSO will hold a site-specific safety meeting for all on-site personnel prior to the start of on-site operations. Daily "tailgate" safety meetings, prior to the start of the day's operations, will also be held. The SSO will also document each person entering the contamination reduction zone (CRZ) or exclusion zone (EZ) on the Daily Site Log included as Attachment E.

The Site Health and Safety Officer is responsible for coordinating with a representative of the medical facility designated in Attachment B explain the nature of the SCAPS operation and determining their willingness and capability of treating a potential chemically contaminated patient. The suitability of the medical facility shall be determined prior to its inclusion in this Health and Safety Plan.

3.1.3 All Employees

All personnel participating in these field activities are required to read and comply with all sections of this plan. All personnel entering the site must sign the Daily Site Log Compliance Agreement Form. Subcontractors and other contractors must comply with 29 CFR 1910.120 training, medical surveillance, and fit testing requirements. Subcontractors and other contractors are responsible for providing their own personal protective equipment, and are directly responsible for the health and safety of their own employees. At least two persons on-site will be trained and certified in emergency first aid and cardiopulmonary resuscitation (CPR). The SSO shall identify and document the certified personnel on Attachment E, "Daily Site Log", prior to the start of field operations. These employees will participate in a Bloodborne Pathogen program, in accordance with 29 CFR 1910.1030, "Bloodborne Pathogens." Some of the requirements of this standard include using universal precautions as the approach to infection control, providing and using handwashing facilities, providing and using personal protective equipment, such as latex gloves. Any Naval Medical Clinic, can provide support in this area.

4. TASK/OPERATION SAFETY AND HEALTH ANALYSIS

4.1 General

The purpose of the SCAPS is to provide in-situ sampling data used to identify and determine the extent of subsurface petroleum contamination and provide a three-dimensional plume visualization for subsurface petroleum contamination. Since the soils are not normally removed from the ground during penetrometer operations, direct exposure to petroleum contamination is minimal. In addition, the hardware which contacts potentially contaminated soils is decontaminated prior to personnel contact.

NOTE:

THIS PLAN APPLIES ONLY TO SAMPLING FOR PETROLEUM PRODUCTS. IT MAY NOT MEET OCCUPATIONAL HEALTH AND SAFETY REQUIREMENTS IF APPLIED TO SITES WHERE OTHER CONTAMINANTS ARE SUSPECTED (SEE ATTACHMENTS FOR SITE-SPECIFIC INFORMATION).

4.1.1 Chemical Hazards

Potential exposure to petroleum products may occur through inhalation, dermal contact, and ingestion. Additionally, the chemicals listed in Table 4-1, "Occupational Health Guidelines and Toxicological Information", (located at the end of the report for convenient field reference) may be encountered during site activities. Exposure to contaminated media is expected to be minimal due to the type of operation.

The following is a list of all Material Safety Data Sheets (MSDSs) which are used in the field for operation of the SCAPS vehicle and equipment. Copies of these MSDSs are available at PWC Environmental Department Headquarters, located at 2730 McKean Street, Building 398, San Diego, CA 92136. Upon request, a copy of these MSDSs will be provided via fax, hand-delivery, or other means. MSDSs are not required on-site for hazardous substances which might be encountered at the site, however if hazardous substances are encountered, MSDSs shall be provided to the site in a timely manner (via fax) upon request.

1. Antifreeze-Navy
2. Battery, Alkaline Manganese Dioxide Cell
3. Battery, Gel-Lead
4. Battery, Lead-Acid, Sealed
5. Battery, Nickel Cadmium
6. Bentonite
7. Brake Fluid, Super Heavy Duty, DOT 3 & 4
8. Cement, Portland
9. Fuel, Diesel No. 2
10. Gasoline, Unleaded
11. Hydraulic Fluid, C3
12. Nitrogen gas
13. Quinine Sulfate, Monohydrate
14. Sikament ESL

4.1.2 Physical Hazards

Physical hazards associated with SCAPS operations include those of heavy equipment, utility power lines, hidden obstacles, noise, heat, cold, and poor illumination. Injuries from physical hazards can be avoided by adopting safe work practices and using caution when working with machinery. Safe work practices are described in Section 9.5.5. The Site Health and Safety Officer will conduct and document regular safety inspections and will make sure that all workers are informed of any potential physical hazards.

4.2 Task-by-Task Risk Analysis

4.2.1 Site reconnaissance and surface geophysical survey

The purpose of site reconnaissance surveys are to determine access requirements and limitations. Surface geophysical surveys are performed to screen proposed push locations for subsurface obstacles that may damage the penetrometer. No chemical hazards are expected during this task. If unusual odors, soil discoloration, or other sign of chemical contamination are noted, the area shall be evacuated immediately. Physical hazards would be associated with uneven terrain, temperature extremes, improper lifting, contact with overhead power lines, and vermin. Level D personal protection equipment is appropriate for these hazards. Observing safe work practices as described in Section 9, Site Control Measures, and the Specific Standard Operating Procedures should eliminate physical hazards.

4.2.2 Probe Operation

The penetrometer probe is pushed into the ground by a hydraulic press. Once in the ground, the sensors are operated remotely from the surface. For the laser induced fluorescence system, the laser excites the soil adjacent to the probe. A second fiber collects and transmits the response from the soil to instruments in the truck. The intensity of the response is proportional to the concentration of petroleum, oil and lubricants in the subsurface soil. Chemical hazards are not expected during this operation. For the piezocone, the forces exerted by the soil are monitored at the surface and real-time data is archived using an on-board CPU. For the GeoVIS, soil images generated are monitored at the surface and archived using the same CPU. Physical hazards may include improper lifting, contact with underground utilities, improper use of laser equipment, and heavy equipment operation. Observing safe work practices described in Section 9, Site Control Measures, and the Specific Standard Operating Procedures, should eliminate physical hazards.

4.2.3 Soil and Water Sampling

Occasionally, the workers may collect soil and water samples. The sampling process is similar to push operations. The sample collection device is hydraulically pressed into the ground and retrieved once the collection device is filled with sample. Soil samples are contained in a stainless steel sleeve and water samples are contained in appropriate sample containers supplied by the laboratory. Once a soil sample is retrieved, the sleeve ends have to be sealed using teflon tape and plastic caps. Groundwater is transferred to sample containers via teflon tubing and/or a bailer. There is opportunity for direct dermal contact with soil and/or groundwater that may be contaminated. Chemical exposures may occur during this operation. The requirement to use personal protective equipment (PPE), described in Section 6, "Personal Protective Equipment", of this plan, combined with the requirement to wash arms, face and hands before eating or smoking should prevent exposure through inhalation, dermal or ingestion pathways.

Physical hazards may include improper use of laser equipment and improper lifting. Observing safe working practices, described in Section 9, Site Control Measures, and the Specific Standard Operating Procedures, should eliminate physical hazards.

4.2.4 System Calibration

The system calibration procedure may include inoculating soil samples (less than 50 grams) with a small amount of petroleum product (less than 2 grams). A small portion of the inoculated sample is placed on the sapphire window. Chemical exposures are expected to be minimal. Physical hazards include exposure to laser light and improper lifting. Safe work practices described in Section 9, Site Control Measures, and the Specific Standard Operating Procedures, should eliminate these hazards.

4.2.5 Equipment Decontamination

Significant quantities of potentially hazardous wastewater will be generated during equipment decontamination operations. Note that to date, all tests of SCAPS decontamination wastewater have yielded no detectable levels of target compounds. The decontamination operations are automated so that the only potential for exposure would be during the removal of the vacuum pump and securing of the drum lid. Chemical exposures may potentially occur during this operation. Level D personal protective equipment described in Section 6, Personal Protective Equipment, should minimize potential exposures. If direct dermal contact with the suspected contaminated water or soil occurs, wash the affected area with soap and water immediately.

Reusable sampling equipment will be decontaminated before and after each use. During decontamination activities, workers shall use personal protective equipment (PPE), described in Section 6, "Personal Protective Equipment".

Physical hazards may include improper lifting. Observing safe working practices, described in Section 9, Site Control Measures, and the Specific Standard Operating Procedures, should eliminate physical hazards.

5. PERSONNEL TRAINING REQUIREMENTS

5.1 General

All on-site personnel who may be exposed to hazardous conditions are required to complete 40-hours of off-site training in accordance with 29 CFR 1910.120. In addition, supervisors must have successfully completed an additional 8 hours of supervisory training. All employees must have three days of supervised field experience. Eight-hour annual refresher training is required for all on-site employees. The personnel training requirements are summarized in Table 5-1. Copies of current training and medical clearance documents are available at the PWC Environmental Department Headquarters, located at 2730 McKean Street, Building 398. Upon request, copies of these documents will be provided via fax, hand-delivery, or other means.

Subcontractor and other contractors are required to submit proof of current training status.

Table 5-1 Personnel Training Requirements

PERSONNEL	TRAINING REQUIRED
All workers	40 hours HAZWOPER training 3 days field work with a trained, experienced supervisor
Supervisors	40 hours HAZWOPER training 3 days field work with a trained, experienced supervisor 8 hours additional supervisory training
All site workers	8 hours annual refresher training
A minimum of two on-site workers	First Aid/CPR training Bloodborne pathogen training

5.2 Training and Briefing Topics

Prior to on-site activities beginning, the Site Health and Safety Officer will brief all site personnel on the following topics:

- a) Identification of the project manager and the alternate project manager
- b) Site History
- c) Physical and chemical hazards
- d) Personal protective equipment requirements
- e) Work tasks
- f) Site control measures
- g) Emergency communication
- h) Emergency procedures
- i) Emergency phone numbers
- j) Emergency routes

5.3 Other

Any other health and safety related topics that may arise before on-site activities begin will be discussed at the in-briefing. Issues that arise while implementing on-site activities will be addressed during tailgate safety meetings. Any changes in procedures or site-specific health and safety related matters will be addressed during these meetings.

6. PERSONAL PROTECTIVE EQUIPMENT

6.1 *Personal Protection Level*

All on-site personnel will be equipped with personal protective equipment appropriate for the hazardous material being handled and the nature of the work being completed. The levels of personal protective equipment to be used for work tasks have been selected based on known or anticipated hazards and expected concentrations of materials found on the site. The site-specific conditions are presented in the attachments to this HASP.

Personnel must wear protective equipment when field activities involve known or suspected atmosphere contamination,; when vapors, gases or particulates may be generated by site activities; or when direct contact with skin may occur. Respirators may be worn to protect lungs, gastrointestinal tract, and eyes against airborne toxicants. Chemical-resistant clothing may be worn to protect the skin from contact with skin-destructive and absorbable chemicals.

The anticipated primary level of protection necessary for field activities at the site will be Level D. Level D protective equipment will be modified to include additional protective equipment where skin contact with contaminants is reasonably anticipated.

6.1.1 Level D Protection

- a) Steel-toed boots with shanks.
- b) Hard hat.
- c) Work pants and shirt or coveralls (disposable or reusable).
- d) Work gloves for equipment operators (optional).
- e) Chemical-resistant gloves (latex or nitrile) for sampling personnel.
- f) Safety glasses or goggles (when appropriate).
- i) Hearing protection (when appropriate)..

When performing normal SCAPS operations at a petroleum site, if there is any indication that a higher level of protection is needed, (i.e., respiratory protection) evacuate the area and request assistance from the facility's health and safety officer.

If the site conditions described in the attachments to this HASP specify the need, the following additional protective equipment may be required for soil or groundwater sampling operations, thus upgrading from Level D to Level C protection.

6.1.2 Level C Protection

- a) Air-purifying respirator equipped with NIOSH/MSA approved combination organic chemical and high efficiency particulate air (HEPA) cartridges.
- b) Disposable, chemical-resistant one-piece suit (such as Tyvek coveralls).
- c) Disposable, chemical-resistant gloves (inner and outer pair).
- d) Disposable, chemical-resistant shoe/boot covers.
- e) Chemical-resistant safety glasses, or face shield attachment to the hard hat.

Meeting all of these criteria permits use of Level C protection:

Measured air concentrations of identified substances, with adequate warning properties, are reduced by the respirator to a level at or below the substances's permissible exposure limit and the concentrations are within the service limit of the respirator cartridge as well as the respirator's protection factor rating.

Atmospheric contaminant concentrations do not exceed IDLH levels, and oxygen content is greater than or equal to 19.5%.

Atmospheric contaminants, liquid splashes, or other direct contact does not adversely affect the small area of skin left unprotected by chemical-resistant clothing.

Job functions are determined not to require self-contained breathing apparatus.

Continual surveillance utilizing direct-reading instruments is conducted to detect changes in air quality necessitating a higher level of respiratory protection.

6.2 Limitations of Personal Protective Equipment

Personal protective equipment designated for use during site activities has been selected to provide protection against contaminants at known or anticipated concentrations in soil or water. However, no protective garment, glove, or boot is entirely chemical resistant, nor does any protective clothing provide protection against all types of chemicals. Permeation of a given chemical through personal protective equipment depends on contaminant concentrations, environmental conditions, the physical condition of the protective garment, and the resistance of the garment to the specific contaminant. Chemical permeation may continue even after the source of contamination has been removed from the garment.

To obtain the optimum use from personal protective equipment, the following procedures will be followed by all site personnel:

- a) Duct tape will be used to ensure that disposable coveralls and gloves are tightly joined when personnel are working within contaminated zones.
- b) When using disposable chemical-resistant coveralls, don a new, clean garment after each rest break (if taken outside the exclusion zone) or at the beginning of each shift
- c) Inspect all clothing, gloves, and boots before and during use for the following:
 - i) imperfect seams
 - ii) non-uniform coatings
 - iii) tears
 - iv) poorly functioning closures
- d) Inspect reusable garments, boots and gloves both before and during use for visible signs of chemical permeation such as the following:
 - i) swelling
 - ii) discoloration
 - iii) stiffness
 - iv) brittleness
 - v) cracks
 - vi) signs of puncture
 - vii) signs of abrasion

Reusable gloves, boots or coveralls exhibiting any of the above signs must be discarded. Reusable personal protective equipment will be decontaminated in accordance with procedures in Section 10, Decontamination, and neatly stored in the support zone, away from contaminated or potentially contaminated materials.

6.3 Work Mission Duration

The Site Health and Safety Officer shall determine the work mission duration. Factors for determining the duration include the following:

- a) Ambient temperatures
- b) Weather conditions

- c) Capacity of personnel to work in the designated level of personal protective equipment.

7. MEDICAL SURVEILLANCE REQUIREMENTS

All employees will be in a medical surveillance program. The content and frequency of the examination will be decided by a board-certified occupational medicine physician based upon anticipated exposures and personal protective equipment. The physician will provide a written opinion as to whether the employee has any detectable medical condition that would place the employee at increased risk from working on a hazardous waste site. The medical examinations can be obtained from the local Navy Medical Treatment Facility. If there is a problem locating this facility, PWCS Environmental Office can be contacted for assistance (see Attachment B, "Emergency Contact List").

8. FREQUENCY AND TYPES OF AIR MONITORING / SAMPLING

8.1 General

Air monitoring will be performed during push operation, soil and water sampling, system calibration, and equipment decontamination (see Sections 4.2.2 - 4.2.5) to determine personnel exposure to airborne hazards and to determine appropriate personal protective equipment levels. All monitoring will be performed as close to the worker's breathing zone as practicable on workers most likely to be exposed to hazardous air contaminants. All air monitoring data will be logged by the equipment, and either recorded on data sheets, or provided by downloading of data from the equipment at the end of the workshift.

8.2 Initial Air Monitoring

Initial monitoring will be performed before beginning any work task to determine background levels and to detect any potentially hazardous situation that might have developed during off-shift periods. The monitoring will be performed using real-time field survey instrumentation, such as a photoionization detector (PID) with a 10.7 eV lamp or an organic vapor analyzer (OVA). Colorimetric detector tubes, for example Draeger tubes, are also acceptable. Lower explosive levels (LEL) and oxygen (O₂) levels will also be determined.

8.3 Periodic Air Monitoring

Air monitoring will be conducted periodically when the following situations arise:

- a) Work begins on a different portion of the site.
- b) Contaminants other than those previously identified are encountered.
- c) A different operation is initiated.
- d) Obvious lithologic changes are noticed during probe activities.
- e) Workers experience physical difficulties.

8.4 Action Levels

Table 8-1 summarizes hazardous conditions, detection methods, and required actions for various conditions which may endanger personnel.

Table 8-1 Action Levels

INSTRUMENT	READING	ACTION
PID/OVA OR Draeger Tubes	> 10 ppm above site background	Evacuate area immediately
	< 10 ppm yet above background	Continue monitoring
Combustible Gas Meter	< 10% LEL	Continue work
	10% - 25% LEL	Stop work, identify source and take corrective actions before proceeding with work
	>25% LEL	Evacuate area immediately
Hydrogen Sulfide Gas Meter	<1-5 ppm	Continue work
	>5 ppm	Stop work, identify source and take corrective actions before proceeding with work
	> 10 ppm	Evacuate area immediately
Carbon Monoxide	<1-25 ppm	Continue work
	25-199 ppm	Stop work, identify source and take corrective actions before proceeding with work
	> 200 ppm	Evacuate area immediately
Oxygen Meter	<19.5% or >22%	Evacuate area immediately

8.5 Calibration

All instruments will be calibrated according to the manufacturer's instructions. This documentation will be logged by the equipment and either recorded on data sheets or provided by downloading of data from the equipment at the end of the workshift. All instruments shall be periodically maintained according to the manufacturer's instructions.

9. SITE CONTROL MEASURES

9.1 General

Work areas on or near the site will, depending on suspected contamination levels, be divided into an exclusion zone (EZ), a contamination reduction zone (CRZ), and a support zone. Access to the EZ will be restricted to authorized personnel. A daily roster will be kept for all personnel working in such an area and shall include: date of each person's entrance into the contaminated zone, the person's name, signature and organization; the time of entry; and the time of exit. Any visitors to the area must be authorized to be on the site. Visitors must comply with all provisions of this HASP. The Site Health and Safety Officer will identify work areas that visitors are authorized to enter and will enforce site control measures.

9.2 Site Maps

Site maps are provided in the work plan. If necessary, the site maps will clearly show the following:

- a) Exclusion zone
- b) Support zone
- c) Decontamination zone
- d) Traffic routes
- e) Hazardous waste collection site(s)
- f) Storage facilities
- g) Parking facilities
- h) Sanitary facilities
- i) Location of telephones
- j) Location of emergency equipment, such as personnel eyewash stations
- k) Physical hazards, such as underground and overhead utilities

9.3 Visitors

At a minimum, the Site Health and Safety Officer will verbally provide a summary of the HASP contents. Otherwise, all site visitors will be required to read the HASP. Visitors are expected to comply with all relevant OSHA requirements and to provide their own personal protective equipment as required by the HASP. Any site visitors who do not meet OSHA training and medical surveillance requirements will not be permitted to enter the contamination reduction zone or the exclusion zone. Visitors who are eligible to enter the contamination reduction zone or the exclusion zone, are required sign the daily site log/compliance agreement form.

9.4 Site Communications Plan

9.4.1 Telephone

Location of telephone services will be determined during site mobilization. In addition, the SCAPS truck has two cellular phones as standard operating equipment. Emergency phone numbers will be prominently posted for easy access. Dialing procedures will be included to access both on-site and off-site emergency numbers.

9.4.2 Visual/Hand Communications

The following hand signals will be used by site personnel in an emergency situation or if verbal communications become difficult.

Table 9-1 Hand Signal Definition

<u>SIGNAL</u>	<u>DEFINITION</u>
Hands clutching throat	No air available or cannot breathe
Hands on top of head	Need assistance
Thumbs up	Okay; I'm all right; I understand
Thumbs down	No; negative
Arms waving upright	Send back-up support
Gripping partner's wrist	Exit area immediately

9.5 Work Zones

The Site Health and Safety Officer has the final authority to determine all work zone boundaries based on his/her experience, personal observations, and existing site conditions.

9.5.1 Exclusion Zone (EZ)

A defined EZ will be established at the site during SCAPS deployment activities. The EZ is defined as the space beneath the SCAPS vehicle when the SCAPS system is deployed. An additional EZ is defined as the space within 10 feet of an unconfined soil or groundwater sample. Visitors will not be permitted to enter the EZ without authorization of the Site Health and Safety Officer.

9.5.2 Contamination Reduction Zone (CRZ)

The CRZ is a transition zone between the exclusion zone and the support zone. A decontamination line will be established within the CRZ. The CRZ decontamination station will contain facilities and equipment, such as a wash basin, bucket, soap, towels and a container in which to collect the wash water, to decontaminate personnel and portable equipment, see Section 10, Decontamination. Visitors will not be permitted to enter the CRZ unless authorized by the Site Health and Safety Officer.

9.5.3 Support Zone

The support zone is situated in a clean area outside the CRZ, where the chance of encountering hazardous materials or conditions is very minimal. Visitors will be permitted to enter the support zone only if authorized by the Site Health and Safety Officer.

9.5.4 Nearest Medical Assistance

The nearest medical treatment facility is provided in Attachment C of this HASP. The Site Health and Safety Officer is responsible for coordinating with a representative of the medical facility to explain the nature of the SCAPS operation and determining their willingness and capability of treating a potential chemically contaminated patient. The suitability of the medical facility shall be determined prior to its inclusion in this Health and Safety Plan.

9.5.5 Safe Work Practices

The following is a list of the specific standard operating procedures used in training all SCAPS personnel. A copy of the detailed information provided for each subject is available from PWC Environmental Department Headquarters, located at 2730 McKean Street, Suite 1, San Diego, CA 92136.

1. Safe Use of Heavy Equipment
2. Heat Stress Prevention
3. Cold Stress Prevention
4. Lockout Procedure
5. Avoidance of Electrical Hazards
6. Site Activities Near Utility and Power Lines
7. SCAPS Laser Safety

Following are general safe work practices, applicable to all work sites.

- a) Workers will be informed of any potential trip and fall hazards during regular health and safety meetings such as the daily tailgate meetings. Trip and fall hazards will be eliminated whenever possible, or clearly identified with yellow caution tape.
- b) Use the "buddy system" at all times in the exclusion zone and the CRZ. Do not perform field work alone. Maintain visual, vocal or radio communication at all times. Observe each other for signs of toxic exposure, heat or cold stress. Some indications of adverse effects include, but are not limited to:

- i) changes in complexion and skin discoloration
 - ii) changes in coordination
 - iii) changes in demeanor
 - iv) excessive salivation and pupillary response
 - v) changes in speech patterns
- c) Site personnel will inform each other of non-visual effects of adverse effects, such as, but not limited to:
 - i) headache
 - ii) dizziness
 - iii) nausea
 - iv) blurred vision
 - v) cramps
 - vi) irritation of the skin, eyes or respiratory tract
- d) All site personnel will enter a designated EZ only through the CRZ. All personnel leaving an EZ must exit through the CRZ and undergo decontamination.
- e) Only vehicles and equipment necessary to complete work tasks (such as drilling rigs and support trucks) will be permitted within the EZ. All nonessential vehicles will remain in the support zone.
- f) Whenever possible, avoid contact with contaminated or potentially contaminated surfaces. Walk around, not through, puddles and discolored surfaces. Do not kneel on the ground or set equipment on the ground. Bag equipment to prevent contamination.
- g) Portable eyewash stations will be located near the site.
- h) Matches and lighters are not permitted in the EZ or the CRZ.
- i) Eating, drinking, using tobacco and applying cosmetics are permitted only in designated areas. These activities are never permitted in the exclusion zone or the CRZ; they may be permitted in the support zone upon approval by the Site Health and Safety Officer.
- j) All personnel, at a minimum, will wash their hands and faces before eating, drinking, smoking or applying cosmetics.
- k) All outdoor work will be stopped and workers will seek cover immediately if thunder storms, strong winds, tornadoes or other severe weather conditions enter the area. The Site Health and Safety Officer or Project Manager may stop work if rain or other weather conditions present a potential health and safety threat.
- l) All employees will follow the emergency procedures outlined in this plan.
- m) Employees will report all injuries/illnesses to their supervisor. This includes minor or slight injuries and near miss incidents.
- n) Duct tape will be used to ensure that disposable coveralls and gloves are tightly secured when personnel are working within contaminated zones.
- o) When temperatures fall below 40 °F, a cold stress protocol will be followed. Employees must be supplied with adequate clothing to maintain body core temperature.

- p) When temperatures exceed 70 °F and personnel are wearing impermeable protective clothing, a heat stress protocol will be followed.

9.5.6 Avoidance of Excessive Noise Exposure

Noise levels are not expected to exceed hazardous levels, 84 decibels A scale (dBA). If it is suspected that this is not the case, for instance, if two people standing next to one another have difficulty conducting a conversation in a "normal" tone, the base safety and occupational health office should be contacted so the noise levels can be measured. If levels are found to exceed 84 dBA, hearing protection is required.

9.5.7 Site Housekeeping

Work areas shall be kept orderly so that if an emergency situation occurs, workers can evacuate. An orderly work area can also reduce slip, trip, and fall accidents.

9.5.8 SCAPS Deployment

Specific procedures for deploying the SCAPS equipment are presented in the Work Plan, a separate document. All pushing activities will be performed in accordance with these requirements and those outlined within this HASP.

- a) The SCAPS crew's minimum personal protective equipment will be Level D as discussed in Section 6, Personal Protective Equipment.
- b) Before beginning the initial push and each morning thereafter, the pushroom operators will conduct a thorough inspection of the truck for any defects or unsafe conditions, such as leaking fuel lines or hydraulic lines or fittings, and inoperable or poorly responding controls or equipment. All guards or safety devices shall be operational and in place over rotating machinery. All wire ropes, slings, clevises and other lifting equipment shall be in satisfactory condition and rated for the work to be performed as required in OSHA 29 CFR 1926.550. Any defects identified during inspections will be corrected before pushing begins.
- c) Extreme care will be used during addition or removal of the rods and during startup of the hydraulic ram and leveling equipment. Injury or death can result from being caught or pinched in pushing equipment. Use of verbal commands, hand signals, and line-of-sight confirmation by field crew members will help workers avoid these types of accidents (see Section 9.4.2, Visual/Hand Communications).

10. DECONTAMINATION

10.1 General

During the SCAPS push operations the probe and rods are decontaminated by a steam/brush system as they are pulled from the ground. The rods are decontaminated before entering the SCAPS truck. All contaminated water and soil will be stored in 55 gallon drums supplied by the activity. Drum transportation will be controlled and handled by the activity.

10.2 Site-Specific Requirements

Minimal personnel decontamination is anticipated since Level D equipment will be utilized and it consists mostly of disposable items. If personnel decontamination is necessary, the following procedure will be used. Disposable personal protective equipment will be placed in barrels to be disposed of as hazardous waste by the facility. Non-disposable personal protective equipment will be physically wiped clean and rinsed to the extent possible. If cloth coveralls are utilized, they will be bagged and sent to a laundry which specializes in handling clothing potentially contaminated with hazardous materials. Hands, face and any other exposed skin will be thoroughly washed with soap and water after removing the personal protective equipment. A shower will be taken as soon as possible.

11. EMERGENCY RESPONSE / CONTINGENCY PLAN

11.1 General

In the unlikely event an emergency situation occurs, all employees will evacuate the site immediately and call the appropriate emergency response group for assistance. An air horn or other predetermined alarm will be used to signal evacuation. Personnel involved in the SCAPS operation are not permitted to assist in emergency response without specific permission from the Site Health and Safety Officer. Prior to the start of work, the Site Health and Safety Officer will determine an emergency meeting location. The emergency meeting location is identified in Attachment C. First aid and emergency equipment, as well as a cellular telephone, shall be located both on the SCAPS truck and on a support truck. The Site Health and Safety Officer, utilizing the Daily Site Log/ Compliance Agreement Form, will account for all employees after the evacuation. Employees will be verbally informed of this procedure prior to the start of work.

11.2 Start-up Requirements

Prior to starting work, the Site Health and Safety Officer will determine which emergency services may be required. All emergency phone numbers will be verified. All site activities will be coordinated with the agencies prior to the start of work. Telephone dialing sequences to contact on-site and off-site telephones will be identified. If special dialing procedures are required, this will be clearly noted on the emergency contact list. A copy of this list will be conspicuously posted or maintained near the telephone.

12. CONFINED SPACE ENTRY PROCEDURES

Confined space entries will not be conducted during SCAPS operations.

13. SPILL CONTAINMENT PROGRAM

13.1 General

A very small spill of relatively non-toxic materials, such as hydraulic fluid will be wiped up and/or absorbed and swept up as much as possible and disposed of in accordance with local site procedures. If a larger spill should occur, or one in which more toxic materials are involved, contact the Navy On-Scene Commander or Spill Response Coordinator listed in Table 2-1 for assistance. The following factors will be considered when determining if assistance is needed:

- a) Availability of adequate spill response equipment
- b) Toxicity of spilled material
- c) Potential impact on the environment
- d) Weather conditions (rain, high wind, etc.)

If any doubt exists regarding the need for assistance, the Navy On-Scene Commander or Spill Response Coordinator listed in Table 2-1 shall be contacted immediately. **All spills, regardless of quantity, must be reported to the local environmental office listed in Attachment B, "Emergency Contact List".**

13.2 Spill Response Equipment

The following spill response equipment will be maintained with the SCAPS unit:

Table 13-1 Spill Response Equipment

ITEM	QUANTITY	ITEM	QUANTITY
Shovel	1 each	Oil sorbent pad (2 ft ²)	20 each
PVC sheeting (10ml)	400 ft ²	Water sorbent pad (5'x5")	1 roll
Broom	1 each	Emergency eye wash station	1 each
3M Powersorb Spill Kit & Salvage Drum	1 each	First-aid kit	1 each
Fire extinguisher (Halon/ABC types)	3 each	Compressed air horn	1 each
Cellular telephone	2 each	Chemical resistant gloves	4 pair

14. UPDATES OF HEALTH AND SAFETY PLAN

Updating of this Health and Safety Plan shall be done as frequently as necessary to ensure safe work conditions. Suggestions should be brought to the attention of the Project Manager or Site Health and Safety Officer.

Attachment A - SITE BACKGROUND AND HISTORY

NCBC Port Hueneme is located in Ventura County, California. In 1985, up to 15,000 gallons of leaded and unleaded fuel was reported missing from two underground storage tanks in use at the Navy Exchange Gas Station. This demonstration will be implemented in a fenced-in area located along the downgradient zone of the dissolved MTBE plume resulting from the release. Although the ground water in this area contains dissolved MTBE, no water samples will be collected using the SCAPS probes or attachments. All water samples will be collected from monitoring wells, and analyzed for tracer (rhodamine) concentration using an on-site test kit.

ATTACHMENT B - EMERGENCY CONTACT LIST

Site Health and Safety Officer: Tim Shields– (619) 524-6947, pager: (888) 516-3453

**Primary Contaminants of Concern: Methyl tertiary butyl ether (MTBE) dissolved in ground water.
Minimum Level of Protection: Level D**

PWC Environmental Office Telephone: (619) 524-6924
PWC Office Mailing Address: 2730 McKean Street, Ste 1. CODE 980
San Diego, CA 92136

Mobile Phone On-Site: (619) 890-9438 (SCAPS truck) or (619) 884-1308 (support truck)

EMERGENCY PHONE NUMBERS:

In the event of any emergency, contact Project Manager or Site Health and Safety Officer.

Ambulance:	9-911 (base phone) 911 (cell phone)	Navy PI: Mark Kram (805) 982-2669
Fire:	(805) 982-4595 (or 911) (cell phone)	SCAPS Project Manager: Jerry Fee (619)524-6945
Base Security:	(805) 982-4591	National Response Center: 1-800-424-8802
Hospital:	(805) 988-2500	Chemtec: 1-800-424-9300
Branch Med Clinic:	(805) 982-6301	Poison Control: 1-800-876-4766
PWC Emergency Duty Desk:	(805) 982-2222	
Underground Utilities:	(805) 989-8263	
Additional Navy Contacts:	Dale Lorenzana (805-982-1681); Ernie Lory (805-982-1299); Bill Major (805-982-1808)	

FIRST AID FOR PETROLEUM HYDROCARBON AND TCE EMERGENCIES

Ingestion: DO NOT INDUCE VOMITING. Call Poison Control; follow instructions. Administer CPR, if necessary. Seek medical attention.

Inhalation: Remove person from contaminated environment. DO NOT ENTER A CONFINED SPACE TO RESCUE SOMEONE WHO HAS BEEN OVERCOME UNLESS PROPERLY EQUIPPED AND A STANDBY PERSON IS PRESENT. Administer CPR if necessary. Seek medical attention.

Skin

Contact: Brush off dry material, remove wet or contaminated clothing. Immediately wash with soap, flush skin thoroughly with water. Seek medical attention if irritation persists.

Eye

Contact: Flush eyes with water for 15 minutes. Seek medication attention.

Exposure

Symptoms: Petroleum Hydrocarbons: Headache, dizziness, nausea, drowsiness, irritation or eyes, nose, throat, breathing difficulties. TCE: Headache, vertigo; visual disturbance; tremors; somnolence; nausea; vomiting; eye irritant; dermatitis; cardiac arrhythmia; paresthesia;

Contingency

Plan: Report incident to Project Manager, Site Health and Safety Officer, or Health and Safety Manger after emergency procedures have been implemented.

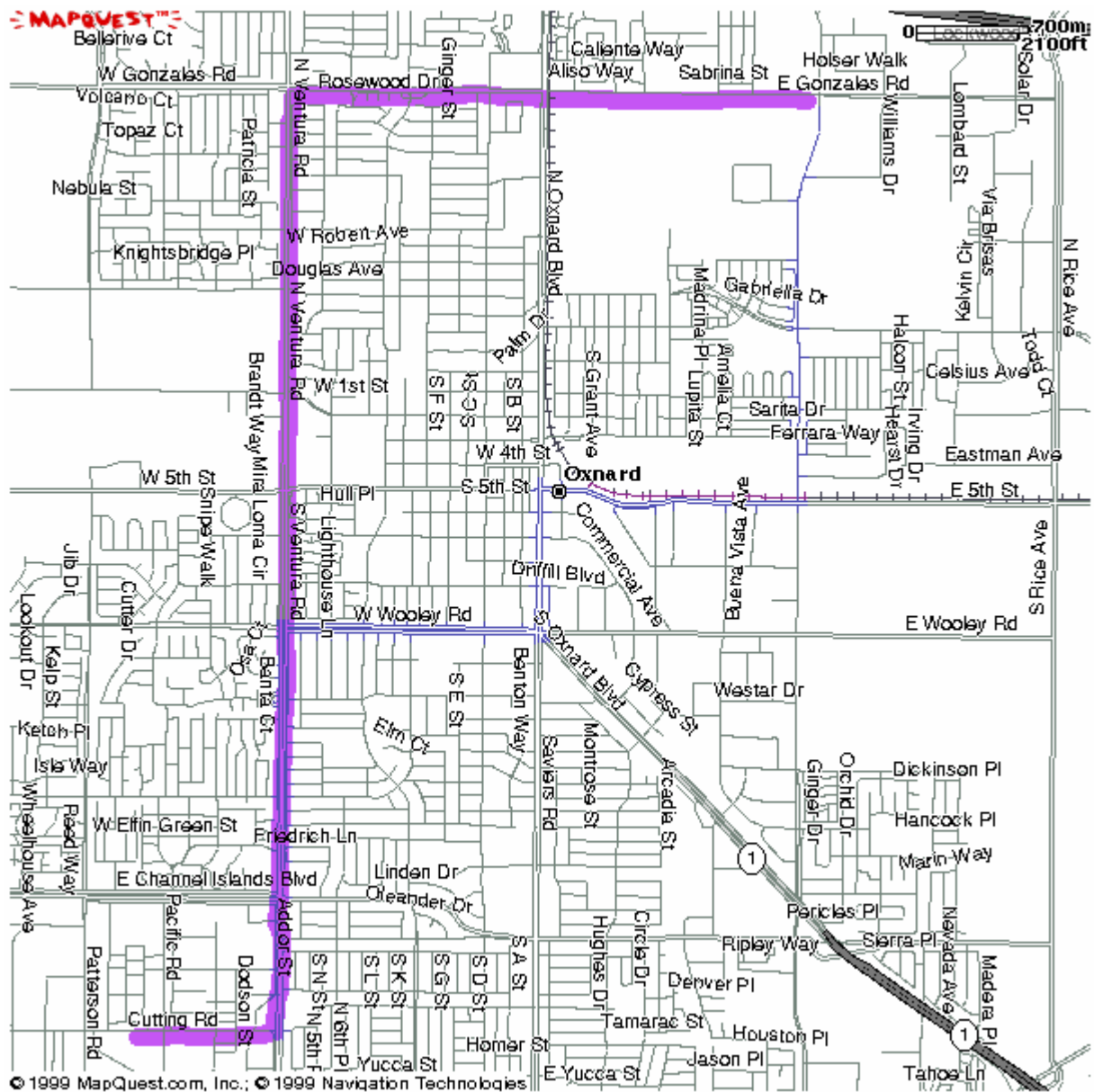
Attachment C - DIRECTIONS & MAP TO NEAREST MEDICAL TREATMENT FACILITY

DIRECTIONS TO ST. JOHN'S REGIONAL MEDICAL CENTER (805) 988-2500

1600 North Rose Avenue
Oxnard, CA 93030

1. Exit NCBC Port Hueneme on Sunkist Road Gate (by SeaBee Museum)
2. Turn left onto Ventura Rd and proceed to Gonzales Ave.
3. Turn right on Gonzales Ave and proceed to St. John's Regional Medical Center, just past Rose Ave. The medical facility is located on the right.

MEDICAL TREATMENT FACILITY MAP(S)



EMERGENCY MEETING LOCATION

SCAPS Support Pickup Truck or location set at daily tailgate meeting.

ATTACHMENT E – TABLE 4.1 – OCCUPATIONAL HEALTH GUIDELINES AND TOXICOLOGICAL INFORMATION

Contaminant	ACGIH TLV (ppm)	NIOSH REL (ppm)	OSHA Ceiling (ppm)	OSHA PEL (ppm)	OSHA STEL (ppm)	NIOSH/OSHA IDLH (ppm)	Ionization Potential (eV)	Routes of Exposure	Symptomology Acute/Chronic
Benzene ^a	10	0.1	15	1	5* *10min peak in any 8hrs	500	9.24	Inhalation Ingestion Contact Skin Absorption	Eye, nose, and respiratory tract irritant; giddiness headache; nausea; staggered gait; fatigue; anorexia; lassitude; dermatitis; bone marrow depressant; CARCINOGEN
Ethylbenzene ^b	100	100	N/A	100	125* *15min peak in any 2hrs	800	8.76	Inhalation Ingestion Contact	Eye and mucus membrane irritant; headache; dermatitis; narcosis; coma.
Toluene ^{b,c}	50	100	300	200	300* *10min max peak per 8hr shift	500	8.82	Inhalation Ingestion Contact Skin Absorption	Fatigue, weakness, confusion, euphoria, dizziness, headache, dilated pupils, lacrimation, nervousness, insomnia, paresthesia, dermatitis.
Xylene, ^{b,c} isomers	100	100	N/A	100	150* *15min peak in any 2hrs	900	8.44- 8.56	Inhalation Ingestion Contact Skin Absorption	Dizziness; excitement; drowsiness, uncoordination, staggering gait; eye, nose, throat irritant; corneal vacuolization; anorexia, nausea, vomiting; abdominal pain; dermatitis.
Methyl tert-Butyl Ether (MTBE)	40 ^d	N/A	N/A	N/A	N/A	N/A	N/A	Inhalation Ingestion Contact Skin Absorption	Loss of appetite, excessive thirst and fatigue. Dangerous fire and explosion hazard.
1,1,1-Trichloroethane ^d (1,1,1-TCA)	350	10	N/A	350	1910* *15min peak in any 2hrs	700	11	Inhalation Ingestion Contact	Headache; lassitude; central nervous system (CNS) depressant; poor equilibrium, eye irritant; dermatitis; cardiac arrhythmia.
JP-4 (Naptha)	N/A	100	N/A	100	N/A	10,000	N/A	Inhalation	Light headedness; drowsiness; eye, nose, and

Notes:	a	The lower value of the two is represented in this table.	f	NIOSH-considered carcinogen.
	b	Common petroleum constituent.	g	TFH is represented as gasoline in this table.
	c	Common constituent of paint.	h	Values are expressed in milligrams per cubic meter.
	d	Common industrial solvent.	i	Asbestos has remote potential that it may be present at the site.
	e	Not available.	j	Values are expressed in fibers per cubic centimeter of air.
			k	Represents the possible pesticides used at the site.

ATTACHMENT E – TABLE 4.1 – OCCUPATIONAL HEALTH GUIDELINES AND TOXICOLOGICAL INFORMATION

Contaminant	ACGIH TLV (ppm)	NIOSH REL (ppm)	OSHA Ceiling (ppm)	OSHA PEL (ppm)	OSHA STEL (ppm)	NIOSH/OSHA IDLH (ppm)	Ionization Potential (eV)	Routes of Exposure	Symptomology Acute/Chronic
JP-5	See Benzene							Ingestion Contact	skin irritant; dermatitis.
1,2-Dichloroethane ^d (DCA)	10	1Ca ^f	100	50	200* *5min peak in any 3hrs	3,000	11.04	Inhalation Ingestion Contact Skin Absorption	CNS depressant; nausea; vomiting; eye irritant, corneal opacity; CARCINOGEN
Methylene ^c Chloride	50	Ca	N/A	25	125* *5min peak in any 2hrs	2,300	11.32	Inhalation Ingestion Contact	Fatigue; weakness; sleepiness; light-headedness; limbs numb, tingling; headache; nausea; eye and skin irritant; CARCINOGEN.
Trichloroethylene ^d	50	Ca ^f	200	100	200/300* *5min peak in any 2hrs	1,000	9.45	Inhalation Ingestion Contact	Headache, vertigo; visual disturbance; tremors; somnolence; nausea; vomiting; eye irritant; dermatitis; cardiac arrhythmia; paresthesia; CARCINOGEN
Diesel Fuel	N/A	N/A	N/A	300	N/A	10,000	N/A	Inhalation Ingestion Contact	Nephrotoxicity; eye, skin, and respiratory tract irritant.
Fuel Oil	N/A	N/A	N/A	100	N/A	10,000	N/A	Inhalation Ingestion Contact	Light headedness; eye, nose, and skin irritant; dermatitis.
Total fuel hydrocarbons ^g (TFH)	300	Ca	N/A	300	500	N/A	N/A	Inhalation Ingestion Contact	CNS depressant; eye, nose and throat irritant; dermatitis; headache.

Notes:	a	The lower value of the two is represented in this table.	f	NIOSH-considered carcinogen.
	b	Common petroleum constituent.	g	TFH is represented as gasoline in this table.
	c	Common constituent of paint.	h	Values are expressed in milligrams per cubic meter.
	d	Common industrial solvent.	i	Asbestos has remote potential that it may be present at the site.
	e	Not available.	j	Values are expressed in fibers per cubic centimeter of air.
			k	Represents the possible pesticides used at the site.

ATTACHMENT E – TABLE 4.1 – OCCUPATIONAL HEALTH GUIDELINES AND TOXICOLOGICAL INFORMATION

Contaminant	ACGIH TLV (ppm)	NIOSH REL (ppm)	OSHA Ceiling (ppm)	OSHA PEL (ppm)	OSHA STEL (ppm)	NIOSH/OSHA IDLH (ppm)	Ionization Potential (eV)	Routes of Exposure	Symptomology Acute/Chronic
4,4'-DDT ^h	1	0.5	N/A	1	N/A	500	N/A	Inhalation Ingestion Contact Skin Absorption	Tongue, lips, and face paresthesia; dizziness; headache; vomiting; eye and skin irritant; tremor.
Chlordane ^{h,k}	0.5	0.5	N/A	0.5	N/A	100	N/A	Inhalation Ingestion Contact Skin Absorption	Blurred vision; confusion; ataxia; delirium, coughing; abdominal pain; nausea; vomiting; diarrhea; tremors, convulsions; anuria. in animals: lung,liver, kidney damage.
Arsenic ^{c,h}	0.01	Ca	N/A	.5*/.01**	0.002***	5	N/A	Inhalation Ingestion	Ulceration of nasal septum; gastrointestinal disturbances; respiratory irritation; skin hyper-pigmentation; CARCINOGEN.
				*Organic Compounds	**Inorganic Compounds				
					***15min max peak any 2hrs				
Beryllium ^{c,h}	0.002	0.005	0.005	0.025*	0.002	N/A	N/A	Inhalation Ingestion	Berylliosis; abnormal low-weight; weakness; chest pain; cough; clubbing of fingers; cyanosis; pulmonary insufficiency; eye irritant; CARCINOGEN.
				*30min peak per 8hr shift					
Chromium ^{c,h}	0.01	0.001	0.1*	0.1*	N/A	15	N/A	Inhalation Ingestion Contact	Irritation to eyes; fibrotic changes to lungs; dermal sensitization; CARCINOGEN.
			*as Chromat es						
Cadmium ^{c,h}	0.01 ^(total) 0.002 ^(resp)	Ca	N/A	0.005	N/A	9	N/A	Inhalation Ingestion	Pulmonary edema; dyspnea; cough; tight chest; pain; headache; chills; muscle ache; nausea; vomiting; diarrhea; mild anemia; CARCINOGEN.
Copper ^{c,h} dusts & mists	1	0.1* *fume	N/A	1	N/A	100* *fume	N/A	Inhalation Ingestion Contact	Irritation to eyes and upper respiratory system; metallic taste; dermatitis in animals; lung, liver, kidney damage; anemia.

Notes:	a	The lower value of the two is represented in this table.	f	NIOSH-considered carcinogen.
	b	Common petroleum constituent.	g	TFH is represented as gasoline in this table.
	c	Common constituent of paint.	h	Values are expressed in milligrams per cubic meter.
	d	Common industrial solvent.	i	Asbestos has remote potential that it may be present at the site.
	e	Not available.	j	Values are expressed in fibers per cubic centimeter of air.
			k	Represents the possible pesticides used at the site.

ATTACHMENT E – TABLE 4.1 – OCCUPATIONAL HEALTH GUIDELINES AND TOXICOLOGICAL INFORMATION

Contaminant	ACGIH TLV (ppm)	NIOSH REL (ppm)	OSHA Ceiling (ppm)	OSHA PEL (ppm)	OSHA STEL (ppm)	NIOSH/OSHA IDLH (ppm)	Ionization Potential (eV)	Routes of Exposure	Symptomology Acute/Chronic
Lead ^{c,h} elemental & inorganic compounds	0.05	0.1	N/A	0.05	N/A	100	N/A	Inhalation Ingestion Contact	Weakness; insomnia; facial pallor; pale eye; anorexia; stomach pain; constipation; colic; anemia; tremor; limp wrist, encephalopathy; neuropathy.
Thallium ^{c,h}	0.1	0.1	N/A	0.1	N/A	15	N/A	Inhalation Absorption Ingestion Contact	Nausea, diarrhea, abdominal pain, vomiting; strabismus; peripheral neuritis; tremors, chest pain; pulmonary edema; psychosis; liver, kidney damage; alopecia.
Zinc ^{c,h}	10	5 ^(fume) 10 ^(dust)	15 ^(total)	5 ^(resp) *15min in any 2hrs as dust	15*	500	N/A	Inhalation	Metal fume fever; chills; muscle ache, nausea, fever; dry throat, cough, weakness; lassitude; metallic taste; headache; blurred vision; low back pain; vomiting; fatigue; tight chest, dyspnea, rales, decreased pulmonary function.
Asbestos ^{i,j}	0.2-2 f/cc	0.1	N/A	0.1-2.0	1 f/cc* *30-min	Ca ^f	N/A	Inhalation Ingestion	Dyspnea, interstitial fibrosis; restricted pulmonary function, finger clubbing; CARCINOGEN with latency period of 20 or more years.
PCBs	N/A	Ca	N/A	N/A	N/A	N/A	N/A	Contact Inhalation	Dermatitis; CARCINOGEN
Freon 113 ^d	1,000	1,000	2,000	1,000	1,250	2,000	11.99	Inhalation Ingestion Contact	Throat irritation; drowsiness; dermatitis.

Notes: a The lower value of the two is represented in this table.
 b Common petroleum constituent.
 c Common constituent of paint.
 d Common industrial solvent.
 e Not available.

f NIOSH-considered carcinogen.
 g TFH is represented as gasoline in this table.
 h Values are expressed in milligrams per cubic meter.
 i Asbestos has remote potential that it may be present at the site.
 j Values are expressed in fibers per cubic centimeter of air.
 k Represents the possible pesticides used at the site.

ATTACHMENT E – TABLE 4.1 – OCCUPATIONAL HEALTH GUIDELINES AND TOXICOLOGICAL INFORMATION

Contaminant	ACGIH TLV (ppm)	NIOSH REL (ppm)	OSHA Ceiling (ppm)	OSHA PEL (ppm)	OSHA STEL (ppm)	NIOSH/OSHA IDLH (ppm)	Ionization Potential (eV)	Routes of Exposure	Symptomology Acute/Chronic
Oil (mist) ^h	5	5	N/A	5	10*	2,500	N/A	Inhalation	None reported.
					*15min peak in any 2hrs				

Notes: a The lower value of the two is represented in this table.
 b Common petroleum constituent.
 c Common constituent of paint.
 d Common industrial solvent.
 e Not available.

f NIOSH-considered carcinogen.
 g TFH is represented as gasoline in this table.
 h Values are expressed in milligrams per cubic meter.
 i Asbestos has remote potential that it may be present at the site.
 j Values are expressed in fibers per cubic centimeter of air.
 k Represents the possible pesticides used at the site.

APPENDIX E

TIME-SERIES GEOPHYSICAL TRACER STUDY

Gary A. Robbins and Benjamin Cagle
Department of Natural Resources Management and Engineering

Lanbo Liu
Department of Civil and Environmental Engineering

University of Connecticut
Storrs, CT

November 10, 2005

Conducted for
Naval Facilities Engineering Service Center
1100 23rd Avenue
Port Hueneme, CA 93043

Acknowledgments

The authors would like to thank the following individuals for their assistance: Dr. Mark Kram, Project Manager; Bryan Long, Kenda Neil, and Dale Lorenzana for their efforts in conducting field testing, data collection and surveying; Dorothy Cannon for logistical support; and Kristina Giano for creating and analyzing the three-dimensional model of the differential resistivity data. This project was funded through a contract (N47408-04-C-7514) with the Naval Facilities Engineering Service Center, Port Hueneme, California and is part of the Environmental Security Technology Certification Program (ESTCP) project 04 E-CU1-010.

Table of Contents

1.0 INTRODUCTION	4
1.1 Background	4
1.2 Objectives	4
1.3 Site Conditions	4
2.0 FIELD TESTING	5
2.1 Hydraulic Conductivity Tests	5
2.2 Gradient Direction and Magnitude Estimates	6
2.3 Background Electrical Conductivity Measurements	8
2.4 Time Lapse DC Resistivity Setup and Methodology	10
2.5 Tracer Injection	14
3. 0 RESULTS	18
3.1 Determination of Differential Resistivity	18
3.2 Differential Resistivity in the Upper and Lower Zones of the Aquifer	19
3.3 Saline Plume Longitudinal and Vertical Variation with Time	22
4.0 IMPLICATIONS AND RECOMMENDATIONS	24
4.1 Flow Path and Velocity of the Saline Tracer in Three-Dimensions	24
4.2 Degree of Hydrodynamic Dispersion	27
4.3 Recommended Locations and Depths for the Piezometers	31
4.4 Implications for the Rhodamine Test	32
5.0 SUMMARY AND CONCLUSIONS	35
6. 0 REFERENCES	36

1.0 INTRODUCTION

1.1 Background

This study was conducted as part of a larger demonstration effort supported by a grant from the Environmental Security Technology Certification Program (ESTCP) 04 E-CU1-010, entitled: *Detailed Hydraulic Assessment Using a High-Resolution Piezocone Coupled to the GeoVIS*. The focus of that study is to demonstrate the use of the SCAPS high-resolution piezocone in combination with the subsurface camera (GeoVIS) as a cost effective and rapid system to determine three-dimensional hydrogeology and ground water flow at contamination sites. To evaluate the effectiveness of this approach the SCAPS will be used to characterize a site at the Naval Facilities Engineering Service Center (NFESC) in Port Hueneme, California. For comparison, the test site will be characterized in three dimensions using a more conventional approach involving the installation of 39 piezometers at 13 locations. Furthermore, a tracer study using Rhodamine dye will be conducted to allow a comparison of velocity and mass flux distribution estimates based on both approaches.

1.2 Objectives

The geophysical study was conducted to help locate and design the piezometer clusters in order to optimize concentration data collection as the tracer migrates in the shallow ground water. The test site used in the overall study is relatively small and flat lying. There are three preexisting perimeter wells at the site within only 50 feet of one another. Given the low hydraulic gradient at the site and the close spacing of the wells, one cannot determine the local hydraulic gradient magnitude and direction with confidence. Furthermore, the previous SCAPS pushes at the well locations revealed that the high permeable layer being tested, although continuous across the site, possesses significant lithologic variation. These factors create uncertainty in locating the piezometer clusters in a manner so as to maximize tracer detection. Ideally the piezometer clusters would be oriented along and on either side of the centerline of tracer migration. The piezometer intakes would be located at depths so as to detect the tracer given advection and dispersion in three-dimensions and instrument limits of detection. The objectives of the geophysical time series tracer test were to empirically determine the direction and rate of tracer migration and the degree of tracer dispersion in three-dimensions. This information was then used to define design parameters for the piezometer clusters. Furthermore, the geophysical data provide information to calibrate an analytical model to help design the Rhodamine dye test.

1.3 Site Conditions

The test site is located on an asphalt covered parking area approximately 50 feet east of building 401 at the Naval Base Ventura County (Figure 1). Prior to this study



Figure 1. DC resistivity geophysical test site.

three SCAPS pushes were conducted at the site and used to determine soil type and well design parameters. Based on the information from the initial pushes, three shallow wells (W-1, W-2 and W-3) were installed in boreholes adjacent to the SCAPS holes (Figure 2). The wells were made of 3/4" PVC with a 3.5 ft. screen and prepack. The screen intervals ranged from 10 to 13.5 feet. Table 1 provides baseline relative location and elevation data. Well W-1 was installed to be the injection well for the tracer test. Wells W-2 and W-3 were installed to help determine the hydraulic gradient and to evaluate the spatial variability in hydraulic conductivity. The stratigraphy of the site based on the SCAPS pushes conducted adjacent to the wells is shown in Figure 3. Based on the SCAPS profiles, all the wells are screened in a silty sand layer that is continuous across the site. At well W-3, the silty sand is interbedded with a sand. At well W-1, the silty sand is interbedded with a sandy silt. Based on the lithology in the screen intervals of the wells, one would expect W-3 to have the highest hydraulic conductivity and W-1 to have the lowest.

2.0 FIELD TESTING

2.1 Hydraulic Conductivity Tests

Prior to conducting the tracer test, hydraulic conductivity tests of the wells were performed over a three day period from February 26 to February 28, 2005. Each well

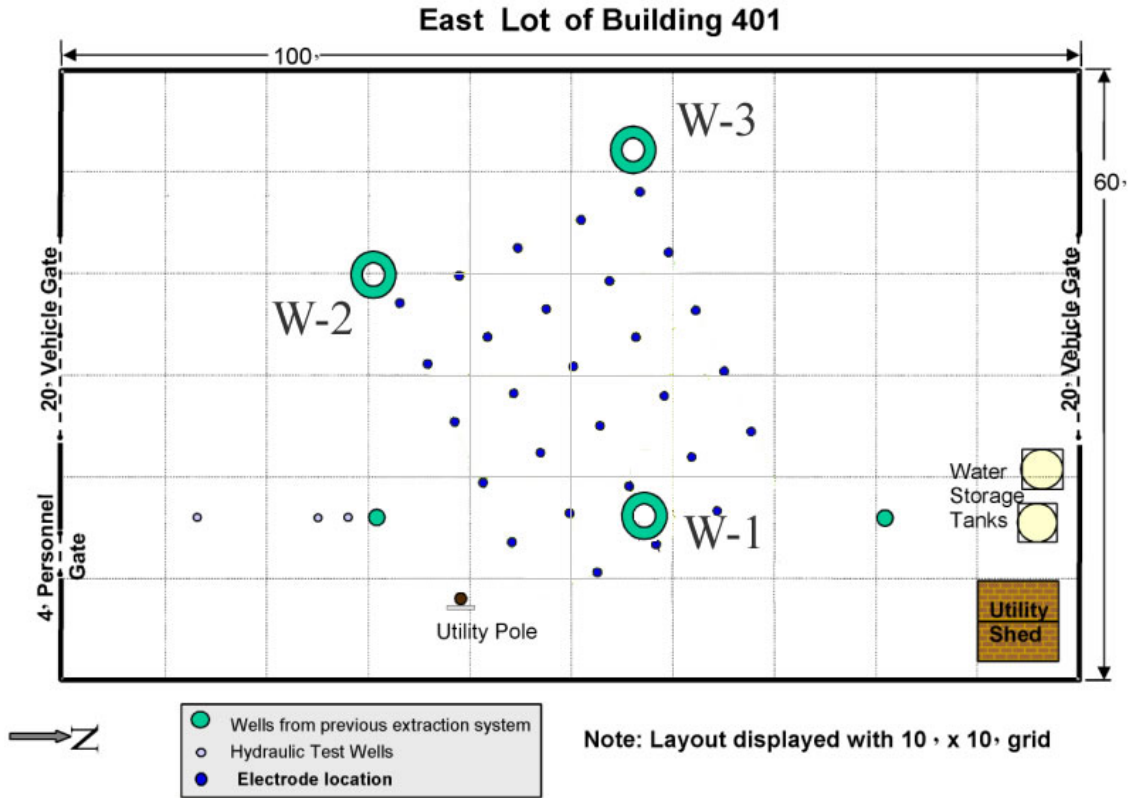


Figure 2. Site layout with geophysical electrodes (7 foot spacing).

was developed by surging and pumping using the method described in Bartlett et al. (2004). Then three pneumatic slug-out tests were performed in each well using a modified version of the Geoprobe Systems pneumatic hydraulic conductivity test system (Bartlett et al.; 2004). Data from the tests are contained in the accompanying spreadsheets in folder KTESTS. The results are summarized in Table 2. The relative variation in hydraulic conductivity amongst the wells was consistent with the lithology determined from the SCAPS pushes. The tests were highly reproducible and yielded a mean hydraulic conductivity of 1.89×10^{-2} cm/s (53.6 ft/day).

2.2 Gradient Direction and Magnitude Estimates

Prior to, during and after the saline tracer test, water level measurements were made in the three wells. They are listed in Table 3. Also shown on the Table are the relative water level elevations computed using the relative well head elevations from Table 1, which were determined by a transit survey. Figures 4 and 5 show the variation in water levels with time. Early variations in the water levels may be due to influences of purging during development and precipitation. During the test period the ground water levels in the wells remained at about 4 feet. The water level in W-2 was consistently shallower than that of the other wells. Well W-1 consistently had the deepest water level.

Table 4 summarizes estimates of the hydraulic gradient direction and magnitude

Table 1. Well Specifications

Well	W-1	W-2	W-3
Rel. Easting (ft)	0.0	-31.6	39.0
Rel. Northing (ft)	0.0	-31.6	4.1
Rel. Well Cover El. (ft)	100	99.52	99.61
Rel Well Head El. (ft)	100	99.59	99.64
Drilled Depth (ft)	14.5	14.5	14.5
Total Well Depth (ft)	13.5	13.5	13.5
Depth to Screen Top (ft)	10	10	10
Screen Length (ft)	3.5	3.5	3.5
Diameter of prepack (ft)	0.27	0.27	0.27
Diameter of hole (ft)	0.27	0.27	0.27
ID Casing (ft)	0.125	0.125	0.125
OD Casing (ft)	0.156	0.156	0.156
Prepack Gradation	20-40	20-40	20-40
PVC schedule 40,	slot 10	slot 10	slot 10
Formation Thickness (ft)	7.2	6.5	7

based on solving a three-point problem for the relative water level elevations in Table 3. The data were processed using Rockworks 2004. It should be noted that the water

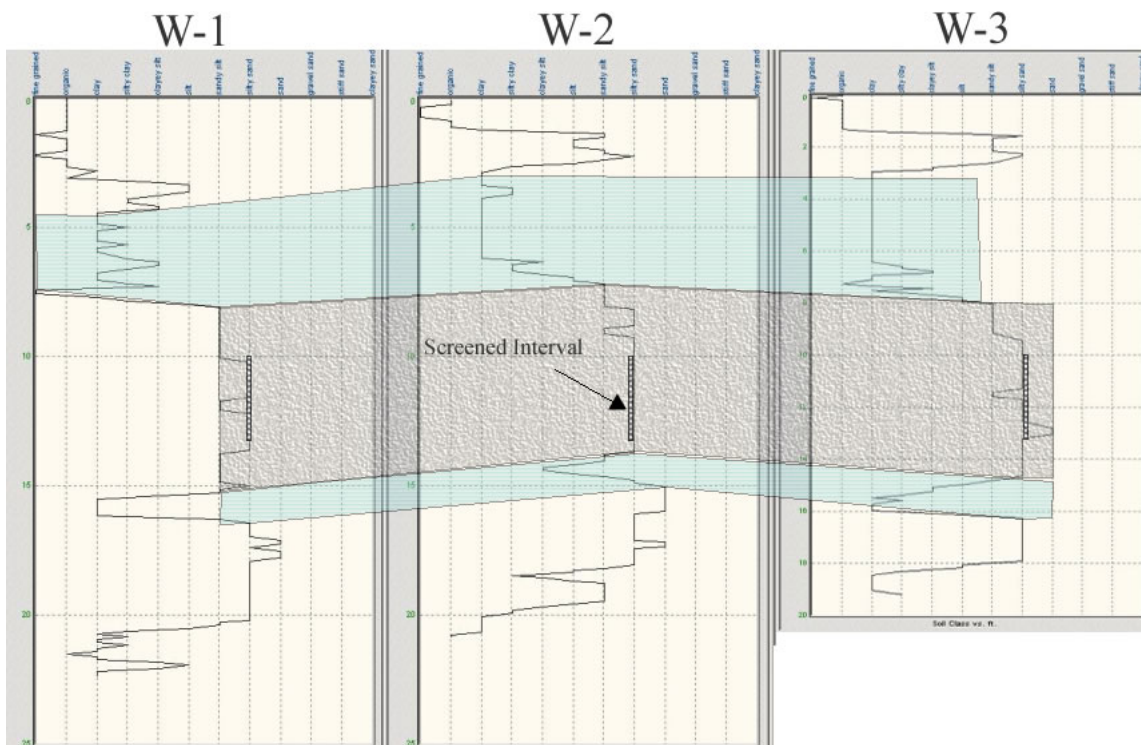


Figure 3. Stratigraphy in vicinity of test site wells.

elevations in the wells differed by less than two tenths of a foot at most monitoring days, making gradient direction and magnitude estimates highly uncertain. The mean gradient was 0.007 and the mean gradient azimuth was 287 degrees. Figure 6 shows the

Table 2. Hydraulic Conductivity Test Results

Well	W-1	W-2	W-3	
date	2/27/2005	2/28/2005	2/27/2005	
Test	K(cm/s)	K(cm/s)	K(cm/s)	
	1	8.52E-03	1.75E-02	2.96E-02
	2	8.69E-03	1.71E-02	2.90E-02
	3	9.61E-03	1.79E-02	3.20E-02
Mean	8.94E-03	1.75E-02	3.02E-02	
Standard Deviation	5.86E-04	4.08E-04	1.59E-03	
%RSD	6.56	2.33	5.26	
Mean of Means (cm/s)	1.89E-02			

Table 3. Water Table Measurements

Date	DTW (ft)			Relative Water Elevation (ft)		
	W-1	W-2	W-3	W-1	W-2	W-3
2/27/05	4.01	3.89	4.27	95.99	95.70	95.37
2/28/05	3.91	4.05	4.3	96.09	95.54	95.34
3/1/05	3.92	4.05	4.3	96.08	95.54	95.34
3/2/05	4.36	3.95	4.09	95.64	95.64	95.55
3/3/05	4.32	3.91	4.06	95.68	95.68	95.58
3/8/05	4.35	3.92	4.06	95.65	95.53	95.72
3/12/05	4.38	4	4.13	95.62	95.46	95.64
3/17/05	4.43	4.07	4.2	95.57	95.39	95.57
3/24/05	4.30	3.9	4.02	95.70	95.57	95.74
4/1/05	4.39	3.99	4.15	95.61	95.44	95.65
4/7/05	4.50	4.1	4.25	95.50	95.34	95.54
4/11/05	4.56	4.17	4.26	95.44	95.33	95.47

mean gradient direction plus and minus one standard deviation superimposed on the site plan map. Based on the mean gradient (0.007) and mean hydraulic conductivity (1.89×10^{-2} cm/s), and assuming an average porosity of 30%, the average linear velocity of the ground water is estimated to be 1.25 ft/day.

2.3 Background Electrical Conductivity Measurements

Following the hydraulic testing, ground water samples were collected and background electrical conductivity (EC) readings were taken in two of the wells. EC readings were taken with a Cole-Parmer handheld instrument calibrated with a 3 mS/cm standard. The EC readings are summarized in Table 5.

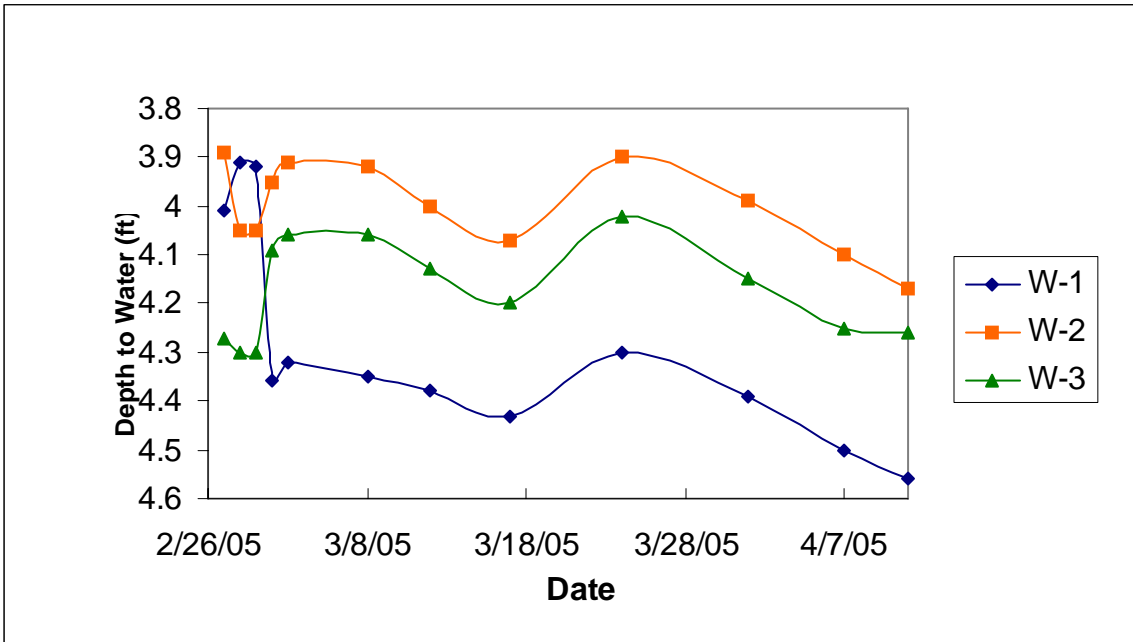


Figure 4. Depth to water levels in perimeter wells.

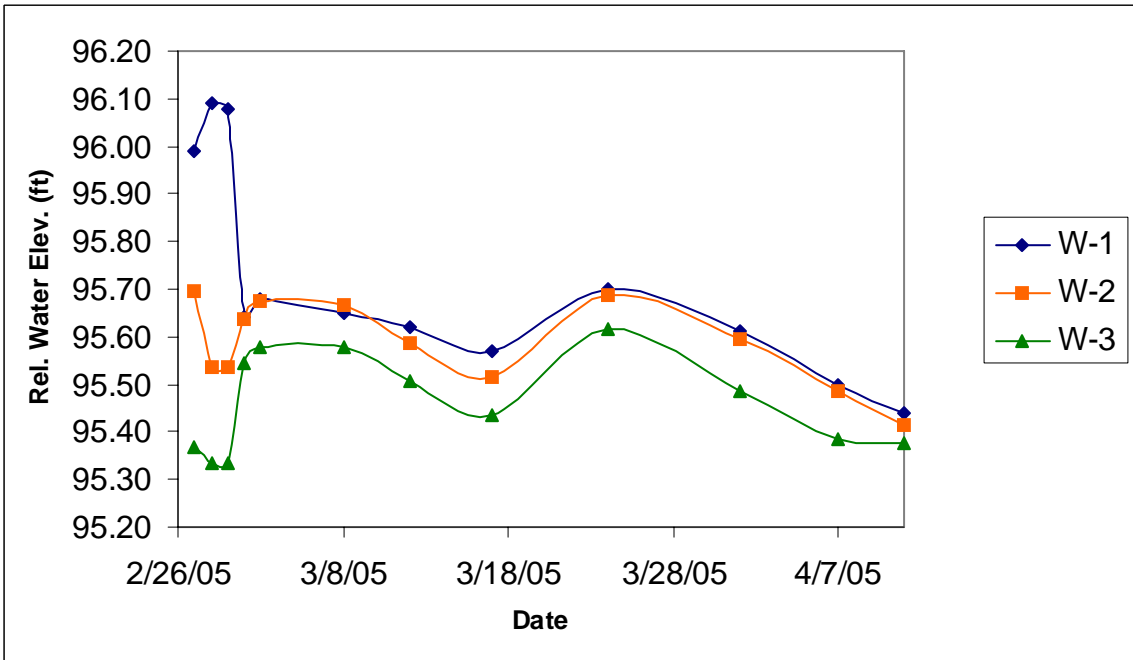


Figure 5. Relative water level elevations in perimeter wells.

Table 4. Ground Water Gradient Magnitude and Direction

Date	Gradient	Azumuth
2/27/05	0.016	291
2/28/05	0.019	275
3/1/05	0.019	275
3/2/05	0.003	225
3/3/05	0.003	225
3/8/05	0.003	324
3/12/05	0.003	302
3/17/05	0.004	297
3/24/05	0.002	309
4/1/05	0.004	311
4/7/05	0.003	311
4/11/05	0.002	299
Mean	0.007	287
Std Dev.	0.007	32
Mean 3/1-4/1	0.005	284
Std Dev.3/1-4/1	0.006	39

Table 5. Background Electrical Conductivity Readings

Well	EC (mS/cm)
W-1	2.83
W-2	Not Measured
W-3	2.98

2.4 Time Lapse DC Resistivity Setup and Methodology

Electrode Array

To track the movement of the saline tracer, a time-lapse DC resistivity survey was conducted. Twenty eight (28) automotive electrodes were installed through the asphalt in a grid pattern with a 7 foot center to center spacing (see Figure 2). Twenty five (25) of the electrodes were installed downgradient of the injection well (W-1) and three (3) were installed upgradient. Electrode locations in the array were designated by (i,j) coordinates with the "i" coordinate oriented Southwest to Northeast and the "j" coordinate oriented Southeast to Northwest. Electrodes at positions (1,1) and (5,1) were lacking. Two additional electrodes were installed at distance from the array along the adjacent road. Electrode B was installed near an electric power pole to the West (harbor direction) about 268 ft from the array. Electrode N was installed near a power pole to the East about 295 ft from the array.

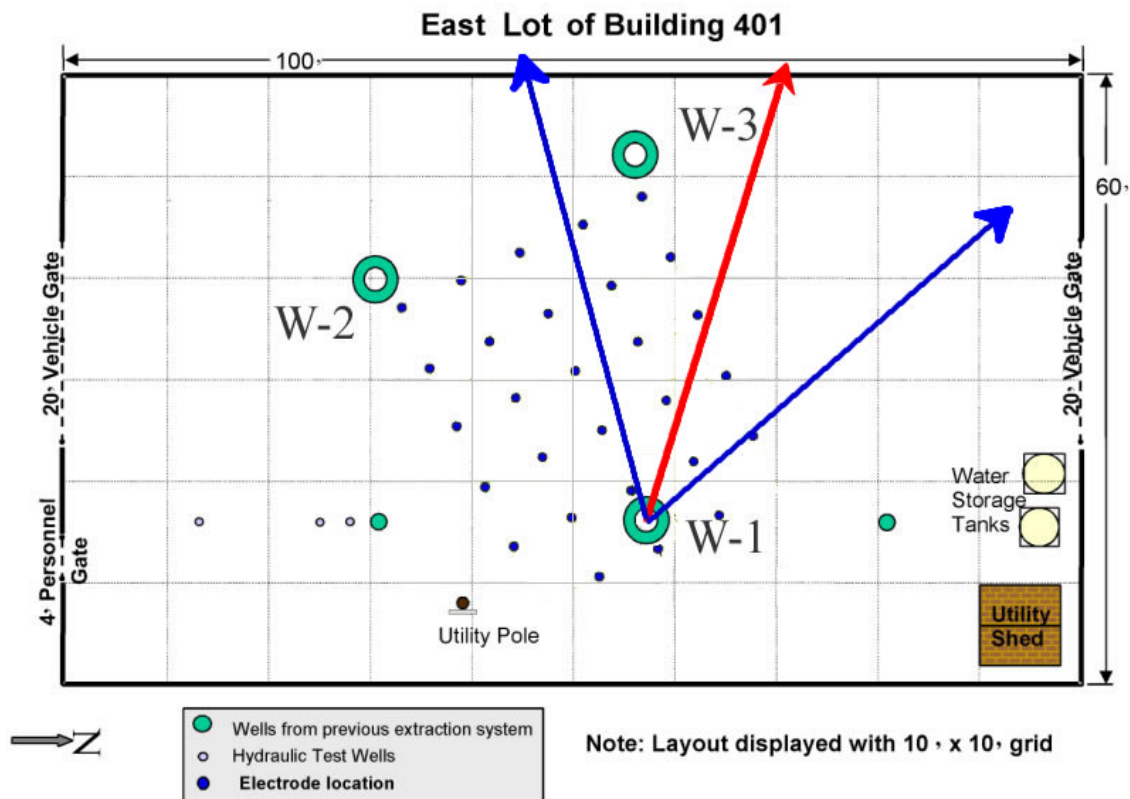


Figure 6. Gradient direction based on water level measurements (red arrow is mean direction, blue arrows are + and - one std. deviation).

Data Acquisition

A DC resistivity pole-pole array was used for data acquisition. The electrodes were connected by wires to an Advanced Geoscience Instruments model Sting R1 resistivity meter with an automatic switch box (see Figure 1). The data acquisition procedure for the pole-pole array entails each of the 28 electrodes serving once as a current injection electrode (A) while the other 27 electrodes work as potential electrodes (M). The distant electrode B serves as the other current electrode. The distant electrode N serves as the other potential electrode.

A complete round of data acquisition takes approximately one working day. First, before the ground resistivity data set was taken, the contact resistances between adjacent electrodes were checked (the 28 electrodes compose 27 pairs). The manufacturer recommends that the contact resistance should be less than 1 to 2 kilo-Ohms for best survey results. At this site, the contact resistance was found to be quite low, mostly around 200 Ohms, indicating the ground is generally conductive. This is consistent with the relatively high electrical conductivity of the ambient ground water. This procedure usually takes only 3 minutes.

Second, data for a Mise-a-la-masse survey was acquired. This acquisition takes 5 minutes. This survey method originates in mineral exploration and entails connecting one of the current electrodes to a conductive ore body. To conduct this survey, one of the current electrodes was put into the ground water in well W-1 where the saline solution was injected. We found, however, that the Mise-a-la-masse method did not generate useful data to monitor the movement of the saline plume. This may have resulted from not maintaining contact with the conductive solution in the ground water as it migrated away from the well.

Third, the pole-pole array data were taken. This procedure usually takes about 3 hours to acquire a total of 756 (28 x 27) readings. This is the main body of each survey.

Fourth, the Mise-a-la-masse data acquisition was repeated.

Finally, the ground contact resistance was measured again for quality control and quality assurance purposes before finishing the resistivity survey. A plot of the contact resistance for all of the surveys is shown as Figure 7. The ground contact resistance appeared to decrease in the course of the study. The highest reading at the beginning of the survey (2/28/05) is about 350 ohms. The highest reading on the last survey day of useful data (4/1/05) is only 242 ohms. This reading occurs at the electrode pair (5,5) and (5,6), the electrodes closest to well W-3.

The site was surveyed thirteen times from 2/28/05 to 4/11/05. The 2/28/05 survey provided a measure of the background resistivity prior to injecting the tracer. Table 6 provides a summary of the field tests performed. Because of instrumentation problems the last two surveys were not analyzed.

Data Processing

In data processing, the resistivity was determined at points in a three-dimensional coordinate system. The origin of the coordinate system ($x=0$, $y=0$, and $z=0$) is at the surface in the Southwest corner of the electrode grid at the virtual electrode array location (1,1). The z -direction is from the surface downward to depth. The y -direction is oriented parallel to a line extending from well W-1 to a point bisecting wells W-2 and W-3. The x -direction is perpendicular to the y -direction.

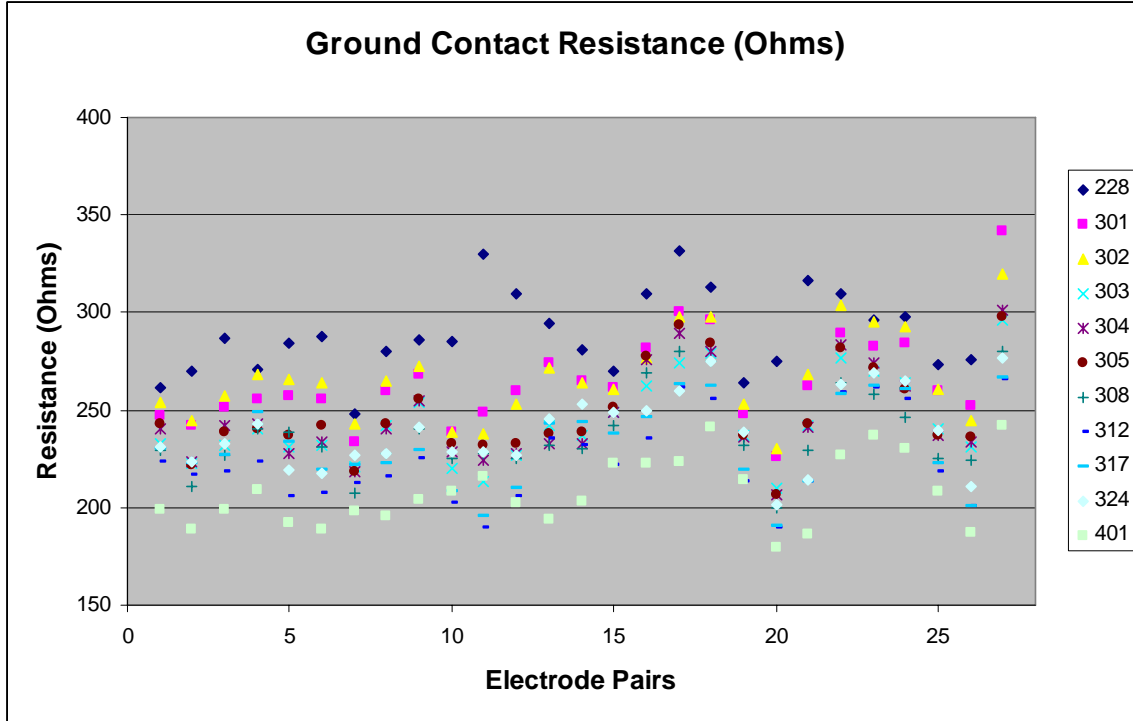


Figure 7. Contact resistance of the electrodes for all survey days (numbers in column to the left refer to the survey date, 228 = 2/28, 301 =3/1, etc.).

The resistivity data were analyzed using a tomographic inversion program based on Zhang et. al. (1995). This method breaks the site into a series of resistivity blocks. The matrix is defined by (the number of sources) x (the number of receivers) x (the number of resistivity blocks). Zhang's program is capable of handling a matrix of 50 x 50 x 20. The inversion is based on the maximum likelihood inverse theory developed by Tarantola and Valette (1982).

The inversion is based on the following equation:

$$(\mathbf{A}_k^T * \mathbf{R}_{dd}^{-1} * \mathbf{A}_k + \mathbf{R}_{mm}^{-1}) \Delta \mathbf{m}_k = \mathbf{A}_k^T * \mathbf{R}_{dd}^{-1} * (\mathbf{d} - \mathbf{G} * \mathbf{m}_k) + \mathbf{R}_{mm}^{-1} * (\mathbf{m}_o - \mathbf{m}_k) \quad (1)$$

where:

- \mathbf{A}_k = sensitivity matrix;
- \mathbf{A}_k^T = transposed sensitivity matrix
- \mathbf{d} = observed data vector
- \mathbf{m} = model vector
- \mathbf{G} = forward modeling operator
- \mathbf{R}_{dd} = data covariance matrix
- \mathbf{R}_{mm} = model covariance matrix
- \mathbf{m}_o = a priori model
- $\Delta \mathbf{m}_k$ = model changes for inversion iteration k

When the increment of the model (here the formation resistivity) is less than a pre-set value of threshold, the iteration stops. This algorithm was used to conduct a tomographic inversion for bulk resistivity for each survey day. Resistivity values were computed for a three dimensional grid with data points between $x = 0$ and 28 feet by 3.5 foot increments, between $y = 0$ and 35 feet by 3.5 foot increments and $z = 0$ to 15 fifteen feet in 1.5 foot increments. Differential resistivity was then computer at each grid node by taking the difference between the resistivity measured on 2/28/05 and that measured on all other survey days.

Table 6: Information on Field Resistivity Tests

Date Surveyed	Personnel	Notes
2/28/2005	Liu, Robbins, Cagle	Background
3/01/2005	Liu, Robbins, Cagle	Conducted immediately after tracer injection
3/02/2005	Liu, Robbins, Cagle	
3/03/2005	Liu, Robbins, Cagle	
3/04/2005	Liu, Robbins, Cagle	Rain. A mistake in PP3D by connected the wire to the injection well A31, so data point 591-577 was replaced by the average of 03 and 05 of March for the 54 data points.
3/05/2005	Liu, Robbins, Neil	
3/08/2005	Neil	
3/12/2005	Neil	
3/17/2005	Neil	The data of March 17 contains a large error of the potential reading at the electrode (4,6) near Well 3. Five readings of rms error reaches 70%.
3/24/2005	Neil	
4/01/2005	Neil	
4/07/2005	Neil	Interrupted survey
4/11/2005	Neil	AC Power failure, last 5 contact resistances were erroneous.

2.5 Tracer Injection

The tracer injection took place on March 1, 2005. A calcium chloride solution was used as the electrical conductivity tracer. The saline solution was prepared by weighing out approximately 90 pounds of granular calcium chloride. The calcium

chloride was then added to 50 gallons of tap water in a plastic drum. The water was circulated in the drum using a peristaltic pump and manual paddle until the calcium chloride was dissolved. It should be noted that the dissolution of the calcium chloride caused the water temperature in the drum to rise. The solution was mixed for approximately an hour. An aliquot was then taken and diluted 400 times for EC measurement. The injection solution had an EC of approximately 55 S/m (540 mS/cm) which was about 180 times that of the background ground water quality. At the time of injection the saline solution had cooled to a temperature of 33°C. The injection system is shown in Figure 8.



Figure 8. Tracer injection system.

The saline solution was injected at a rate to maintain the drawup in the injection well (W-1) at 1 foot or less to help avoid perturbations to the ambient flow field. This was accomplished by lowering a water level sounder to within 1 foot of the water table (4.30 ft BGS) prior to the injection. The saline water was then injected into the well using a peristaltic pump. The injection rate was then lowered if the water level sounder detected a rise in the water level. The injection rates were set using the numbers on a variable rate switch on the pump. The numbers were calibrated to injection rate after the test by pumping water to a volumetric flask for a given time period. The pump calibration plot is shown in Figure 9. Using the calibration curve, the injection rate history was developed and is shown in Figure 10. The injection took approximately 38 minutes. Figure 11 shows the cumulative volume injected as a function of time. The mean injection rate was 1.7 gpm. Immediately after the test, 2.2 liters of freshwater were injected into the well to flush the saline solution out of the well bore that was above the

screen. The water levels in the other wells were monitored before, during and immediately after the injection. No water level changes were detected.

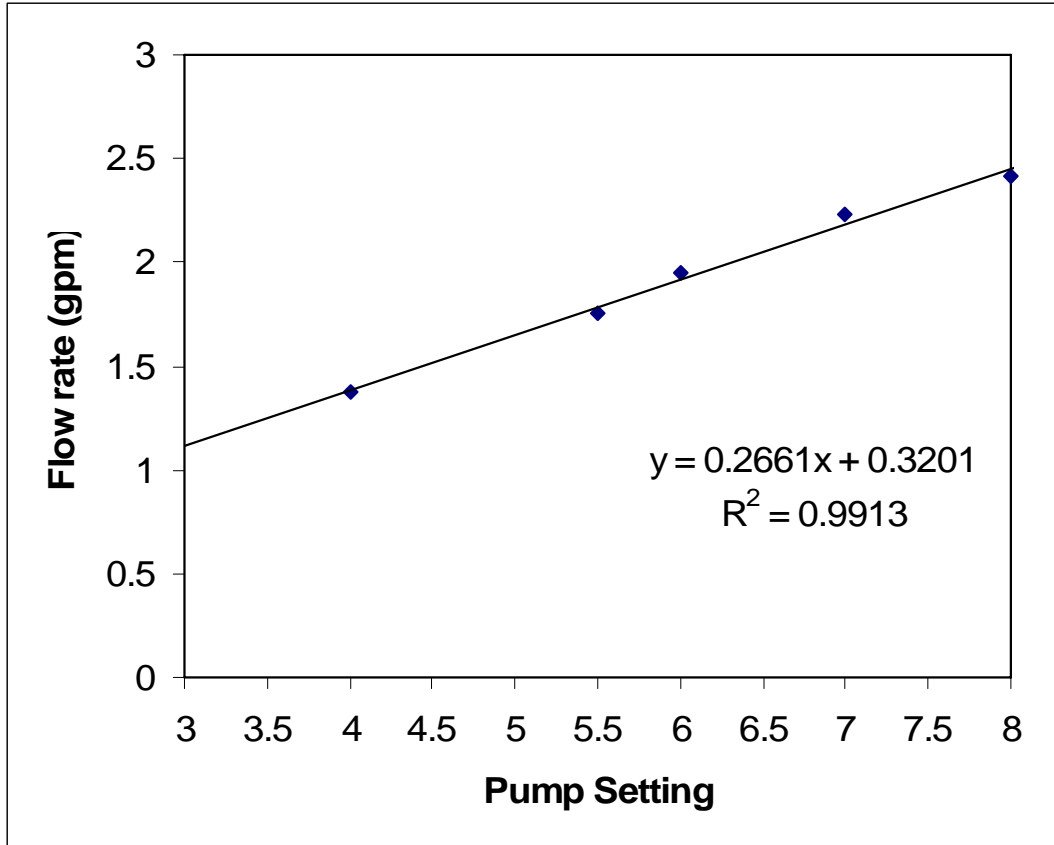


Figure 9. Pump calibration curve.

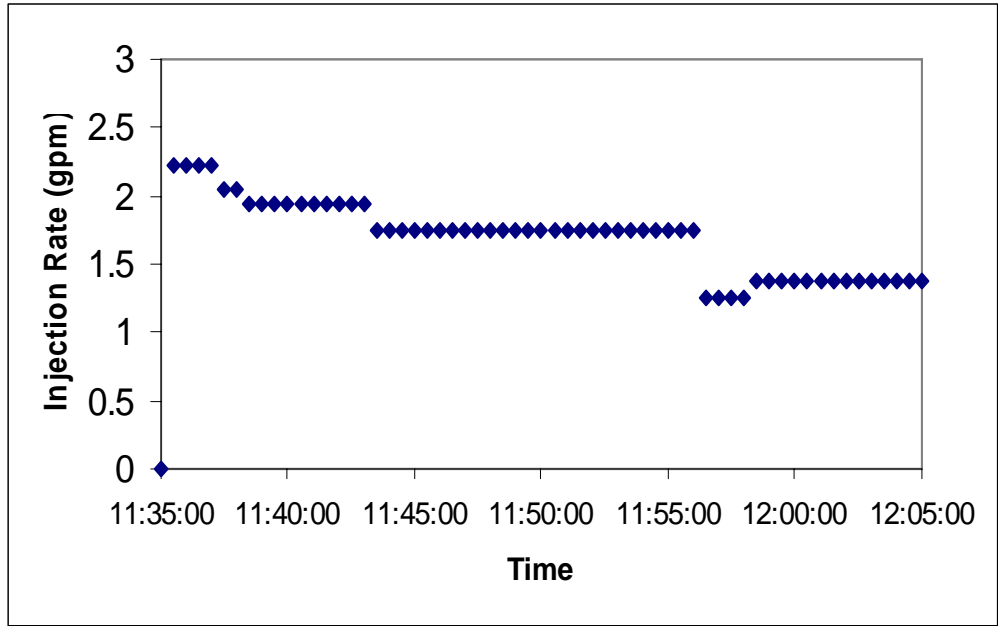


Figure 10. Injection rate variation.

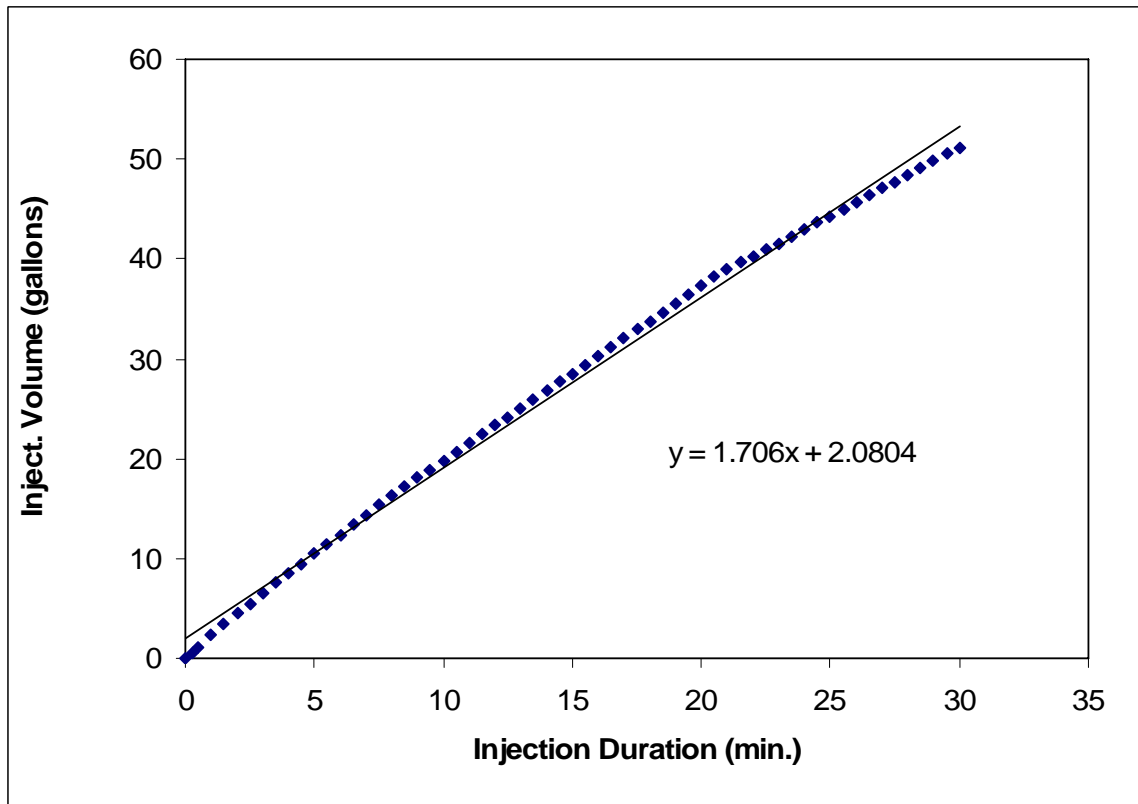


Figure 11. Cumulative injection volume.

3.0 RESULTS

3.1 Determination of Differential Resistivity

The background resistivity for February 28, 2005 is shown in Figure 12. The silty sand zone of interest (about 9 to 15 feet) is characterized by having a higher background resistivity than the layers above and below it. Within this zone, there appears to be an anomaly in the northeast corner of the grid (lower right) that trends southwestward (toward the top). The result serves as the background for doing differences to image the movement of the saline plume.

To show how the saline plume detection works, Figures 13 and 14 were developed. Figure 13 shows the resistivity inversion results for April 1, 2005, the last useful survey day. The differential resistivity for April 1, 2005 (the difference of Figures 12 and 13) is shown as Figure 14. One can observe by this time, the main portion of the tracer had migrated southwestward (toward the top) beyond the probe array. However, some tracer still remains emanating from the source, especially between depths of 9 and 10.5 feet.

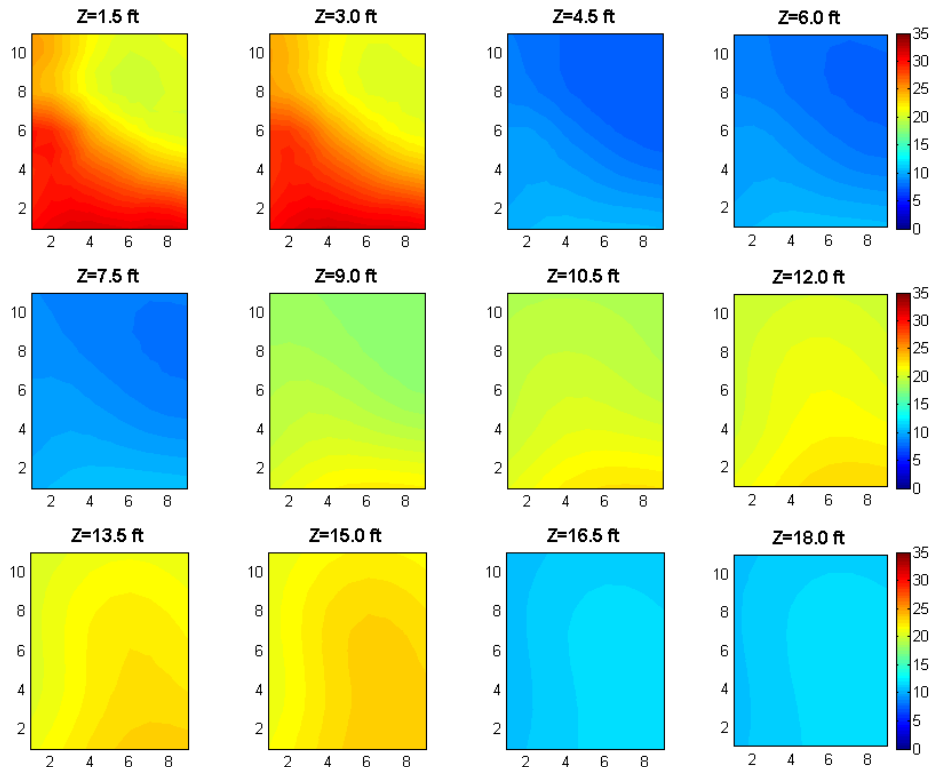


Figure 12. Tomographic inversion results for the formation resistivity on February 28, 2005 at depth 1.5 ft to 18 ft.

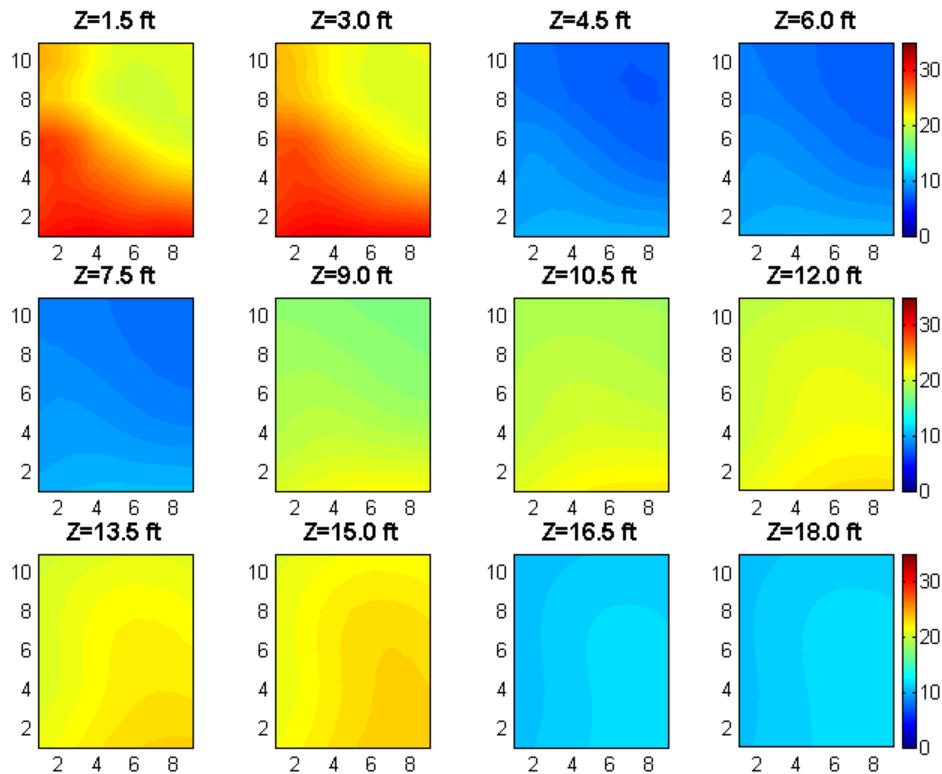


Figure 13. Tomographic inversion results for the formation resistivity on April 1, 2005 at depth 1.5 ft to 18 ft. The unit of the color bar is in Ohm-meters.

3.2 Differential Resistivity in the Upper and Lower Zones of the Aquifer

Figures 15 and 16, show maps of the differential resistivity within the silty sand formation where the saline solution was injected. From the figures, it would appear that the groundwater flow direction is westsouthwest, and that the average velocity is somewhat less than a foot per day. There is no significant difference between the upper zone ($z=10.5-12.0$ ft) and lower zone ($z=13.5-15.0$ ft) of the formation. It appears the flow rate was not constant over time. The saline tracer moved slower at first and much faster at a later time. This is consistent with the variation in hydraulic conductivity at the site. The hydraulic conductivities at wells W-2 and W-3 are 2 and 3 times higher, respectively, than that of W-1.

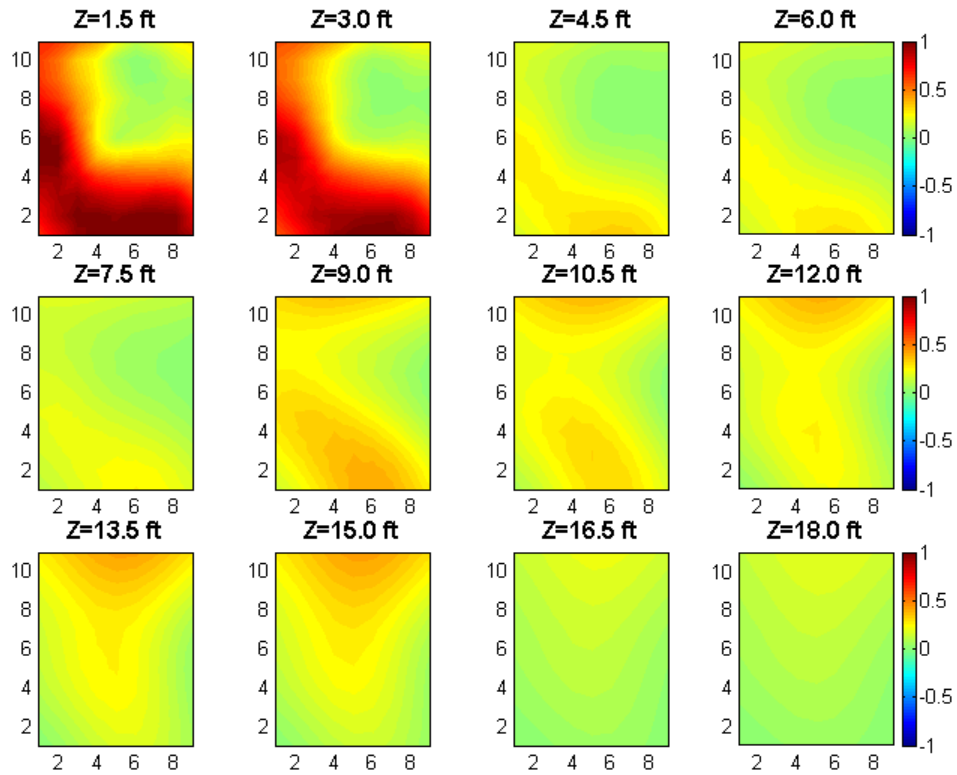


Figure 14. Differential Resistivity by subtracting the results for April 1, 2005 from the results of February 28, 2005. The unit of the color bar is in Ohm-meters.

Depth: 10.5 - 12.0 ft

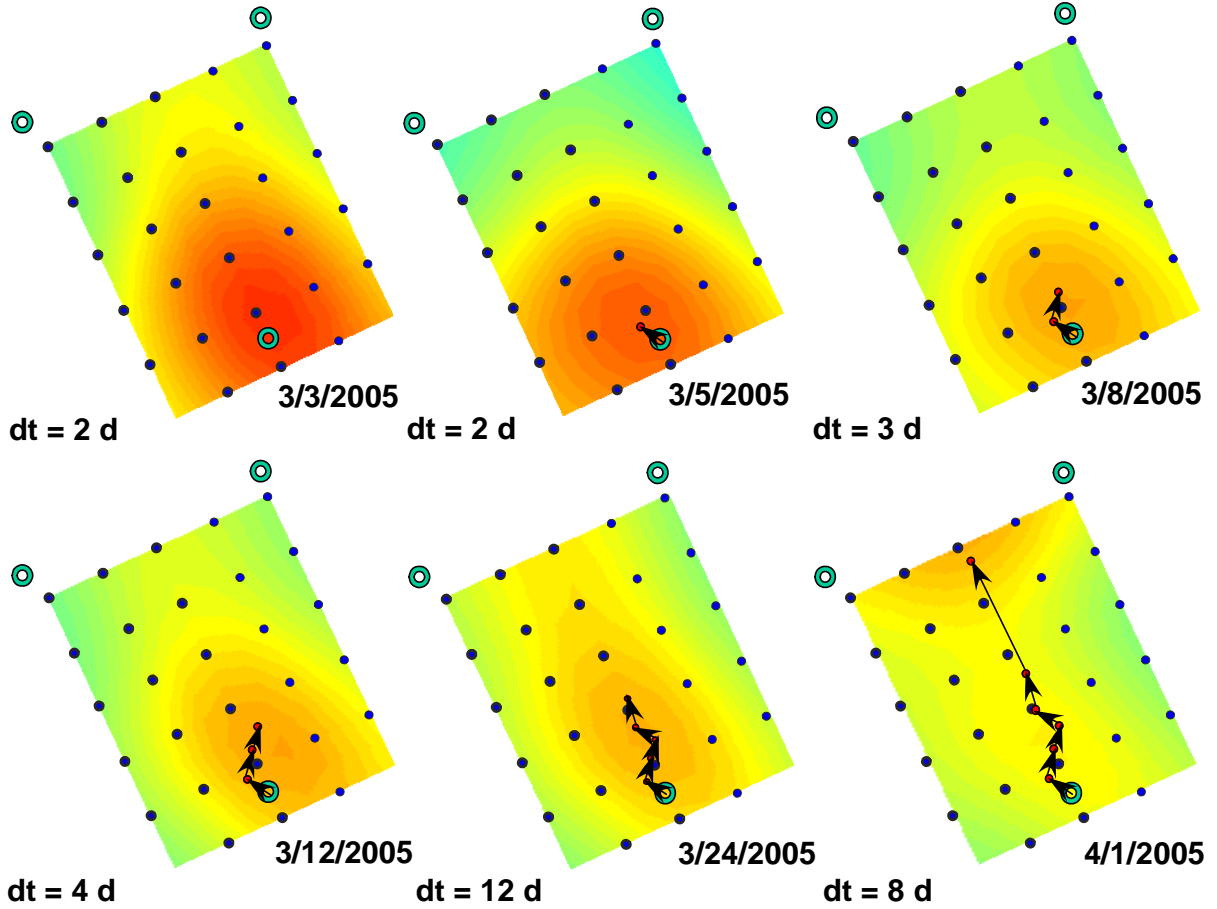


Figure 15. Contours of the differential electric resistivity in the upper zone of the silty sand formation ($z=10.5-12.0$ ft) between the date of survey (marked for each contour) and February 28, 2005. The full scale of the color code (red to blue) is +2 to -2 Ohm-meter. Warm color means conductivity increases (resistivity decrease) and cool color means conductivity decreases and resistivity increases. The dt value refers to time in days between the mapped survey shown and the previous survey.

Depth: 13.5 - 15.0 ft

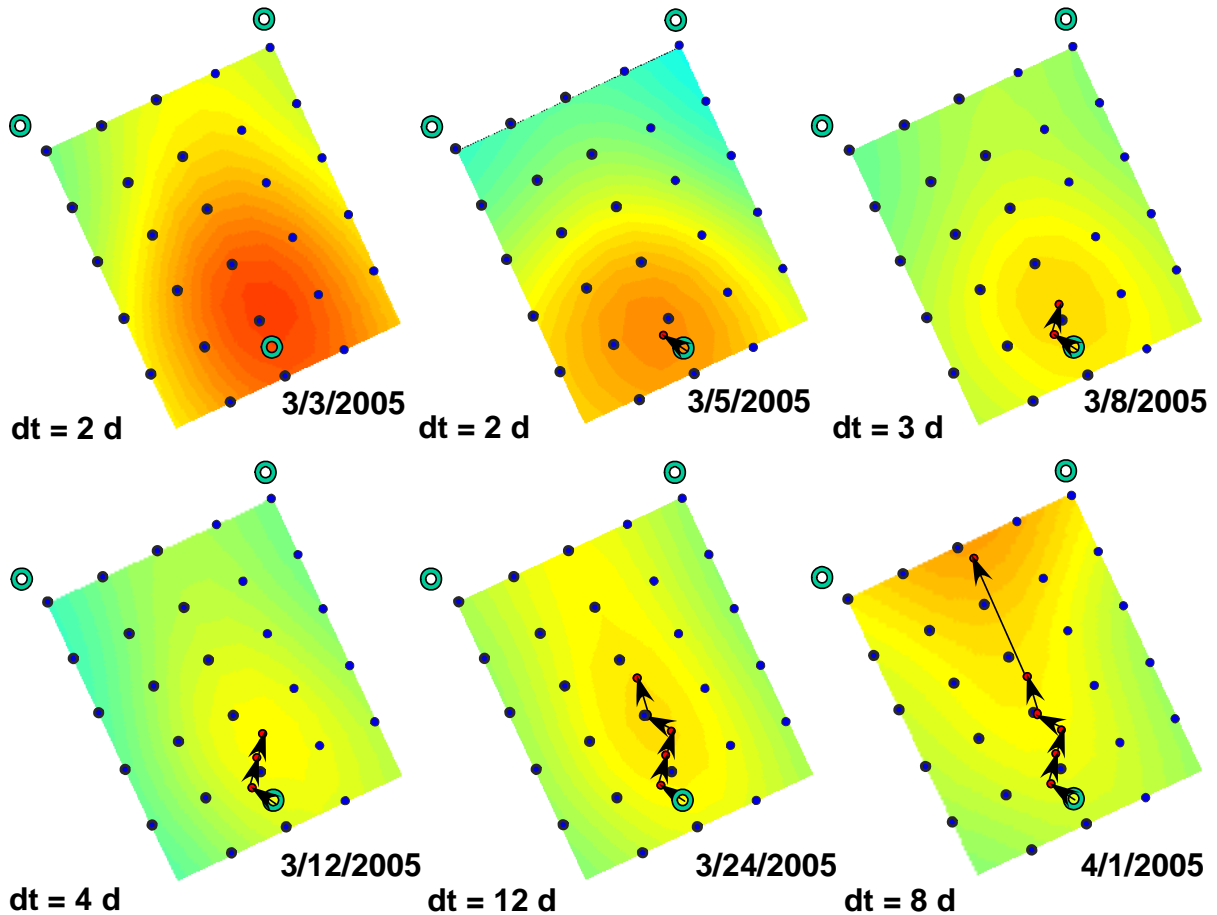


Figure 16. Contours of the differential electric resistivity in the lower zone of the silty sand formation ($z=13.5-15.0$ ft) between the date of survey (marked for each contour) and February 28, 2005. The full scale of the color code (red to blue) is +2 to -2 Ohm-meter. The dt value refers to time in days between the mapped survey shown and the previous survey.

2.3 Saline Plume Longitudinal and Vertical Variation with Time

The salt plume longitudinal variation with time is shown in Figure 17. Each curve expresses the differential electric resistivity (in Ohm-meters) along the centerline ($x = 14$ ft) in the Y-direction in the upper zone ($z=10.5-12.0$ ft, left panel) and lower zone ($z=13.5-15.0$ ft, right panel) of the aquifer. The symbols for each curve denote the number of days after the tracer injection.

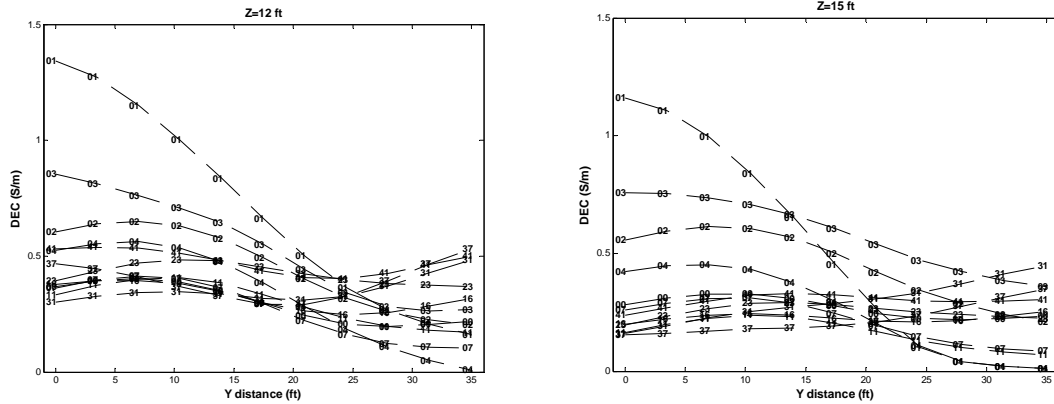


Figure 17. The differential electric resistivity in the central YZ plane at the depth of 10.5-12.0 ft (left panel) and 13.5-15.0 ft (right panel). The data points are labeled with the day after salt water injection. The unit of the vertical axis is in Ohm-meters.

Figure 18 shows the longitudinal differential electric resistivity profile at $x=14$ ft along the YZ plane, the central vertical plane of the electrode array. The differential electric resistivity in the surface layer ($z=0-3$ ft) bears no significance to groundwater flow and is severely affected by daily meteorological conditions and should be excluded in the discussion of groundwater flow. The vertical profile of the differential electric resistivity shows that the center of mass of the saline water pulse rises somewhat (from 12 to 10 feet) as it migrates and disperses across the site.

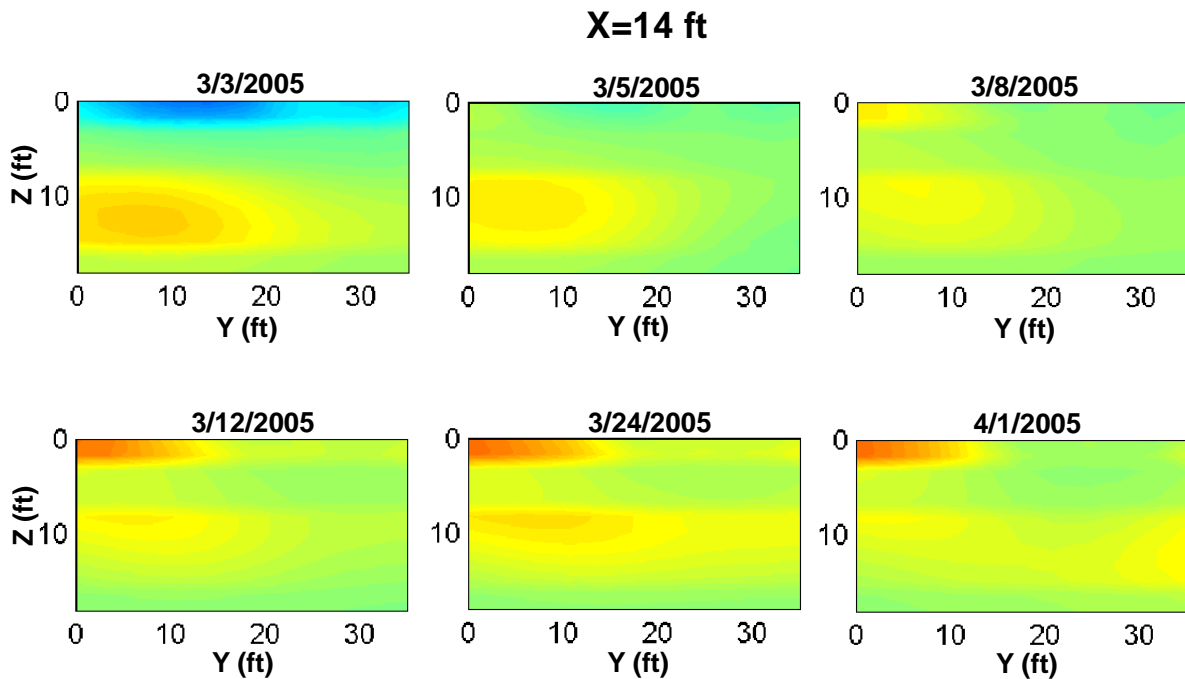


Figure 18. Contours of the differential electric resistivity in the vertical plane ($x=14.0$ ft). Full scale of the color code (red to blue) is +2 to -2 Ohm-meter.

4.0 IMPLICATIONS AND RECOMMENDATIONS

To further examine the differential resistivity results, three-dimensional models of the differential resistivity for select survey days were created in Rockworks 2004. These models used only differential resistivity data below the water table ($z > \text{or} = 4.5$ feet). The models were then used to develop the animation, cross sections and maps discussed below to evaluate the following:

- (1) the flow path of the saline tracer in three-dimensions;
- (2) the flow velocity as a function of time after injection;
- (3) the degree of hydrodynamic dispersion;
- (4) the optimum locations and depths for the piezometers; and
- (5) implications for the Rhodamine dye tracer test.

4.1 Flow Path and Velocity of the Saline Tracer in Three-Dimensions

The attached animation depicts the change in the differential resistivity as a function of time (survey dates 3/1, 3/3, 3/5, 3/8, 3/12, 3/24 and 4/1). The surface of the animation corresponds to a depth of 10.5 ft. This depth was chosen to permit viewing the main portion of the anomaly within the sandy silt. Maps and cross sections were generated to depict the maximum resistivity anomalies in plain and cross sectional views for select survey dates (3/1, 3/3, 3/5, 3/8, 3/12, 3/24 and 4/1). These are contained in Appendix A. Certain dates were not contoured or used in the animation owing to problems in surveying as noted in Table 6 (3/4, 3/17, 4/7 and 4/11). The data for 3/2 exhibited anomalously high resistivity differences in comparison to other survey dates and was also excluded from analysis.

Map Pattern

The variations in differential resistivity with time did not follow a simple instantaneous source model as initially anticipated. We anticipated seeing a pulse shaped anomaly migrating away from the injection well by advection and dispersion at a rate of about 1 ft/day. Early on from 3/1 to 3/5 the anomaly is pulse shaped and elongated in a southwestward direction but remains centered within only a few feet of the injection well. From 3/5 to 3/8 and 3/8 to 3/12 the anomaly remained elongated in a southwestward direction but the center of the anomaly moved northwestward. Also, despite this apparent movement, the center of the anomaly still remained within 5 feet of the injection well. From 3/12 to 3/24, the center of the anomaly appeared to have moved more rapidly (8 feet in 12 days from the 3/12 survey position (0.67 ft/day)) in a southwestward direction. The anomaly on 3/24 has a maximum point located about 7 feet from the injection well (effective velocity of 7 feet in 23 days or 0.3 ft/day) and appeared to exhibit tailing. The 4/1 data appeared to indicate the anomaly significantly accelerated sometime after 3/24. The anomaly migrated beyond the survey area (at a minimum rate of 22 feet in 7 days or a velocity of 3.1 ft/day). The apparent increase in velocity is consistent with the hydraulic data that shows the hydraulic conductivity increases in the direction of the downgradient wells and the geologic data from the SCAPS pushes that show the presence of a coarser sand layer near well W-3.

During the survey period, the differential resistivity anomaly was expected to exhibit a decrease in intensity with time as the tracer spread. Instead, the intensity of the anomaly oscillated between sampling dates. Figure 19 shows a map view of trend lines for the different survey dates that track the centerline of the resistivity anomalies across the geophysical electrode grid. For reference, the vertical line of electrodes is along an azimuth of 244 degrees. The trend lines exhibit a curve linearity trending toward the southwest near the injection well then turning toward the west-southwest with distance.

Profile Patterns

Figure 20 is a vertical projection of the of trend lines that track the centerline of the resistivity anomalies in cross section. As can be seen here, the anomaly appears to get shallower with distance from the injection well and with time. This likely results from the change in saline solution density as it migrates downgradient. The trend lines fall within the depth interval of 9 to 15 ft within the silty sand layer. The most intense portion of the anomaly in cross section during the survey period was within the depth range of 9 to 13 feet and extended downgradient about 15 feet from the injection well on 3/24.

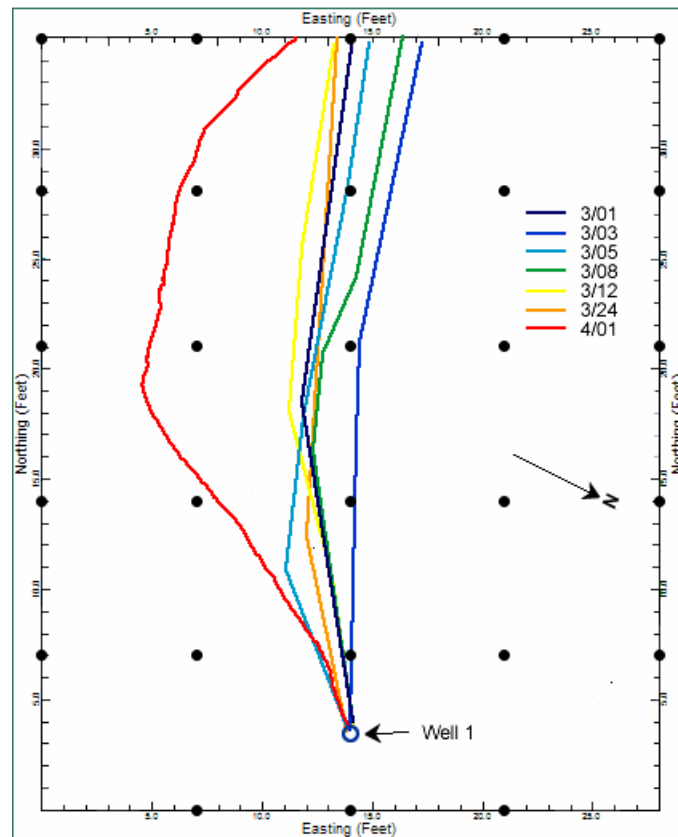


Figure 19. Lines depicting trends in the differential resistivity anomalies (black dots are the geophysical electrode points).

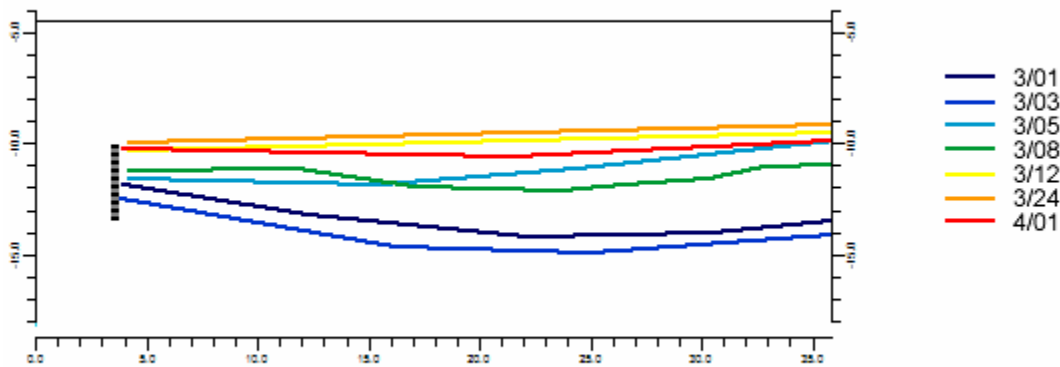


Figure 20. Vertical cross section of the geophysical test site depicting possible flow paths in the differential resistivity anomalies (scales are in feet, the horizontal distance is relative to the upgradient electrode location, the vertical scale is depth below the surface).

4.2 Degree of Hydrodynamic Dispersion

The geophysical data was used to approximate the degree of hydrodynamic dispersion to characterize the site for the Rhodamine dye study. The differential geophysical data were analyzed at survey day 3/24/05 (23 days after injection). A differential resistivity contour map and vertical cross section were used to develop longitudinal, transverse and vertical differential resistivity profiles. It is assumed that these profiles are directly proportional to concentration profiles of the saline tracer. This assumption is based on Archie's law where the formation resistivity and ground water resistivity are directly proportional as expressed by:

$$\rho = a\phi^{-m}S^{-n}\rho_w \quad (2)$$

where:

$\tilde{\rho}$ = effective formation resistivity;

ρ_w = pore water resistivity;

ϕ = porosity;

S = saturation;

a = 0.5-2.5;

m = 1.3-2.5;

n = 2.

Except at high concentration, the ground water resistivity should be directly proportional to the diluted saline solution concentration.

The parallelepiped model of Hunt (1978) was used to calibrate for hydrodynamic dispersion coefficients (and dispersivities) in the longitudinal, transverse and vertical directions.

For the longitudinal direction, along the centerline of flow, the parallelepiped model may be written:

$$C = .5C_{\max} \left[\operatorname{erf} \left(\frac{(x - vt + X/2)}{(2D_x t)^{.5}} \right) - \operatorname{erf} \left(\frac{(x - vt - X/2)}{(2D_x t)^{.5}} \right) \right] / \operatorname{erf} \left(\frac{(X/4)}{(2D_x t)^{.5}} \right) \quad (3)$$

Where:

C = concentration

C_{\max} = the maximum concentration

x = longitudinal distance from the injection well

X = source dimension in x

v = average linear velocity = x/t

t = time since injection

D_x = hydrodynamic dispersion coefficient in x

The dispersivity is taken as $\alpha_x = D_x/v$.

For the horizontal transverse direction, the parallelepiped model may be written:

$$C = .5C_{\max} \left[\operatorname{erf} \left(\frac{(y + Y/2)}{(2D_y t)^{.5}} \right) - \operatorname{erf} \left(\frac{(y - Y/2)}{(2D_y t)^{.5}} \right) \right] / \operatorname{erf} \left(\frac{(Y/4)}{(2D_y t)^{.5}} \right) \quad (4)$$

Where:

y = a transverse distance from the centerline of flow

Y = source dimension in y

D_y = hydrodynamic dispersion coefficient in y

The dispersivity is taken as $\alpha_y = D_y/v$

For the vertical transverse direction, equation (3) above is also applicable.

To calibrate the model, an Excel spreadsheet was developed that allowed iterating the above equations to derive "best fit" dispersion coefficients by minimizing the sum of the square differences between contoured differential resistivity values ("observed") and model predicted values along the three differential resistivity profiles.

Figure 21 and Figure 22 are map and longitudinal profile views, respectively, of the differential resistivity values for 3/24/05. The center of the anomaly traveled about 7 feet from the injection well in 23 days in a southwestward direction, giving an average linear velocity of 0.304 ft/day. The injection source was assumed to be rectangular in

shape having a vertical dimension (Z) equal to the screen length of the injection well of 3.5 feet. The Y and X dimensions were assumed equal and estimated using an injection volume of 50 gallons and assuming a formation porosity of 30%. This resulted in Y and X source dimensions of 2.5 feet.

Figures 23, 24, and 25 show the contour (observed) points and best fit curves. Estimated dispersion coefficients are tabulated in Table 7. The longitudinal dispersion

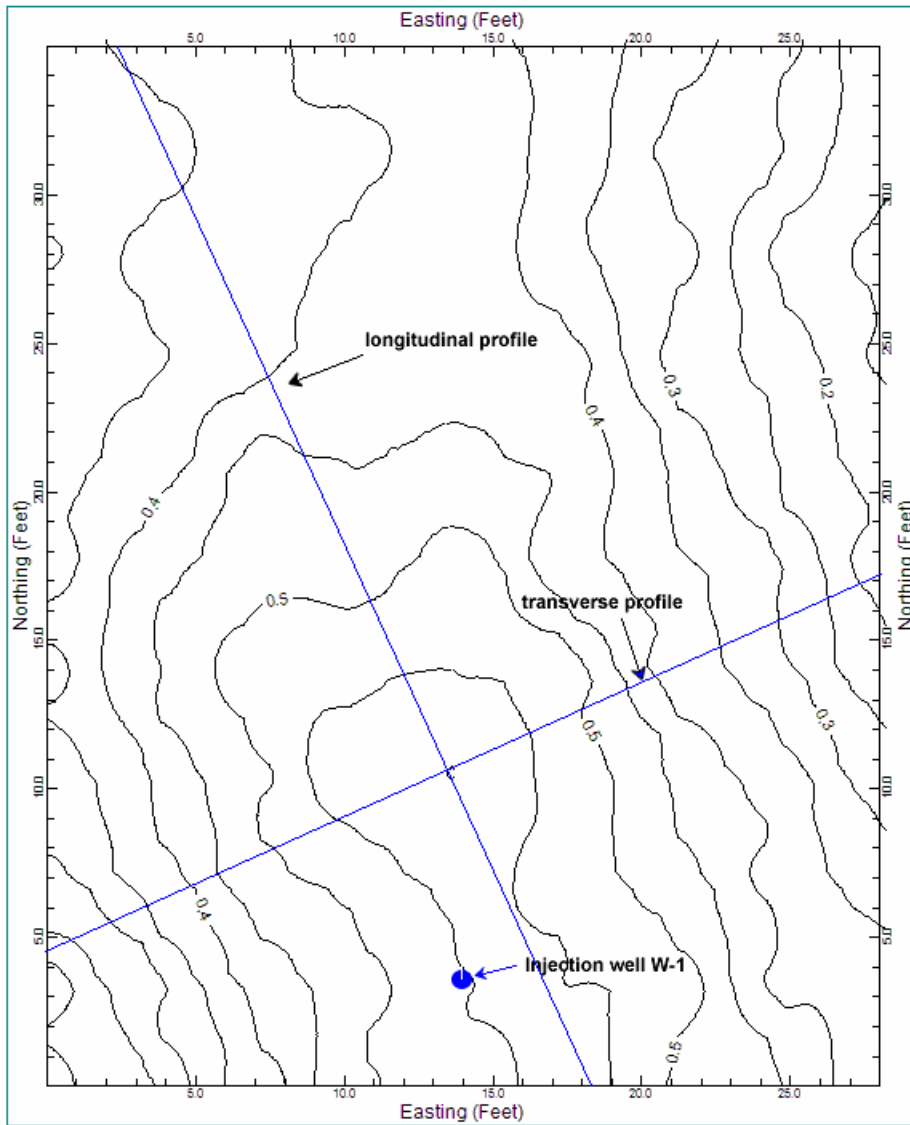


Figure 21. Differential resistivity contour map for 3/24/05 (depth = 10.5 ft.).

coefficient appears quite high in consideration of the travel distance of the plume. This value results from having a long longitudinal anomaly at a relatively low velocity. To a lesser extent, the transverse dispersion coefficient also appears high, perhaps because of the same reason. The vertical spreading is very much constrained. However, the vertical

spreading is asymmetrical with more spreading below 10.5 feet than above, perhaps due to the saline solution density.

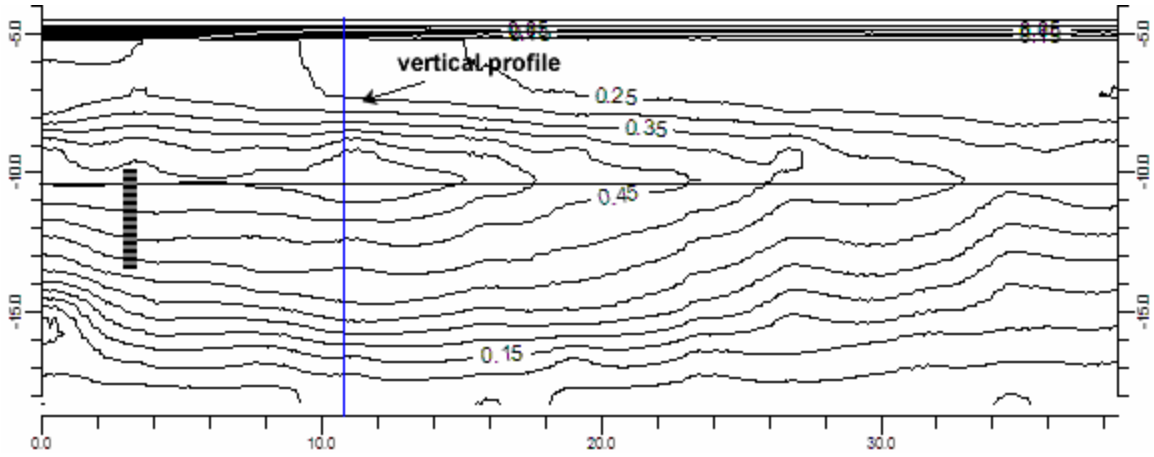


Figure 22. Differential resistivity profile for 3/24/05 (scales are in feet, the horizontal distance is relative to the upgradient electrode location, the vertical scale is depth below the surface).

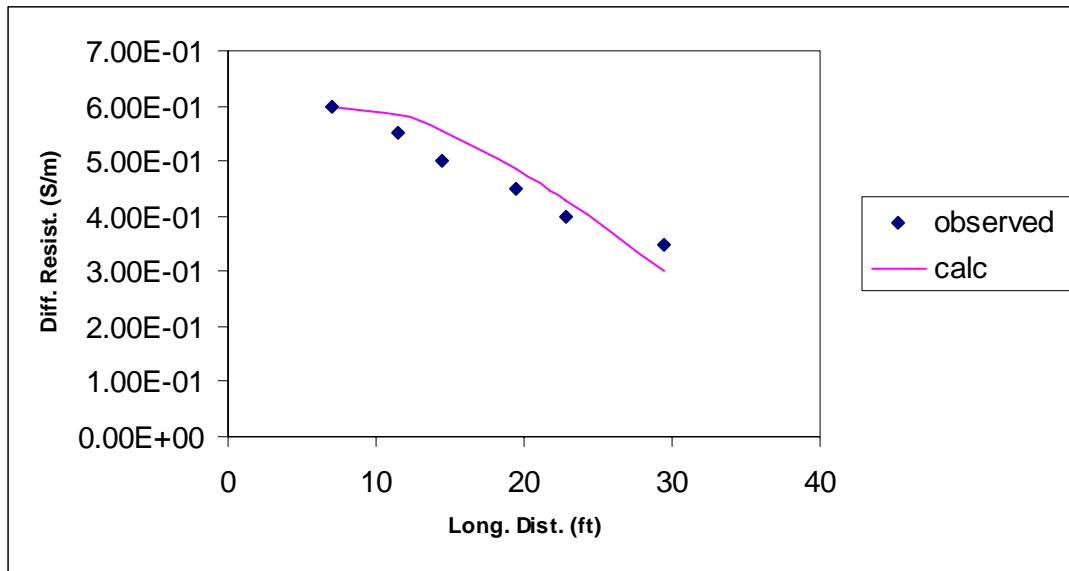


Figure 23. Longitudinal dispersion coefficient calibration for 3/24/05.

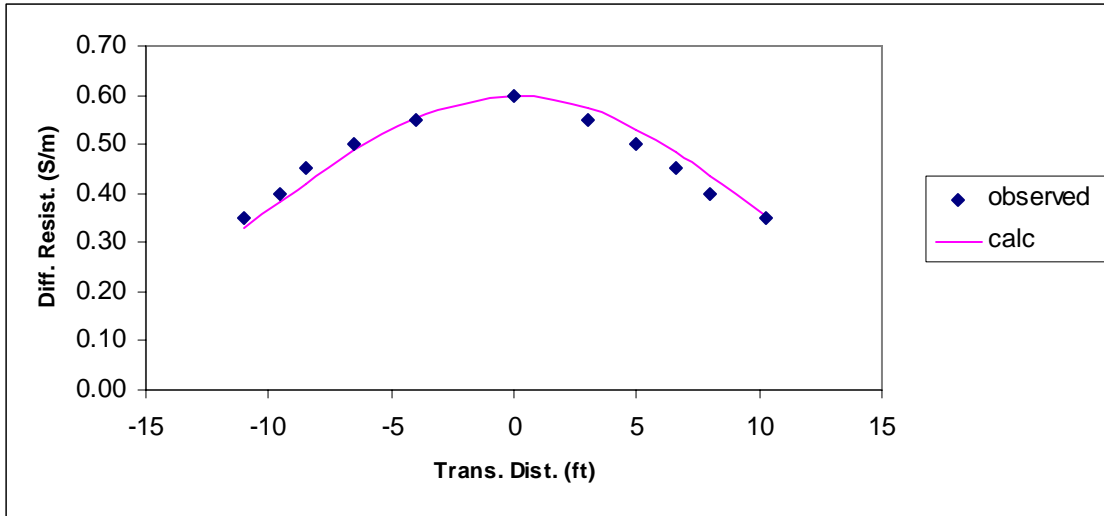


Figure 24. Transverse dispersion coefficient calibration for 3/24/05.

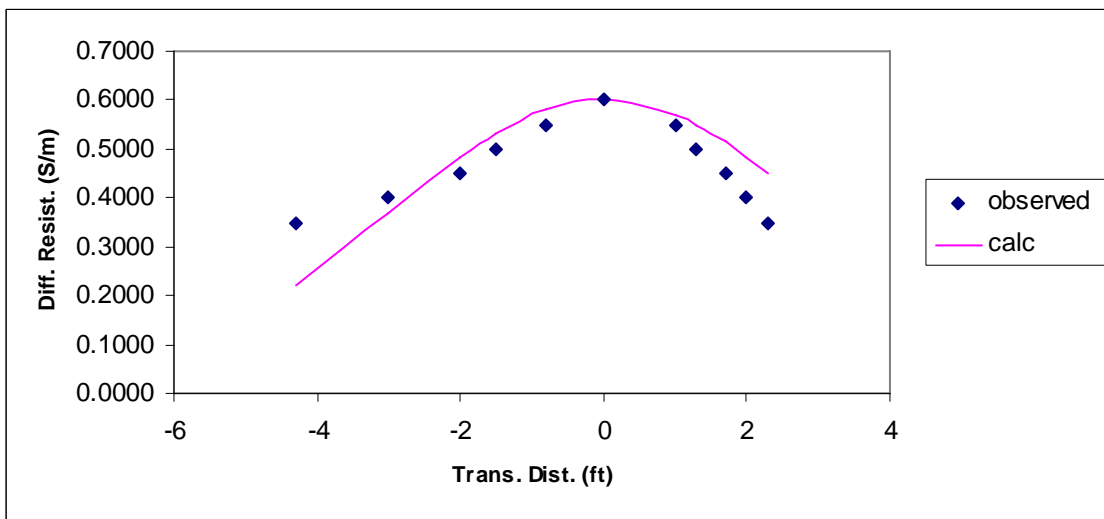


Figure 25. Vertical dispersion coefficient calibration for 3/24/05.

Table 7. Dispersion Best Fit Calibration Results

Date	3/24/05
X (cm)	76.9
Y (cm)	76.9
Z (cm)	106.7
v (cm/s)	1.07E-04
v (ft/day)	0.30
Dx (cm ² /s)	8.60E-02
Dy (cm ² /s)	2.40E-02
Dz (cm ² /s)	1.93E-03
α_x (cm)	800
α_y (cm)	220
α_z (cm)	18

4.3 Recommended Locations and Depths for the Piezometers

Figure 26 depicts the recommended configuration for the 13 piezometer clusters. It is recommended that the cluster grid be oriented with an azimuth of approximately 234 degrees. This azimuth is the approximate mean of the trendlines shown in Figure 19, in consideration of the travel distance of the anomalies and fitting straight-line paths to trends that exhibited curvature. It is recommended that the clusters be spaced 5 feet apart given the relatively narrow nature of the geophysical anomaly and the low velocity encountered which would curtail transverse spreading over the test site. It is recommended that the screen intervals be set at 8 to 8.5 feet, 10.5 to 11 feet and 13.5 to 14 feet. The 10.5 to 11 foot depth interval falls at the center of the profile trend lines shown in figure 20. The other intervals represent a compromise given the geology, the low vertical dispersion, the observed variations in vertical trends of the geophysical anomalies with time and distance and the need to obtain vertical separation between the piezometers.

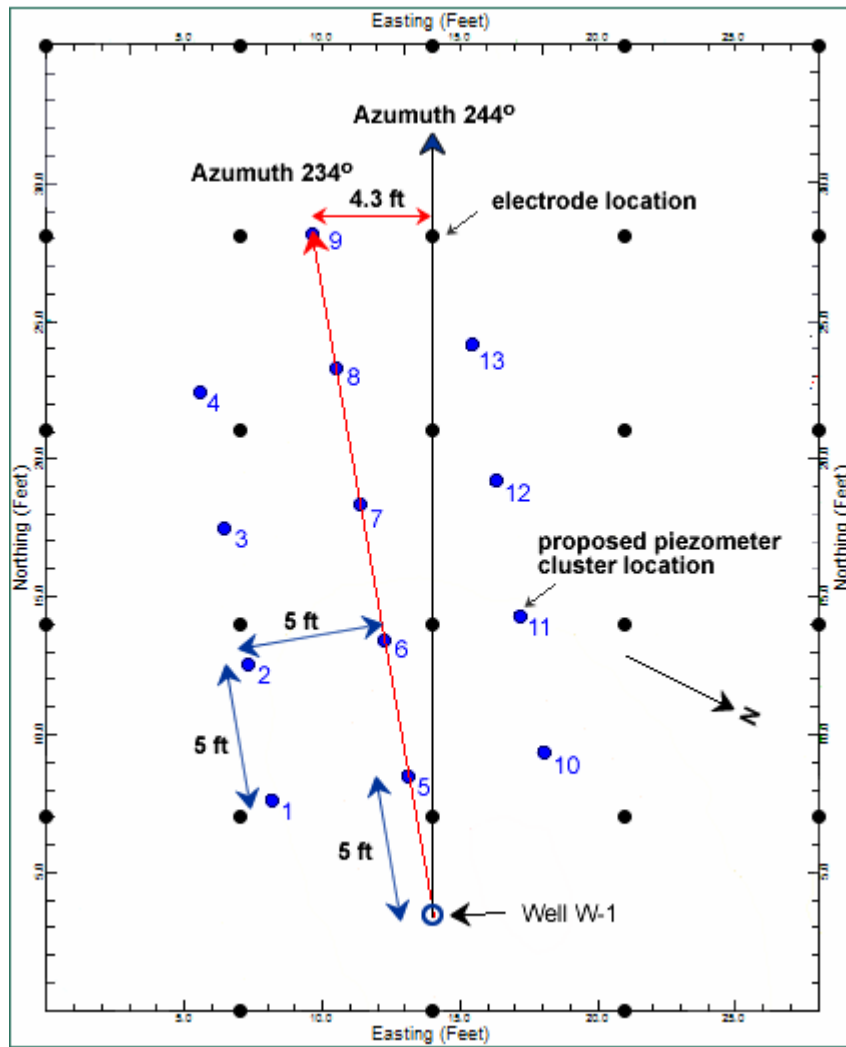


Figure 26. Recommended piezometer cluster locations.

4.4 Implications for the Rhodamine Test

Using the calibration information in Table 7 and the recommended probe locations, calculations were performed to evaluate the detection of the dye. Table 8 lists the input parameters. Using the parallelepiped model, the concentrations of the dye at the recommended cluster locations and depths were estimated for 7, 14, 21 and 28 days.

Figure 27 shows the results of the calculations for the centerline probes at the 10 to 11.5 foot depth. The concentrations predicted fall within the range of 26 to 2 ppb. In all cases the dye should be readily detectable with the Turner-Designs handheld unit. Figure 28 summarizes the estimated concentrations for the off-centerline piezometers at the depth of 13.5 to 14 feet. These piezometers should exhibit the lowest concentrations. The concentration range predicted varies from 5 to 0.5 ppb. Although the concentrations predicted are substantially lower than those for the centerline, they should still be readily quantifiable.

Table 8. Input Parameters for the Rhodamine Dye Model

Co ($\mu\text{g/l}$)	200000
injection volume (cc)	2000
X (cm)	7.9
Y (cm)	7.9
Z (cm)	106.7
v (cm/s)	1.07E-04
porosity (%)	30.00
Dx (cm ² /s)	8.60E-02
Dy (cm ² /s)	2.40E-02
Dz (cm ² /s)	1.93E-03
α_x (cm)	800
α_y (cm)	220
α_z (cm)	18

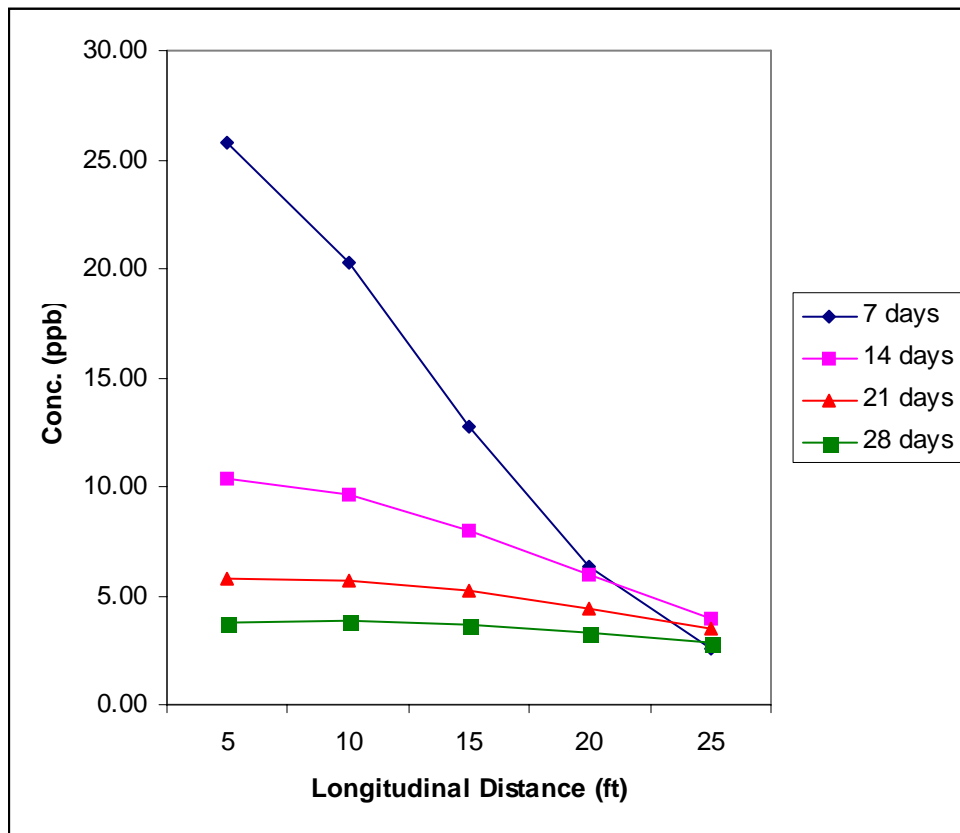


Figure 27. Estimated concentrations of Rhodamine dye for the recommended piezometer centerline clusters at the 10.5 to 11 ft. depth for 4 periods after injection.

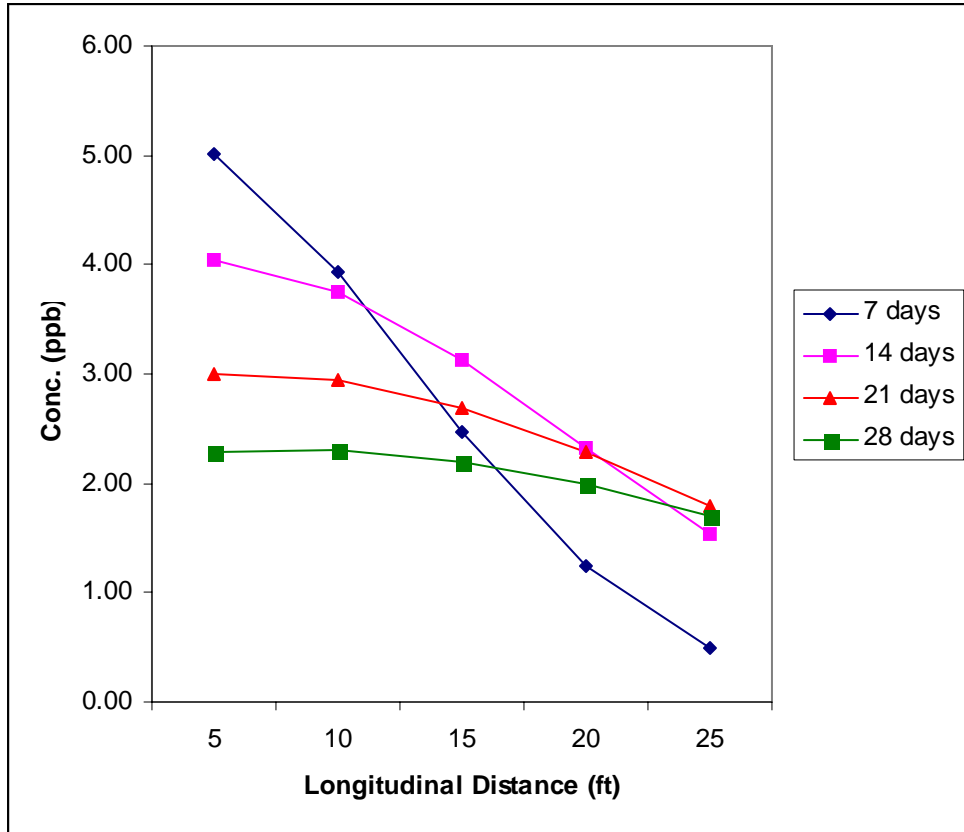


Figure 28. Estimated concentrations of Rhodamine dye for the recommended piezometer off centerline clusters at the 13.5 to 14 ft. depth for 4 periods after injection.

5.0 SUMMARY AND CONCLUSIONS

- The hydraulic conductivity of the three on-site wells which are screened within the silty sand zone was found to vary by a factor of 3, increasing toward well W-3 and had a mean value of 1.89×10^{-2} cm/s.
- The mean hydraulic gradient in the test site area was found to be 0.007 and had an azimuth of 287 degrees. Given the low gradient and close spacing between the three existing on-site wells, these values are considered highly uncertain.
- The differential resistivity anomaly did not exhibit a simple pulse-like behavior nor trend in the gradient direction estimated by the water level elevations in the perimeter wells.
- The geophysical test results suggests the follow:
 - The saline tracer had an apparent flow path from well W-1 that trended northwestward in the immediate vicinity of the well, then turned southwestward across most of the site and then turned west-southwest near the western boundary of the site. Given the low pumping rate, and lack of draw up in the other wells during the tracer injection, the migration of the saline tracer was most likely influenced by the natural heterogeneity in the silt sand formation. Given the low gradient, tidal affects and infiltration may have also been important in influencing the tracer migration.
 - The apparent flow velocity varied by perhaps an order of magnitude from about 0.3 to 3 ft/day in the downgradient direction;
 - The longitudinal dispersion in the test site area is substantially greater than the lateral and vertical dispersion.
- Based on the trends in the geophysical data, a piezometer grid was recommended that is oriented in a direction having a 234 degree azimuth. This direction differs substantially from the 287 degree azimuth suggested using the water level data from the perimeter wells. This difference may be due to error in estimating the gradient direction from the well data because of the low gradient encountered, or it may be due to formation anisotropy.
- Based on the geology, the geophysical anomaly and other practical considerations, three screened depths were recommended for the piezometers (8-8.5 ft, 10.5 to 11 feet and 13.5 to 14 feet).
- The geophysical data was used to calibrate a parallelepiped model. The model was then used to simulate the Rhodamine dye test. Concentrations were calculated for the recommended piezometer locations. It was found that the dye should be quantifiable at all piezometer locations between 7 and 28 days following injection.

6. 0 REFERENCES

Bartlett, S.A., Robbins, G.A., Mandrick, J.D., Barcelona, M.J., McCall, W., and Kram, M., 2004, Comparison of Hydraulic Conductivity Determinations in Direct Push and Conventional Wells, Naval Facilities Engineering Service Center, contract no. N47408-03-C-7407.

Hunt, B., 1978, Dispersive Sources in Uniform Groundwater Flow, J. Hydraulics Div., Proc. of the Amer. Soc of Civil Eng., v. 104, No hy 1, p. 75-85.

Tarantola, A., and Valette, B., 1982, Generalized nonlinear inverse problems solved using the least squares criterion, Rev. Geophys. Space Phys., v. 20, p. 219-232.

Zhang, J., Mackie, R. L., and Madden, T. R., 1995, 3-D resistivity forward modeling and inversion using conjugate gradients, Geophysics, v. 60, p.1313-1325.

APPENDIX F

Comparison of Hydraulic Conductivity and Head Values Obtained from the Piezometer Cluster with those Determined Using the High-Resolution Cone Penetrometer System (SCAPS)

Gary A. Robbins, Meredith Metcalf
Department of Natural Resources Management and Engineering
University of Connecticut
Storrs, CT

Mark Kram
Naval Facilities Engineering Service Center
Port Hueneme, CA

June 6, 2007

Conducted for
Naval Facilities Engineering Service Center
1100 23rd Avenue
Port Hueneme, CA 93043

Acknowledgments

The authors would like to thank the following individuals for their assistance: Dale Lorenzana for assisting in field testing; and Dorothy Cannon for logistical support. We are also grateful to Geoprobe Systems for providing the pneumatic slug test equipment used in this study and Wes McCall for his continual advice and support. This project was funded through a contract (N47408-04-C-7514) with the Naval Facilities Engineering Service Center, Port Hueneme, California and is part of the Environmental Security Technology Certification Program (ESTCP) project CU-0421.

Table of Contents

1.0 INTRODUCTION	4
1.1 Background	4
1.2 Objectives	4
2.0 FIELD TESTING	5
2.1 Hydraulic Conductivity Testing.....	5
2.2 Head Testing	6
3. 0 COMPARISON OF RESULTS.....	6
3.1 Comparison of Hydraulic Conductivity Determinations	6
3.2 Comparison of the Hydraulic Head Determinations	10
4. 0 CONCLUSIONS	12
5. 0 REFERENCES	12

1.0 INTRODUCTION

1.1 Background

This study was conducted as part of a larger demonstration effort supported by a grant from ESTCP, entitled: *Detailed Hydraulic Assessment Using a High-Resolution Piezocone Coupled to the GeoVIS, CU-0421*. The focus of that study is to demonstrate the use of a high-resolution piezocone and a subsurface camera probe (GeoVIS) deployed using a cone penetrometer system as a cost effective and rapid approach to determine three-dimensional hydrogeology and ground water flow characteristics at contamination sites. To evaluate the effectiveness of this approach, the Navy Site Characterization and Analysis Penetrometer System (SCAPS) was used to characterize a site at the Naval Facilities Engineering Service Center (NFESC) in Port Hueneme, California. For comparison, the test site has been characterized in three dimensions using a more conventional approach involving the installation of 39 customized short screen (e.g., 6-inch length) monitoring wells at 13 locations (**Figure 1**).

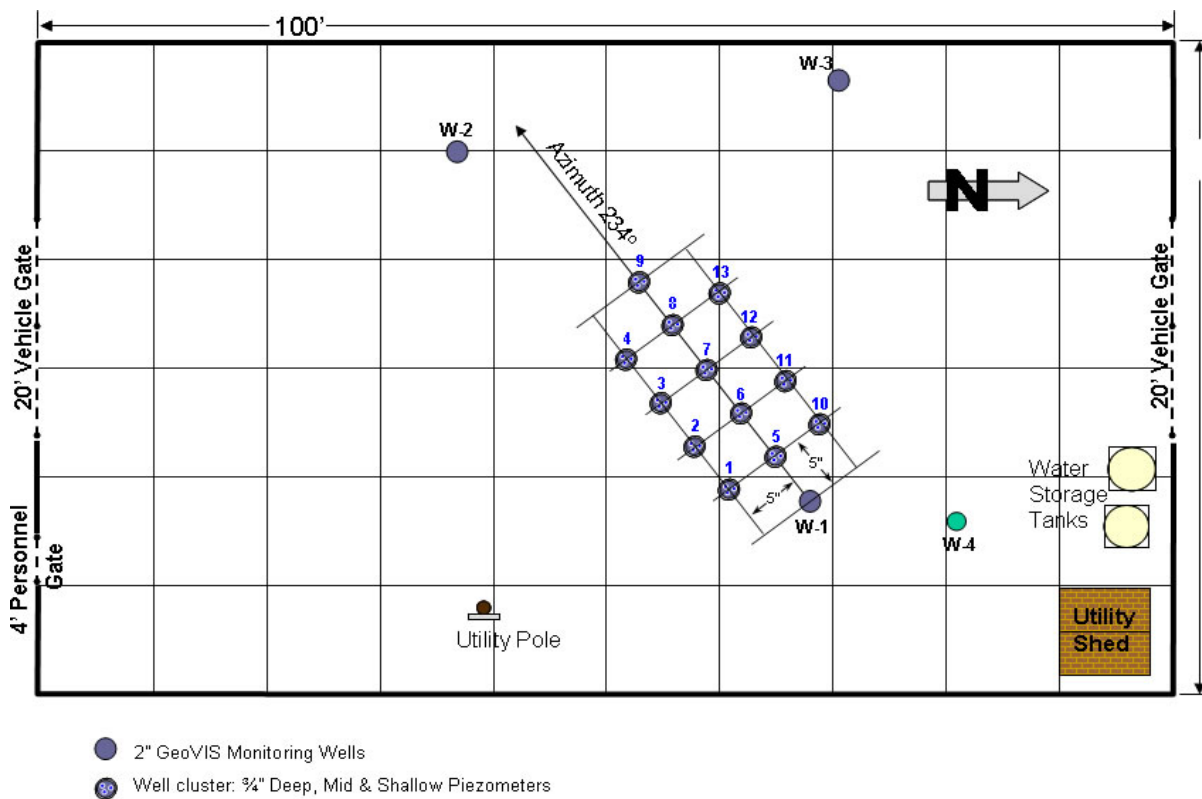


Figure 1. Well Cluster Test Site

1.2 Objectives

In this portion of the study hydraulic conductivity (K) and hydraulic head (H) values determined from the monitoring well clusters were compared to those determined using the high resolution piezocone, a direct push probe deployed by the SCAPS. The objective is to determine

whether the K and H values measured with the high-resolution piezocone compare favorably to the values collected from co-located conventional monitoring wells.

2.0 FIELD TESTING

2.1 Hydraulic Conductivity Testing

Robbins (2005) described the methods and results of slug testing conducted in the 13 clusters of wells at the test site. Each cluster consists of three monitoring wells constructed of 3/4-inch PVC with 6-inch long prepacked screens. The wells were screened over depth intervals of approximately 8-8.5 feet (shallow), 10-10.5 ft (middle), and 13.5 - 14 ft (deep). These depths were chosen to bracket a high permeable sand layer identified during preliminary site investigations consisting of piezocone deployment to determine the soil type profile in three test cell perimeter locations (**Figure 2**). Monitoring wells WC-1M and WC-4M were found to be broken and were not tested in the Robbins study. Subsequently, replacement wells were installed at these locations and depths, and their results are reported here along with an analysis of the K values determined in Robbins (2005). The mean K value for each well was determined based on hydraulic tests run in triplicate.

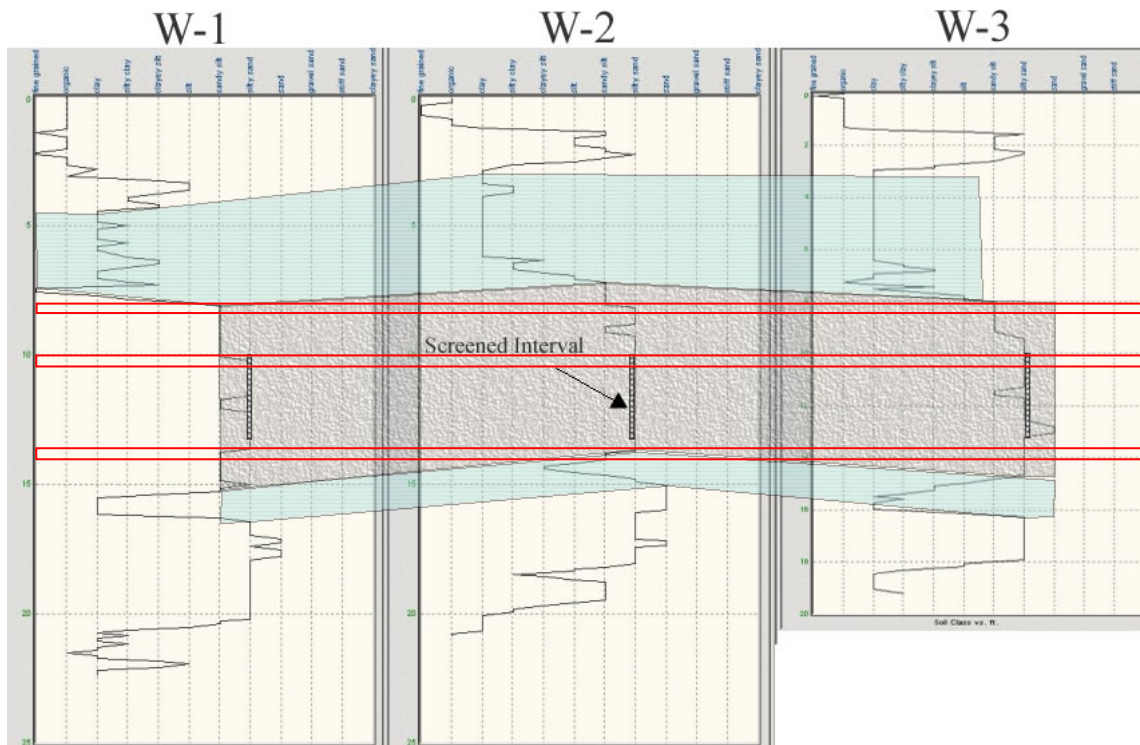


Figure 2. Test site stratigraphy based on preliminary SCAPS piezocone pushes. Also shown are the screen intervals of three monitoring wells that surround the test site and the depth intervals (in red) of the piezometer screens.

The high resolution piezocone reports K values based on two different approaches. The first approach correlates soil type, determined using the load cell resistance to force and sleeve friction and pore pressure readings, with K values (Campanella and Robertson, 1989). This provides an order of magnitude level of resolution for K. The second approach is similar to a slug test. It uses the Parez and Fauriel (1988) relationship to determine a K value based on the time required for 50 percent pressure dissipation. This method provides a maximum, minimum and mean K values based on a graphical relationship, and a K value based on a formula.

2.2 Head Testing

Depth to water in each monitoring well was determined using a Solinst water level meter model number 31850. H was then determined by subtracting depth to water from surveyed surface elevations. Given the shallow depth to water at the site, measurement reproducibility is on the order of ± 0.02 feet.

To define H using the high resolution piezocone, the probe is advanced to several depths beneath the water table. At each depth the increased water pressure created by the advancing probe is allowed to dissipate back to hydrostatic conditions. This results in a hydrostatic pressure-depth profile at each location. The hydrostatic pressure profile is then extrapolated to zero pressure, which corresponds to the depth of the water table. H is derived by subtracting the depth to the water table from a surveyed surface elevation tied to a reference (e.g., mean sea level). The method is reported to have a resolution of approximately 0.08 ft (1 inch).

On a side note, final dissipation pressure values can be used for modeling purposes. A gradient builder function has been incorporated into GMS to allow for three-dimensional assessment of flow. Alternatively, water table elevations derived from multiple final dissipation pressure values for a single push (e.g., the hydrostatic pressure profile) can be used for modeling and to establish boundary conditions.

3.0 COMPARISON OF RESULTS

3.1 Comparison of Hydraulic Conductivity Determinations

Table 1 and Figure 3 summarize the K results. K_{well} refers to the average of the triplicate conductivity tests performed in the monitoring wells. It should be noted that the monitoring well slug tests resulted in K values that were highly reproducible with an average relative standard deviation ($100 * \text{Std. Dev.} / \text{Mean}$) of only 8.5 percent. These tests also showed that the test cell can be described as a three layer system with a relatively higher permeable zone situated between shallow and deep lower permeability zones. The boundaries between these zones appear relatively sharp but the depth of the boundaries did vary somewhat across the test cell. Although the monitoring well depths are relatively consistent at each cluster, some of the shallower wells and most of the deeper wells do not intersect the low permeable zones.

The high-resolution piezocone K values are based on measurements collected from a depth that is approximately at the center of the screen sections of the monitoring wells. On

average, the vertical difference between the center of the screen and the location of the piezocone sensor unit was about 0.11 feet. The SCAPS probe push locations were offset from the monitoring well clusters by 1 to 1.5 feet in map view. K_{\min} , K_{\max} and K_{mean} refer to K values based on graphical relationships in Parez and Fauriel (1988). K_{form} refers to K values calculated using the dissipation formula provided in Parez and Fauriel (1988). It should be noted that all the K values from the Parez and Fauriel (1988) study are linearly related. K_{lc} refers to the K value based on the Robertson and Campanella (1989) correlation between hydraulic conductivity and load cell-based soil type.

Table 1 and Figure 3 summarize the results for all the K determinations. The K values taken together irrespective of stratigraphy best fit a log normal distribution with the exception of K_{lc} , which by its order of magnitude nature does not fit a continuous function. Given the K value affinities to log normal distributions, geometric means and geometric standard deviations were also included along with arithmetic means and arithmetic standard deviations in Table 1. Figure 3 is a confidence interval plot of log K values showing the range for two standard deviations about the geometric mean. Comparison of arithmetic and geometric mean values show that on average the K_{mean} and K_{lc} values are within about a factor of 2 of the K_{well} values. On average the K_{\min} , K_{\max} and K_{form} values fall within a factor of 5 or better of the K_{well} values.

K values derived from piezocone pushes differed widely from those derived from slug tests conducted in the adjacent monitoring wells. To some extent this may be due to the vertical variations in site stratigraphy. The monitoring wells provide a K determination averaged over 0.5 feet of screen. The individual high resolution piezocone K determinations are essentially measurements at a specific depth. Given this higher resolution, they are subject to more variability than the screened wells. To examine this further, data from the middle zone was used to develop Table 2 and Figure 4. The piezometer determinations exhibit a percent RSD of 44, which can be taken as a measure of horizontal heterogeneity. The piezocone determinations based on the Parez and Fauriel (1988) relationships exhibit a higher variability and a somewhat lower mean K value relative to that of the monitoring well determinations. In general, K values are known to vary in a lognormal manner, having more frequent lower values than higher values. This may explain the results observed here, given the depth discrete measurements of the piezocone. The mean K value based on the method of Robertson and Campanella (1989) is similar to that of the monitoring well determinations but also exhibits a higher percent RSD than the monitoring wells. Here the higher percent RSD maybe due to using a K value scale where the magnitude of hydraulic conductivity varies by a factor ten between soil types.

Table 1. Comparison of Hydraulic Conductivity Values

Well	K_{well} (cm/s)	K_{min} (cm/s)	K_{max} (cm/s)	K_{mean} (cm/s)	K_{form} (cm/s)	K_{lc} (cm/s)
WC-01-S	1.19E-04	1.56E-05	6.69E-05	4.13E-05	2.61E-05	1.00E-03
WC-01-M Alt	2.91E-03	1.12E-03	1.12E-02	6.14E-03	2.51E-03	1.00E-03
WC-01-D	2.52E-03	1.39E-04	9.12E-04	5.25E-04	2.69E-04	1.00E-02
WC-02-S	6.95E-04	1.09E-03	1.08E-02	5.96E-03	2.45E-03	1.00E-04
WC-02-M	6.12E-03	4.16E-04	3.41E-03	1.91E-03	8.71E-04	1.00E-03
WC-02-D	4.27E-03	1.41E-04	9.31E-04	5.36E-04	2.74E-04	1.00E-02
WC-03-S	2.65E-05	6.02E-05	3.36E-04	1.98E-04	1.10E-04	1.00E-03
WC-03-M	2.81E-03	2.60E-04	1.93E-03	1.10E-03	5.26E-04	1.00E-02
WC-03-D	2.40E-03	1.03E-04	6.43E-04	3.73E-04	1.96E-04	1.00E-02
WC-04-S	5.28E-05	1.08E-04	6.75E-04	3.91E-04	2.05E-04	1.00E-03
WC-04-M Alt	5.97E-03	1.55E-04	1.04E-03	5.98E-04	3.02E-04	1.00E-02
WC-04-D	7.08E-04	5.60E-05	3.08E-04	1.82E-04	1.02E-04	1.00E-03
WC-05-S	4.16E-05	1.64E-05	7.09E-05	4.37E-05	2.74E-05	1.00E-04
WC-05-M	6.15E-03	2.18E-04	1.57E-03	8.95E-04	4.36E-04	1.00E-03
WC-05-D	1.39E-03	8.96E-05	5.41E-04	3.15E-04	1.68E-04	1.00E-02
WC-06-S	2.53E-05	2.67E-05	1.27E-04	7.67E-05	4.61E-05	1.00E-04
WC-06-M	8.59E-03	1.19E-04	7.60E-04	4.39E-04	2.28E-04	1.00E-03
WC-06-D	2.07E-03	6.77E-05	3.87E-04	2.27E-04	1.25E-04	1.00E-03
WC-06-S	2.53E-05	2.67E-05	1.27E-04	7.67E-05	4.61E-05	1.00E-04
WC-07-M	5.12E-03	2.19E-04	1.58E-03	8.99E-04	4.38E-04	1.00E-02
WC-07-D	4.89E-03	6.11E-04	5.40E-03	3.00E-03	1.31E-03	1.00E-03
WC-08-S	7.52E-05	1.77E-04	1.23E-03	7.02E-04	3.50E-04	1.00E-05
WC-08-M	3.36E-03	1.53E-04	1.02E-03	5.88E-04	2.98E-04	1.00E-03
WC-08-D	2.14E-03	6.18E-04	5.47E-03	3.04E-03	1.33E-03	1.00E-03
WC-09-S	1.05E-03	1.50E-03	1.58E-02	8.66E-03	3.43E-03	1.00E-04
WC-09-M	2.09E-03	2.53E-04	1.87E-03	1.06E-03	5.11E-04	1.00E-03
WC-09-D	2.29E-03	2.14E-04	1.54E-03	8.75E-04	4.27E-04	1.00E-03
WC-10-S	1.50E-03	1.22E-04	7.82E-04	4.52E-04	2.34E-04	1.00E-04
WC-10-M	2.61E-03	2.04E-04	1.45E-03	8.29E-04	4.07E-04	1.00E-03
WC-10-D	1.89E-03	4.08E-05	2.11E-04	1.26E-04	7.27E-05	1.00E-02
WC-11-S	7.50E-05	3.15E-05	1.54E-04	9.29E-05	5.50E-05	1.00E-04
WC-11-M	7.33E-03	2.11E-04	1.51E-03	8.59E-04	4.21E-04	1.00E-03
WC-11-D	1.54E-03	4.31E-05	2.26E-04	1.34E-04	7.71E-05	1.00E-02
WC-12-S	3.52E-05	2.15E-05	9.77E-05	5.96E-05	3.65E-05	1.00E-03
WC-12-M	2.94E-03	4.98E-05	2.67E-04	1.59E-04	8.98E-05	1.00E-03
WC-12-D	1.23E-03	3.20E-05	1.57E-04	9.47E-05	5.59E-05	1.00E-02
WC-13-S	1.04E-03	7.00E-03	1.00E-01	5.35E-02	1.78E-02	1.00E-04
WC-13-M	4.60E-03	1.10E-04	6.89E-04	3.99E-04	2.09E-04	1.00E-02
WC-13-D	3.74E-03	9.30E-05	5.66E-04	3.29E-04	1.75E-04	1.00E-02
Arithmetic Mean	2.47E-03	4.09E-04	4.51E-03	2.46E-03	9.40E-04	3.56E-03
Std. Dev.	2.25E-03	1.13E-03	1.61E-02	8.59E-03	2.87E-03	4.37E-03
Geometric Mean	1.02E-03	1.32E-04	8.63E-04	5.00E-04	2.56E-04	1.13E-03
+ Std. Dev.	6.45E-03	4.95E-04	4.19E-03	2.35E-03	1.05E-03	6.99E-03
- Std. Dev.	1.62E-04	3.54E-05	1.78E-04	1.06E-04	6.24E-05	1.81E-04

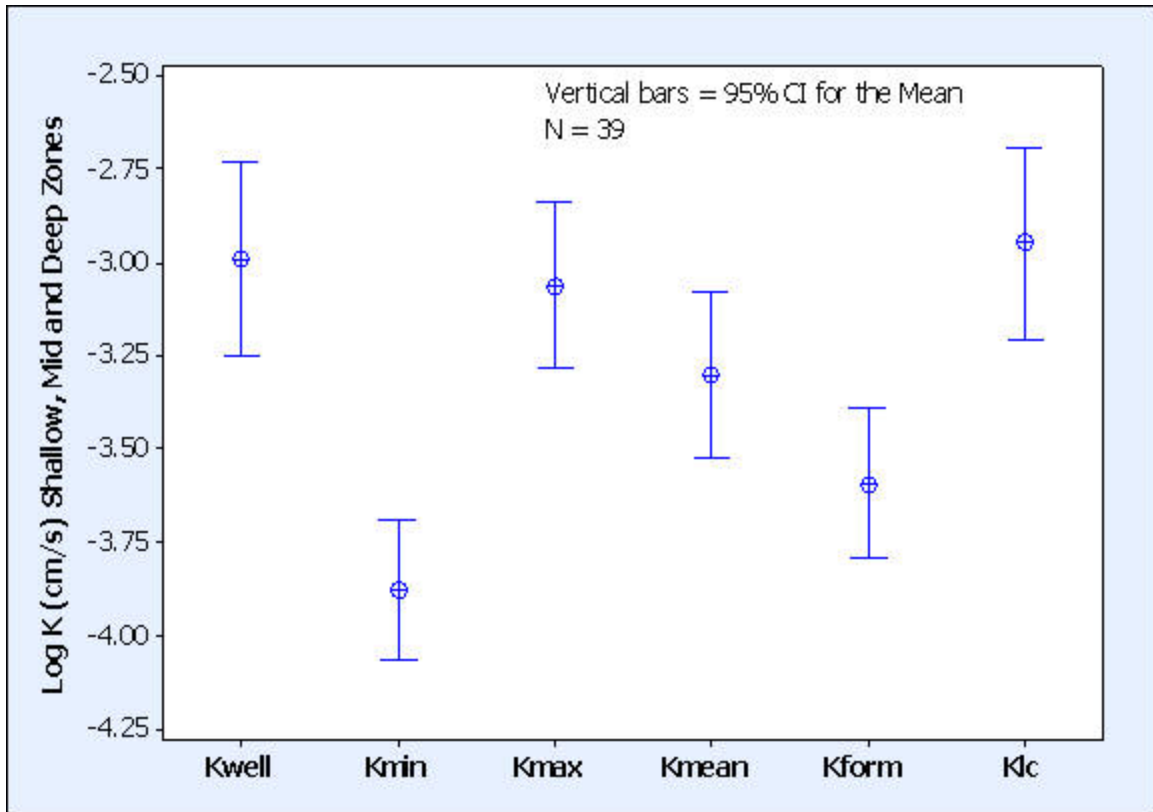


Figure 3. Comparison of all K values (Circles are the geometric mean values).

Table 2. Middle Zone Hydraulic Conductivity Comparison

Well	K_{well} (cm/s)	K_{min} (cm/s)	K_{max} (cm/s)	K_{mean} (cm/s)	K_{form} (cm/s)	K_{lc} (cm/s)
WC-01-M Alt	2.91E-03	1.12E-03	1.12E-02	6.14E-03	2.51E-03	1.00E-03
WC-02-M	6.12E-03	4.16E-04	3.41E-03	1.91E-03	8.71E-04	1.00E-03
WC-03-M	2.81E-03	2.60E-04	1.93E-03	1.10E-03	5.26E-04	1.00E-02
WC-04-M Alt	5.97E-03	1.55E-04	1.04E-03	5.98E-04	3.02E-04	1.00E-02
WC-05-M	6.15E-03	2.18E-04	1.57E-03	8.95E-04	4.36E-04	1.00E-03
WC-06-M	8.59E-03	1.19E-04	7.60E-04	4.39E-04	2.28E-04	1.00E-03
WC-07-M	5.12E-03	2.19E-04	1.58E-03	8.99E-04	4.38E-04	1.00E-02
WC-08-M	3.36E-03	1.53E-04	1.02E-03	5.88E-04	2.98E-04	1.00E-03
WC-09-M	2.09E-03	2.53E-04	1.87E-03	1.06E-03	5.11E-04	1.00E-03
WC-10-M	2.61E-03	2.04E-04	1.45E-03	8.29E-04	4.07E-04	1.00E-03
WC-11-M	7.33E-03	2.11E-04	1.51E-03	8.59E-04	4.21E-04	1.00E-03
WC-12-M	2.94E-03	4.98E-05	2.67E-04	1.59E-04	8.98E-05	1.00E-03
WC-13-M	4.60E-03	1.10E-04	6.89E-04	3.99E-04	2.09E-04	1.00E-02
Arithmetic Mean	4.66E-03	2.68E-04	2.17E-03	1.22E-03	5.58E-04	3.77E-03
Std. Dev.	2.06E-03	2.72E-04	2.81E-03	1.54E-03	6.18E-04	4.32E-03
%RSD	44	101	129	126	111	115
Geometric Mean	4.25E-03	2.03E-04	1.44E-03	8.21E-04	4.03E-04	2.03E-03

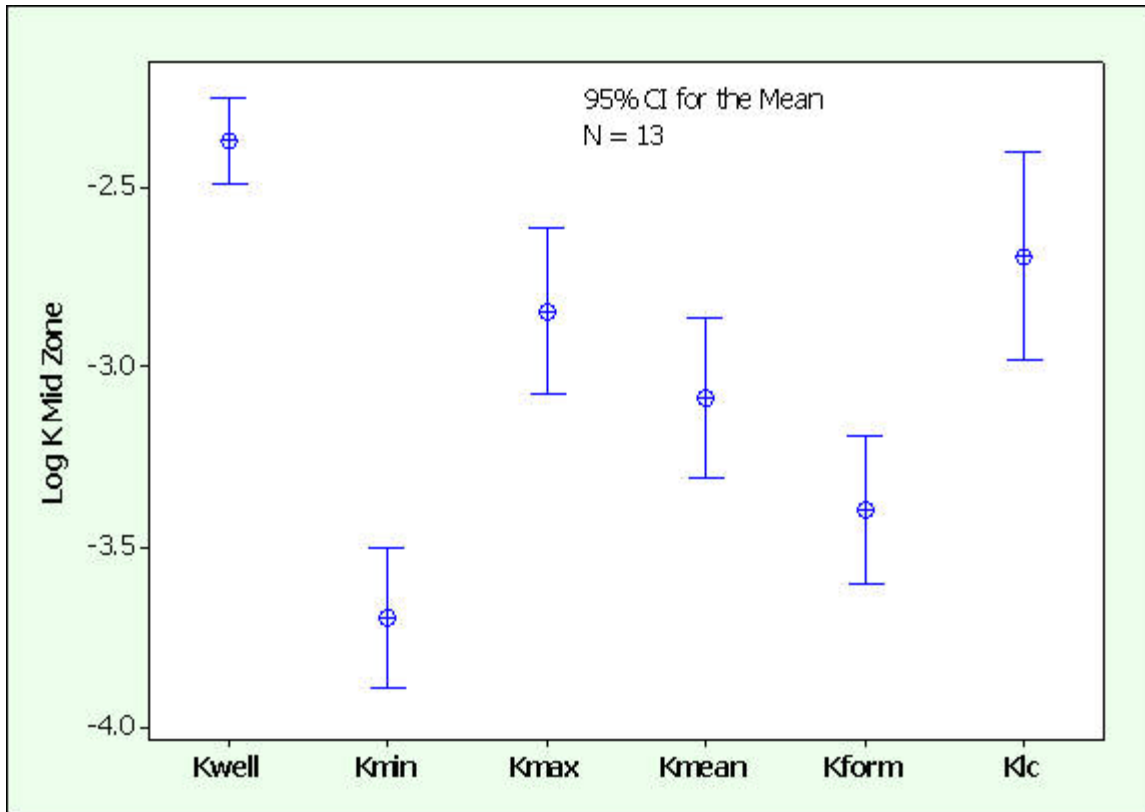


Figure 4. Comparison of Middle Zone K values (Circles are the geometric mean values).

3.2 Comparison of the Hydraulic Head Determinations

Hydraulic Head values were determined in the monitoring wells during the SCAPS deployment. These values are compared to the H values determined from the high resolution piezocone in Table 3. The monitoring well data did not reveal any discernible vertical or horizontal gradients. It should be noted that the well clusters are aligned along the hydraulic gradient for a distance of only 25 feet and the cluster locations span only 10 feet across. Within the limits of resolution for both methods, the piezocone results agree closely with the monitoring well H values with respect to finding no discernible vertical or horizontal gradients, mean value of the hydraulic head and the degree of variability.

Table 3. Comparison of Monitoring Well and High Resolution Piezocone H Values

Well	Well H (ft)	Piezocone H (ft)
WC-01-S	5.18	5.49
WC-01-M Alt	5.45	5.54
WC-01-D	5.46	5.47
WC-02-S	5.44	5.44
WC-02-M	5.43	5.49
WC-02-D	5.46	5.42
WC-03-S	5.46	5.43
WC-03-M	5.44	5.49
WC-03-D	5.45	5.37
WC-04-S	5.43	5.55
WC-04-M Alt	5.41	5.51
WC-04-D	5.43	5.52
WC-05-S	5.46	5.53
WC-05-M	5.45	5.52
WC-05-D	5.47	5.51
WC-06-S	5.43	5.47
WC-06-M	5.44	5.49
WC-06-D	5.45	5.46
WC-07-S	5.43	5.53
WC-07-M	5.43	5.58
WC-07-D	5.45	5.54
WC-08-S	5.41	5.50
WC-08-M	5.41	5.50
WC-08-D	5.43	5.50
WC-09-S	5.38	5.37
WC-09-M	5.41	5.41
WC-09-D	5.42	5.38
WC-10-S	5.45	5.51
WC-10-M	5.45	5.57
WC-10-D	5.46	5.49
WC-11-S	5.44	5.52
WC-11-M	5.43	5.56
WC-11-D	5.44	5.56
WC-12-S	5.43	5.55
WC-12-M	5.42	5.53
WC-12-D	5.44	5.44
WC-13-S	5.41	5.52
WC-13-M	5.42	5.57
WC-13-D	5.41	5.49
Mean	5.43	5.49
Std. Dev	0.05	0.05
%RSD	0.83	0.99
Minimum	5.18	5.37
Maximum	5.47	5.58
Range	0.29	0.21

4.0 CONCLUSIONS

- The high resolution piezocone derived hydraulic conductivity values were on average similar to those obtained from monitoring wells. Differences at any individual location may be attributed to averaging hydraulic conductivity values over the well screen or more focused depth specific determinations from the piezocone, which is more sensitive to vertical heterogeneities. Differences between well data and high resolution piezocone derived hydraulic conductivity values were in general much less than one order of magnitude.
- Within the limits of resolution, the high resolution piezocone hydraulic head determinations agreed closely with those derived from co-located monitoring wells. Differences between well and high resolution piezocone derived head values were on average less than 0.08 feet (1 inch).

5.0 REFERENCES

- Parez and Fauriel (1988). "Le piezocone ameliorations apportees a la reconnaissance de sols." *Revue Francaise de Geotech* 44: 13-27
- Robbins, G. A., 2005, GEOVIS/SCAPS Well Cluster Test Site Hydraulic Conductivity, Naval Facilities Engineering Service Center Port Hueneme, CA, Environmental Security Technology Certification Program (ESTCP) project CU-0421, November 21,
- Robertson, P.K. and R.G. Campanella, 1989. *Guidelines for Geotechnical Design Using the Cone Penetrometer Test and CPT with Pore Pressure Measurement*, 194pp.

APPENDIX G

RHODAMINE WT TRACER TEST

Gary A. Robbins
Department of Natural Resources Management and Engineering
University of Connecticut
Storrs, CT

Kenda Neil
Naval Facilities Engineering Service Center
Port Hueneme, CA

June 7, 2007

Conducted for
Naval Facilities Engineering Service Center
1100 23rd Avenue
Port Hueneme, CA 93043

Acknowledgments

The authors would like to thank the following individuals for their assistance: Dale Lorenzana, Meredith Metcalf and Jessica Chau for assisting in field testing; and Dorothy Cannon for logistical support. Dr. Mark Kram, Project Manager, provided funding and technical assistance. This project was funded through a contract (N47408-04-C-7514) with the Naval Facilities Engineering Service Center, Port Hueneme, California and is part of the Environmental Security Technology Certification Program (ESTCP) project CU-0421.

Table of Contents

1.0 INTRODUCTION 4

1.1 Background 4

1.2 Objectives 5

2.0 TEST METHODS 5

2.1 Dye Preparation and Injection 5

2.2 Field Sampling..... 6

2.2.1 Sample Collection 6

2.2.2 Sample Packaging and Shipping 7

2.3 Laboratory Analysis 7

2.3.1 Sample Rhodamine Analysis 7

2.3.2 Sample Turbidity Analysis 8

2.3.3 Cleaning 8

3.0 RESULTS 8

4.0 DISCUSSION 13

5.0 CONCLUSION 17

6.0 REFERENCES 17

1.0 INTRODUCTION

1.1 Background

This study was conducted as part of a larger demonstration effort supported by a grant from ESTCP CU-0421, entitled: *Detailed Hydraulic Assessment Using a High-Resolution Piezocone Coupled to the GeoVIS*. The focus of that study is to demonstrate the use of a high-resolution cone penetrometer system (SCAPS) in combination with a subsurface camera (GeoVIS) as a cost effective and rapid system to determine three-dimensional hydrogeology and ground water flow at contamination sites. To evaluate the effectiveness of this approach the SCAPS was used to characterize a site at the Naval Facilities Engineering Service Center (NFESC) in Port Hueneme, California. For comparison, the test site has been characterized in three dimensions using a more conventional approach involving the installation of 39 customized short screen (e.g., 6-inch length) monitoring wells at 13 locations (**Figure 1**). The wells were screened at depths of approximately 8-8.5 feet (shallow), 10-10.5 ft (middle), and 13.5 - 14 ft (deep).

To further compare the SCAPS with conventional site assessment, a tracer study was conducted in an attempt to obtain concentration data for comparing model simulations based on the different site characterization data sets. The design of the tracer

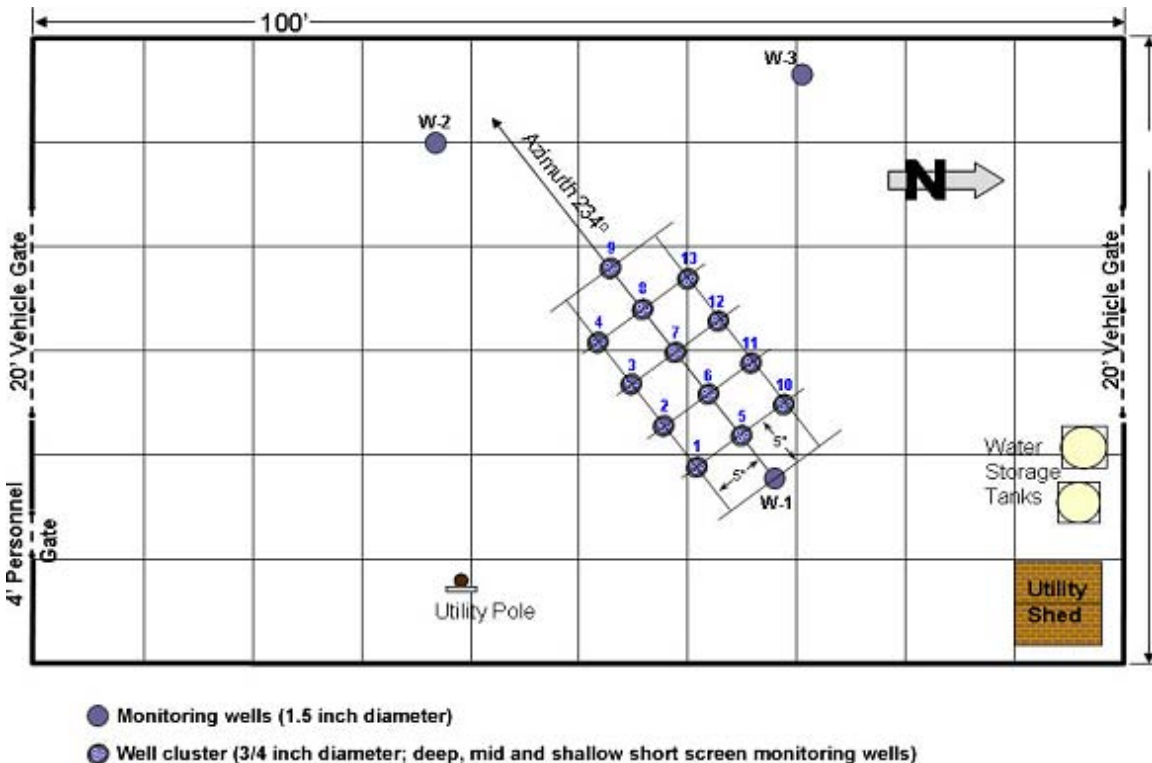


Figure 1. Well Cluster Test Site.

study was based on an analysis of data collected in a time series geophysical test (Robbins et al. 2005) and permitting constraints. The Navy had available at the site a portable fluorometer for detecting Rhodamine WT dye.

1.2 Objective

The objective of this study was to collect concentration distribution data for one or more periods at the well clusters for model input.

2.0 TEST METHODS

2.1 Dye Preparation and Injection

Rhodamine WT Dye was used as the tracer. A solution of 200,000 ppb Rhodamine WT was prepared from a Turner Designs 10-108 calibration standard and spring water. To prepare the solution, 0.42460 (~ 0.42) grams of Rhodamine WT were weighed in a glass beaker and added to a 2,000-ml volumetric flask. To assure minimum loss of dye, the beaker was rinsed several times with water and the rinseate was added to the flask. An additional volume of de-ionized water was added to completely fill the flask to the 2,000 ml mark.

MW-1 (**Figure 1**) located 5 feet upgradient from the well cluster network was used as the injection well. The well was constructed of 1.5" ID PVC, having a prepacked screen situated at a depth between 10 to 13.5 feet. To minimize tracer lag in the well head dead space above the well screen after injection, a small bore mechanical packer system was developed and inserted into the well just above the screen (**Figure 2**). The packer, based on McCabe (1996), consisted of a 1/2" diameter, 2.5 feet long slotted PVC pipe connected by fittings to 1/2" OD aluminum pipe. The aluminum pipe had an inner diameter of 1/4" and 3 foot long sections were connected together by fittings. The connection between the injector screen and aluminum pipe was fabricated with three expandable rubber plugs separated by spacers. After lowering the packer system into the well, and positioning the plug just above the well screen, expansion of the plugs was accomplished by screwing a butterfly bolt down at the surface on a threaded pipe which pushed a washer down on an outer 1/2" PVC pipe which in turn compressed the plugs against a lower fixed washer and the sides of the well. A valve with a hose barb was connected to the threaded pipe at the surface. Tubing was connected to the hose barb and then to a peristaltic pump for injecting the tracer. Following tracer injection the valve was closed and the injection system was left in place until the test was terminated.

The 2 liters of tracer was injected on July 25, 2006 by pumping the tracer out of the volumetric flask into the well through the packer system (**Figure 3**). This took several minutes and was followed by an injection of 200 ml of clean water to flush the tracer from the injector dead space.

2.2 Field Sampling

2.2.1 Sample Collection

Groundwater samples were collected between August and the end of October 2006 using low flow sampling. Prior to actual sample collection, depth-to-water measurements were taken. In an attempt to minimize flow field disturbance, the following procedure was followed. Purging was performed at a very low purge rate, between 40 to 80 milliliters per minute. After the water level stabilized during pumping, approximately 100 ml were further purged out of the aquifer. A sample was then collected in a 40-ml VOA vial. Following sample collection, depth-to-water measurements were taken a second time. In addition to depth-to-water measurements, the following data were also collected: date, time, well identification, flow rate (in ml/sec), sample color and visual description of samples. All data were recorded on field data sheets.

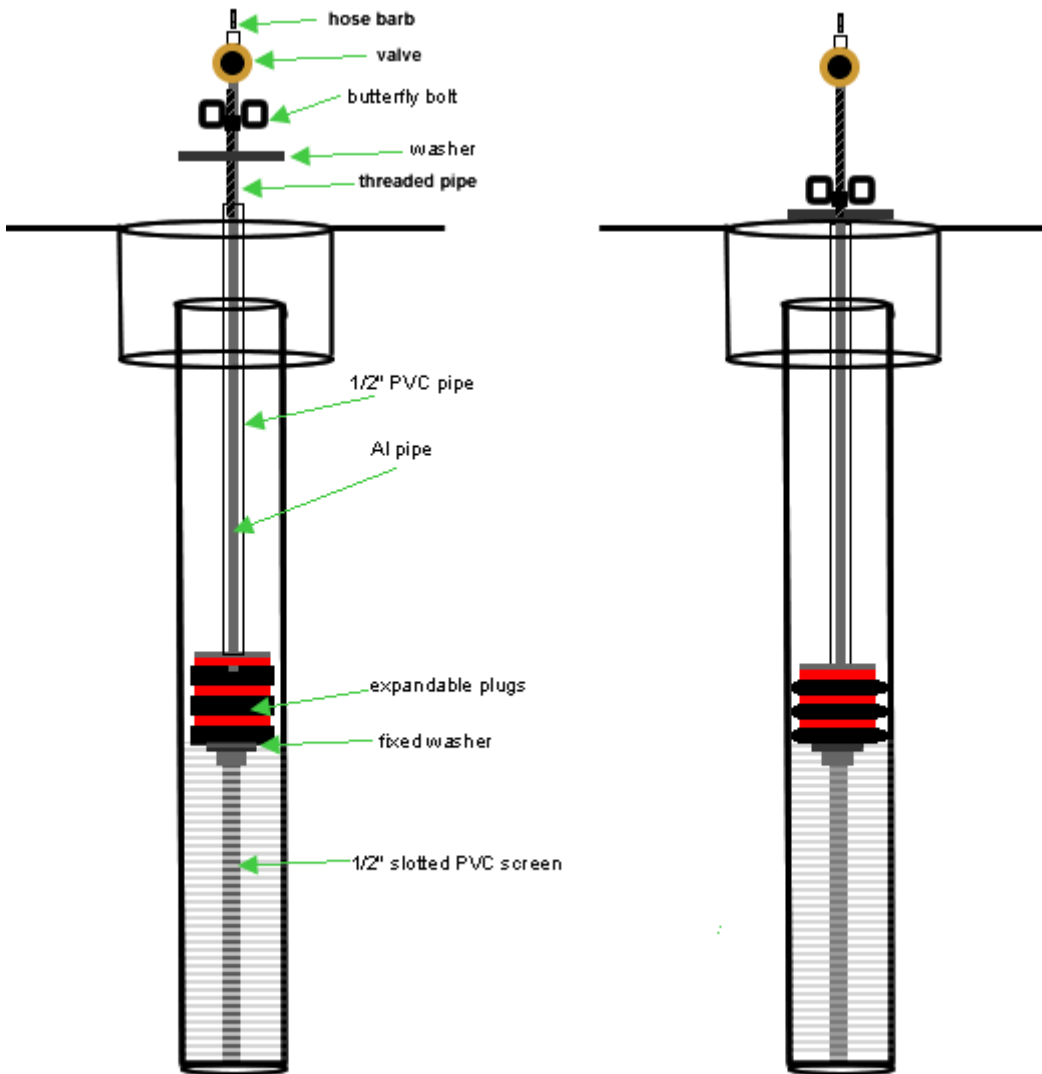


Figure 2. Packer system for dye injection (left: plug unexpanded, right: plug expanded).



Figure 3. Tracer injection.

2.2.2 Sample Packaging and Shipping

Samples were packaged in a UV light-resistant box and transported to the NFESC facility laboratory for analyses. All samples were stored in darkness in the laboratory for at least 24 hours prior to analysis to allow suspended solids to settle and to allow sample temperatures to equilibrate to that of the laboratory standard.

2.3 Laboratory Analyses

2.3.1 Sample Rhodamine Analyses

Samples were analyzed using a Turner Designs *Aquafluor*TM handheld fluorometer/turbidimeter. All samples were measured for both fluorescence and turbidity. Fluorescence was measured in parts per billion (ppb), and turbidity was measured in Nephelometric Turbidity Units (NTU). The instrument has a dynamic linear range for Rhodamine WT between a detection limit of 0.4 to over 300 ppb. It has a detection range for turbidity between 0.5 and 150 NTU. Prior to sample analysis, the *Aquafluor*TM meter was calibrated with a primary standard using *Aquafluor*TM User's Manual guidelines. Samples were analyzed in clean, dry 5-ml methacrylate cuvettes (by Turner Designs). The cuvettes were filled with a 3-ml solution volume for analysis. One aliquot of sample was analyzed 3 times each for both turbidity and fluorescence. The following (sample) data were collected and recorded: date and time of sample collection and analysis, and laboratory (air and sample) temperatures.

A 100-ppb Rhodamine WT solution was prepared and used for the Fluorometer calibration. To prepare the standard, 0.49274 (~ 0.50) grams of Rhodamine WT tracer injection solution was weighed out in a glass beaker and added to a 1,000-ml flask. The

beaker was rinsed several times with de-ionized water and also added to the flask. An additional volume of de-ionized water was added to completely fill the flask.

2.3.2 Sample Turbidity Analysis

Prior to each sample analysis, the Fluorometer was calibrated with both a blank and standard. Hach StablCal® (0 and 100 NTU) standards were used. Standards were shaken well before Fluorometer readings were collected and recorded.

2.3.3 Cleaning

All glassware and plastic material were washed thoroughly with a solution of non-florescent detergent (Liquinox™). The material was then rinsed 3 times each with tap water and de-ionized water and allowed to air dry.

3.0 RESULTS

Several days following the tracer injection (7/31/06), samples were collected from several downgradient wells within the cluster network and at the site perimeter to evaluate potential false negative detections that may result from turbidity. Thereafter samples were collected on approximately weekly bases from select wells through the end of October 2006. In all, sampling was conducted 11 times. During four of the sampling periods, samples were collected from all of the wells within the cluster network.

Tables 1 and 2 summarize the rhodamine and turbidity results. The data in the table represent averages determined on analyzing each sample in triplicate. Precision was very high and typically less than 5 percent RSD ($100 * \text{Mean} / \text{Std. Dev.}$) for rhodamine and turbidity. The highest rhodamine concentration observed was only about 30 ppb and the highest turbidity measured was about 38 NTU.

Initial background readings on samples taken on July 31, 2006 from downgradient wells outside of and within the cluster network showed an apparent background level of rhodamine and a linear relation between the apparent rhodamine readings and turbidity (**Figure 4**). The instrument manufacturer notes that turbidity could cause either suppression of or an apparent enhancement in readings depending on its nature (Turner Designs, 2007). Based on observations made during development efforts, the turbidity here is characterized by silt or clay sized material, with little organic matter being observed. Laboratory experiments subsequently conducted at the University of Connecticut using the same model instrument showed that similar sized material caused false positive readings when added to tap water (**Figure 5**). Also, a linear increase in rhodamine concentration reading with turbidity was observed when silt sized crushed rock was added to a 100 ppb standard (**Figure 6**).

Recognizing that turbidity could vary from well to well and between sampling rounds, several approaches were tried to remove turbidity influences. Early on,

Table 1. Measured Rhodamine Results (ppb) for Each Sampling Round

Well	8/8/06	8/9/06	8/16/06	8/22/06	8/30/06	9/1/06	9/6/06	9/12/06	9/19/06	9/26/06	10/3/06	10/11/06	10/24/06
PZ-01-S			6.1			4.5		10.5					8.6
PZ-02-S			8.1			16.6		8.3					9.6
PZ-03-S			3.2			2.1		1.8					1.5
PZ-04-S			-1.6			0.6		5.8					9.8
PZ-05-S			6.7		11.8	11.5	17.9	12.8	17.4	16.0	15.9	8.6	12.8
PZ-06-S			9.4			12.4		15.9					16.7
PZ-07-S			8.0			6.5		12.1					7.3
PZ-08-S			6.8			7.2	9.8	8.8					14.4
PZ-09-S			5.4			3.1		29.7					27.4
PZ-10-S			7.3			11.1		14.7					16.4
PZ-11-S			7.5			12.5		6.1					5.9
PZ-12-S			1.3			3.9		17.7					13.2
PZ-13-S			4.7			17.1	9.0	9.3					12.6
PZ-01-M-alt			6.2			14.6		12.0					11.4
PZ-02-M	10.0		6.4	2.0	5.2	10.6	14.6	7.0	8.4	11.5	17.0		13.2
PZ-03-M			5.1			7.6		11.0					12.5
PZ-04-M-alt			8.5			9.7		9.9					9.8
PZ-05-M			6.1		3.7	9.1	11.2	9.5	16.9	16.2	10.3	13.7	11.9
PZ-06-M	10.9		4.7	2.8	21.1	10.3	11.7	9.4	11.0	9.9	14.6		10.2
PZ-07-M			3.3			7.1		10.0					9.9
PZ-08-M			5.9			7.9	8.5	9.8					8.9
PZ-09-M			5.2			-0.1	8.2	19.8					25.5
PZ-10-M			2.8			12.7		15.3			18.4	14.4	12.9
PZ-11-M	8.0		4.2	1.5	12.0	12.1	14.4	7.7	16.2	14.4	14.9	15.2	8.1
PZ-12-M			7.0			9.4		11.7				6.6	10.5
PZ-13-M			5.4			5.6	7.5	7.8			14.1	13.8	13.2
PZ-01-D			10.8			9.0		9.0					8.5
PZ-02-D			4.3			12.2		13.3					9.6
PZ-03-D			4.7			11.7		13.0					7.5
PZ-04-D			4.7			8.5		11.3					17.2
PZ-05-D			6.4		10.4	8.4	15.6	12.4	14.4	6.8	6.4	11.1	7.4
PZ-06-D			2.2			2.8		9.5					10.2
PZ-07-D			3.6			9.2		11.8					10.9
PZ-08-D			2.2			9.0	6.9	7.5					9.8
PZ-09-D			10.6			5.6	10.5	5.2					9.0
PZ-10-D			4.2			9.8		10.2					14.3
PZ-11-D			5.0			10.0		10.1					12.8
PZ-12-D			8.9			9.7		12.4					9.2
PZ-13-D			3.6			8.6	5.5	12.5					11.4
MW-01									32.3				11.4
MW-01									14.3				
MW-02			5.5										
MW-03			4.0										
MW-04		14.2	1.2										
MW-05		1.5	1.8										

Table 2. Measured Turbidity Results (NTU) for Each Sampling Round

Well	8/8/06	8/9/06	8/16/06	8/22/06	8/30/06	9/1/06	9/6/06	9/12/06	9/19/06	9/26/06	10/3/06	10/11/06	10/24/06
PZ-01-S			0.0			3.6		7.7					6.2

PZ-02-S			8.1			19.2		8.2					10.0
PZ-03-S			0.9			2.3		-0.1					1.1
PZ-04-S			1.2			2.8		8.5					8.1
PZ-05-S			6.4		15.4	15.5	16.7	11.9	19.0	17.3	18.9	7.3	12.6
PZ-06-S			9.1			13.4		22.6					20.8
PZ-07-S			7.1			14.0		14.8					8.2
PZ-08-S			7.5			10.5	10.0	9.3					15.8
PZ-09-S			5.5			5.1		37.8					32.8
PZ-10-S			4.9			14.3		17.5					17.7
PZ-11-S			7.7			14.9		8.5					5.1
PZ-12-S			4.3			9.0		19.0					13.0
PZ-13-S			6.0			21.6	11.6	9.5					12.9
PZ-01-M-alt			7.3			18.2		13.8					14.6
PZ-02-M	11.5		4.5	5.5	6.9	15.2	10.7	11.1	6.3	12.4	18.1		13.0
PZ-03-M			6.5			11.8		13.2					13.6
PZ-04-M-alt			6.3			10.8		9.5					10.9
PZ-05-M			4.3		5.3	10.6	10.6	14.0	19.1	17.8	14.9	15.7	11.1
PZ-06-M	6.9		4.3	5.8	25.8	12.5	11.6	11.5	10.4	10.4	19.2		12.4
PZ-07-M			4.4			9.9		12.1					10.2
PZ-08-M			4.9			10.0	8.8	9.4					9.4
PZ-09-M			4.9			3.9	9.0	23.0					27.7
PZ-10-M			3.3			15.0		17.9			21.2	16.4	16.6
PZ-11-M	6.9		3.1	5.1	11.9	17.2	11.5	9.4	13.9	14.5	19.2	13.9	8.3
PZ-12-M			5.8			11.3		14.9				6.8	11.1
PZ-13-M			4.3			9.0	5.6	8.7			16.2	11.9	12.7
PZ-01-D			7.7			10.2		10.4					10.8
PZ-02-D			3.9			14.3		12.5					10.6
PZ-03-D			4.3			12.8		15.7					9.5
PZ-04-D			1.7			10.9		12.8					24.6
PZ-05-D			4.8		11.2	13.9	13.3	12.5	15.3	5.7	9.2	9.5	10.3
PZ-06-D			2.5			5.4		14.4					9.9
PZ-07-D			4.2			13.1		14.1					10.9
PZ-08-D			2.9			9.3	8.7	6.4					10.2
PZ-09-D			8.2			7.7	9.8	6.6					10.0
PZ-10-D			3.5			14.4		12.1					16.4
PZ-11-D			3.5			10.8		12.9					15.4
PZ-12-D			7.6			12.2		12.6					8.1
PZ-13-D			3.7			9.2	3.6	12.8					10.2
MW-01									13.3				13.0
MW-01			2.6						3.7				
MW-02			3.5										
MW-03		17.5	2.2										
MW-04		5.5	1.7										
MW-05		1.5	1.8										

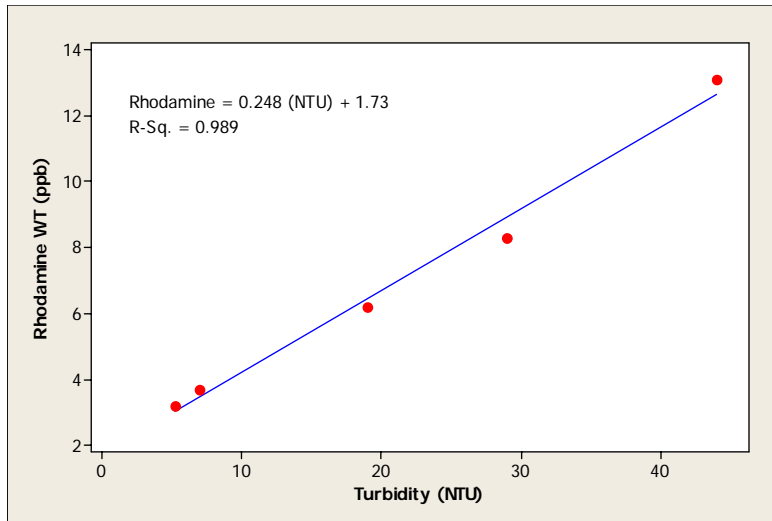


Figure 4. Apparent rhodamine readings due to turbidity (samples collected on July 31, 2006). experiments were performed using the rhodamine standard to test whether samples could be filtered using syringe filters without impacting rhodamine readings, but rhodamine adsorption was observed on available filters. Tests were also conducted to see if centrifuging samples prior to analysis would work, but this was found to be impractical. As an alternative means to resolve the issue, samples were left to settle for twenty four hours and then an aliquot was drawn off for analysis. Even though low levels of turbidity were achieved using this approach, a correlation between rhodamine readings and turbidity was still observed. A correction was applied using the regression in **Figure 4** as an attempt to correct readings for turbidity. However, as data were obtained it became apparent that the correction was not sufficient to remove the turbidity influence.

The instrument manufacturer suggests a multivariate approach to develop a correction (Turner Designs, 2007). To test this approach, the rhodamine analytical standard was diluted with distilled water and with ground water from the site to generate a relation between actual concentration, apparent concentration and turbidity. The approach overcompensated for turbidity, resulting in an inverse relation between rhodamine and turbidity. The instrument manufacturer approach assumes that the level of turbidity is constant and that the only factor that changes is the concentration of rhodamine, which is not the case here. Several other QC tests were conducted. The turbidity of the 100 ppb rhodamine standard was measured on several occasions and consistently registered near zero NTU. The rhodamine standard was systematically diluted with clean water to test the instrument functionality. The clean water standard concentration diluted in a relatively linear manner with the degree of dilution down to about 6 ppb, the limit of the dilution.

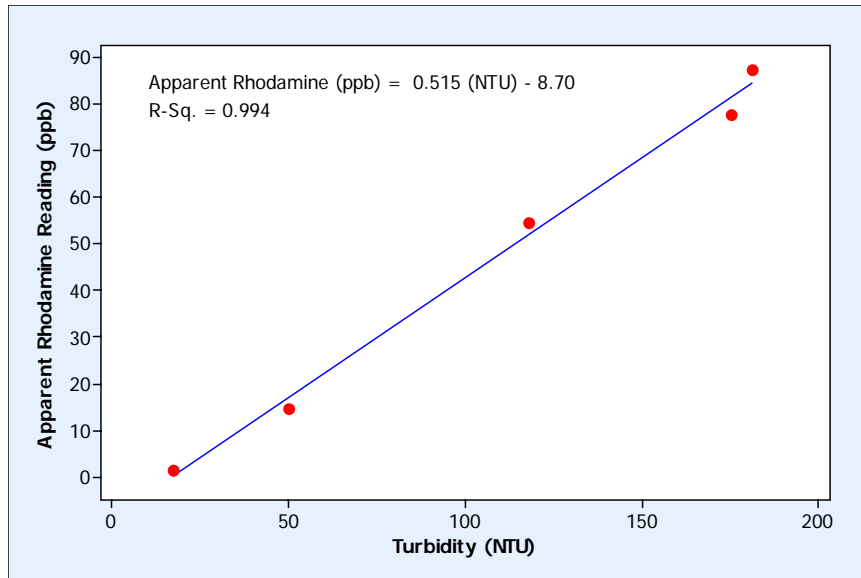


Figure 5. Apparent rhodamine correlation with turbidity based on adding silt to clean tap water.

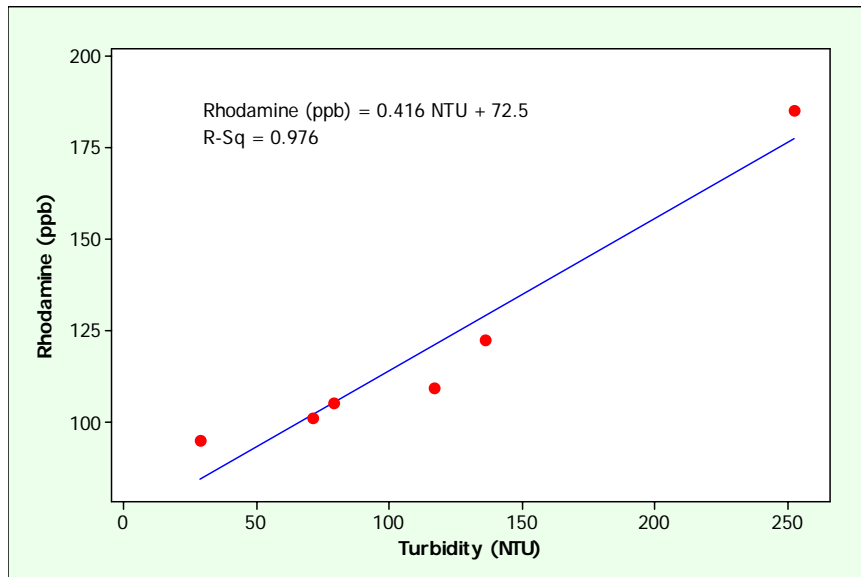


Figure 6. Influence of turbidity on 100 ppb rhodamine standard concentration.

Figure 7 shows the relation between apparent rhodamine readings and turbidity for all the sampling rounds. Each sampling round resulted in about the same linear increase in measured rhodamine concentration with turbidity.

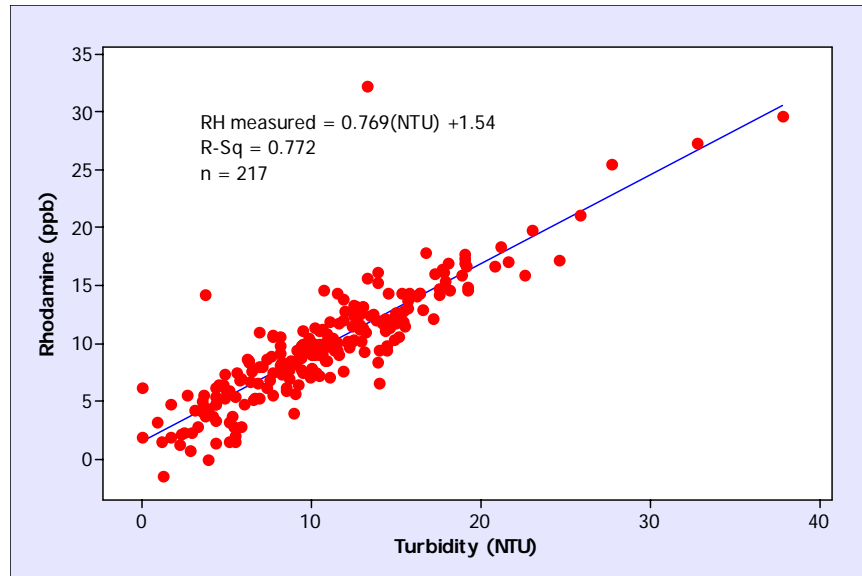


Figure 7. Measured Rhodamine and Turbidity (217 samples).

Temporal and spatial variations in rhodamine and turbidity readings were examined through developing graphs of readings with time, and by 2D and 3D contouring of sampling rounds. Ideally, the tracer concentration distribution would appear as a bullseye shaped pulse in map and cross sectional views that would migrate through the well clusters with time. Furthermore, at any well that detected the tracer, it was expected to observe an increase and then decrease in concentration with time as the tracer migrated in a pulse configuration. Although at some wells the concentration did increase then decrease with time, the rhodamine response mimicked the turbidity levels, as exemplified in **Figure 8** for well 5-M, the closest mid-level well to the injection well. Furthermore, the timing of peak concentrations amongst the wells in the cluster network was not consistent with a migrating pulse of tracer. Similarly, one could not discern spatial trends in concentration data in the four rounds of sampling where all the cluster wells were sampled that were definitively consistent with a migrating pulse of tracer. Overall, the tracer concentration appeared to increase throughout the test area with time.

4.0 DISCUSSION

The lack of definitive tracer observation is likely in part a result of masking by turbidity interference. In Robbins et al. (2005) analytical model predictions for the site were made based on calibration of dispersion parameters with a salt tracer conducted as part of a time series resistivity study to evaluate the ground water flow direction. Based on the parameters in **Table 3** from Robbins et al. (2005), analytical modeling predicted rhodamine concentrations on the order of those observed (up to about 30 ppb at PZ 05-M). Numerical modeling conducted as part of this study used the parameters in **Table 4** to predict tracer concentrations. In comparison, the numerical model distributed the injected mass over a somewhat larger source volume, resulting in lesser initial

concentration. The velocity used in the initial modeling was higher than that used in the numerical modeling. The velocity used in the initial modeling was based on higher

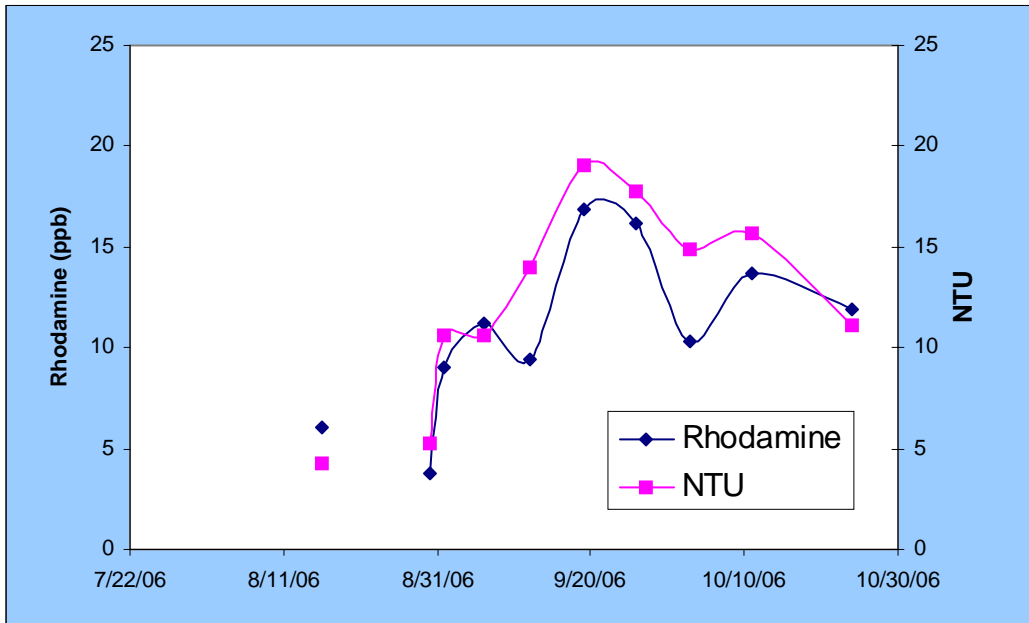


Figure 8. Variation in rhodamine and turbidity with time at PZ-05-M.

Table 3. Input Parameters for the Rhodamine Dye Model (after Robbins et al., 2005)

Co ($\mu\text{g/l}$)	200000
injection volume (cc)	2000
X (cm)	7.9
Y (cm)	7.9
Z (cm)	106.7
v (cm/s)	1.07E-04
porosity (%)	30
α_x (cm)	800
α_y (cm)	220
α_z (cm)	18

hydraulic conductivity values derived from tests conducted in perimeter wells. The numerical modeling used the hydraulic conductivity values derived in the cluster network, which were about an order of magnitude less than that of the perimeter wells. For conservatism, in light of the lower velocity, the dispersivity values were reduced by a factor of 10 in the numerical model. This resulted in higher predicted concentrations up to about 280 ppb at PZ-05-M. Given difficulties in numerical model calibration, owing to the low gradient and lack of definitive head boundaries, and lack of dispersion calibration, this prediction could easily be off by an order of magnitude.

Other factors that could have contributed to the lack of definitive tracer observation include the following:

Table 4. Input Parameters for the Numerical Rhodamine Dye Model

Co ($\mu\text{g/l}$)	19500 (0.4 g)
injection volume (cc)	not relevant- assume instant dilution in cell
X (cm)	30.48
Y (cm)	30.48
Z (cm)	74.07
v (cm/s)	Mean: 8.47E-06, Max: 1.2E-04
porosity (%)	30
α_x (cm)	80
α_y (cm)	22
α_z (cm)	1.8

Rhodamine dye is known to adsorb onto organic matter and biodegrade. However, given the sandy nature of the sediment, especially in the mid-zone, and the short distance of travel between the injection and the first cluster of short screen wells (5 ft), the contributions of these processes is considered minor.

It is possible that the rhodamine was diluted during the injection to the point where it became undetectable, especially in light of turbidity interference.

Given the low mean velocity, it is possible that the pulse of tracer moved almost in a plug flow fashion, between the wells. Recall the dye was injected over a screened vertical length between depths of 10 to 13.5 feet and the wells in the cluster network were screened at depths of approximately 8-8.5 feet (shallow), 10-10.5 ft (middle), and 13.5 - 14 ft (deep).

The hydraulic conductivity values determined for the perimeter wells 1, 2 and 3, were 8.94E-03, 1.75E-02, 3.02E-02, respectively and averaged 1.89E-02 cm/s. These values are greater than those observed in the cluster network wells. The initial SCAPS pushes also show that the zone between the mid and deep short screen wells has relatively high and variable conductivity. It is possible that the tracer took a higher conductivity path between the depth intervals of the well screens.

Although the rhodamine initial concentration was relatively low (200 ppm) and the ground water total dissolved solids at the site is relative high, density driven flow could have occurred and resulted in the tracer diving below the middle or deep wells intakes or moving above the middle well intakes.

It is possible given the duration of the test that water level changes may have resulted in the tracer moving in some direction other than that of the well cluster layout. Tidal influences on the hydraulic gradient were tested early on in the site characterization

efforts by measuring depth to water (DTW) in perimeter wells 1, 4 and 5 hourly over a 10 hour period. The results are shown in **Table 5**. No influence was observed within measurement error.

Table 5. Tidal Measurements (12/15/05)

Time of Day	MW-01	MW-04	MW-05	Azimuth	Gradient
	DTW (ft)	DTW (ft)	DTW (ft)	degrees	ft/ft
7:00	4.95	4.74	4.74	252	0.002
8:00	4.98	4.76	4.74	253	0.002
9:00	4.96	4.76	4.74	253	0.002
10:00	4.96	4.73	4.72	253	0.002
11:00	4.96	4.72	4.72	250	0.003
12:00	4.97	4.74	4.73	253	0.002
13:00	4.97	4.74	4.72	255	0.003
14:00	4.97	4.75	4.73	255	0.002
15:00	4.96	4.74	4.72	255	0.002
16:00	4.96	4.73	4.72	253	0.002
17:00	4.97	4.75	4.72	257	0.002
	Local Tide				
Tide	Time	Elev. ft			
Low	1:47	2.4			
High	8:06	6.5			
Low	15:33	-1.0			
High	22:13	3.7			

Between 2/26/06 and 3/29/06 water levels in MW-1 (the injection well) were monitored to evaluate how readily water levels at the test site responded to rainfall events. Water levels were measured at least once a day manually. Despite the fact that the site is overlain with asphalt, ground water levels responded relatively rapidly to precipitation events as shown in **Figure 9**. The rapid response of the ground water to precipitation suggests that leakage from nearby catch basins, drainage pipes and water mains could temporarily impact the flow field and the movement of the tracer, given the low gradient at the site.

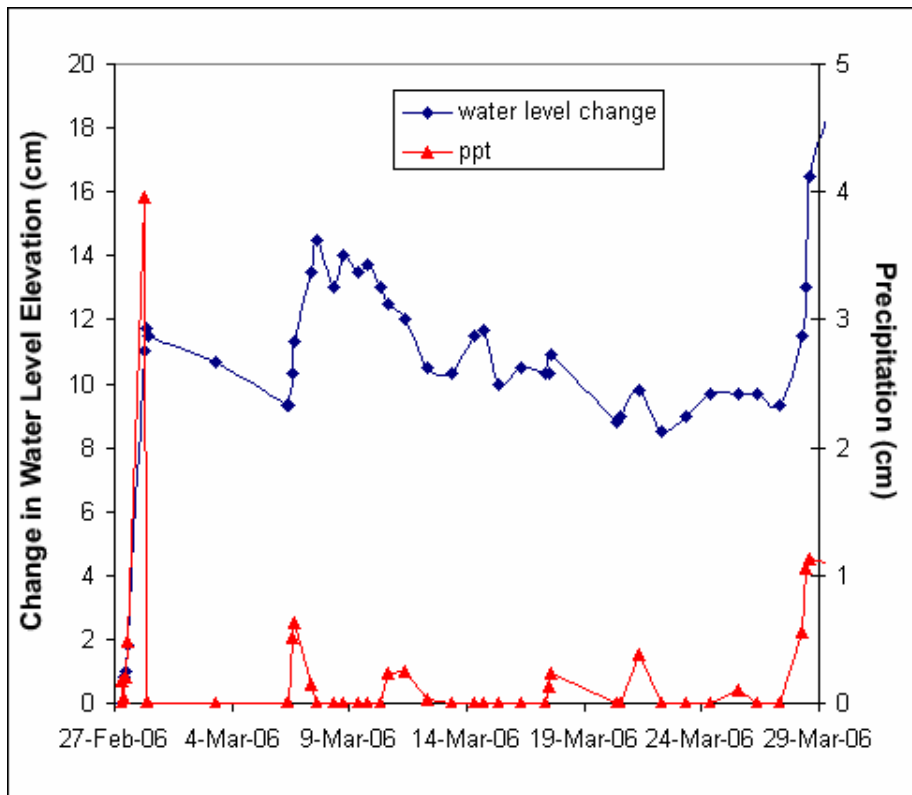


Figure 9. Water level changes in MW-1 in response to precipitation.

5.0 CONCLUSIONS

Owing to turbidity interference and other possible factors, there was a lack of definitive tracer observation on-site. Given the sensitivity of the handheld analytical equipment to turbidity, it necessitates the use of higher initial concentrations of rhodamine and developing an approach to negate turbidity influences, if the equipment is to be used in a ground water tracer study where turbidity is not constant. Despite the instruments low limits of detection and large linear range, its use in ground water studies is thwarted by its sensitivity to turbidity. If additional studies of this nature are to be performed at the Port Hueneme test site, it is suggested that they consist of force gradient testing to circumvent difficulties associated with the low natural gradient. Consideration might also be given to an alternative tracer.

6.0 REFERENCES

- McCabe, D., 1996, Evaluation of a Method for Obtaining Multilevel Hydrogeologic Data from Ground Water Monitoring Wells, M.S., Thesis, Dept. of Geology and Geophysics, University of Connecticut, Storrs, CT.
- Robbins, G.A., Cagle, B, and Lanbo, L., 2005, Time-Series Geophysical Tracer Study, Naval Facilities Engineering Service Center Port Hueneme, CA, Environmental Security

Technology Certification Program (ESTCP) project CU-0421, November 10, 36 p. with appendices

Robbins, G. A., 2005, GEOVIS/SCAPS Well Cluster Test Site Hydraulic Conductivity, Naval Facilities Engineering Service Center Port Hueneme, CA, Environmental Security Technology Certification Program (ESTCP) project CU-0421, November 21, 12 p. with appendices

Turner Designs, 2007, Effects Of Turbidity On In Vivo Chlorophyll Fluorescence, http://www.turnerdesigns.com/t2/esci/turbidity_effects.html

Tracer Injection Field Notes

7/25/06

Dye Injection Rhodamine Tracer Test

200 ppm Vol - 200 L

~~500,000~~

- pics taken
- pumped dye - 200ml
- " H₂O into well
- also 200ml
- 11:18 - injection (end) -
Rhodamine
- H₂O - followed after dye
(200ml).

<u>Mezo</u>	<u>Meters</u>	<u>LOC</u>
3-S	1.479, 1.479	" - N
3-M	1.445, 1.445	" - N
3-D	1.382, 1.381	" - N.
<hr/>		
4-S	1.465, 1.465	" - N
4-M (M)	1.443, 1.445	" - N
4-D	1.392, 1.394	" - N
<hr/>		
5-S	1.477 , 1.488, 1.485, 1.486	
5-M	1.4670 , 1.470	
5-D	1.448, 1.447, 1.448	
<hr/>		
6-S	1.452	
6-M	1.426, 1.427	
6-D	1.395, 1.397, 1.396	
<hr/>		
7-S	1.680 (1.680?) ✓ OR	
7-M	1.435	
7-D	1.407, 1.408	

7/25/06 Depth to water.

nw-4	(1) 2.679 M	Top of standpipe
	(2) 2.678 M	" " "
	(3) 2.678 M	" " "
nw-5	(1) 2.698 M	Top of standpipe
	(2) 2.698 M	" " "
MW-2	2.580 M.	Top of "
nw-3	(1) 2.621 M.	" " "
	(2) 2.621 M	" " "

Piezometers	Meters	Measured @
1-S	1.470, 1.469	Top of casing
1-M	1.460 , 1.405 , 1.461	" "
1-D	1.390, 1.390	" "

Piezo	Meters	(a) T.O.C
2-S	1.486, 1.487	
2-M	1.444, 1.443, 1.444	
2-D	1.402, 1.401,	

	1.442, 1.442	TOC-N
8-M	1.357, 1.358	
8-D	1.417, 1.417	
9-S	1.442, 1.367 1.441	TOC-N
9-M	1.376, 1.376	
9-D	1.360, 1.360	
10-S	1.438, 1.438	TOC-N
10-M	1.384, 1.385	
10-D	1.375, 1.378	
11-S	1.440, 1.440	
11-M	1.402, 1.402	
11-D	1.353, 1.351	
12-S	1.444, 1.444	
12-M	1.420, 1.420	
12-D	1.401, 1.410	

U	1.395, 1.395	7.
13-M	1.361, 1.360	4
13-D	1.312, 1.312	4

Flow Rate from water bottle

① $500\text{ml} / 32\text{sec}$

② $380\text{ml} / 70\text{sec}$

Flow Rate into well

- 400 ml

123.2 cm - ext.

4
 RHE 414.8 cm
 13.61'

5
 13.80'

Piezo 5

W.H.E. md 10.03'

	Well 4	5	Piezo 5
RHE	13.61'	13.80	10.03
OTW	<u>8.78'</u>	<u>8.85</u>	<u>4.82'</u>
H ₂ O Elev	4.83'	4.95'	5.21'
Σ east (x)	6195995.56	6195962.43	6196057.51
v (y)	1883406.75	1883499.81	1883491.51

~~Strike 141.521°
 Dip 0.25°~~

Hyd. grad 232°
~~Dip Direction 299.521~~
 mag. grad .004

CBC 51

1.640 m - Notch

Azimuth 234° - computer

APPENDIX H - GMS Workshop

GMS-SCAPS Workshop Agenda

August 31, 2005 – San Diego, California

- 1) Introduction to GMS
 - a. Background
 - b. Installation/Registration
 - c. GUI Layout
 - d. Modules
 - e. Project Explorer
 - f. Viewing angles
 - g. 3D Viz intro
- 2) Starting a New Project
 - a. Coordinate Systems
 - b. Units
 - c. Background Images
- 3) Importing SCAPS data
 - a. Overview of data import options
 - b. Import file format
 - c. Import process
- 4) Borehole Module
 - a. Stratigraphy vs. Sample Data
 - b. Display options
 - c. Conversion to scatter points
- 5) Geostatistics
 - a. Scatter point modules
 - b. 2D geostatistics
 - c. 3D geostatistics
- 6) 3D Visualization
 - a. Contouring
 - b. Cross-sections
 - c. 3D vectors
 - d. Iso-Surfaces
 - e. Animation
- 7) Flux/Velocity Tools
 - a. Equations/assumptions
 - b. Seepage/flux builder tools
 - c. Visualization
- 8) Mass Calculator
- 9) Applications
 - a. Building MODFLOW models
 - b. Boundary conditions/inverse modeling issues
 - c. MODPATH
 - d. MT3DMS

GMS-SCAPS Workshop

San Diego, California
August 31, 2005

Quick Facts

- First version released early 1995
- Current version is v5.1/6.0
- Developed by EMRL at BYU
- Partially sponsored by DoD
- Distribution and tech support handled by EMSI
- Thousands of users in over 90 countries

GMS Web Site

- <http://www.ems-i.com/>
- General info. on GMS
- News
- Demo versions of GMS
- Models (MODFLOW, FEMWATER, etc.)
- Bug fixes posted periodically

GMS Mailing List

- Used to
 - Post news on GMS
 - Ask questions of fellow users
 - Share tips
- To subscribe
 - Send a message to majordomo@ems-i.net with “subscribe gms-l” in the message

Modules in GMS

- Boreholes
- TINs
- Solids
- 2D Meshes
- 2D Grids
- 2D Scatter Points
- 3D Meshes
- 3D Grids
- 3D Scatter Points
- Map
- GIS

Contact Information

- DOD Users
 - Clarissa Hansen, USACOE
 - 601-634-2102
 - Clarissa.M.Hansen@erdc.usace.army.mil
- Other Users
 - Jeff Davis, EMSI
 - 801-302-1400
 - jeff@ems-i.com
- Norm Jones
 - njones@byu.edu
 - 801-42207569

Overview of Steps

- Import SCAPS data as boreholes
- Convert to 3D scatter points
- Interpolate to 3D grid
- Run flux/seepage velocity data set builder
- Visualize results

Getting Started on a Modeling Project

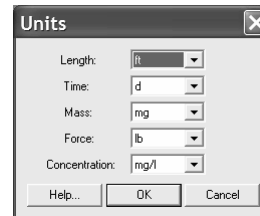
Coordinate systems, units, base maps

Basic Steps

1. Select units
2. Define a coordinate system
3. Establish a base map
4. Build a conceptual model

Units

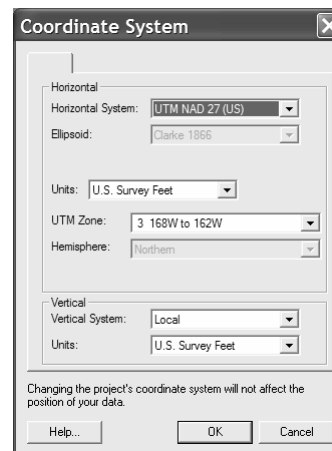
- Select “Units” command in Edit menu
- Controls text labels displayed in interface as a units reminder
- Helps ensure consistent units



Item	Value	Units
Horizontal k	0.0	(ft/d)
Vertical k	0.0	(ft/d)
Horizontal anisotropy	1.0	
Vertical anisotropy (Kh/Kv)	1.0	
Specific storage	0.0	(1/ft)
Specific yield	0.0	
Long. disp.	0.0	
Porosity	0.3	

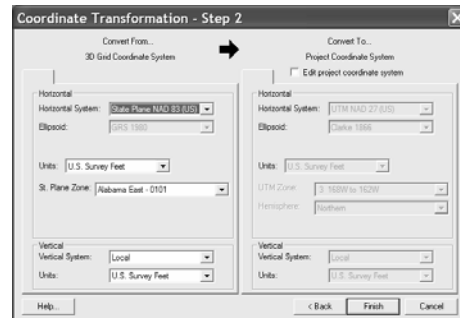
Coordinate Systems

- Select “Coordinate System...” command in Edit menu
- Defines default system for project
- Individual objects can be transformed to selected system



Transforming Objects

- To transform the coordinate system of individual objects:
 - Import object (scatter point set, obs. wells, etc.)
 - Right click on object in Data Tree and select “Transform...” command



Defining a Base Map

- Uses:
 - Provides a reference for on-screen digitizing
 - Enhances display of model data
- Options
 - Digital images
 - CAD drawings
 - GIS maps

Digital Images

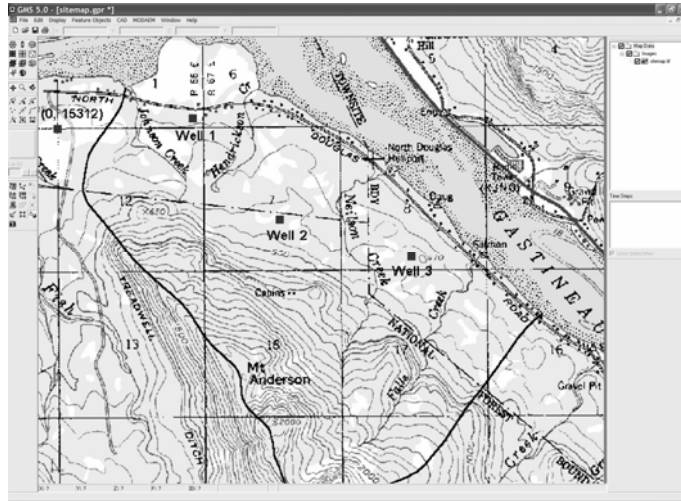


Image Files

- Sources
 - Scanned maps
 - Aerial Photos
 - Internet (see next slide)
 - Mapping/GIS companies
- Can be pre-processed using image editing utilities such as Paint Shop Pro
- TIFF Files (*.tif)
- JPEG Files (*.jpg)

Online Sources for Digital Maps

- <http://emrl.byu.edu/gishydrodata/images.htm>
- http://mcmcweb.er.usgs.gov/drg/free_drg.html
- www.gisdatadepot.com
- <http://mapping.usgs.gov/>

Importing Image Files

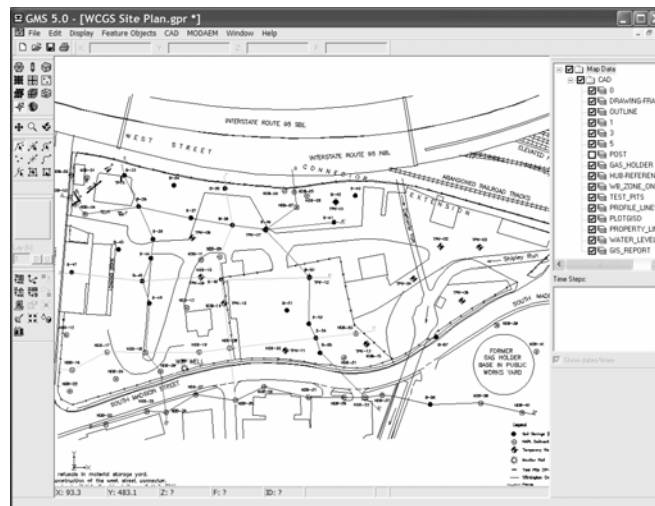
- Use Open command in File menu
- Select image file
- Make sure file has proper extension
 - *.tif, *.tiff for TIFF files
 - *.jpg, *.jpeg for JPEG files

Registering Images

- Identify 2 or 3 points on image where global coordinates are known
- Enter coordinates for each point
- Not required for “geo-referenced” image files



CAD Drawings



Importing CAD Data

- Use Open command in File menu
- *.dwg, *.dxf extension for file

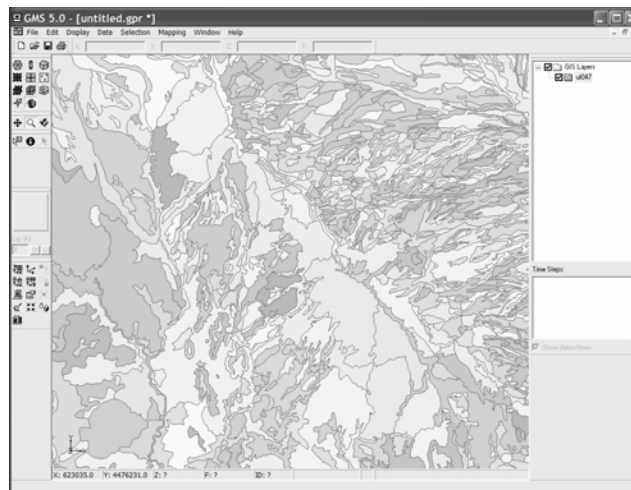
GIS Maps

- Imported via GIS module
- Can be used to import ANY GIS database
- See “Importing GIS Data” lecture

To Import GIS Data

1. Switch to GIS module
2. Select “Enable ArcObjects” from Data Menu (if appropriate)
3. Select the “Add Data” command
4. Select and open file

Sample GIS Map



(soil type)

Data Import

Importing SCAPS Data to GMS

File Format

	A	B	C	D	E	F	G	H	I	J	K
1	Push	x	y	z	Soil Class	Soil Class	(Hydraulic Head	K (min)	K (max)	K (mean)	K (calculated) K
2	Piezocone 0007.mdb	1838959.43	6264897.54	0.333	7	4	0.321	6.98E-03	9.97E-03	8.47E-03	1.29E-05
3	Piezocone 0007.mdb	1838959.43	6264897.54	-1.65	8	8	1.6	6.98E-03	9.98E-03	8.48E-03	1.84E-05
4	Piezocone 0007.mdb	1838959.43	6264897.54	-3.665	8	8	1.921	6.98E-03	9.97E-03	8.47E-03	1.45E-05
5	Piezocone 0007.mdb	1838959.43	6264897.54	-5.667	7	5	2.354	6.98E-03	9.97E-03	8.48E-03	1.61E-05
6	Piezocone 0002.mdb	1839027.56	6264856.01	0.643	7	4	0.305	7.00E-03	1.00E-02	8.50E-03	3.28E-04
7	Piezocone 0002.mdb	1839027.56	6264856.01	-1.34	8	8	0.673	7.00E-03	1.00E-02	8.50E-03	5.23E-04
8	Piezocone 0002.mdb	1839027.56	6264856.01	-3.355	8	8	1.183	7.00E-03	1.00E-02	8.50E-03	6.06E-04
9	Piezocone 0002.mdb	1839027.56	6264856.01	-5.357	7	5	1.521	7.00E-03	1.00E-02	8.50E-03	4.85E-04
10	Piezocone 0003.mdb	1839011.08	6264907.86	-0.442	6	4	0.34	7.00E-03	1.00E-02	8.50E-03	1.24E-03
11	Piezocone 0003.mdb	1839011.08	6264907.86	-2.443	6	5	0.759	7.00E-03	1.00E-02	8.50E-03	1.37E-03
12	Piezocone 0003.mdb	1839011.08	6264907.86	-4.42	6	3	1.107	7.00E-03	1.00E-02	8.50E-03	1.87E-03
13	Piezocone 0003.mdb	1839011.08	6264907.86	-6.303	7	4	1.572	7.00E-03	1.00E-02	8.50E-03	1.35E-03
14	Piezocone 0004.mdb	1839046.26	6264970.03	0.505	8	8	0.725	7.00E-03	1.00E-02	8.50E-03	4.80E-04
15	Piezocone 0004.mdb	1839046.26	6264970.03	-1.619	7	4	1.045	7.00E-03	1.00E-02	8.50E-03	1.03E-03
16	Piezocone 0004.mdb	1839046.26	6264970.03	-3.372	7	4	1.405	7.00E-03	1.00E-02	8.50E-03	1.49E-03
17	Piezocone 0004.mdb	1839046.26	6264970.03	-5.418	7	4	1.864	7.00E-03	1.00E-02	8.50E-03	1.17E-03
18	Piezocone 0005.mdb	1839062.73	6264918.18	0.755	8	8	0.818	7.00E-03	1.00E-02	8.50E-03	6.13E-04
19	Piezocone 0005.mdb	1839062.73	6264918.18	-1.369	7	4	1.045	7.00E-03	1.00E-02	8.50E-03	1.03E-03
20	Piezocone 0005.mdb	1839062.73	6264918.18	-3.122	7	4	1.405	7.00E-03	1.00E-02	8.50E-03	1.49E-03
21	Piezocone 0005.mdb	1839062.73	6264918.18	-5.168	7	4	1.864	7.00E-03	1.00E-02	8.50E-03	1.17E-03
22	Piezocone 0006.mdb	1838994.61	6264959.7	0.258	6	4	0.34	7.00E-03	1.00E-02	8.50E-03	1.24E-03
23	Piezocone 0006.mdb	1838994.61	6264959.7	-1.743	6	5	0.759	7.00E-03	1.00E-02	8.50E-03	1.37E-03
24	Piezocone 0006.mdb	1838994.61	6264959.7	-3.72	6	3	1.107	7.00E-03	1.00E-02	8.50E-03	1.87E-03
25	Piezocone 0006.mdb	1838994.61	6264959.7	-5.603	7	4	1.572	7.00E-03	1.00E-02	8.50E-03	1.35E-03
26	Piezocone 0001.mdb	1838975.91	6264845.7	0.393	7	4	0.315	7.00E-03	1.00E-02	8.50E-03	9.65E-04
27	Piezocone 0001.mdb	1838975.91	6264845.7	-1.59	8	8	0.675	7.00E-03	1.00E-02	8.50E-03	5.23E-04
28	Piezocone 0001.mdb	1838975.91	6264845.7	-3.605	8	8	1.177	7.00E-03	1.00E-02	8.50E-03	8.50E-04
29	Piezocone 0001.mdb	1838975.91	6264845.7	-5.607	7	5	1.519	7.00E-03	1.00E-02	8.50E-03	5.45E-04
30											
31											

File Format, Cont.

- Can be created/saved
 - to text file
 - to spreadsheet
- Required columns
 - X, Y, Z
 - Data sets
 - ☞ Any number
 - ☞ Any order

Steps

1. Import table
 - Open text file, or
 - copy table to clipboard and paste into GMS
2. Follow steps in Data Import Wizard

Import Wizard, Step 1

File Import Wizard - Step 1 of 2

File import options

Set the column delimiters:

Delimited Fixed Width

Space Tab Semicolon

Comma Other: Text qualifier:

Treat consecutive delimiters as one Skip leading delimiters

Start import at row: Heading row

File preview

	Push	x	y	z	Soil Cla
1	Push	x	y	z	Soil Cla
2	Piezococone 0007.mdb	1838959.429999999900	6264897.540000000000	0.333	7
3	Piezococone 0007.mdb	1838959.429999999900	6264897.540000000000	-1.650	8
4	Piezococone 0007.mdb	1838959.429999999900	6264897.540000000000	-3.665	8
5	Piezococone 0007.mdb	1838959.429999999900	6264897.540000000000	-5.667	7

Help < Back Next > Cancel

Import Wizard, Step 2

File Import Wizard - Step 2 of 2

GMS data type:

Borehole sample data

No data flag -999.0 Name: GMS Export

File preview

Type	Name	X	Y	Z	Data set	Data set
Header	Push	x	y	z	Soil Class (load...	Soil Class (pore...
	Piezococone 000...	1838959.4299...	6264897.5400...	0.333	7	4
	Piezococone 000...	1838959.4299...	6264897.5400...	-1.650	8	8
	Piezococone 000...	1838959.4299...	6264897.5400...	-3.665	8	8
	Piezococone 000...	1838959.4299...	6264897.5400...	-5.667	7	5
	Piezococone 000...	1839027.5600...	6264856.0099...	0.643	7	4
	Piezococone 000...	1839027.5600...	6264856.0099...	-1.340	8	8

First 20 lines displayed.

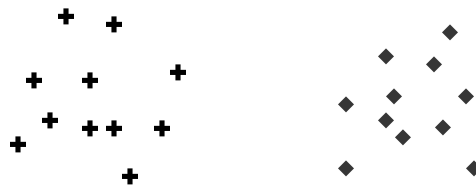
Help < Back Finish Cancel

2D & 3D Geostatistics in GMS

Data Interpolation Using the
Scatter Point Modules

Scatter Point Sets

- Each set contains a list of points with an xy location
- Each set contains a list of data sets



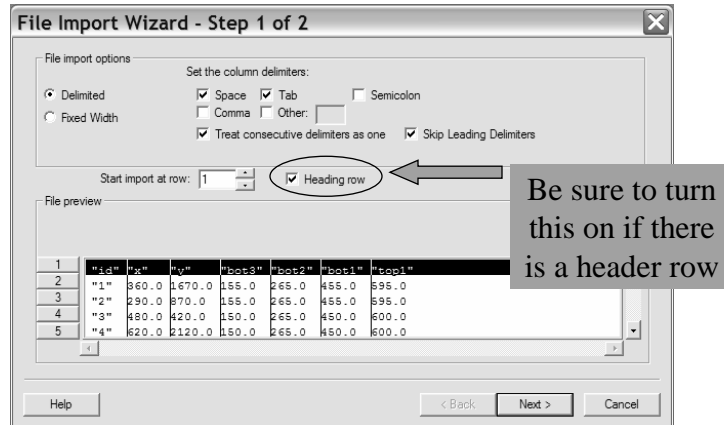
Scatter Data Import Options

- Tabular scatter point text files
 - Save to *.txt file
 - Imported through Open command in File menu
- Copy from Excel and paste to GMS
- Follow *Text Import Wizard*

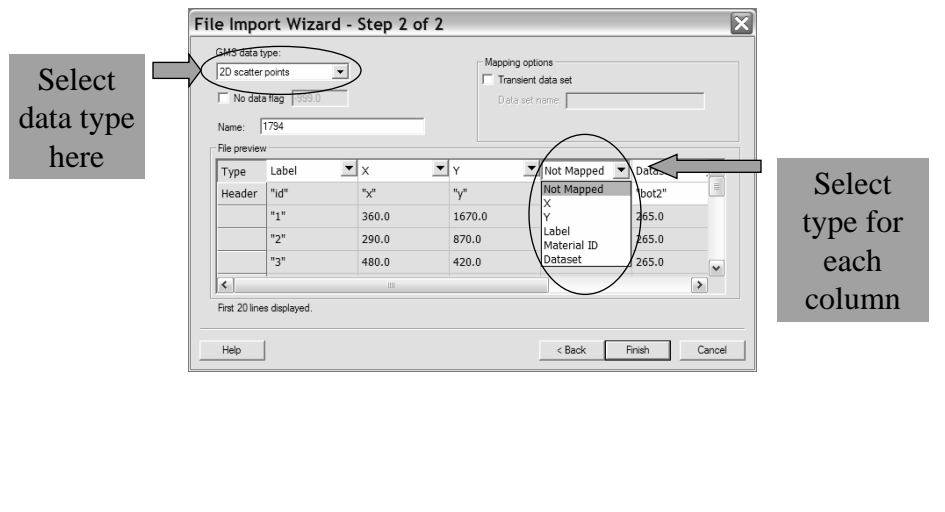
Sample Point Data

	A	B	C	D	E	F	G
1	id	x	y	top1	bot1	bot2	bot3
2	1	360.0	1670.0	450.0	345.0	200.0	100.0
3	2	290.0	870.0	445.0	340.0	195.0	95.0
4	3	480.0	420.0	450.0	350.0	200.0	100.0
5	4	620.0	2120.0	455.0	245.0	200.0	100.0
6	5	990.0	1820.0	470.0	355.0	210.0	115.0
7	6	890.0	1190.0	465.0	350.0	205.0	110.0
8	7	1030.0	710.0	475.0	360.0	215.0	130.0
9	8	910.0	590.0	470.0	350.0	210.0	125.0
10	9	1520.0	2100.0	530.0	405.0	275.0	185.0
11	10	1410.0	1560.0	510.0	390.0	260.0	210.0
12	11	1520.0	910.0	530.0	405.0	275.0	185.0
13	12	1320.0	430.0	560.0	445.0	305.0	210.0
14	13	2120.0	1850.0	580.0	475.0	350.0	260.0
15	14	1980.0	1200.0	575.0	455.0	330.0	250.0
16	15	2100.0	950.0	580.0	465.0	350.0	255.0
17	16	2530.0	1720.0	565.0	490.0	370.0	335.0
18	17	2710.0	1020.0	550.0	480.0	390.0	350.0
19	18	2610.0	560.0	555.0	490.0	385.0	345.0
20	19	3090.0	1590.0	515.0	450.0	385.0	350.0
21	20	3040.0	790.0	512.5	447.5	382.5	347.5
22	21	3050.0	420.0	512.5	447.5	382.5	347.5
23	22	495.0	1250.0	450.0	345.0	200.0	100.0

Import Wizard – Step 1



Import Wizard – Step 2



Interpolation

- You can interpolate from any one of the scatter point data sets to:
 - TIN Elevations
 - Meshes (2D or 3D)
 - Grids (2D or 3D)
 - MODFLOW data array layers
- A new data set is created on the object being interpolated to

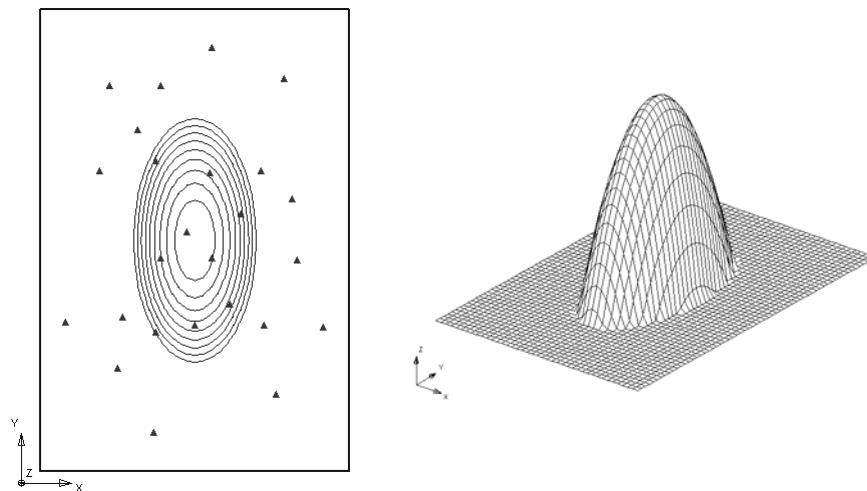
2D Interpolation Schemes

- Linear
- Inverse Distance Weighted
- Clough-Tocher
- Natural Neighbor
- Kriging

Comparing Schemes

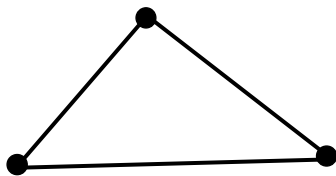
- We will use an elliptical control function to generate a set of points
- Grid will be constructed around points
- Each scheme will be used to interpolate from points to grid
- Interpolated values will be compared to control function

Elliptical Control Function



Linear Interpolation

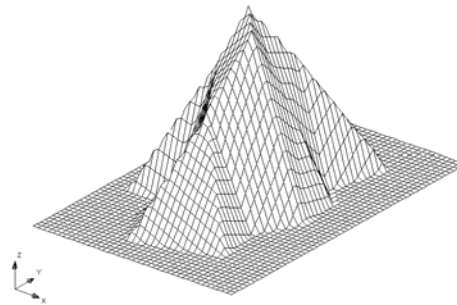
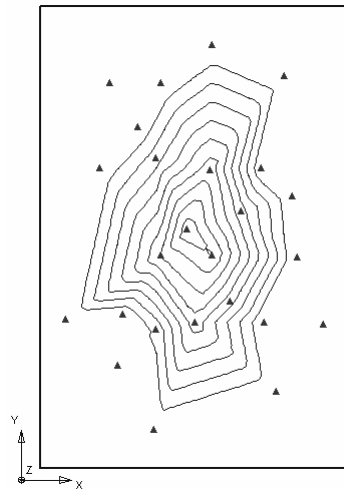
- Scatter point set is triangulated.
- Interpolated function is assumed to vary linearly across each triangle.



$$Ax + By + Cz + D = 0$$

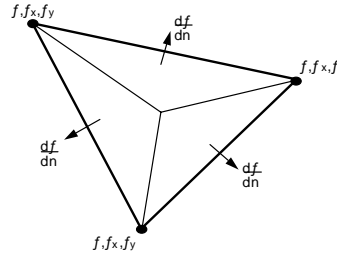
$$f(x, y) = -\frac{A}{C}x - \frac{B}{C}y - \frac{D}{C}$$

Linear Interpolation



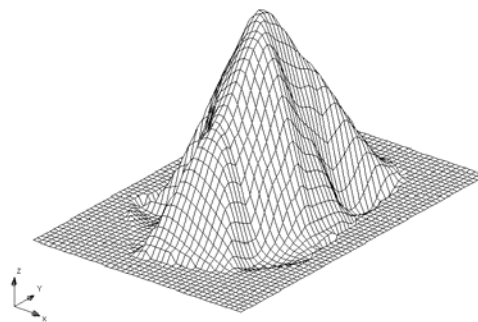
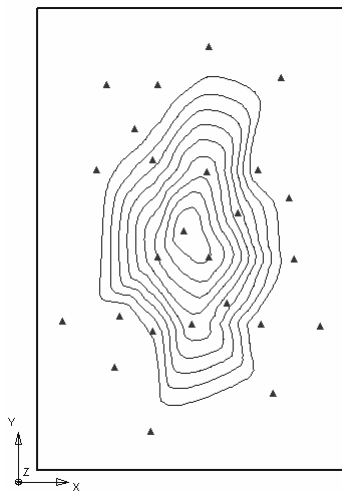
Clough-Tocher Interpolation

- Adapted from finite element analysis
- Steps
 - Points are triangulated
 - Cubic function is fitted over each triangle



$$f(x,y) = \sum_{i=0}^3 \sum_{j=0}^{3-i} c_{ij} x^i y^j$$

Clough-Tocher



Inverse Distance Weighted (IDW)

$$f(x, y) = \sum_{i=1}^n w_i f_i$$

$$w_i = \frac{\left[\frac{R - h_i}{Rh_i} \right]^2}{\sum_{j=1}^n \left[\frac{R - h_j}{Rh_j} \right]^2}$$

$$h_i = \sqrt{(x - x_i)^2 + (y - y_i)^2}$$

R = Distance to most distant point in interpolation subset

IDW Nodal Function Options

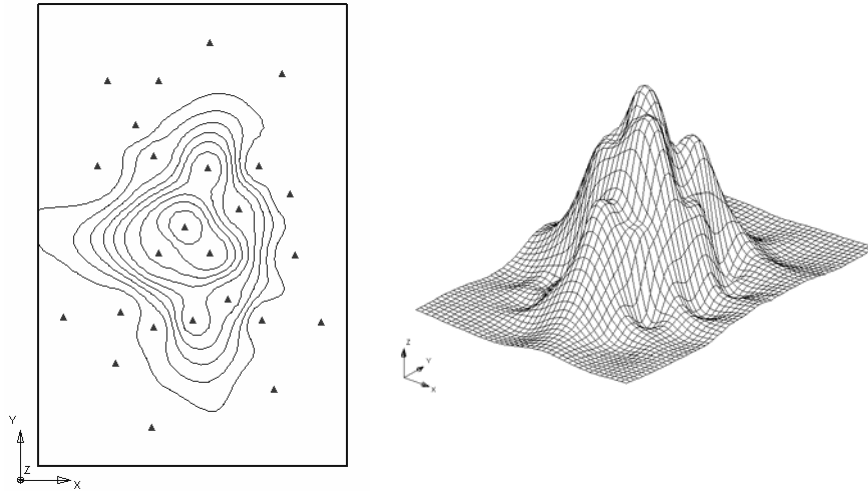
- Constant (Shepard's Method)

$$f(x, y) = \sum_{i=1}^n w_i f_i$$

- Gradient Plane
- Quadratic

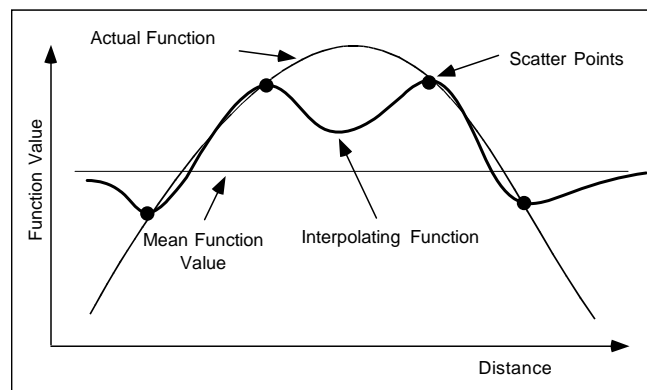
$$f(x, y) = \sum_{i=1}^n w_i Q_i(x, y)$$

IDW - Constant



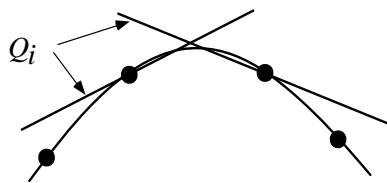
IDW - Constant

- Does not infer local maxima/minima

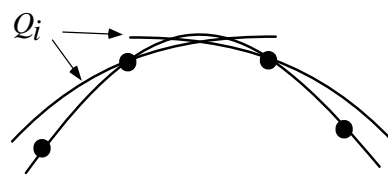


Nodal Functions

- Higher order functions are fit through each scatter point and "blended" or averaged to produce interpolating function
- Better infers trends

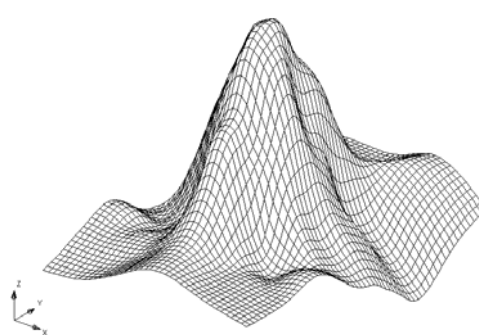
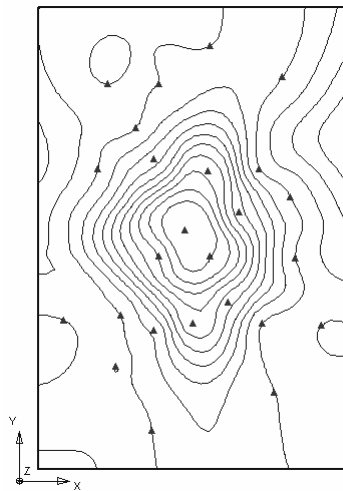


Gradient Plane (Linear)

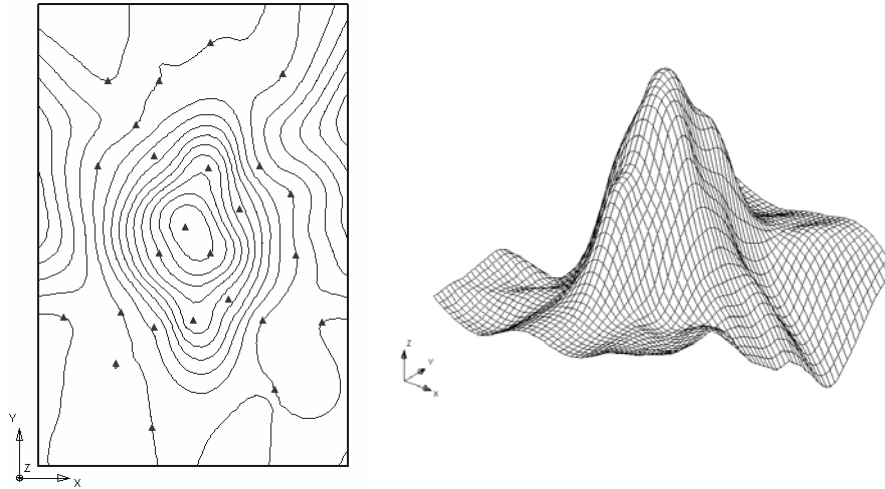


Quadratic

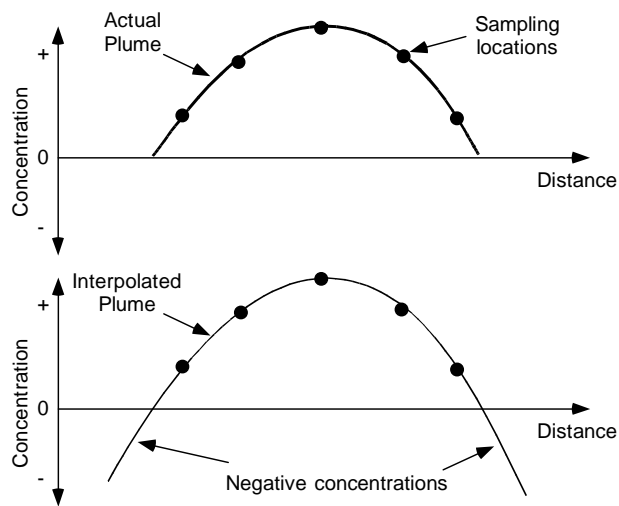
IDW - Gradient Planes



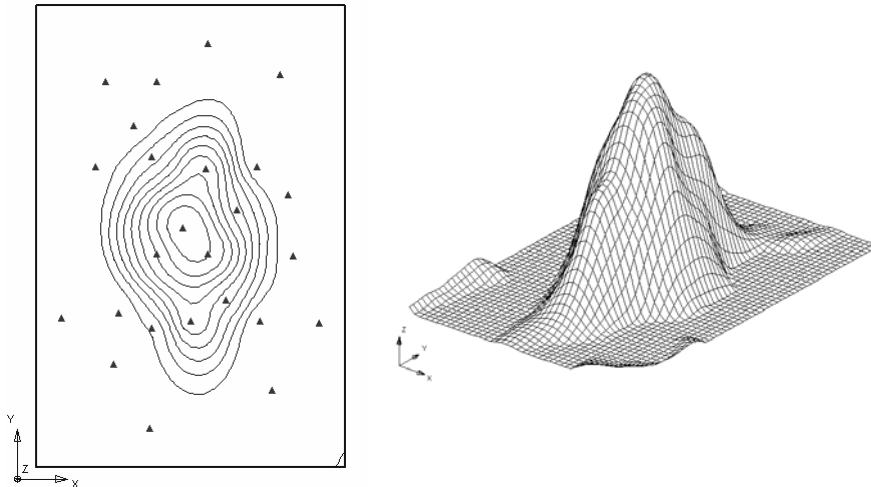
IDW - Quadratic



Negative Concentrations



IDW - Quadratic Truncated

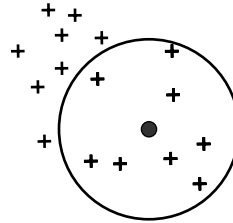


Points Used in Interpolation

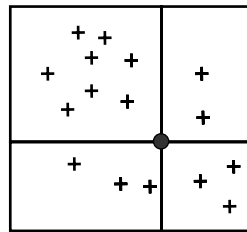
- Points used in interpolation can be:
 - all points
 - subset of points in the vicinity of interpolation point
- Using a subset simplifies computations

Subset Options

- Use nearest n points



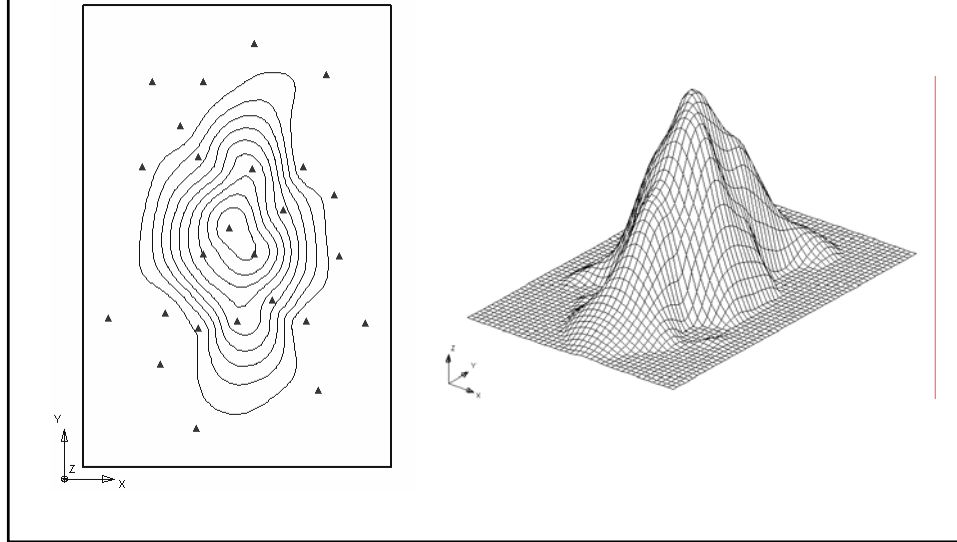
- Use nearest n points in quadrant
 - Reduces ill effects of clustering



Natural Neighbor Interpolation

- Similar to IDW but a special technique is used to determine weights
- Weights are based on both topology and distance
- Works well with clustered data
- See GMS Help Document for details

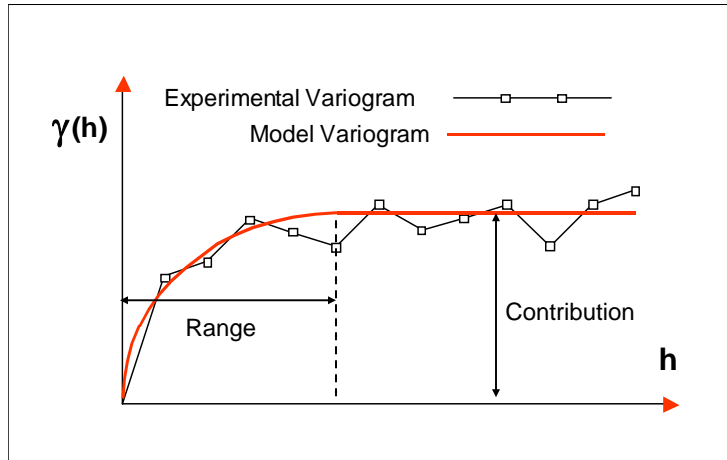
Natural Neighbor - Truncated



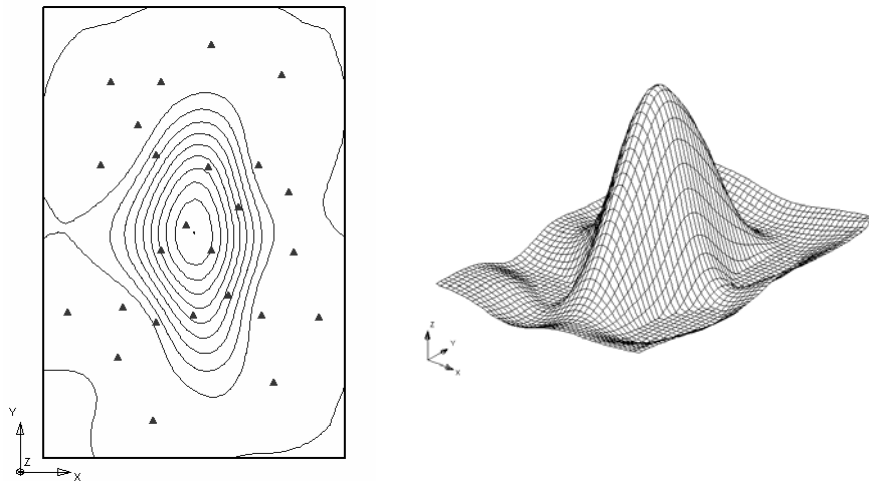
Kriging

- An optimal set of weights is computed at each interpolation point
- Optimal weights are computed from model variogram
- GMS kriging code is based on GSLIB and UNCERT codes

Variograms



Kriging



Summary

- Poor
- Average
- Good

Scheme	Speed	Ease of Use	Extrapolation	Accuracy
Linear	●	●	○	○
Clough-Tocher	●	●	○	○
IDW	●	●	●	●
Natural Neighbor	●	●	●	●
Kriging	○	○	●	●

3D vs. 2D Geostatistics

- Equations are basically the same
- Z component is added

- 2D

$$f(x, y) = \sum_{i=1}^n w_i f_i$$

- 3D

$$f(x, y, z) = \sum_{i=1}^n w_i f_i$$

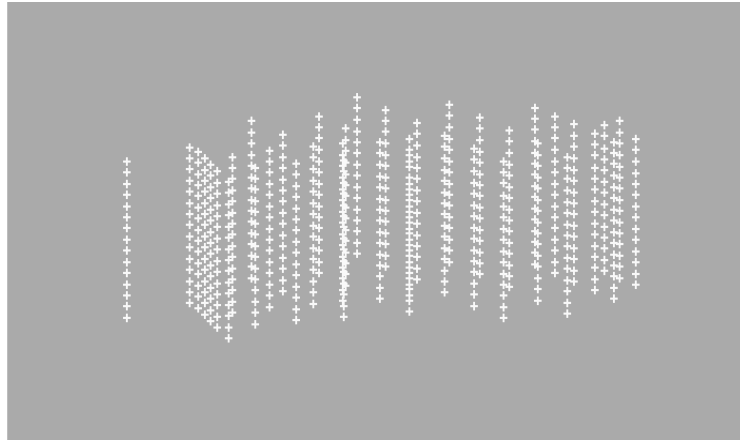
3D Methods Supported

- Inverse Distance Weighted (IDW)
- Natural Neighbor
- Kriging

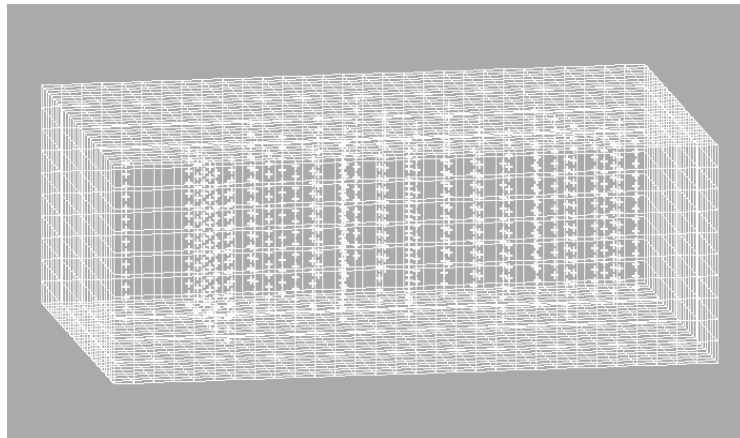
3D Plume Characterization

- Enclose sampling locations (scatter points) with 3D grid
- Interpolate to grid nodes
- Compute iso-surfaces from grid

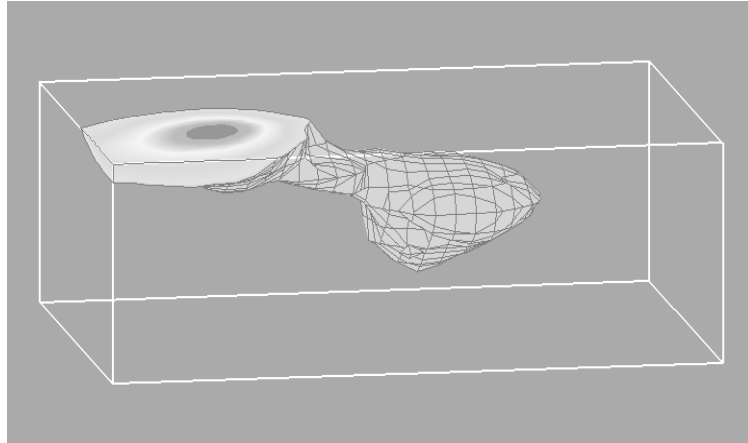
3D Scatter Points



3D Grid



Iso-surfaces



Seepage/Flux Data Set Builder Tools

Converting SCAPS Data to 3D Data Sets

Before attempting conversion:

- Import SCAPS data as borehole data sets
- Convert borehole sample data to 3D scatter points
- Interpolate to 3D grid

Data Sets Required

- The following data sets must exist on the 3D grid:
 - Head (total hydraulic head)
 - Horizontal hydraulic conductivity
 - Porosity (must be between 0 – 1)
- Any set of names can be used
- Mesh-centered grid should be used

Darcy's Law

$$V_s = \frac{V_d}{n} = \frac{ki}{n}$$

V_s = seepage velocity

V_d = Darcian velocity

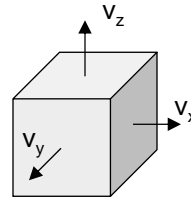
K = hydraulic conductivity

n = effective porosity

Darcy's Law in 3D

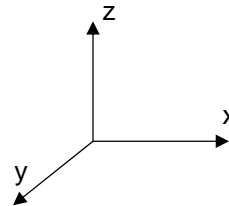
General case:

$$\begin{bmatrix} v_x \\ v_y \\ v_z \end{bmatrix} = \begin{bmatrix} k_{xx} & k_{xy} & k_{xz} \\ k_{yx} & k_{yy} & k_{yz} \\ k_{zx} & k_{zy} & k_{zz} \end{bmatrix} \begin{bmatrix} \partial h / \partial x \\ \partial h / \partial y \\ \partial h / \partial z \end{bmatrix}$$



The tensor is symmetric, i.e.:

$$\begin{aligned} k_{yx} &= k_{xy} \\ k_{zx} &= k_{xz} \\ k_{zy} &= k_{yz} \end{aligned}$$



Darcy's Law in 3D

If x , y , and z axes coincide with principal axes of permeability:

$$\begin{bmatrix} v_x \\ v_y \\ v_z \end{bmatrix} = \begin{bmatrix} k_{xx} & 0 & 0 \\ 0 & k_{yy} & 0 \\ 0 & 0 & k_{zz} \end{bmatrix} \begin{bmatrix} \partial h / \partial x \\ \partial h / \partial y \\ \partial h / \partial z \end{bmatrix}$$

$$v_x = -k_h \frac{\partial h}{\partial x}$$

$$v_y = -k_h \frac{\partial h}{\partial y}$$

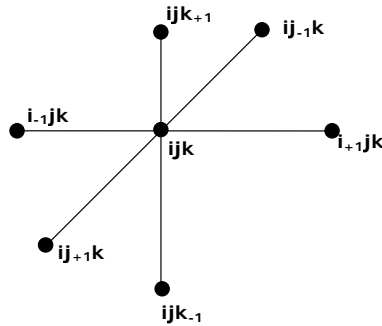
$$v_z = -k_z \frac{\partial h}{\partial z}$$

In most cases

$$\begin{aligned} k_{xx} &= k_{yy} \\ k_{xx} &> k_{zz} \end{aligned}$$

Calculating Hydraulic Gradient

For an interior node:



$$\frac{\partial h}{\partial x} = \frac{\frac{h_{i-1jk} - h_{ijk}}{x_{i-1jk} - x_{ijk}} + \frac{h_{ijk} - h_{i+1jk}}{x_{ijk} - x_{i+1jk}}}{2}$$

Mass Flux

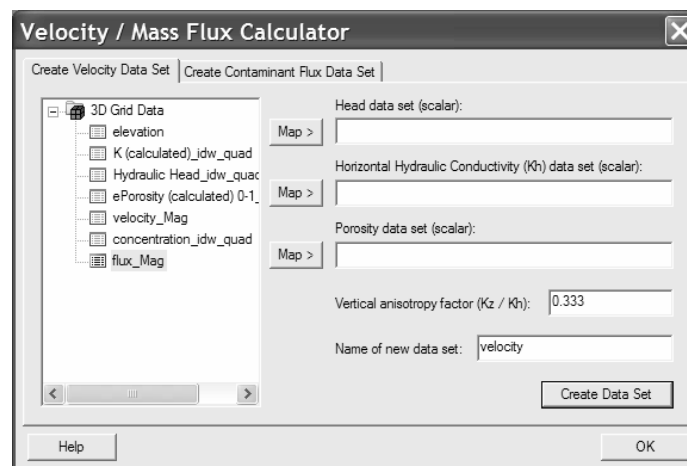
- Computed as seepage velocity data set multiplied by concentration data set
- Resulting units:

$$\frac{M}{L^2 * T}$$

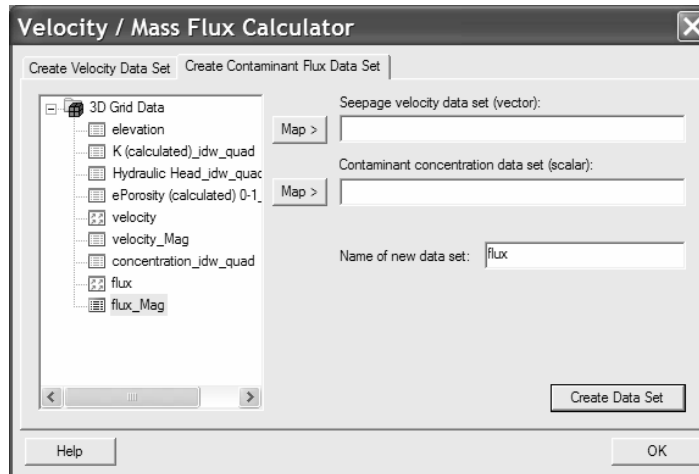
Launching Calculator

- Highlight 3D grid object in Project Explorer
- Select the following command:
 - Data|Advanced|Velocity/Mass Flux Calculator

Velocity Calculator



Mass Flux Calculator



Velocity and Mass Flux Calculators

This tutorial gives an overview of the *Velocity* and *Mass Flux* calculators. These calculators are in the 3D Grid module of GMS and were designed to be used with imported sample data – i.e. data obtained from borehole geophysical logs or cone penetrometer logs.

1.1 Velocity Calculator

The *Velocity* calculator takes three scalar data sets and from them creates a vector data set representing seepage velocity. The three input data sets are *head*, *porosity* and *hydraulic conductivity*. The calculations are based on Darcy's Law:

$$\mathbf{v}_s = \frac{\mathbf{v}_d}{n} = \frac{\mathbf{k}\mathbf{i}}{n}$$

Where \mathbf{v}_s is the seepage velocity, \mathbf{v}_d is the Darcy velocity, n is the effective porosity, \mathbf{k} is the hydraulic conductivity, and \mathbf{i} is the head gradient.

In 3D, the equation is:

$$\begin{bmatrix} v_x \\ v_y \\ v_z \end{bmatrix} = - \begin{bmatrix} k_{xx} & k_{xy} & k_{xz} \\ k_{yx} & k_{yy} & k_{yz} \\ k_{zx} & k_{zy} & k_{zz} \end{bmatrix} \begin{bmatrix} \partial h / \partial x \\ \partial h / \partial y \\ \partial h / \partial z \end{bmatrix}$$

If we assume $k_x = k_y = k_h$ and $k_z = (\text{anis factor}) * k_h$ then this equation simplifies to:

$$\begin{bmatrix} v_x \\ v_y \\ v_z \end{bmatrix} = - \begin{bmatrix} k_h & 0 & 0 \\ 0 & k_h & 0 \\ 0 & 0 & k_z \end{bmatrix} \begin{bmatrix} \partial h / \partial x \\ \partial h / \partial y \\ \partial h / \partial z \end{bmatrix}$$

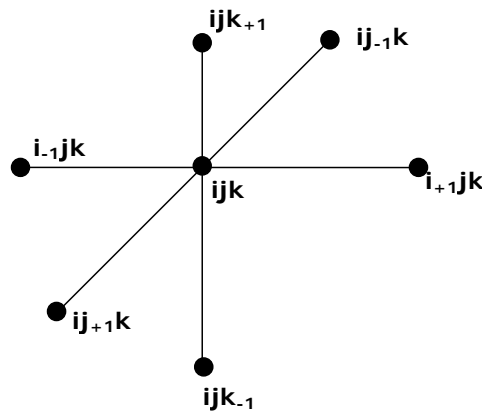
Or:

$$v_x = -k_h \frac{\partial h}{\partial x}$$

$$v_y = -k_h \frac{\partial h}{\partial y}$$

$$v_z = -k_z \frac{\partial h}{\partial z}$$

Thus, the first step is to calculate the hydraulic gradient vector. This is done using simple finite differences. For an interior node (ijk):



We can compute the dh/dx as:

$$\frac{\partial h}{\partial x} = \frac{\frac{h_{i+1jk} - h_{ijk}}{x_{i+1jk} - x_{ijk}} + \frac{h_{ijk} - h_{i-1jk}}{x_{ijk} - x_{i-1jk}}}{2}$$

The gradients in the other direction are computed in a similar fashion.

1.2 Mass Flux Calculator

The *Mass Flux* calculator multiplies a seepage velocity data set by a concentration data set to create a vector data set representing mass flux. The units for mass flux are mass per unit area per unit time, or:

$$\frac{M}{L^2 * T}$$

Multiplying the seepage velocity, which has units of length over time (L/T), by a concentration, which has units of mass per volume (M/L³), results in units of:

$$\frac{L}{T} * \frac{M}{L^3}$$

This reduces to $\frac{M}{L^2 * T}$ which are the correct units for mass flux.

1.2.1 Outline

This is what you will do:

1. Import SCAPS data.
2. Create 3D scatter points.
3. Create a bounding 3D Grid.
4. Interpolate to the 3D Grid.
5. Run the calculators.
6. View the results.

1.2.2 Required Modules/Interfaces

You will need the following components enabled to complete this tutorial:

- Sub-surface characterization
- Grid
- Geostatistics

You can see if these components are enabled by selecting the *File / Register*. If you do not have these components enabled, you can complete the tutorial in *Demo Mode*. You can switch to *Demo Mode* by selecting the *File / Demo Mode* menu command.

1.3 Getting Started

Let's get started.

1. If necessary, launch GMS. If GMS is already running, select the *File / New* command to restore the program settings to their default state.

1.4 Import Sample Data

We will start by importing sample data.

1. Select the *Open* button .
2. In the *Open* dialog, locate and open the directory entitled **sampcalc**.
3. Change the *Files of type:* to **Text Files (*.txt,*.csv)**.
4. Select the file named **GMS Export.txt** and click *Open*.
5. In step 1 of the *File Import Wizard*, select the options shown in the figure below and click *Next*.

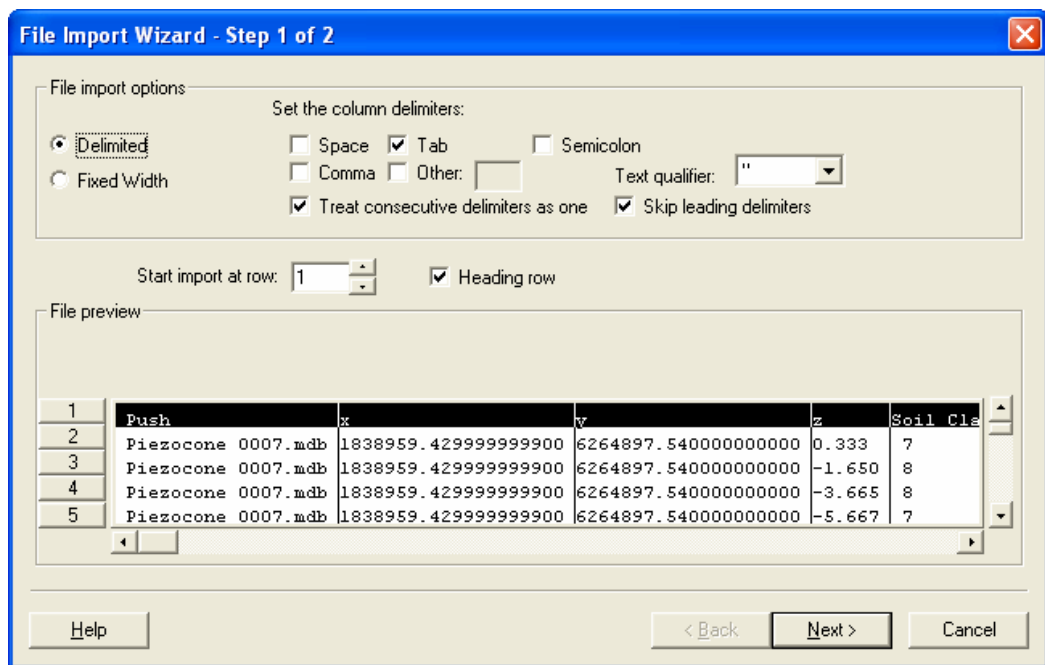


Figure 1.1 File Import Wizard step 1

6. In step 2 of the *File Import Wizard*, change the *GMS data type* to **Borehole sample data**. Change the first column *Type* to **Name**. Make sure everything else is as shown in the figure below and click *Finish*.

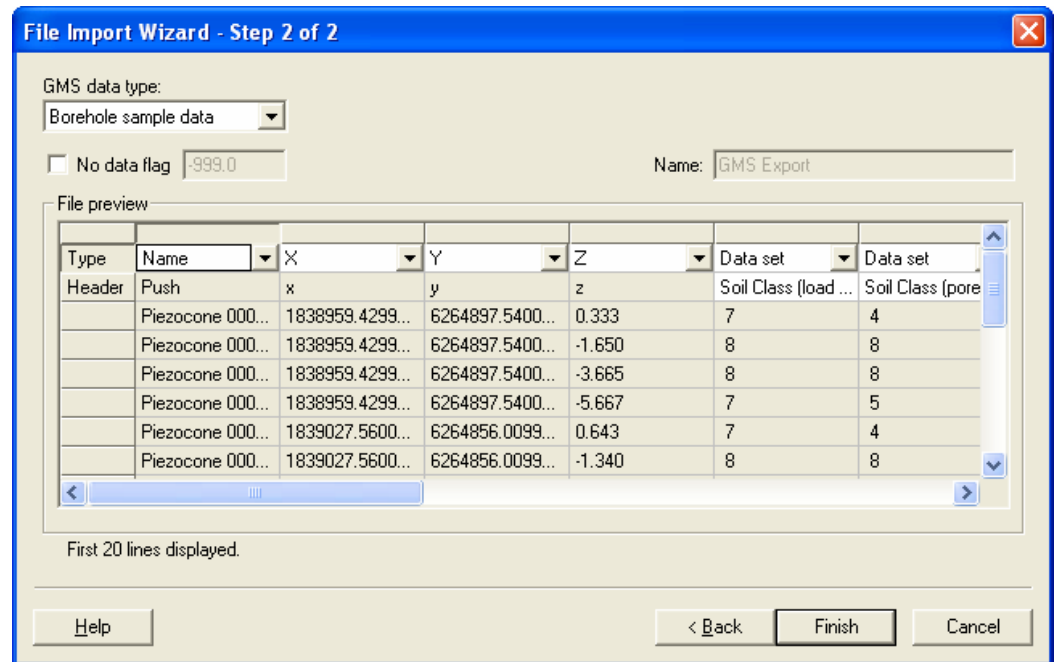


Figure 1.2 File Import Wizard step 2

By default, the imported data are shown in plan view. To better see the data:

7. Switch to oblique view by clicking the *Oblique View* button .

1.5 Changing the Display Options

Next, we'll adjust the display options so that the boreholes are more visible. Boreholes consist of two types of information: stratigraphy (sand, silt, clay, etc.) and sample data (data set values measured at point locations along the borehole). In this case, we wish to focus on the sample data, so we will turn off the display options related to the stratigraphy. We will also exaggerate the z scale.

1. Click on the *Display Options* button .
2. Turn **off** the *Borehole edges* option.
3. Turn **off** the *Borehole faces* option.
4. Change the *Z magnification* to **3**.
5. Click *OK*.

1.6 Convert to Scatter Points

We need to interpolate the sample data to a 3D grid. Interpolation is done using scatter points, so we must convert the borehole sample data to scatter points.

1. Select the *Boreholes/Advanced/Sample Data* → *3D Scatter Points* menu command.

This dialog is used to filter borehole sample data. In many cases, the borehole sample data are densely sampled in the vertical direction. Since this can lead to difficulties with 3D interpolation, this dialog can be used to thin the sample data. However, our sample data are quite sparse and no filtering is needed.

2. Accept all the default settings and click *OK*.
3. Accept the default name for the new scatter point set and click *OK*.

1.7 Changing the Display Options

At this point, you should see a set of symbols appear at the location of the borehole sample data locations. Before proceeding, we will hide the borehole sample data.

1. In the *Project Explorer*, turn **off** the *Borehole Data*  folder.

We will also adjust the display of the scatter points so the data values are plotted and the point color is adjusted based on the data value.

2. Click on the *Display Options* button .
3. Under the *Scatter Point Symbols* option, change the *Color* option to **data**.
4. Turn **on** the *Scatter point scalar values* option.
5. Change the *Z magnification* to **3**.
6. Click *OK*.

1.8 Creating the Bounding Grid

Now that we have scatter point data, we are ready to interpolate the measured values to a grid so that we can visualize the data in three dimensions. First we will create a 3D grid which bounds our scatter points. Two types of grids are supported in GMS: cell-centered (data values at cell centers) and mesh-centered (data values at cell corners). We will use a mesh-centered grid since this type of grid is best-suited for 3D visualization.

1. In the *Project Explorer*, expand the *3D Scatter Data* folder if necessary so the *scatter* object is visible.
2. Right-click on the *scatter* object and select the *Bounding 3D Grid* command from the pop-up menu.
3. Change the values to be as shown in the dialog below and click *OK*.

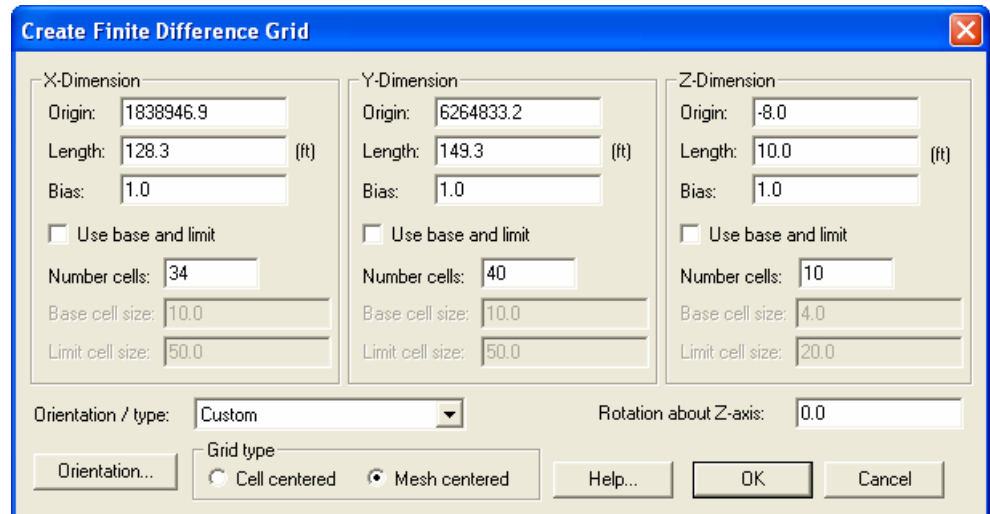


Figure 1.3 Creating the Bounding Grid

You should now see a 3D grid.

4. Select the *Frame* button to frame the data in the window.

1.9 Changing the Display Options

We'll change the display options so that only the outline of the grid is visible for now.

1. In the *Project Explorer*, select the *3D Grid Data* object.
2. Click on the *Display Options* button.
3. Turn **off** the *Cell edges* option.
4. Turn **on** the *Grid shell* option.

1.10 Interpolating K to the 3D Grid

Next, we'll interpolate the hydraulic conductivity data from the scatter points to the 3D grid.

1. In the *Project Explorer*, select the *3D Scatter Data*  folder.
2. Select the *Interpolation/Interpolation Options* menu command.
3. In the *3D Interpolation Options* dialog, select the *Inverse distance weighted* method.
4. Select the *Options* button next to the *Inverse distance weighted* option.
5. Change the *Nodal function* to be *Quadratic* and click *OK*.
6. Click *OK* to exit the *3D Interpolation Options* dialog.
7. In the *Project Explorer*, expand the *scatter*  object so that you can see the data sets underneath it.
8. Select the *K (calculated)* data set so that it's the active data set.
9. In the *Project Explorer*, right-click on the *scatter*  object and select the *Interpolate To/3D Grid* menu command.
10. Click *OK* to perform the interpolation.

1.11 Changing the Display Options

Now that the data values are interpolated to the 3D grid, we'll turn on grid contours to help visualize the data.

1. In the *Project Explorer*, select the *3D Grid Data*  object.
2. Click on the *Display Options* button .
3. Turn **on** the *Contours* option.
4. Select the *Grid contours* option.
5. Click *OK*.

Next we will try color-fill contours.

6. Select the *Data/Contour Options* menu command.
7. Change the *Contour method* option to **Linear and color fill**.

8. Click *OK*.

1.12 Interpolating Head to the 3D Grid

Now we'll interpolate the head data from the scatter points to the 3D grid.

1. In the *Project Explorer*, select the *Hydraulic Head*  data set under the *scatter*  object.
2. In the *Project Explorer*, right-click on the *scatter*  object and select the *Interpolate To/3D Grid* menu command.
3. Click *OK* to exit the dialog and perform the interpolation.

1.13 Normalizing the Porosity

We need to interpolate porosity to the grid, but first we need to put it in the right form. We want porosity to range from 0 to 1. Currently our porosity values are 28 to 33.

1. In the *Project Explorer*, right-click on the *ePorosity (calculated)*  data set and select the *Properties* command from the pop-up menu.
2. Notice that the min is 28 and the max is 33. Click *OK*.
3. Select the *Data/Data Calculator* menu command.
4. Double click on the *ePorosity (calculated)* data set to add it to the expression field.
5. Add “/100” after the letter in the expression field to divide the data set by 100.
6. Change the text in the *Result* field to “**ePorosity (calculated) 0-1**”.
7. Make sure the data calculator looks like the figure below.

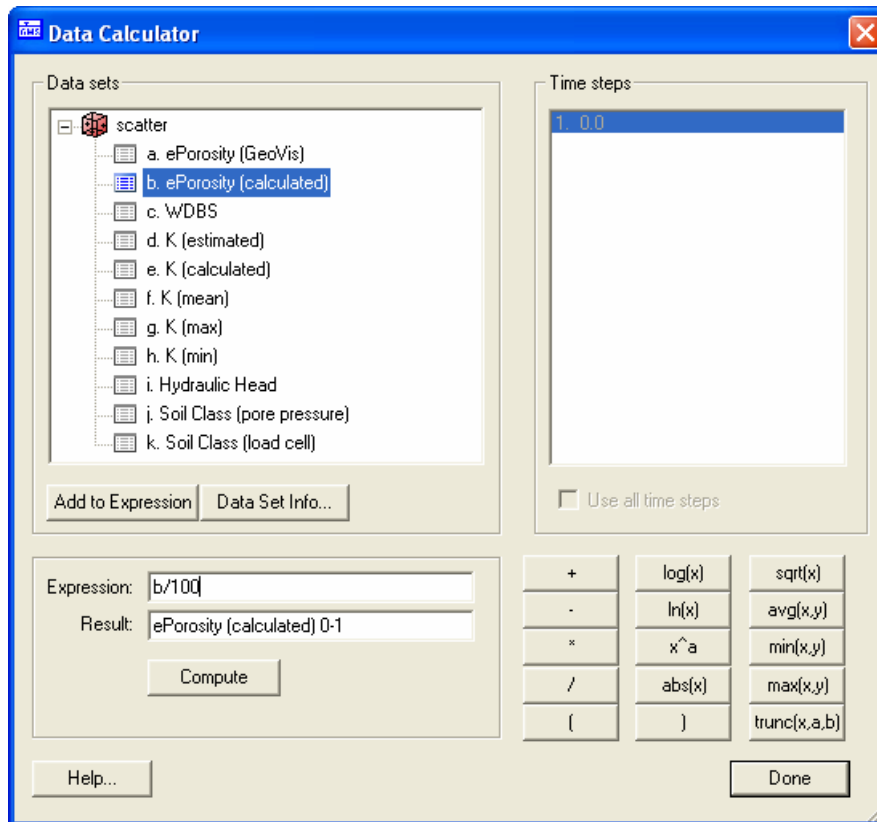


Figure 1.4 Data Calculator

8. Select the *Compute* button.
9. Select the *Done* button.
10. In the *Project Explorer*, right-click on the new *ePorosity (calculated) 0-1* data set and select the *Properties* command from the pop-up menu.
11. Notice the values range between 0.28 and 0.33. Click *OK*.

1.14 Interpolating Porosity to the 3D Grid

Now we'll interpolate the porosity data from the scatter points to the 3D grid.

1. In the *Project Explorer*, right-click on the *scatter*  object and select the *Interpolate To/3D Grid* menu command.
2. Click *OK* to exit the dialog and perform the interpolation.

1.15 Computing Seepage Velocity

The 3D Grid now has all the data sets necessary to compute the seepage velocity.

1. In the *Project Explorer*, select the *3D Grid Data*  object.
2. Select the *Data|Velocity / Mass Flux Calculator* menu command.
3. In the tree of data sets on the left of the dialog, select the *Hydraulic Head_idw_quad*  data set.
4. Click the first (top) *Map >* button. This puts the path to the head data set in the field.
5. Now select the *K (calculated)_idw_grad*  data set on the left and click the middle *Map >* button.
6. Now select the *ePorosity (calculated) 0-1_idw_quad*  data set on the left and click the bottom *Map >* button.
7. Click the *Create Data Set* button.
8. Click *OK*.

1.16 Changing the Display Options

We'll turn on grid vector arrows to visualize the velocity field.

1. Click on the *Display Options* button .
2. Turn **off** the *Contours* option.
3. Turn **on** the *Vectors* option.
4. Select the *Options* button to the right of the *Vectors* option.
5. Turn **on** the *Vary length (a) according to magnitude* option.
6. Turn **on** the *Auto-compute scaling ratio* option.
7. Turn **on** the *Vary color according to magnitude* option.
8. Turn **on** the *Display every 3rd vector* option.
9. Click *OK* twice to exit both dialogs.
10. Use the zoom  and rotate  tools to examine the vectors at different places on the grid.

1.17 Interpolating Concentrations

The *Velocity/Mass Flux Calculator* can also be used to create a mass flux data set. To do so, we need some concentration data. We'll import some, then interpolate it to the 3D grid.

1. In the *Project Explorer*, right-click on the *scatter*  object and select the *Import Data Set* menu command.
2. Select and open the file named **concentration.h5**.
3. In the *Project Explorer*, right-click on the *scatter*  object and select the *Interpolate To/3D Grid* command from the pop-up menu.
4. Select the *Interpolation Options* button.
5. Turn **on** the *Truncate values* option.
6. Select the *Truncate to specified range* option.
7. For the *Min* enter **0.0** and for the *Max* enter **100.0**.
8. Click *OK* twice to exit both dialogs.

1.18 Changing the Display Options

We'll turn on grid iso-surfaces to see the concentration data.

1. In the *Project Explorer*, select the *3D Grid Data*  object.
2. Click on the *Display Options* button .
3. Turn **off** the *Vectors* option.
4. Turn **on** the *Iso-surfaces* option.
5. Select the *Options* button to the right of the *Iso-surfaces* option.
6. Change the *Number of iso-surfaces* value to **3**.
7. Click the *Default* button.
8. Click *OK*.

You should see three colored iso-surfaces representing the contaminant at three different concentrations.

1.19 Computing Mass Flux

The 3D Grid has all the data sets necessary to compute a mass flux data set so we'll do that now.

1. Select the *Data/Velocity/Mass Flux Calculator* menu command.
2. Select the *Create Contaminant Flux Data Set* tab.
3. In the tree of data sets on the left of the dialog, select the *velocity*  data set (make sure you don't select the *velocity_Mag* data set).
4. Click the top *Map >* button.
5. Now select the *concentration_idw_quad*  data set on the left and click the lower *Map >* button.
6. Click the *Create Data Set* button.
7. Click *OK*.

1.20 Changing the Display Options

We'll turn the vector arrows back on to see the mass flux data.

1. Click on the *Display Options* button .
2. Turn **on** the *Vectors* option.
3. Turn **off** the *Iso-surfaces* option.
4. Click *OK*.
5. Use the zoom  and rotate  tools to examine the vectors at different places on the grid.

1.21 Conclusion

This concludes the tutorial. Here are the things that you should have learned in this tutorial:

- The *Velocity/Mass Flux Calculator* can be used to create a vector data set representing seepage velocity.
- You must have a head data set, a hydraulic conductivity data set, and a porosity data set in order to create a seepage velocity data set.

- You can use the *Velocity/Mass Flux Calculator* to create a mass flux data set given a seepage velocity data set and a concentration data set.

APPENDIX I

Detailed Hydraulic Assessment Using a High-Resolution Piezocone Coupled to the GEOVIS

*Report on Development and Testing of Groundwater
Flow and Tracer Transport Models*

Second Draft

Jessica Furrer Chau
Amvrossios Bagtzoglou

Department of Civil and Environmental Engineering
University of Connecticut
Storrs, CT

June 14, 2007

Conducted for
Naval Facilities Engineering Service Center
1100 23rd Avenue
Port Hueneme, CA 93043

Acknowledgements

We wish to thank our project manager Mark Kram for guidance and encouragement, our collaborator Gary Robbins for helpful discussions, and Norm Jones and Tim Shields for assistance with GMS. This project was funded through a contract (N47408-04-C-7514) with the Naval Facilities Engineering Service Center, Port Hueneme, California and is part of the Environmental Security Technology Certification Program (ESTCP) project CU-0421.

Table of Contents

1. Model Development	1
1a. Grid Setup.....	1
1b. Generation of Hydraulic Head and Hydraulic Conductivity Fields	3
1c. MODFLOW Simulations	6
1d. Flow Model Validation	7
1e. MT3D Simulations of Tracer Test	7
2. Modeling the Tracer Test	8
2a. Model Scenarios	8
2b. Error Measures for Evaluation of Model Scenarios	9
3. Tracer Test Modeling Results	10
4. Results of Model Comparisons	13
4a. Comparison of Modeled Vs. Measured Concentrations	13
4b. Model Intercomparisons: Concentration and Flux	16
5. Tracer Test Discrepancies	18
6. Conclusions	19
References	20
Appendix A: Input Parameters, Initial and Boundary Conditions	21

1. Model Development

1a. Grid Setup

A 3-D model of the site was constructed using GMS. A rectangular computational domain was delineated to include the piezometer grid as well as monitoring wells MW-1, 2 and 3 in order to constrain head measurements. In map view, the grid was 45×60 cells (1 cell = 1 ft \times 1 ft), aligned along the assumed flow direction. The alignment was chosen both to reduce numerical instabilities in the flow simulations and to facilitate imaging of the domain along the rows and columns of the piezometer grid. Figure 1 shows the grid layout with the locations of wells.

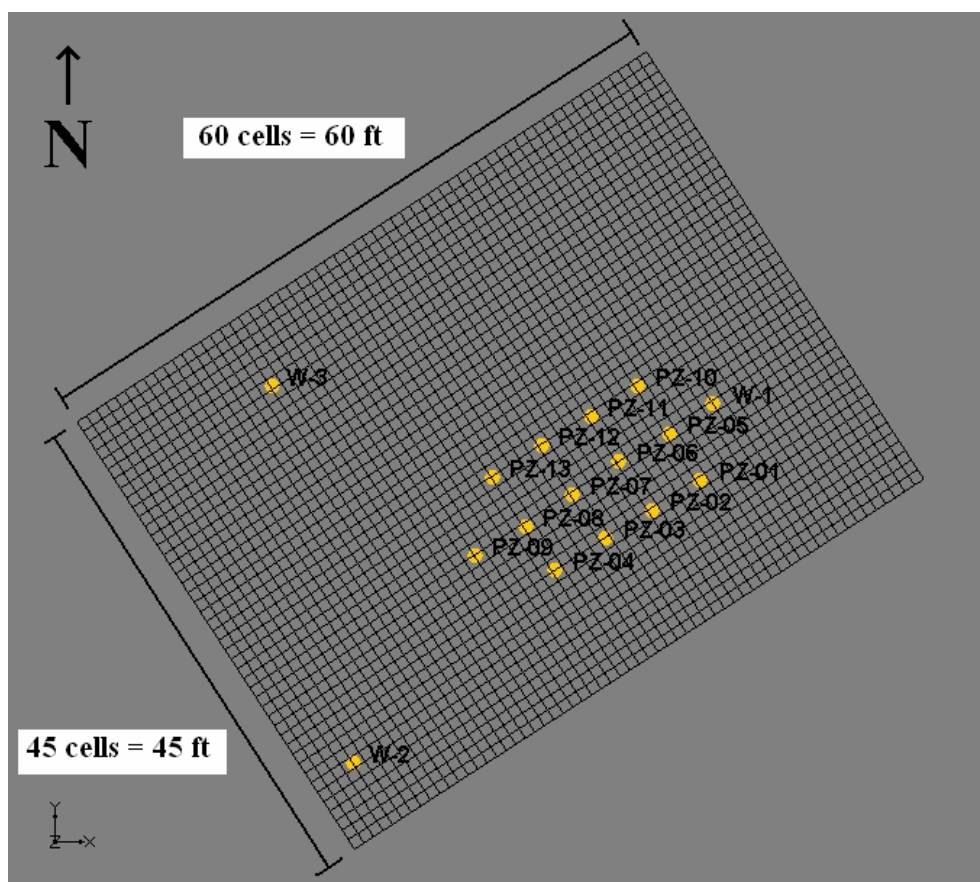
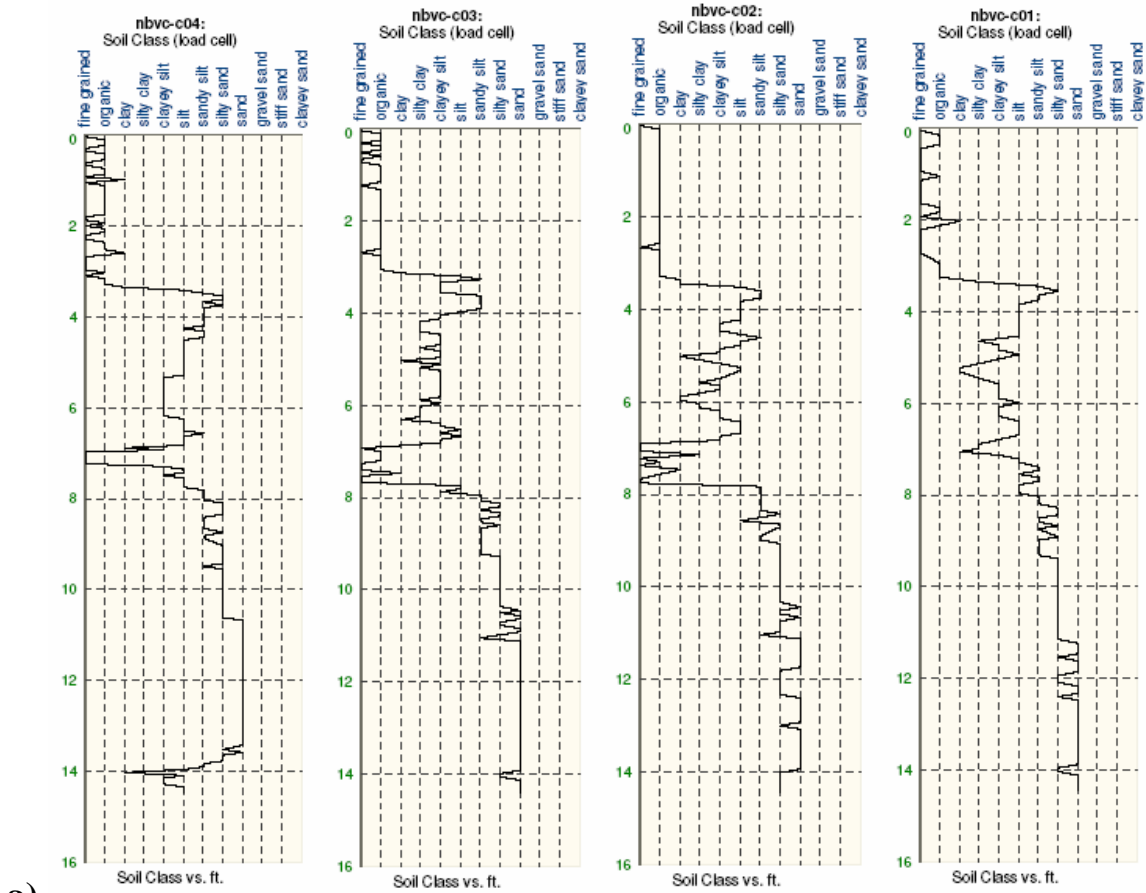


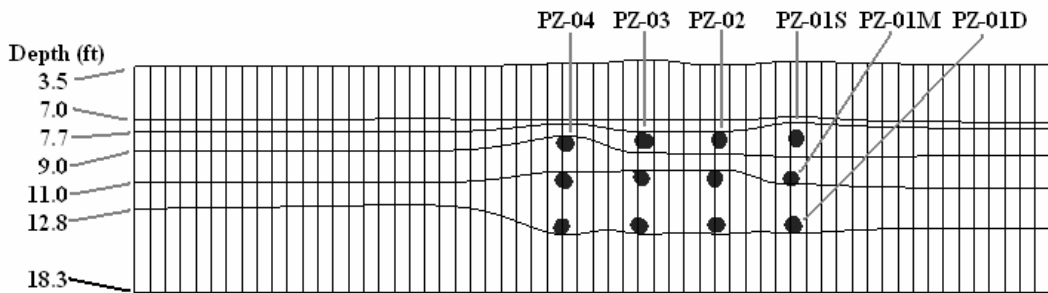
Figure 1. Map view of computational grid. W-1, W-2, and W-3 are simple monitoring wells, while PZ-01 – PZ-13 are nests of piezometers screened at three depths.

The computational grid was divided into six vertical layers, using stratigraphy information inferred from the SCAPS probes. Load cell pressures (recorded as a continuous function of depth) were translated on the basis of a lookup table to a given soil class (e.g., sand, silty sand, etc.). Figure 2a shows the stratigraphy inferred from these soil class profiles for one row of the piezometer grid (wells PZ-01 to 04). Layer boundary elevations were drawn from this approximation of the stratigraphy and interpolated to produce the six layers in the model. Figure 2b shows the resulting layer

boundaries along the same row of the piezometer grid. For most of the nested piezometers, the inlets were located in layers 3 (shallow piezometers), 4 (middle) and 5 (deep), with some exceptions.



a)



b)

Figure 2. a) Stratigraphy inferred from SCAPS pushes for row 1 of piezometer cluster (PZ-01 – PZ-04). Vertical axis is depth below ground surface in feet. b) GMS grid showing layer boundaries for same vertical transect, showing location of screen centers for nested piezometers. Piezometers were denoted by number and depth (Shallow, Middle, and Deep).

1b. Generation of Hydraulic Head and Hydraulic Conductivity Fields

Continuous data were generated by interpolating field measurements made at or near the wells. Head values obtained by either depth-to-water measurements or SCAPS pushes were interpolated using the inverse-distance-weighted algorithm available in GMS. The resulting hydraulic head fields were more or less constant with depth, as shown in the 3-D contours depicted in Figure 3. For both sets of measurements, the head variation across the entire field was less than 0.5 ft.

Comparison of Fig. 3a (interpolated well heads) and 3b (interpolated SCAPS heads) shows the SCAPS data to be more variable, and not constant with depth in the upgradient portion of the piezometer cluster.

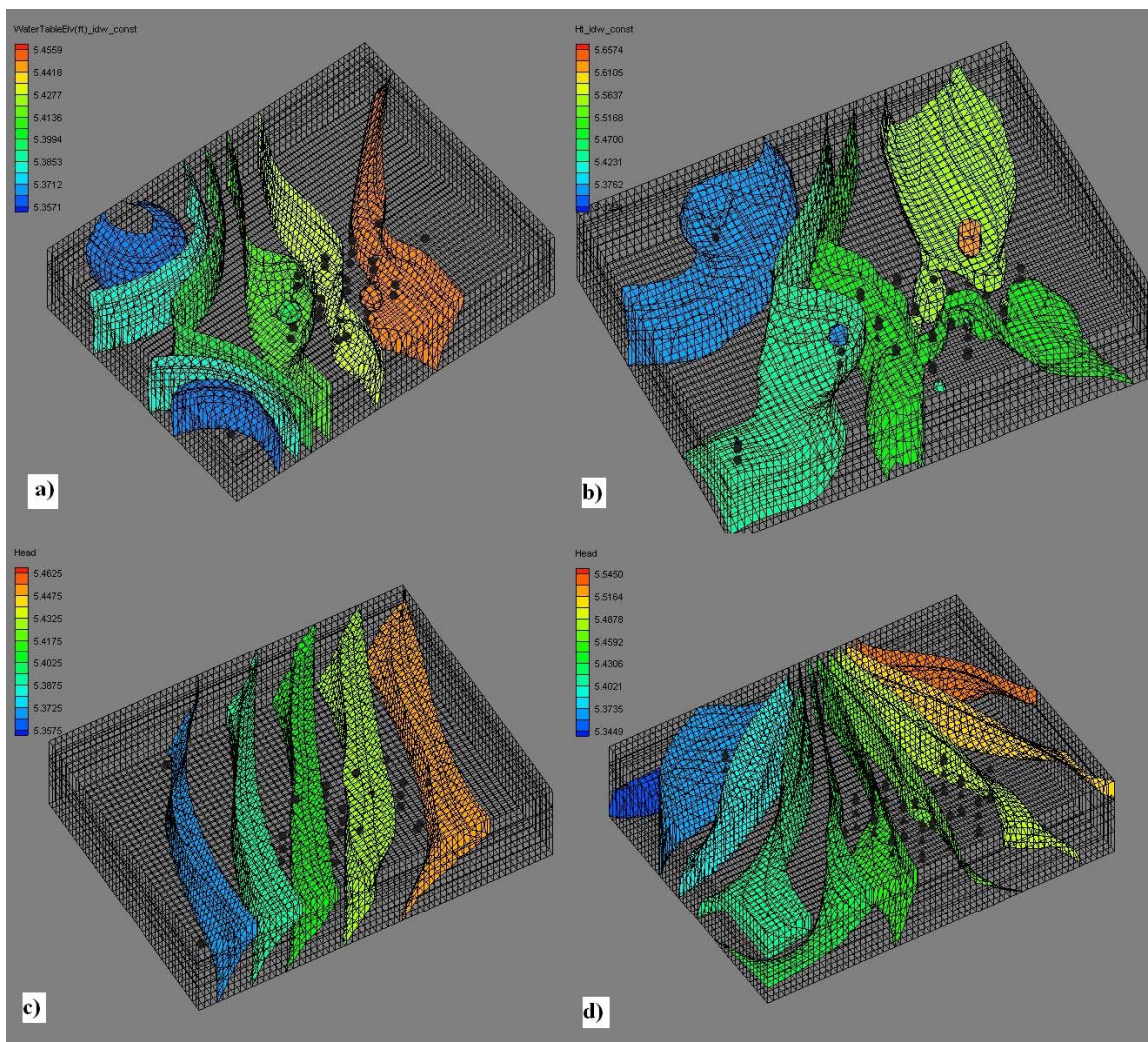


Figure 3. a) Interpolated well head measurements, b) interpolated SCAPS heads, c) steady-state well heads, d) steady-state SCAPS heads. Steady-state heads are a driven by MODFLOW boundary conditions, as detailed in Section 1c below. Contours are at intervals of 0.02 ft.

Representations of the hydraulic conductivity fields were also generated from both well-based measurements (slug tests) and SCAPS measurements (dissipation tests for K_{mean} , K_{min} , and K_{max} and load cell pressures for K_{lookup}). Kriging based on directional variograms was used to interpolate the measurements to the entire field. Variograms were constructed using the GMS geostatistics module along three orthogonal directions. The centerline of the test cluster was assumed to be the main flow direction. As one would expect, the K measurements exhibited higher variability on a smaller spatial scale in the vertical direction, evidenced by the higher sill and shorter range in the variograms shown in Figure 4. The geometry of the test cluster and the limited number of data points is responsible for the shape of the variograms shown. Along the vertical and horizontal orthogonal directions, only three points were available for sampling for each variogram, therefore they reach a maximum around 5 (horizontal direction) or 3 (vertical direction) and drop off when the number of pairs available for sampling goes to one. Given this limited dataset, it is likely that the variability in these directions is higher than indicated here, but as we are most concerned with the K variations within the test cluster itself, this should not present a problem for our modeling and interpretation.

Since the kriging algorithm assumes a normally distributed parameter but hydraulic conductivity is usually found to be log-normally distributed, the K measurements were log-transformed, and new variograms were constructed, before kriging was performed. A spherical model was fitted to each direction and anisotropy ratios were determined from the range parameters of each variogram. Figure 5 shows 2-D K distributions at the depth of the middle piezometers for all K distributions considered.

Through the course of modeling this site, it became clear that the kriged K values did not adequately represent the observed stratigraphy. That is, the measurements taken in a sandy layer were extrapolated to the boundaries of the domain, without regard for the presence of overlying silt layers. As a refinement, the kriged values were used for the sand layers in which the piezometer inlets were located, while the confining layers above were overwritten with a constant average K value for sandy silt (10^{-4} cm/s), silt (10^{-5} cm/s) and fine-grained soil (10^{-7} cm/s) as deemed appropriate. This change did not produce a large difference in the results (as measured by the resulting tracer concentration profiles), but it makes the model a more realistic representation of the stratigraphy of the site.

It should be noted that while the well-based measurements yielded three datapoints with depth (one at each piezometer), the SCAPS measurements were taken at a higher vertical density. Besides the continuous profiles such as those in Fig. 2a, five discrete measurements were processed at each well location, one at the depth of the screen center of each of the piezometers, as well as one measurement slightly above the shallow piezometer and one below the deep piezometer. Interpolations of hydraulic head and hydraulic conductivity for SCAPS scenarios used all five measurements at each location, and so contain slightly more detailed information as a function of depth than the well-derived datasets. It would be possible to construct an even more highly-detailed interpolation of the hydraulic conductivity field using the continuous SCAPS data pictured in Fig. 2a, utilizing Markov Chain transitional probabilities as an interpolation method. However, since MODFLOW only allows one value of K or hydraulic head per grid node, full utilization of the dense vertical resolution would have required a highly-refined grid. Since head values were not available at the higher resolution, there would be

a mismatch between the data density of different parameters within the same model, as well as issues of comparability between models (SCAPS vs. well-based) of different spatial resolution. For these reasons, we opted to use only the discrete hydraulic conductivity data for the SCAPS-based simulations presented here.

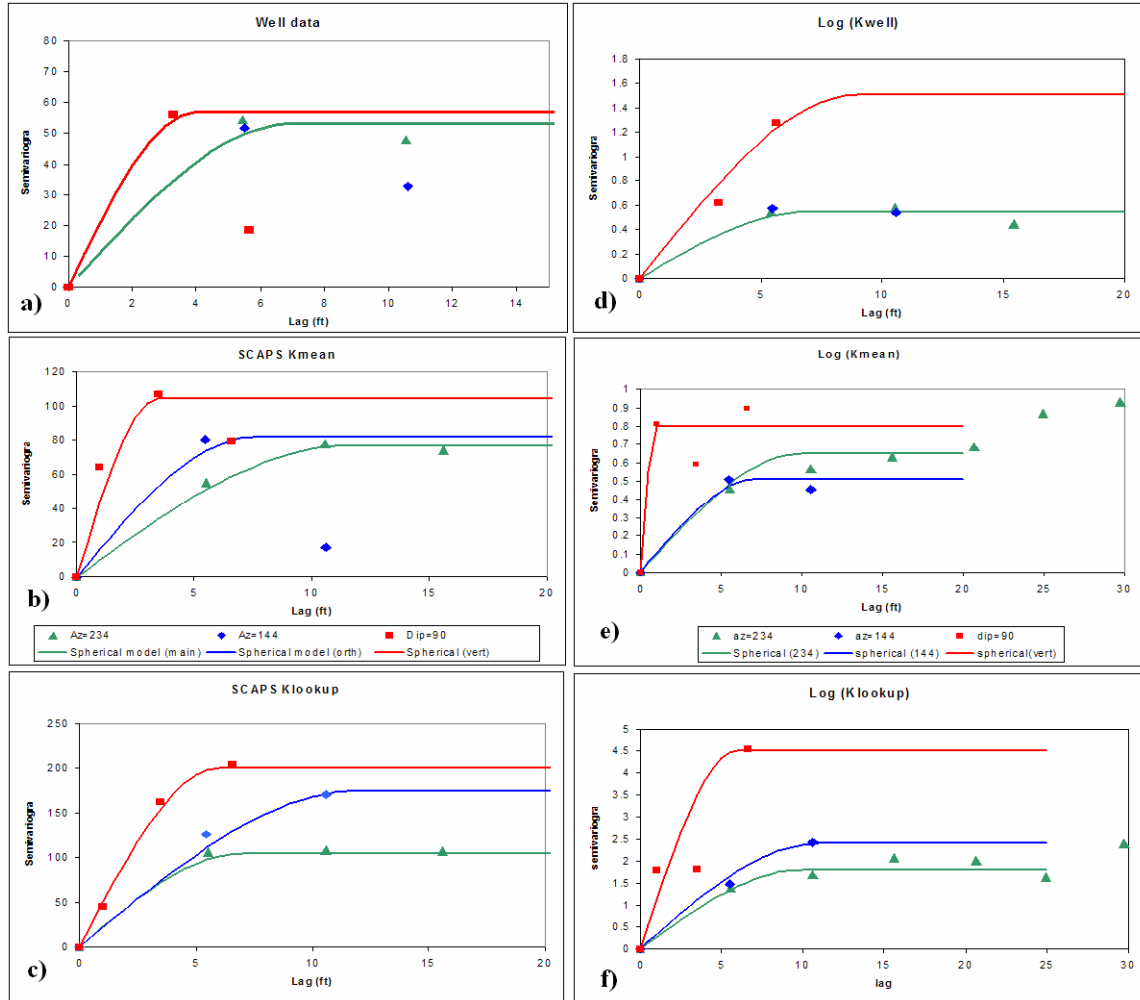


Figure 4. Directional variograms for hydraulic conductivity measurements for **a)** K_{well} , **b)** $SCAPS K_{mean}$, and **c)** $SCAPS K_{lookup}$. Graphs **d)**, **e)** and **f)** are the corresponding variograms for $\log(K)$. Azimuth of 234 represents the centerline of the piezometer cluster and was assumed to be the main flow direction. Azimuth of 144 is orthogonal to 234 in the horizontal direction, while dip of 90 is orthogonal in the vertical direction.

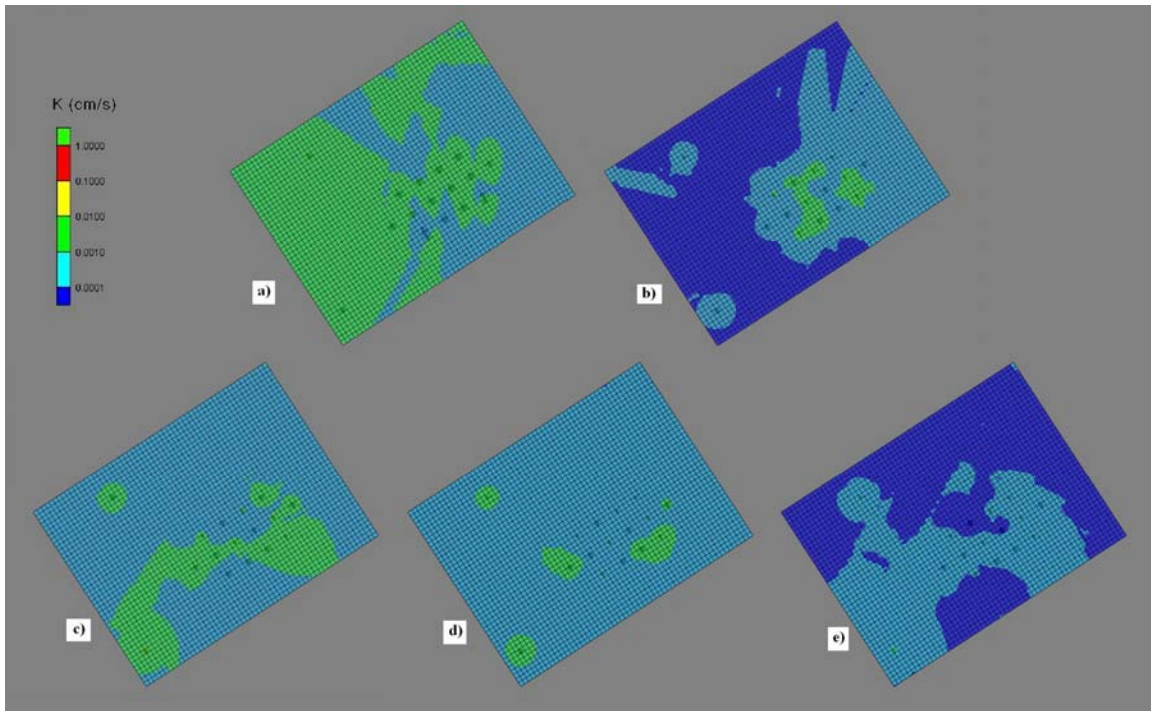


Figure 5. Hydraulic conductivity distributions for a) K_{well} , b) K_{lookup} , c) K_{max} , d) K_{mean} , and e) K_{min} . K values are in cm/s and each contour represents an order of magnitude change in K .

1c. MODFLOW Simulations

Using the MODFLOW module in GMS, flow simulations were conducted on the computational grid using the hydraulic conductivity distributions described previously. Given the lack of natural boundary conditions (e.g., rivers, lakes) at the site, interpolated head measurements were used to generate specified head boundaries for the flow simulations in the following manner. Head measurements were interpolated as described above and extrapolated out to the boundaries to provide a full field of head measurements. From this extrapolation, head values were recorded every 15 feet along the boundary of each layer. The corresponding nodes were set as specified-head nodes, and the head values between these nodes were linearly interpolated to form a full boundary of specified-head nodes along the four sides of the grid. No-flow boundary conditions were applied at the top and bottom of the computational domain. The interpolated head measurements were also used as initial conditions for the flow simulations. The model was run to generate a steady-state head distribution (Figs. 3c and 3d), which was then used as a basis for simulations of the tracer test. Input parameters, boundary conditions, and initial conditions for both flow and transport simulations are summarized in Appendix A.

The extrapolation method described above produced a steady-state head distribution for the well data that matched the assumed flow conditions at the site (relatively constant horizontal gradient, minimal vertical gradient, flow direction roughly along the piezometer cluster). These assumptions were based on previous water level

measurements taken at the site. In contrast, the SCAPS steady-state head distribution exhibits a confluence of head contours along the north-western boundary of the grid, causing the contours to radiate out across the grid from a relatively small portion of the boundary. This is a result of extrapolating the variable upgradient SCAPS data shown in Fig. 3b to the boundaries of the grid. While this extrapolation produces a head distribution over the whole grid which does not correspond to assumed flow conditions at the site, it should be noted that the anomalies are not in the area of the piezometer cluster. Focusing on the area of the cluster, where the tracer transport takes place, the head distribution is relatively constant with depth, the gradient is roughly constant, and the flow direction is roughly along the cluster. In fact, the flow direction based on well data is approximately 30° to the right of 234°, while the SCAPS heads give a flow direction approximately 30° to the left. This is apparent in the tracer contours shown in Section 3.

1d. Flow Model Validation

Because of the low variation in hydraulic head across the field (less than 0.5 ft over a distance of 60 ft), individual head measurements could not be used to constrain the flow field. This was attempted, but the resulting flow field contained highly irregular flow patterns because the expected magnitude of the errors in head measurements were high relative to the variation across the whole field. For example, the well with the lowest head measurement would become a “sink” in the flow field and all stream lines would converge in it. Since this was clearly not a realistic description of the site’s flow conditions, only the boundary heads were used to constrain the model. Validity of the steady-state head distribution was verified by comparing the measured and modeled heads. For the well-based flow models, the average percent error of modeled head in all 39 piezometers was 0.2%, with a maximum percent error of 0.5%. Absolute differences were within 0.03 ft. For the SCAPS-based models, percent errors were slightly higher at 0.9% (average) and 2.3% (maximum), with absolute differences within 0.13 ft. In comparison, the resolution in manual water level measurement is around 0.02 ft, while the corresponding resolution for the SCAPS head measurement is 0.08 ft. Therefore the larger errors for the SCAPS models are expected due to the lower resolution of the method.

1e. MT3D Simulations of Tracer Test

Tracer test simulations were conducted using the MT3D module in GMS. The transport simulations were dependent on the previously-conducted MODFLOW flow simulations for the delineation of boundary conditions; contaminant transport follows the flow of water and is subject to dispersion. Steady-state flow conditions were assumed to drive the transport. The initial concentration in the grid cell containing MW-1 was set by assuming conservation of mass (0.4 g of rhodamine injected), and the rhodamine mass was calculated throughout each simulation using the GMS mass calculator to verify that conservation of mass was maintained. Initial concentrations were zero in all other cells.

Additional inputs to the MT3D module were dispersivity values and a porosity distribution. As the well scenarios did not have a measured porosity distribution, an average value of 30% was assumed, while for the SCAPS scenarios an inverse-distance-

weighted interpolation of the measured porosity data was used. The reader can refer to Table 1 for scenario descriptions. Dispersivity values were obtained from previous calculations done at the site, associated with the salt tracer test conducted in the summer of 2005. The dispersivity values used were $\alpha_x=2.63$ ft, $\alpha_y=0.72$ ft, and $\alpha_z=0.06$ ft, with x oriented along the assumed flow direction. The molecular diffusion coefficient of Rhodamine is 3.35×10^{-4} ft²/day [Rani et al., 2005].

Concentrations within the computational grid were recorded on a weekly basis, starting with one week after the injection and continuing for 168 days. This represented the time period between the July 25, 2006 injection and January 29, 2007. The actual tracer test was terminated in October 24, 2006, so data up to day 91 were included for analysis.

Concentration values at each grid node containing a well were obtained using the “Active Data Set Time Series” option from GMS’s Plot Wizard menu. These values were used to generate breakthrough curves at each well for each scenario, and for the error analysis described in Section 3 of this report. Flux distributions were calculated using the Velocity/Mass Flux Calculator in GMS. Inputs were continuous distributions of concentration, kriged hydraulic conductivity (Fig.5), interpolated or average porosity, and interpolated head (Figs. 3a and 3b).

2. Modeling the Tracer Test

2a. Model Scenarios

In order to observe the similarities and differences between site characterization data derived from traditional well-derived measurements (slug tests, water level measurements) vs. SCAPS measurements (dissipation tests, load cell pressure lookup values), several permutations of the generic flow and transport model were chosen for evaluation. The steady-state head distribution was derived from interpolations of either hand-measured depth-to-water or observations made with the SCAPS method. The hydraulic conductivity field was based on either slug test measurements, piezocone dissipation tests (K_{mean} , K_{max} , K_{min}) or load cell pressure lookup values (K_{lookup}). Porosity was either an average value for the soil type or a lookup value based on load cell pressure. The list of modeled scenarios is given in Table 1.

Each scenario was set up as a copy of the same GMS flow and transport model; therefore, the grid and boundary conditions (constant head boundaries) remained constant throughout all scenarios. The initial input of tracer also remained constant. The boundary values of head, initial head distribution, and the K and porosity distributions changed from model to model, depending on the input.

The information obtained from each modeled scenario included 2-D and 3-D images of tracer concentration and flux distribution, as well as predicted tracer concentrations in each well and piezometer. Flux values at every grid cell were also recorded. Fluxes were calculated using concentration values from the transport model and head distributions interpolated from measurements, to eliminate as much as possible the effects of directionality in the steady-state head distributions.

Scenario	Head	K	Porosity
1	Well	Well	Average
2a	SCAPS	SCAPS K_{mean}	SCAPS
2b	SCAPS	SCAPS K_{min}	SCAPS
2c	SCAPS	SCAPS K_{max}	SCAPS
2d	SCAPS	SCAPS K_{lookup}	SCAPS
3	Well	Well	SCAPS
4a	Well	SCAPS K_{mean}	SCAPS
4b	Well	SCAPS K_{min}	SCAPS
4c	Well	SCAPS K_{max}	SCAPS
4d	Well	SCAPS K_{lookup}	SCAPS
5	Unif. grad.	Average	Average

Table 1. Data sources for inputs to modeled scenarios.

2b. Error Measures for Evaluation of Model Scenarios

Model performance in predicting both concentration in each well and flux distribution in the well cluster was evaluated. Three commonly-used error measures were chosen to analyze the performance of the various model scenarios. The root mean squared error (RMSE) is given by

$$RMSE = \sqrt{\frac{\sum_{t=1}^T \sum_{i=1}^n (y_{o,i,t} - y_{m,i,t})^2}{n * T}},$$

where n is the total number of observation points in space, T is the number of time points, $y_{o,i,t}$ is the observed tracer concentration in well i (or flux value at grid cell i) at time t , and $y_{m,i,t}$ is the modeled concentration in well i (or flux value at cell i) at time t . RMSE has the same units as the y values.

Another error measure that is frequently used in hydrological modeling [e.g., Hossain et al., 2004; Melesse and Wang, 2006] is model efficiency (E) [Nash and Sutcliffe, 1970], given by

$$E = 1 - \frac{\sum_{t=1}^T \sum_{i=1}^n (y_{o,i,t} - y_{m,i,t})^2}{\sum_{t=1}^T \sum_{i=1}^n (y_{o,i,t} - \bar{y}_o)^2},$$

where $\bar{y}_o = \frac{\sum_{t=1}^T \sum_{i=1}^n y_{o,i,t}}{n * T}$ is the average of the observed data. E is analogous (but complementary) to the coefficient of determination in that it indicates what fraction of the observed variance is accounted for by the model under consideration. It has a value of 1

for a perfect model (when $y_{o,i} = \overline{y_{m,i}}$ for all i), while a value of 0 indicates that the model is no better than assuming $y_{m,i} = \overline{y_o}$ for all i . A negative value indicates that the variance in the model is greater than that of the observed values.

Finally, the mean absolute percent error (MAPE) is given by

$$MAPE = \frac{\sum_{t=1}^T \sum_{i=1}^n 100 * |(y_{o,i,t} - y_{m,i,t}) / y_{o,i,t}|}{n * T}$$

It has the advantage of being a dimensionless measure of error, but division by the observed value leaves it sensitive to small observed values. In our case, this presented problems when comparing modeled fluxes, as many of the computed fluxes were 0 or much less than 1. To overcome this problem, we applied a threshold to the observed values (0.01 ppb for concentration and 0.0001 $\mu\text{g}/\text{ft}^2/\text{d}$ for flux) below which the datapoint was discarded. This has the effect of eliminating division by very small numbers (and zero), but also of eliminating potentially large errors wherein the model prediction is large but the observed value is small. Therefore, this threshold-based method can be expected to underestimate the MAPE. For this reason, the other two error measures are given more consideration in the discussion that follows.

3. Tracer Test Modeling Results

Figure 6 shows time series of concentration contours in the middle layer (at the depth of the injection well) for four scenarios: 1 (well-based), 2a (SCAPS K_{mean}), 2d (SCAPS K_{lookup}), and 5 (constant average parameters). These are the scenarios which are discussed in most detail in the following error analysis. Figure 7 shows flux isosurfaces for the same scenarios and times. The isosurfaces are generated at fluxes of 30 $\mu\text{g}/\text{ft}^2/\text{day}$, which is equivalent to a concentration of 35 ppb moving at the average groundwater velocity at the site (0.03 ft/day).

These two figures address the difference in main flow direction between the well heads and SCAPS heads. As stated above, both flow directions were within approximately 30° of the centerline of the piezometer cluster (234°), but the well heads predict flow slightly to the right of the cluster, while SCAPS heads predict flow slightly to the left. In considering the predicted flow directions, it is important to note that there is a significant difference in the reproducibility and zone of influence of the methods used to obtain the hydraulic head data. The depth-to-water measurements were taken in triplicate with excellent reproducibility (detailed in the accompanying tracer test report). The SCAPS pushes, however, were performed once for each depth. Furthermore, the zone of influence of the head measurements is spread or averaged over a 6-inch screen, while the SCAPS dissipation test is essentially a point measurement. Therefore, given the non-reproducibility and the point nature of the SCAPS measurement, it is unreasonable to think that the well and SCAPS measurements fundamentally disagree on flow direction. It is quite possible that another sampling campaign would generate a very different head distribution, with a different flow direction. In our opinion, the fact that there exists a

fairly consistent main flow direction demonstrates that the two methods are in good agreement. Nevertheless, the difference does affect the magnitude of the error measures used to evaluate similarity of the models, as will be explained in Section 4.

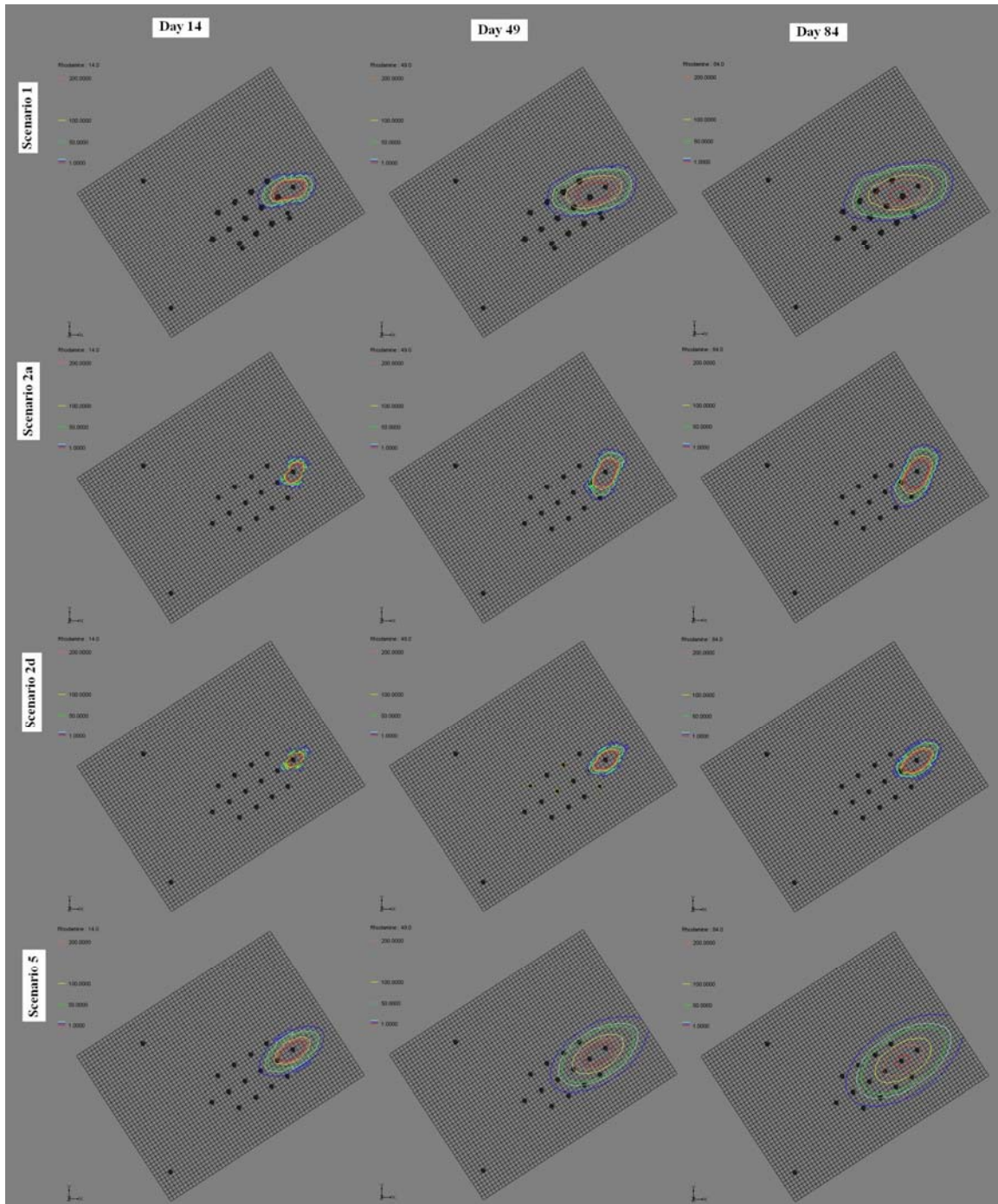


Figure 6. Tracer concentrations at the depth of the injection well for various scenarios and 3 timepoints.

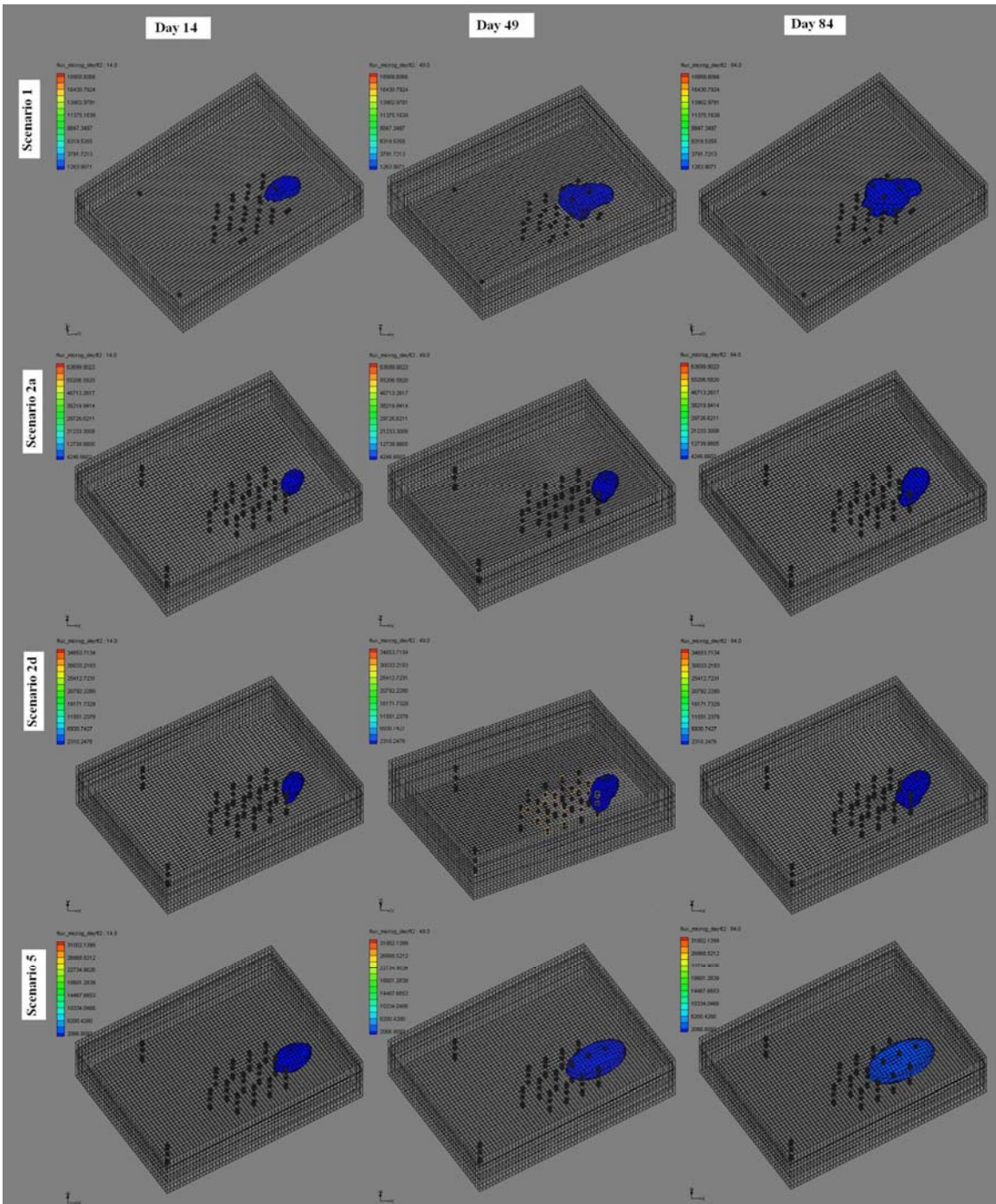


Figure 7. Isosurfaces showing a flux value of 30 µg/ft²/day, which represents a concentration of 35 ppb moving at the average groundwater velocity at the site (0.03 ft/day).

4. Results of Model Comparisons

4a. Comparison of Modeled vs. Measured Concentrations

For reasons to be discussed in Section 4, the modeled Rhodamine WT concentrations did not match the experimental values well. The observed concentrations did not indicate a well-defined plume moving through the piezometer cluster, instead exhibiting sporadic peaks with little spatial or temporal continuity. In contrast, the GMS flow models, which were based on hydraulic head information (water levels or SCAPS data) collected at the site, predicted that the plume would move in the general direction of the piezometer cluster. Therefore, each of the models predicted concentration values in the cluster that rose and fell in a predictable pattern, peaking at around 10-400 ppb depending on the scenario (see Table 2). The highest measured concentration value in any piezometer throughout the test was around 30 ppb. Figure 8 shows measured and modeled breakthrough curves for two piezometers at medium depth along the centerline of the cluster, PZ-05M (closest to the injection well) and PZ-06M (next closest). The breakthrough curves and the error measures in Table 2a clearly demonstrate the lack of agreement between the measured and modeled tracer concentrations.

Scenario	Concentrations (ppb)		Fluxes ($\mu\text{g}/\text{ft}^2/\text{d}$)		
	Maximum	Average	Maximum	Average (all grid cells)	Average (pz. cluster)
Measured	29.7	9.8			
1	420.6	21.6	13854.6	2.0	7.1
2a	131.8	3.2	60664.5	2.5	8.8
2b	4.3	0.1			
2c	159.2	5.2			
2d	82.1	2.0	34750.5	2.4	8.5
3	277.7	11.5			
4a	54.9	1.2			
4b	1.1	0.0			
4c	135.8	3.6			
4d	3.0	0.1			
5	368.2	20.4	22968.0	2.2	7.7

Table 2. Maximum and average values of concentration and flux for selected scenarios. Minimum values are zero in all cases. Concentration values are for the 39 piezometers only, while flux values are for all nodes in a box around the piezometer cluster.

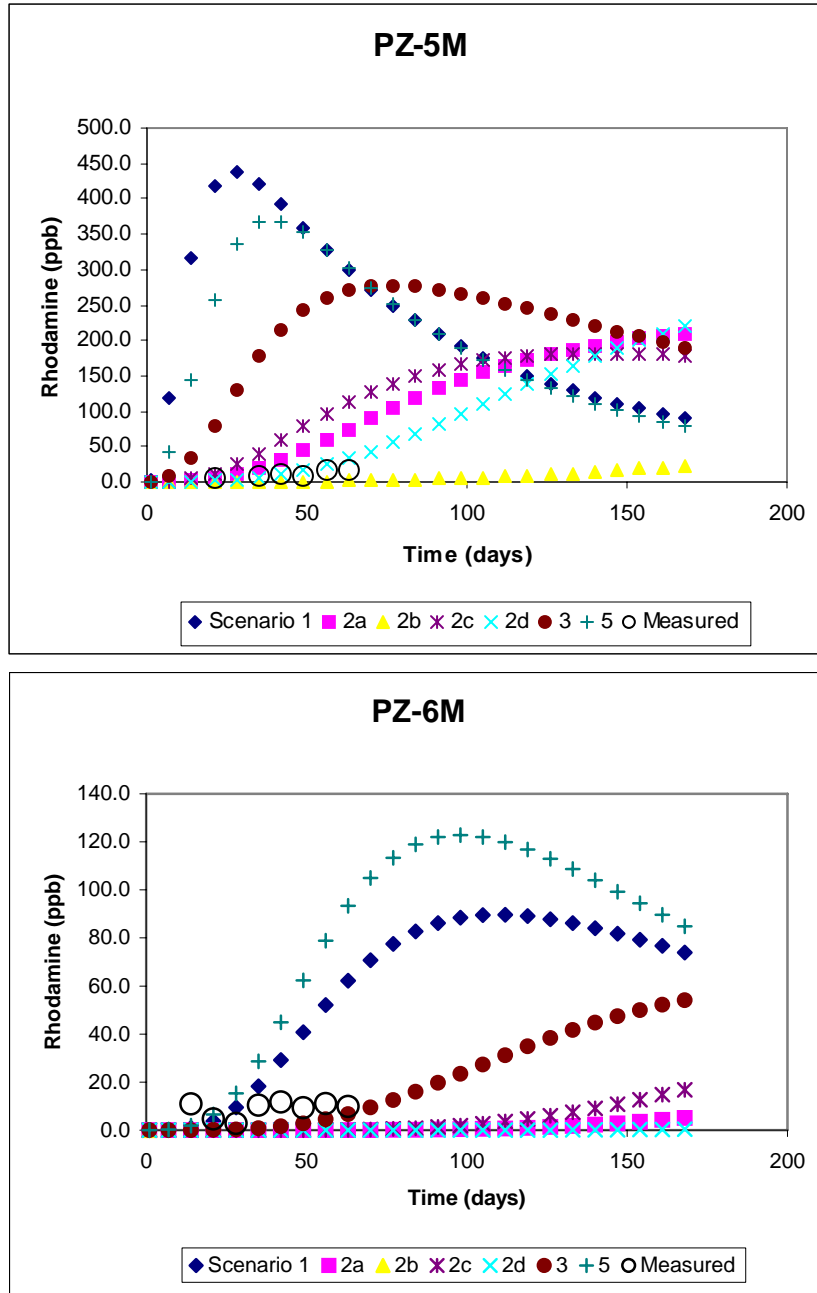


Figure 8. Breakthrough curves for piezometers PZ-05M and PZ-06M, both located along centerline of cluster nearest the injection well in the middle layer.

a) Comparisons with Measured Data

Scenario	MAPE (%)	RMSE (ppb)	E
1	258.6	70.78	-230.43
2a	111.0	16.83	-12.08
2b	98.4	10.74	-4.33
2c	123.3	22.14	-21.63
2d	103.4	12.39	-6.09
3	177.6	48.86	-109.28
4a	98.2	11.02	-4.61
4b	98.9	10.79	-4.38
4c	114.6	17.80	-13.63
4d	98.3	10.72	-4.31
5	224.2	64.13	-188.98

b) Comparisons with Model Scenario 1

Scenario	MAPE (%)	RMSE (ppb)	E
2a	47.1	63.76	0.17
2b	51.7	73.22	-0.09
2c	181.1	59.09	0.29
2d	48.6	68.65	0.04
3	47.7	37.29	0.72
4a	50.8	69.77	0.01
4b	51.7	73.39	-0.09
4c	49.4	62.53	0.21
4d	51.4	73.23	-0.09
5	665.6	18.90	0.93

c) Comparisons with Model Scenario 5

Scenario	MAPE (%)	RMSE (ppb)	E
1	106.5	18.90	0.91
2a	70.3	56.15	0.22
2b	73.4	66.61	-0.09
2c	67.1	50.84	0.36
2d	70.5	61.54	0.07
3	67.7	28.79	0.80
4a	72.1	63.01	0.02
4b	73.4	66.79	-0.10
4c	70.0	55.38	0.24
4d	72.9	66.62	-0.09

Table 3. Results of model-data and inter-model comparisons of concentration.

4b. Model Intercomparisons: Concentration and Flux

In order to evaluate the ability of the SCAPS methodology to produce site characterization data comparable with more traditional methods, we performed model intercomparisons to elucidate the differences in flux and concentration produced by the two methods.

Two scenarios were selected as “baseline” cases: Scenario 1 used only the traditional well-derived measurements for site characterization, and Scenario 5 used simplified site characterization (constant head gradient, K , and porosity), consistent with the level of detail that would likely be used by an environmental practitioner or consultant. These were selected in order to evaluate the degree to which the SCAPS characterization methods produced modeled data that agreed with more traditional measures. Tables 3b and 3c show error measures for concentrations compared against Scenarios 1 and 5, respectively.

Upon inspection of E and RMSE, two scenarios stand out as similar to Scenario 1. For Scenario 3, which was identical to Scenario 1 except for the porosity distribution, $E = 0.72$, indicating that 28% of the variance in Scenario 1 is due to the effect of porosity. Surprisingly, Scenario 5, which used all average parameters, accounted for 93% of the variance in Scenario 1, and gave the lowest RMSE value of ~19 ppb. Perhaps this is because the parameter values used in Scenario 5 were averages of the well-derived data. Paradoxically it gave the highest MAPE (>650%).

Aside from the two most similar models, another level of similarity to Scenario 1 was shared by Scenarios 2a, 2c, and 4c. Here the variance in Scenario 1 captured by the other models was around 20%, and the RMSE values were in the neighborhood of 60 ppb. These used the SCAPS K_{mean} (2a) and K_{max} (2c and 4c) hydraulic conductivity distributions. Figure 9 shows histograms for K_{well} with these two K distributions, with outlier datapoints above 30 ft/day removed. The distributions are somewhat similar, except that the well K s are more evenly distributed and the SCAPS K s appear to be more log-normally distributed. Their similarity at the higher end of the distribution is a possible reason for the reasonable match between models that use K_{well} and those that use K_{mean} and K_{max} . Furthermore, the similarity in error measures between Scenarios 2c and 4c shows that head distribution in this case was not as significant a contributor as the K distribution to the modeled concentration.

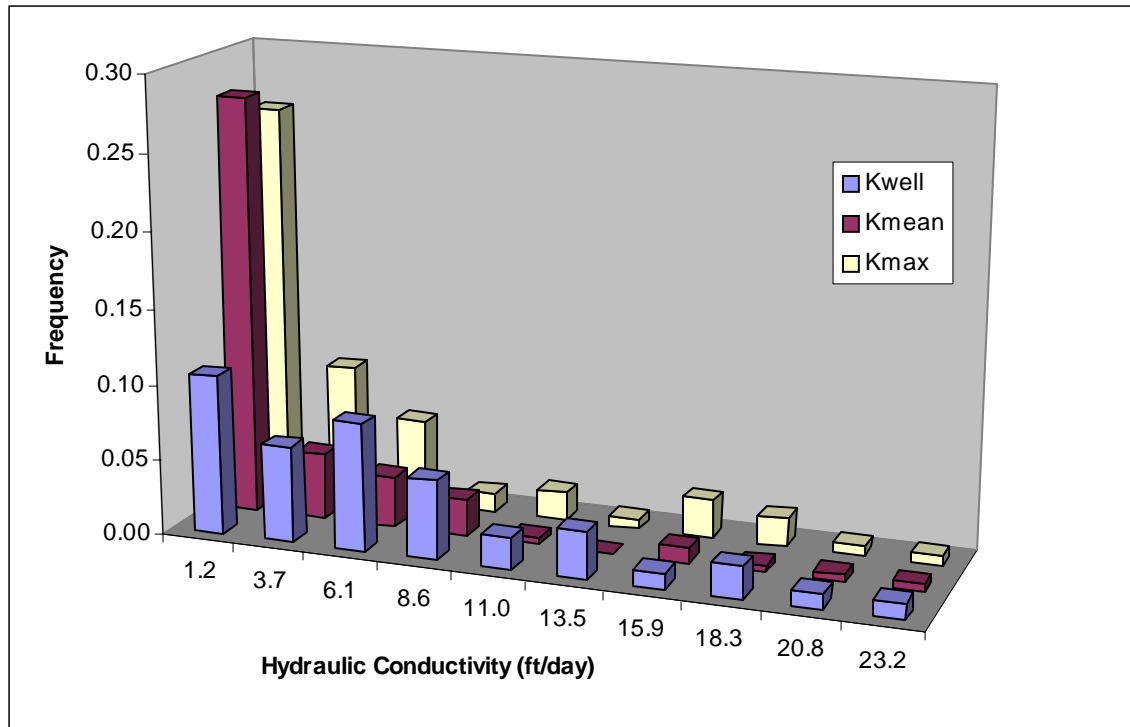


Figure 9. Relative frequency of K values for three conductivity distributions: K_{well} , K_{mean} , and K_{max} . Outlier data points above 30 ft/day were removed; outliers represented 5-10% of the data.

An alternate way of evaluating the different site characterization methods is to compare all models to a very generic model, in this case Scenario 5. We did this, and found similar results to the Scenario 1 comparisons described previously. Scenarios 1 and 3 were the best match according to E and RMSE, with a second level of close similarity displayed by models 2a, 2c, and 4c.

Similarly for flux comparisons, we chose a few representative models and compared them against Scenarios 1 (well data) and 5 (constant average parameters). The SCAPS models chosen for comparison were Scenarios 2a (K_{mean}) and 2d (K_{lookup}); these models represent two different estimation methods for hydraulic conductivity associated with the SCAPS probe, and furthermore contain only SCAPS-derived measurements. Therefore, they are the best choices with which to fulfill the objective of evaluating the SCAPS methodology in contrast to more traditional measurements. Only the fluxes from the grid cells within 5 ft of the piezometer cluster (20 ft \times 35 ft \times 15 ft box) were analyzed. Calculated error measures for fluxes are shown in Table 4.

MAPE values were around 100-200% for comparisons to both Scenarios 1 and 5, and model efficiencies (E) were all negative, indicating poor agreement between models. RMSE values ranged between 80 and 250 $\mu\text{g}/\text{ft}^2/\text{day}$; in comparison the maximum fluxes in the models were between 13,000 and 60,000 $\mu\text{g}/\text{ft}^2/\text{day}$ with average values around 2 $\mu\text{g}/\text{ft}^2/\text{day}$ (Table 2). Examination of three error measures shows that the SCAPS models (Scenarios 2a and 2d) matched the average model (Scenario 5) better than the well-based model (Scenario 1). This is not surprising since Scenario 5 lacked the spatial distribution of parameters that would produce highly-individualized flux predictions. Model efficiency for comparison of Scenario 1 with Scenario 5 is close to zero, indicating that

the spatially-distributed parameters in the model contribute only slightly to the “modeled” variance; it is only slightly worse than using the average value for all parameters, which would be identical to the baseline (Scenario 5).

To answer the fundamental question of how the SCAPS scenarios compare with the more traditional scenarios, we need to look at either concentration or flux error measures, as the picture is different in each case. For concentration, comparing Scenarios 2a (SCAPS K_{mean}) and 2d (SCAPS K_{lookup}) with the baseline scenarios, MAPEs are under 100% and E 's are between 0 and 20%. These would seem to indicate that the differences between models are significant, but certainly within an acceptable range. Looking at flux error measures, MAPEs are between 100 and 200%, and E s are all negative. This indicates that the SCAPS models do not capture the variance characteristics of the baseline models for fluxes. However, the concentration and flux error measures are consistent in that the SCAPS models (Scenarios 2a and 2d) are closer to the average well-based model (Scenario 5) than they are to the spatially-distributed well-based model (Scenario 1). This is likely related to the directionality of well vs. SCAPS head distributions, which would produce differences in modeled concentrations, whereas in Scenario 5 the flow proceeded in the assumed flow direction (234°) and so acts as a “bridge” between the two spatially-distributed models.

Baseline Scenario	Scenario for Comparison	MAPE (%)	RMSE ($\mu\text{g}/\text{ft}^2/\text{d}$)	E
1	2a	203.3	245.94	-13.89
1	2d	142.2	189.69	-7.86
5	1	228.3	83.91	-0.03
5	2a	107.8	181.72	-3.82
5	2d	117.3	140.49	-1.88

Table 4. Error measures for flux comparisons. Fluxes for all timesteps and for a portion of the computational grid containing the piezometer cluster were aggregated for calculation of error measures.

5. Tracer Test Discrepancies

As mentioned above, the tracer test yielded results which were quite unexpected and puzzling. Based on a previous salt-tracer test at the site and on hydraulic head measurements from monitoring wells at the perimeter of the site, assumptions were made about the direction and magnitude of the head gradient. It was recognized from the beginning that the gradient at the site was very low (around 0.002), resulting in a groundwater velocity of about 0.03 ft/day. The low gradient makes prediction of local flow direction difficult, as very small fluctuations (or measurement errors) in head can have a large effect on the flow field. A forced-gradient tracer test could potentially have removed the difficulties with modeling the low gradient at this site. Based on the salt tracer test, the main flow direction was assumed to have azimuth 234°, and the piezometer cluster was oriented accordingly.

As the tracer test progressed, it became apparent that there was a problem with either the Rhodamine collection and measurement or the conceptual model of the site.

There was no strong evidence of a plume moving through the test cluster, just sporadic “hot spots” which did not persist or move in an expected fashion. There is little evidence for a highly heterogeneous domain in which preferential flowpaths would be important. Various measures were taken to find out the source of the problem, but none produced any conclusive result. These are detailed in an accompanying report. We hypothesize that what happened is a combination of one or more of the following: a) the tracer moved in a direction other than through the piezometer cluster, or below it, and we just caught the edges, b) the Rhodamine WT did not act as a conservative tracer due to biological or other degradation, c) the collection of water samples in a relatively dense 3-D network disturbed the flow field and created transient preferential flowpaths, creating an irregular distribution of tracer, d) small-scale temporal variations in the flow field (not accounted for in the steady-state flow model) were important in determining tracer concentrations in the piezometers, or e) the instrument used to measure tracer concentrations was faulty or greatly affected by varying turbidity (contrary to vendor’s assurances). Each of these possible scenarios has arguments for and against it; based on the accompanying analysis by our collaborator it seems that the last option is the most likely. Nevertheless, this model testing exercise is still valid in regards to comparing models against each other and, thus has merit in evaluating the SCAPS method’s usefulness.

6. Conclusions from Data Analysis

Comparison of well-based (Scenario 1) vs. SCAPS-based tracer predictions (Scenarios 2a–2d) shows that the two models were in relatively good agreement, with MAPE values around 50% for all but Scenario 2c (SCAPS K_{\max}). Model efficiencies ranged from modest ($E > 0.15$ for Scenarios 2a and 2c) to low ($E < 0.05$ for Scenarios 2b and 2d), and RMSE’s were in the range of 60 – 70 ppb. Differences in flow directions, while relatively minor, contributed to observed errors by moving high concentrations from the right side of the cluster (Scenario 1) to the left side (Scenarios 2a-2d). For this reason our main recommendation for use of SCAPS data in future studies would be to obtain replicate measurements with closely-spaced pushes, thereby alleviating the “all or nothing” quality of the data and allowing for more conventional statistical comparisons (e.g., Student t-Test, ANOVA, etc.).

Comparison of modeled with observed tracer test data shows that models based on traditional (well-based) measurements and the SCAPS measurements were indistinguishable in terms of performance for the conditions present in this site and tracer test. This statement is made with the caveat that the model performances were all unsatisfactory due to the unexpected tracer test results. Therefore, the observed variances in error measures were quite large, and the finding that no model result is significantly different from the others is primarily influenced by the large variances. Due to the very low observed gradient and suspicion that the detection instrumentation is influenced by turbidity, it is likely that a forced gradient tracer test with well-constrained models and either a better detection instrument or an alternative tracer would have provided more

appropriate data with which to evaluate the site characterization method under evaluation, as a superior prediction versus observation agreement are anticipated.

References

Hossain, F., E.N. Anagnostou, and K.-H. Lee, 2004. A non-linear and stochastic response surface method of Bayesian estimation of uncertainty in soil moisture simulation from a land surface model, *Nonlinear Processes in Geophys.*, 11, 427-440.

Melesse, A.M. and X. Wang, 2006. Multitemporal scale hydrograph prediction using artificial neural networks, *J. American Water Resources Association*, 42, 1647-1657.

Nash, J.E. and J.V. Sutcliffe, 1970. River flow forecasting through conceptual models, Part I: A discussion of principles, *J. Hydrol.*, 10, 282-290.

Rani, S.A., B. Pitts, and P.S. Stewart, 2005. Rapid diffusion of fluorescent tracers into *Staphylococcus epidermis* biofilms visualized by time lapse microscopy, *Antimicrobial Agents and Chemotherapy*, 49, 728-732.

Appendix A

This table lists input parameters and boundary and initial conditions for the MODFLOW flow simulations and MT3D transport simulations.

	Input Parameters	Boundary Conditions	Initial Conditions
MOD-FLOW	Head distribution (well or SCAPS) K distribution (well or SCAPS) K anisotropy ratios (from variograms)	Specified head (side boundaries) No-flow (top & bottom boundaries)	Interpolated head (well or SCAPS)
MT3D	Porosity distribution (well or SCAPS) Dispersivities (from salt tracer test)** Rhodamine molecular diffusion coeff.**	Dependent on MODFLOW**	Rhodamine concentration at injection well set to conserve mass (0.4 g total). Zero concentration elsewhere.

** Refer to Section 1e for explanation or specific parameter values.

APPENDIX J

STANDARD OPERATING PROCEDURE

DATA ACQUISITION USING THE HIGH RESOLUTION PIEZOCONE SYSTEM

REVISION DATE: JUNE 12, 2007

Prepared by Jerome Fee

Reviewed by Fred Essig

Approved by Timothy Shields

TABLE OF CONTENTS

1.0	PURPOSE	1
2.0	BACKGROUND	1
3.0	APPLICABILITY	1
4.0	DEFINITIONS	1
5.0	REFERENCES	4
6.0	APPARATUS AND MATERIALS	4
7.0	PROCEDURES	5
7.1	Probe Preparation	5
7.2	Calibrate the Pressure Transducer as Follows:.....	6
7.3	Prepare the Data Collection Software and Collect Data as Follows:	8
7.4	Post Process the Data File and Set the T50 as Follows:.....	12
7.5	View the Final Hydrostatic Pressure Profile:.....	14
7.6	Exporting Data Files for GMS Model	16

ATTACHMENT 1 DATA COLLECTION SHEET
ATTACHMENT 2 EXAMPLE *PIEZOCONE.CAL* CALIBRATION FILE

STANDARD OPERATING PROCEDURE

DATA ACQUISITION USING THE HIGH RESOLUTION PIEZOCONE SYSTEM

1.0 PURPOSE

This Standard Operating Procedure (SOP) describes a procedure for collecting groundwater data using the high precision piezocone and WinOCPT software.

2.0 BACKGROUND

Groundwater assessment and remediation projects require determination of the direction and rate of groundwater and contaminant flow. Monitoring wells are typically used to estimate these parameters. However, detailed three-dimensional groundwater and contaminant flow pathways cannot be delineated using conventional monitoring well data because screens are typically set to a single depth range that does not allow for measurement of head values at discrete depths.

A piezocone is a direct push sensor probe consisting of a porous element connected to a customized transducer that converts pore pressure to water level. A high-resolution piezocone (U.S. Patents 6,208,940 and 6,236,941) is a recently developed sensor probe capable of generating highly resolved hydraulic head values (plus or minus 1 inch of water level) while simultaneously collecting critical cone penetrometer test (CPT) soil information. The high-resolution piezocone was developed by the U.S. Navy for use on the Navy's Site Characterization and Analysis Penetrometer System (SCAPS) trucks.

The data acquisition system consists of three parts: the SCAPS data acquisition computer system running WinOCPT software, a wire umbilical cord, and the high precision piezocone probe. The procedures for calibrating the system and collecting data are presented in the following sections.

3.0 APPLICABILITY

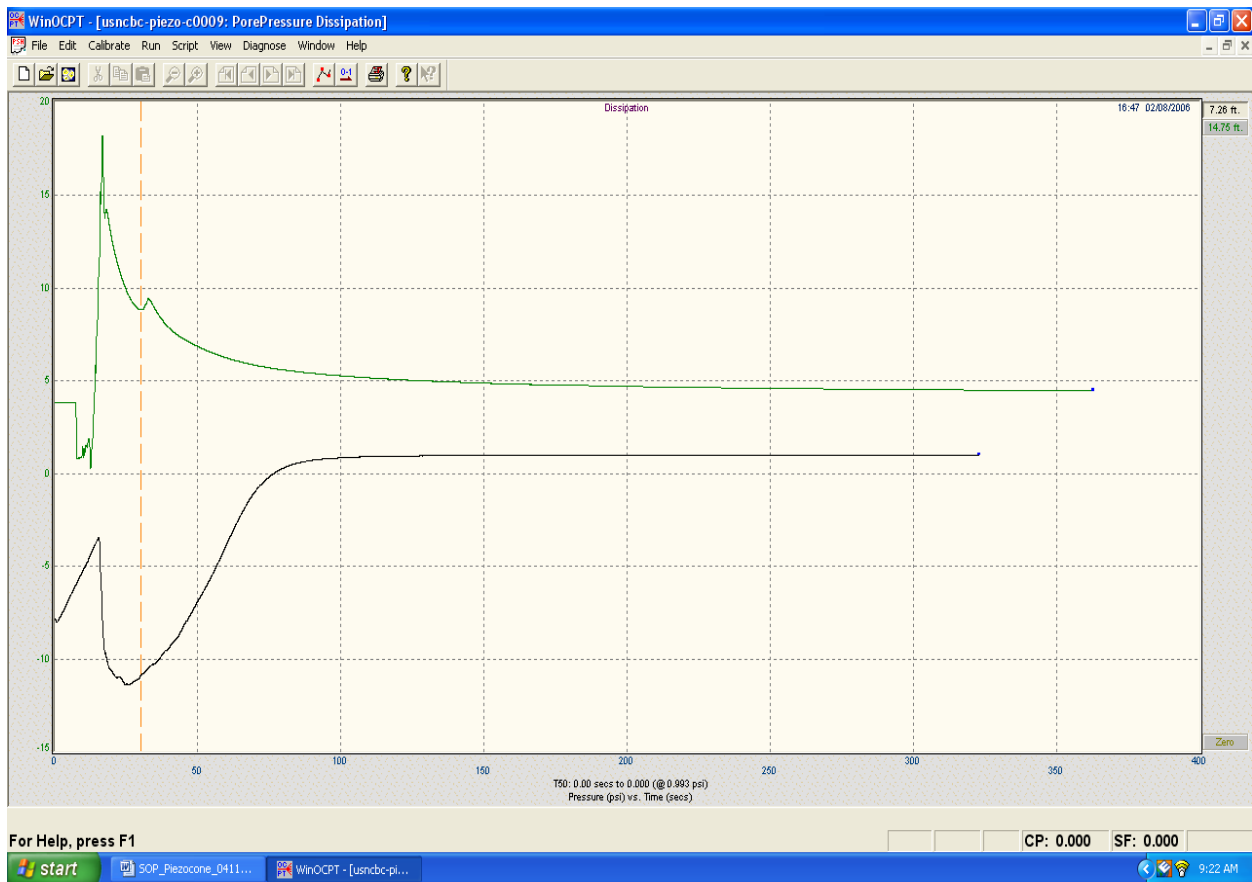
This procedure is applicable for investigations using WinOCPT and Groundwater Modeling System (GMS) software to collect and analyze high-precision piezocone data. When imported into GMS, the high-resolution piezocone data can allow users to generate three-dimensional distributions of hydraulic head, gradient, seepage velocity, and contaminant flux. Furthermore, these distributions can be used for fate and transport modeling and remediation design.

4.0 DEFINITIONS

Cone Penetrometer Test (CPT) – Hydraulic rams on the CPT truck are used to push an instrumented probe into the ground. The probe collects cone pressure and sleeve

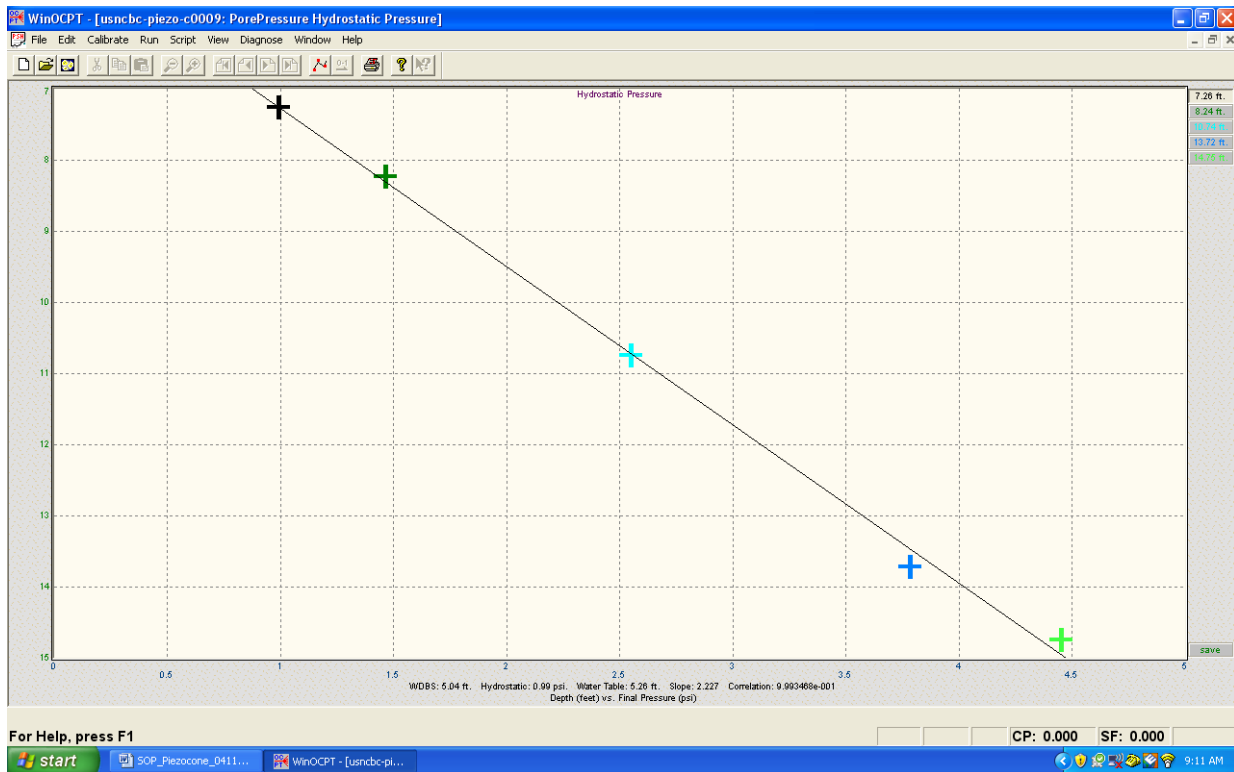
friction data. This test relates cone pressure and sleeve friction to soil behavior classification. CPT data can be used to objectively describe physical soil properties.

Pressure Dissipation Curve – The pore pressure dissipation curve represents observed changes in pressure over time as measured via a transducer in the high-resolution piezocone for a specific depth. The final pressure represents the hydrostatic pressure, which is a reflection of the weight of water measured at that specific depth. The rate of dissipation is used to determine the hydraulic conductivity of the soil adjacent to the probe during the dissipation test. The examples of pressure dissipation curves are plotted below.



Hydrostatic Pressure Profile (HPP) – The HPP represents final pressures measured for a single push depicted as depth on the ordinate, and pressure on the abscissa. The HPP best fit line can be extrapolated to the zero pressure depth, which represents the water table. In some cases, some of the final pressures fall off the single best fit line. These cases may represent a confined aquifer. For instance, if it is suspected that a clay zone represents a vertical boundary to flow, final piezocone pressures above the depth of clay should not fall on the same line as final pressures below the depth of the clay.

An example HPP for an unconfined aquifer is plotted below.



Mandrel – Interior lower portion of the probe to which the strain gauges are mounted. The mandrel is covered by the cone and sleeve.

Push – The act of using the CPT truck to push a probe into the soil. A push is the result of this action.

SCAPS – Site Characterization and Analysis Penetrometer System. A system to obtain real time, subsurface assessment data on soil and chemical characteristics using a variety of instrumented probes.

T50 – The time required for 50 percent of the initial pore pressure to dissipate to a final pressure. This value is used to calculate and estimate hydraulic conductivity.

WinOCPT – Software used to calibrate, control, and record high-resolution piezocone data.

5.0 REFERENCES

ASTM D6067, *Standard Test Method for Using the Electronic Cone Penetrometer for Environmental Site Characterization*. Annual Book of ASTM Standards, v.04.08.

Kram, Mark L., Gary Robbins, Ross Batzoglou, Jessica Chau, Meridith Metcalf, Norm Jones, 2006. *Detailed Hydraulic Assessment Using a High-Resolution Piezocone and 3-D Conceptual Models*, in Proceedings of the Groundwater Resources Association Symposium on High Resolution Site Characterization and Monitoring, Long Beach, CA, November 14-15, 2006.

Kram, Mark L., Gary Robbins, Renduo Zhang, Lanbo Liu, Norm Jones, 2006. *Detailed Hydraulic Assessment Using a High-Resolution Piezocone Coupled to the GeoVIS*, in Proceedings of the North American Environmental Field Conference, Tampa, FL.

6.0 APPARATUS AND MATERIALS

- CPT truck
- High-resolution piezocone data acquisition system
- Data acquisition umbilical
- Calibration yoke
- Tubing
- Vacuum pump
- Valves
- Pressure regulator
- Pressure calibrator
- Pressure calibration vessel
- Digital thermometer
- Ice chest
- Expendable materials including:
 - 1.44-inch-diameter filter elements impregnated with glycerin.
 - O-rings and o-ring lube
 - Glycerin

7.0 PROCEDURES

7.1 Probe Preparation

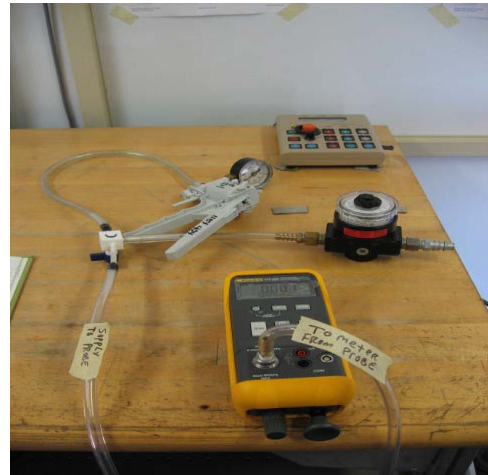
1. Remove cone.
2. Remove sleeve.
3. Remove the front seal assembly from the sleeve.
4. Check all O-ring assemblies.
5. Remove any soil or dirt.
6. Replace all O-rings as necessary.
7. Apply O-ring lube to all seal seat areas.
8. Check for any moisture behind the sleeve assembly in the area of the mandrel.
9. Replace sleeve and seal assembly.
10. Half fill the center of the cone receptacle with glycerin.
11. Using a small probe or dental tool, sweep all interior surfaces to eliminate void spaces or bubbles. It is critical to the data collection process that all of the bubbles are removed from the internal space between the transducer and the filter element.
12. Place glycerin-impregnated filter element on cone with the interior rounded edge of the element facing the cone tip.
13. With the filter element pulled back to expose the ports drilled into the side of the cone, begin to thread the cone and filter element onto the glycerin-filled cone receptacle. Screw the cone onto the probe until glycerin is seen oozing out of the ports.
14. When all of the bubbles are pushed out of the ports in the cone, slide the filter element forward into contact with the cone piece and complete tightening the cone by hand. Use paper towel to contain the extra glycerin that leaks from the cone ports.
15. Place a nitrile glove finger securely over the end of the probe to prevent glycerin from leaking. **Make sure to handle and store the prepared cone in the vertical position with cone facing down. Storing the piezocone assembly on its side will adversely affect calibration or push baseline results and can introduce bubbles into the system.**
16. Plug the piezocone umbilical into the prepared piezocone probe assembly. Gently insert the cord (male plug) into the probe socket (female plug). Carefully rotate the probe while pushing the cable in until the cable seats into position.

Pull the securing ring down the umbilical and thread onto the probe assembly by hand (make sure that the threaded connection is snug).

17. Move the probe selector switch on the data acquisition system to the piezocone position.

7.2 Calibrate the Pressure Transducer as Follows:

1. The sensor will need to be calibrated only once after a new pressure transducer is installed. The specific transducer number is entered in the calibration table. During the setup for a scripted push, there is a prompt for a transducer number so the WinOCPT software can link with the correct calibration data.
2. Prepare the piezocone probe with a new filter element (see section 7.1).
3. Remove the nitrile glove finger and place the piezocone inside the pressure calibration vessel (filter element first) and snugly tighten the locking bolts.
4. Place the two lengths of clear plastic tubing on the pressure vessel.
5. Connect one clear tube from the pressure vessel to the vacuum pump/air supply regulator and air hose using the "T" valve assembly.
6. Connect the other clear hose from the pressure vessel to the pressure calibrator.
7. Turn on the power of the pressure calibrator to the on position and make sure it is reading psi.
8. Tape a digital thermometer to the outside of the pressure vessel so that the temperature of the bath can be monitored during calibration.
9. Set the digital thermometer to read out in degrees centigrade.
10. Place the cone and pressure assembly into an ice chest on the floor with the attached hoses leading to the pressure apparatus and the calibrator on a work bench above. **Note that the probe and pressure vessel may not be stable in the vertical position and should be secured to the side of the bench as needed.**



11. Open the National Instruments measurement and automation software on the data acquisition computer.
 - a. Expand the tab labeled “devices and interfaces”, then expand sub-tab labeled “Traditional NI-DAQ Devices”.
 - b. Right click on sub-tab “PCI-6033E (device 1)” icon and press the drop down labeled “Test Panels”. An A/D card monitoring window will appear.
 - c. Set the program drop down to display channel 5.
 - d. With the “Data Mode” radio button selected on “strip chart”, the program will begin displaying the data from the temperature sensor in the piezocone probe.

12. Introduce ice and/or water into the bucket and stabilize the system at the desired temperature. Monitor the temperature using the external thermometer. Verify the temperature is stabilized using the National Instruments software set to display channel 5 of the A/D card. Note: The system may take several minutes to temperature stabilize for each of the temperature/pressure calibration runs. During the calibration process, it is necessary to keep the pressure calibration vessel at a stable temperature. This can be done by introducing additional water or ice to the bucket and stirring the mixture. Carefully monitor the temperature throughout the calibration process.



13. Once the pressure vessel and probe calibration apparatus is temperature stabilized as described above, reset the National Instruments software to display channel 6 of the A/D card. This will start the program displaying the pressure data from the piezocone probe.
14. A sample data collection sheet is included as Attachment 1 of this SOP. Use the sheet as a model and make sure to collect all of the required fields.
15. Start collecting the calibration data by switching on the vacuum pump bringing the pressure cell to the first desired negative pressure.
16. Use the vacuum pump / pressure regulator to adjust the gross pressure inside the test cell. Use the pressure calibrator controls to make fine pressure

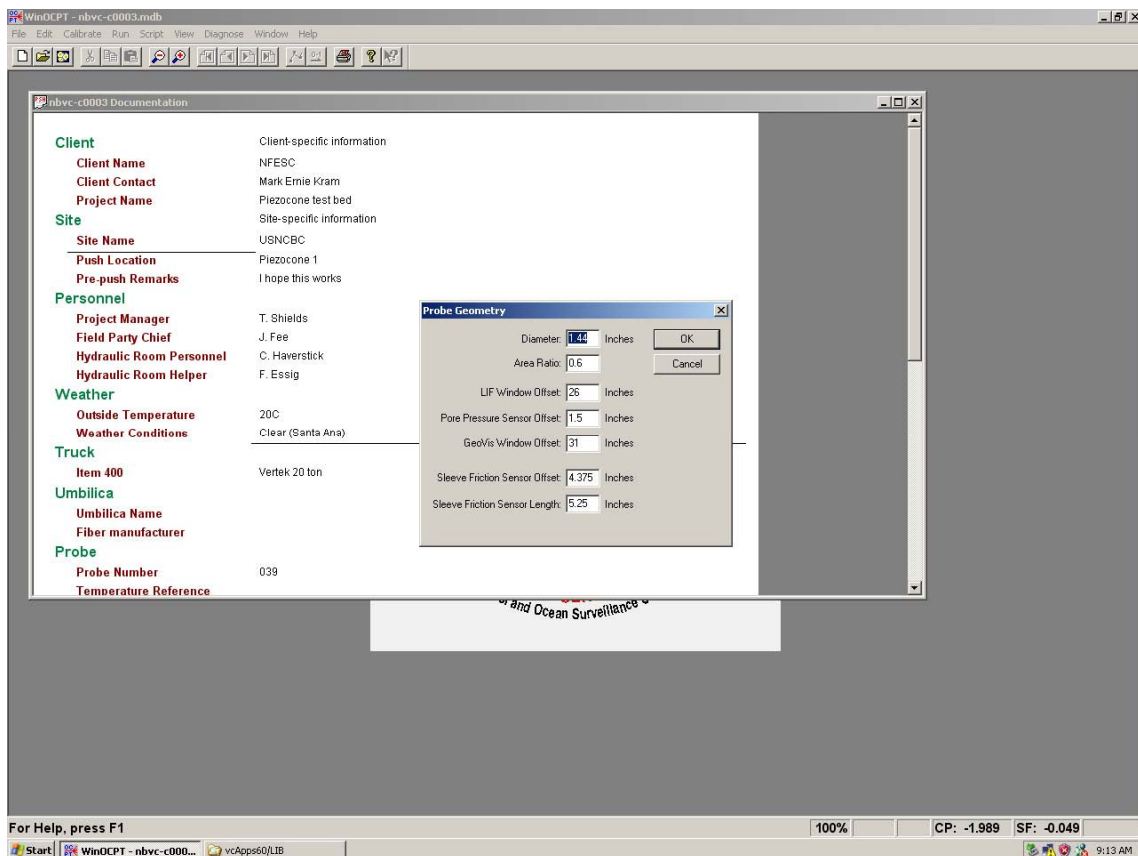
adjustments. Slowly adjust the pressure system to each target value. Do not exceed 25 psi, the maximum calibrated range of the transducer.

17. Simultaneously record the voltage and the pressure using the hold key on the pressure calibrator and clicking on the "one shot" radio button located in the "data mode" box of the A/D software. Carefully record each value in the data collection sheet (Attachment 1). **Note: The fields of the software report the result in volts and the final values required in the calibration table are millivolts. Divide volts by 1000 to get the values to millivolts.**
18. In the middle of the calibration (i.e. at zero pressure) it will be necessary to switch between negative and positive pressure. This will be accomplished by turning off the vacuum pump, closing the valve, and opening the valve leading to the pressure regulator and adjusting the pressure.
19. Turn up the pressure regulator and adjust the calibrator controls to get calibration readings at each of the positive pressure readings. Note: The maximum pressure of the regulator is NO MORE THAN 50 psi. Adjust the system upward slowly while observing the pressure calibrator.
20. Repeat the above process for each target temperature. A minimum of three temperatures is required to run the software. Make sure that all of the temperatures and pressures are recorded to the highest degree of accuracy. The overall accuracy of the system is contingent on the accuracy of the calibration data.
21. Locate the *Piezocone.cal* file in the default directory *C:\Program Files\Paladin Software\WinOCPT* on the data acquisition computer.
22. Make a backup/archive copy of the *Piezocone.cal* file. All of the backup and archive calibration files are kept in the *C:\Program Files\Paladin Software\WinOCPT* subdirectory.
23. If this is the first calibration for the transducer, it will be necessary to add another new paragraph in the *Piezocone.cal* file with the correct sensor serial number. It is most expeditious to copy an existing sensor paragraph, paste it below the last existing entry, then edit the copied information.
24. Using the values in the completed data collection sheet, edit the *Piezocone.cal* file. See Attachment 2 for an example of the *Piezocone.cal* file. Edit each file entry as outlined in the instruction included inside the file.

7.3 Prepare the Data Collection Software and Collect Data as Follows:

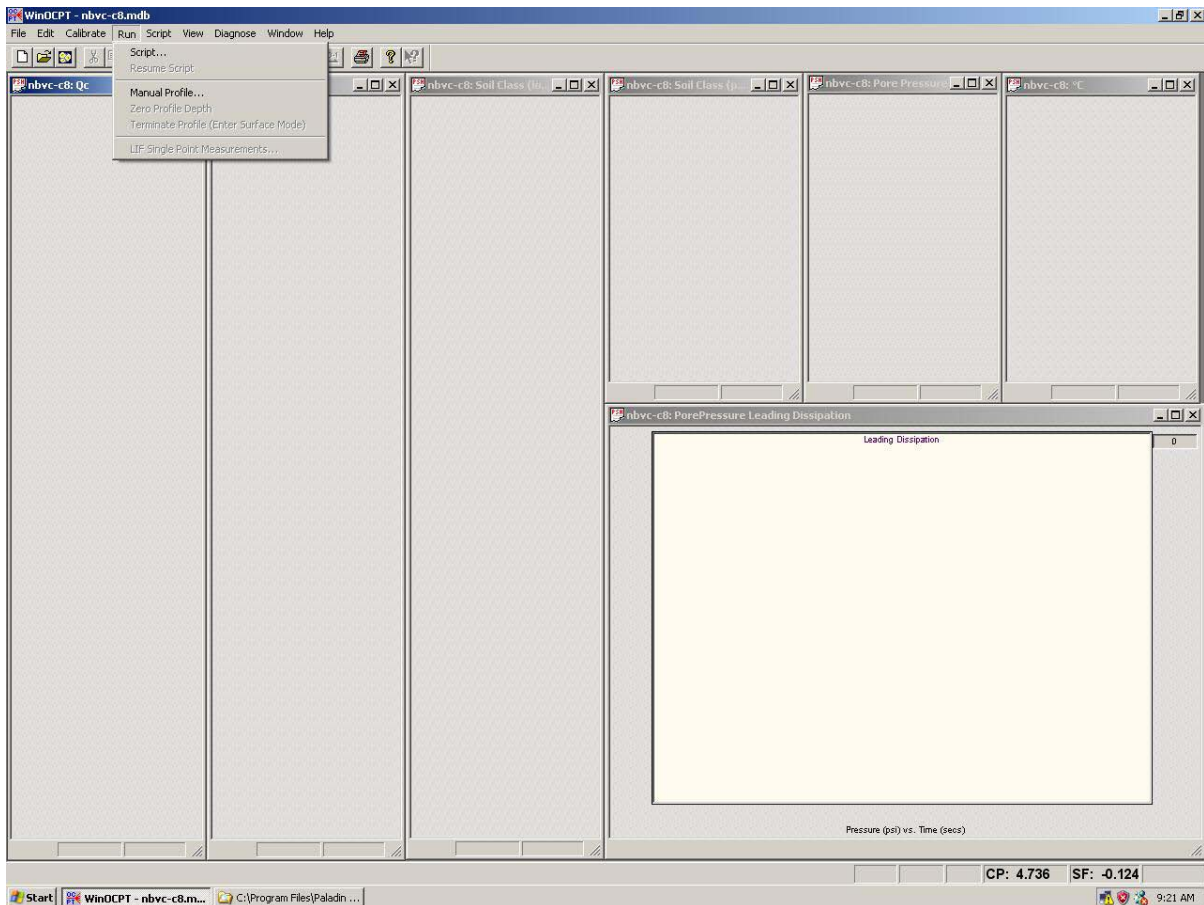
- Start WinOCPT program

- From the FILE menu click on “new”.
- Type in a new file name as directed.
- The system will ask if you desire to select project data template from a previous push. If desired you can select a template push file as presented in the dialog box. If no template is desired, you can press the no button and accept the default values.
- From the EDIT drop down menu select edit probe geometry. Edit the values in the dialog until the parameters match the values show in the following figure:

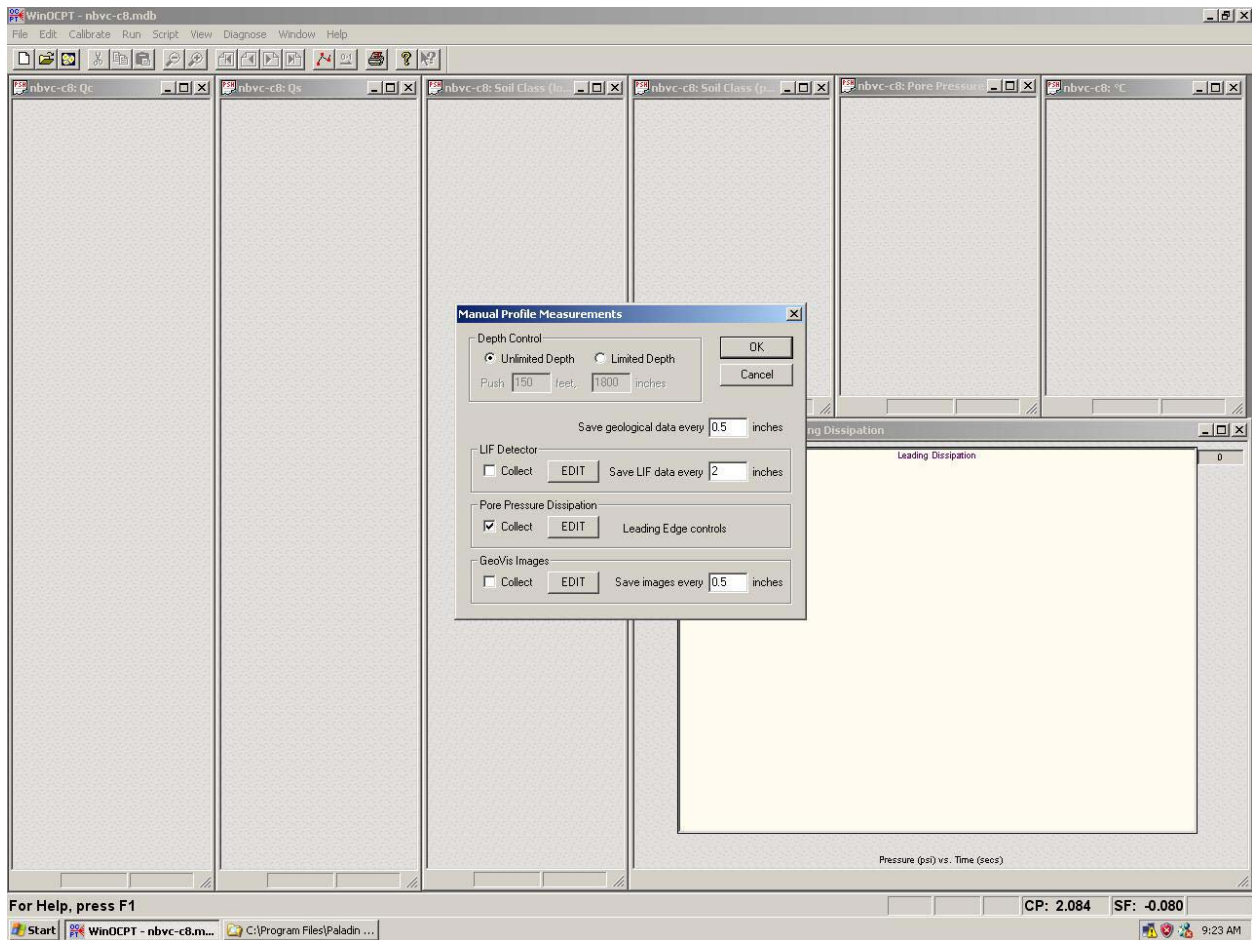


- From the FILE menu click on “load views”.
- Select “*Piezo.view*” or other custom site-specific view from the list and click “OK”. The system will add push windows to the active display. The following screen will then appear:

Data Acquisition using the High Resolution
Piezocone System
Revision Date: 06/12/2007



- From the RUN menu click on “manual profile”.
- Have the push operator advance the probe through the rod washer to ground surface.
- The “Manual Profile Measurements“ dialog box appears. Make sure that “Pore Pressure Dissipation” and “Unlimited Depth” are both selected. Click on the OK button to move to the next window.



- Another dialog appears asking you if the probe is at ground level.

Wait for the SCAPS operator to bring the probe to ground surface before continuing. Also before proceeding make sure that all of the system sensors are idle. If loads are being applied to any of the sensors an error will be generated.

It should be noted that it is very important for the validity of the data that the baselines are collected at the very top of the push immediately before the push is started. Execution of these baseline readings in any other place or position will negatively impact the data quality.

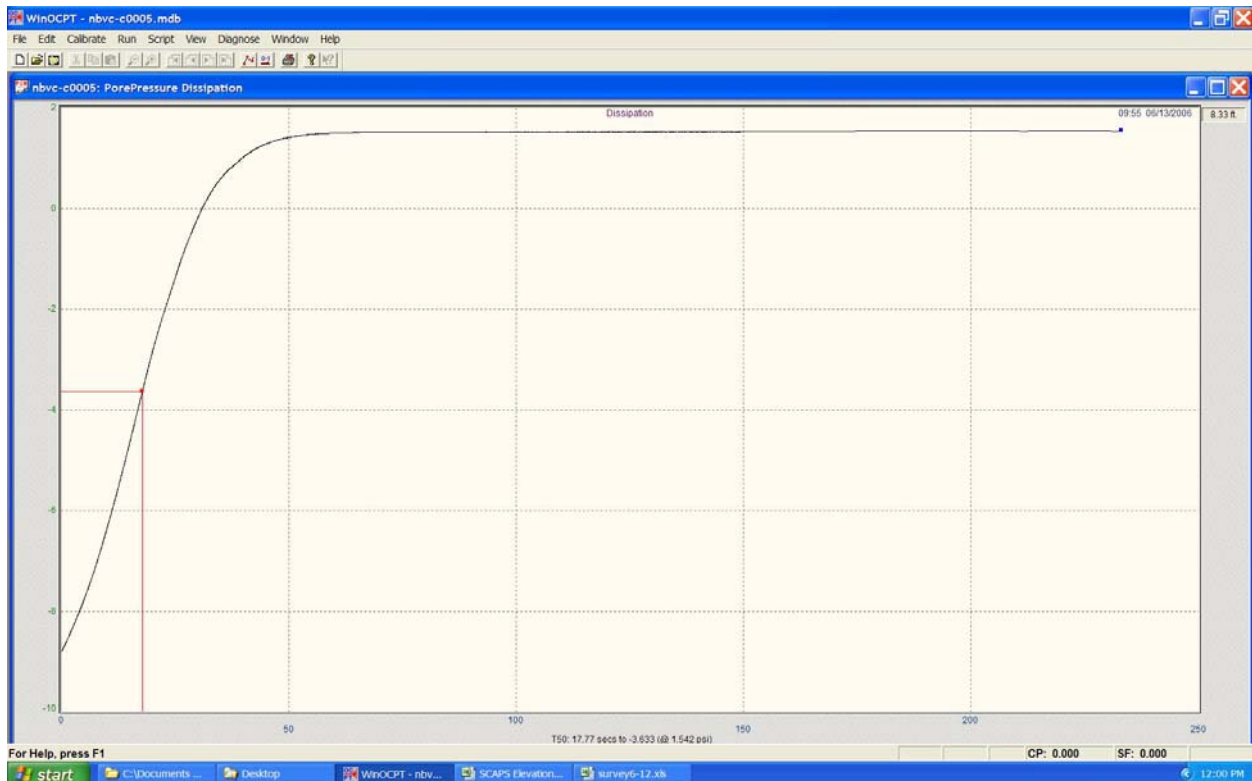
- When the probe is at the ground surface, click on “OK”.
- The system will now go through a series of boxes setting the sensor baselines.
- Note and record the approximate zero level of the pressure system in the SCAPS Data Acquisition Logbook (for later comparison).
- Tell the pushroom operator to “begin the push”.

- When the SCAPS operator begins to push the probe in the ground verify that the system is correctly collecting data.
- Wait for the pushroom operator to reach the first dissipation depth.
- When the number in the upper right hand corner of the dissipation window reaches the desired depth, click on the “capture” button in the lower right hand corner of the dissipation window. It is critical to correlate the commencement of the dissipation collection mode with the operator stopping the push. It is desirable to stop the push head as close to the same time as the software capture button is pushed as possible. Ensure that the capture button is not pressed before the operator stops (this results in a depth error in the push data).
- The pressure observed will typically start at a high positive or negative pressure and the pressure will dissipate to the ambient hydrostatic pressure.
- **Warning: maximum rated pressure for the system is plus or minus 25 psi. Pressures greater or less than the operational range will register as the maximum value. Pressures above 400 psi will potentially damage the transducer.** If pressures above 25 psi are observed the push should be aborted immediately to avoid damaging the pressure transducer.
- When the pressure transducer stabilizes (i.e. the pressure becomes flat wandering within +- .025 psi of a final dissipated pressure) Click on the “monitor” button in the lower right hand corner of the dissipation window to continue the push.
- Repeat the process for each of the desired depths. *It should be noted that to obtain an accurate piezometric surface, it is necessary perform a minimum of four dissipation tests in each push.*
- When the total desired depth is reached, stop the data collection process. From the run menu click on “Terminate profile”. The software will ask if you are sure. Click on “yes”. Tell the pushroom operator “bring the probe up”:
- With the probe dangling vertically in the push jaws, bring up the diagnose geological sensors window. Press “U” for units. Verify that all of the sensors unloaded are within the 1% of the original zero load readings. Verify that the pressure sensor is no more than 0.035 psi from the prerecorded zero load readings. Record the readings in the Data Acquisition Logbook.

7.4 Post Process the Data File and Set the T50 as Follows:

- The post processing of the data fields permanently changes the data files. Before proceeding, copy the original unaltered push data into an archive directory for safekeeping. Copy the files to be post processed to another directory created to separate the processed data. *Make sure to navigate to the correct directory to process the data each time.*

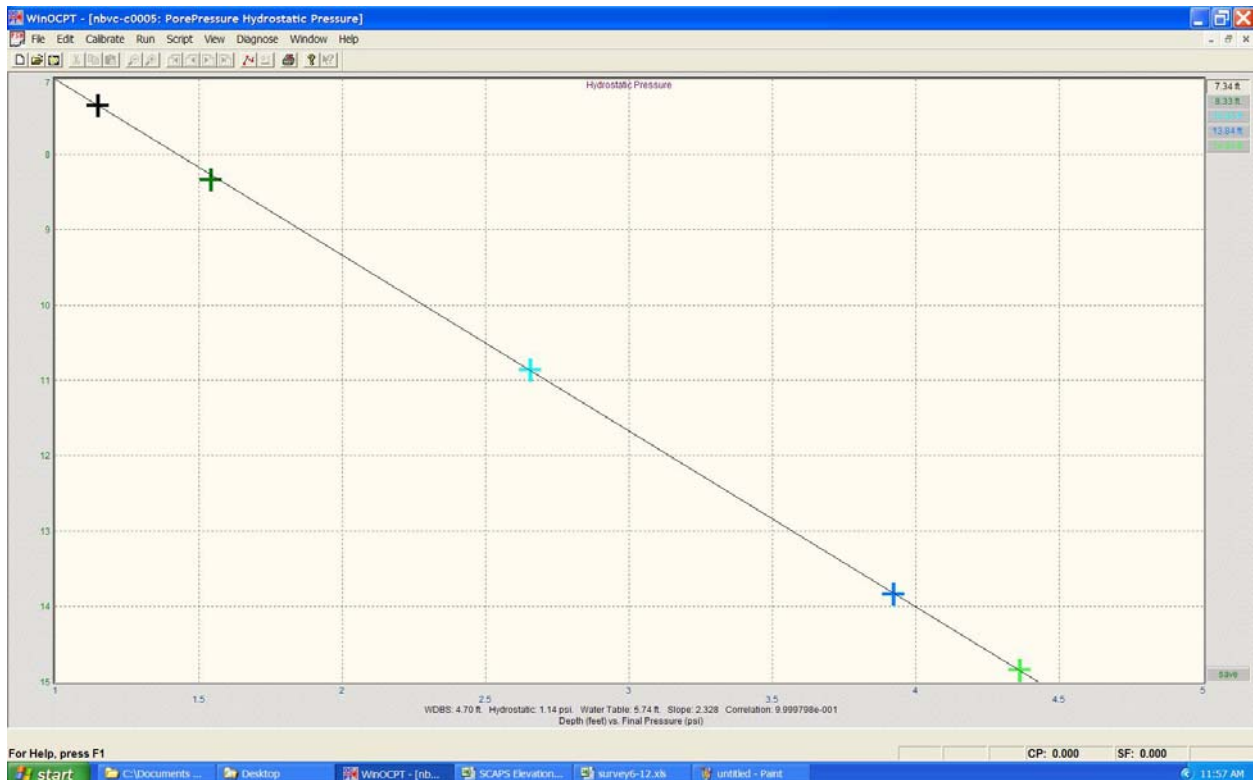
- From the VIEW menu click on “plots”. From the list select the heading “Standard Dissipation”.
- The push dissipation depths for the push will come up in the right hand window.
- Select the first depth and click on “OK”.
- Use the mouse to select the correct dissipation start time by sliding the line across the dissipation window.
- Once the desired depth is displayed, click on zero. *This step removes all of the pressure data before the start of the dissipation. It is critical to select the correct location to truncate the data. To ensure that the correct location is selected refer to notes taken during the push.*



- Review the newly created pore pressure dissipation profile (see graphic above). Make sure that the final pressure is set to the correct pressure.
- The final pressure will not automatically set itself correctly. To change the final dissipation pressure, drag the mouse across the display.
- Repeat the above steps for each of the dissipation in the push.

7.5 View the Final Hydrostatic Pressure Profile:

- From the VIEW menu click on “plots”.
- In the list on the left hand side of the window select “hydrostatic pressure”.
- In the list on the right hand side of the window highlight and select all of the dissipation depths. Press the OK button.
- The Final Hydrostatic Pore Pressure window appears (see graphic below)



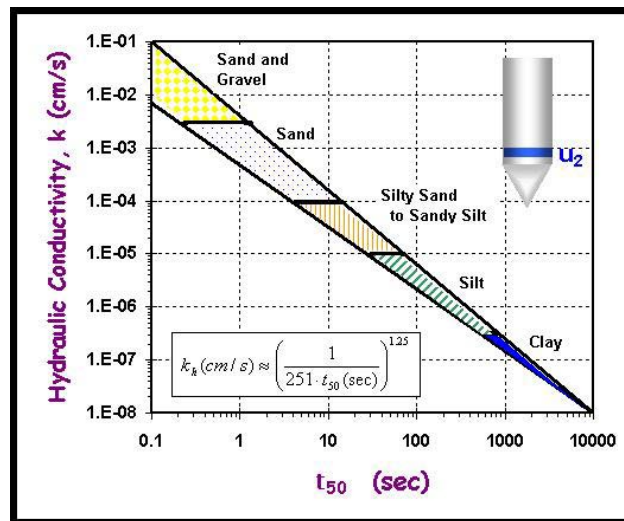
- Take note of the slope, intercept, R^2 , and correlation values.
- Compare to same graphs from other pushes.

Note: curve outliers should not be included in the calculation and will be marked on the display as such. Surficial outliers could be an indicator of perched groundwater conditions. Carefully compare all of the data points for line fit. Poorly fitting points should be eradicated by highlighting the depth window on the display and pressing the delete key. Once the line is satisfactory, press the “save” button on the bottom right corner of the plot. A box will appear, prompting the user to enter X (easting) and Y (northing) coordinates. Enter the X and Y values and press “OK”.

The data displayed typically includes:

- CPT load cell soil classification

- Hydraulic Conductivity (Robertson) “Load Cell Estimate from soil classification.
- Hydraulic Conductivity (Parez and Fauriel) from T50 measurements at each dissipation depth derived from figure below.



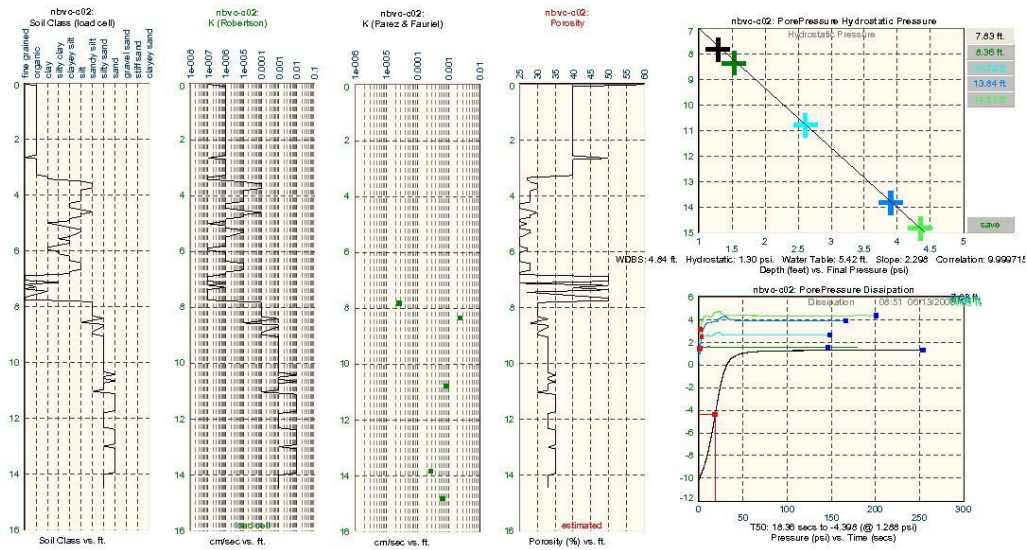
- Porosity, estimated from soil classification.
- Hydrostatic Pressure Plot
- Standard Dissipation Plot

These displays and others are selected as needed in WinOCPT under the View drop down menu within either the “strips” option (geological tab) or within the “plots” option (pore pressure tab).

The hydraulic conductivity estimated from soil classification (Robertson) strip chart uses pore pressure data by default. To view hydraulic conductivity (Robertson) based on a load cell estimate, right click on the strip chart and select “load cell estimate” from the menu.

In general select the hydraulic conductivity (Robertson) display that best conforms to the soil classification and the Parez and Fauriel hydraulic conductivity.

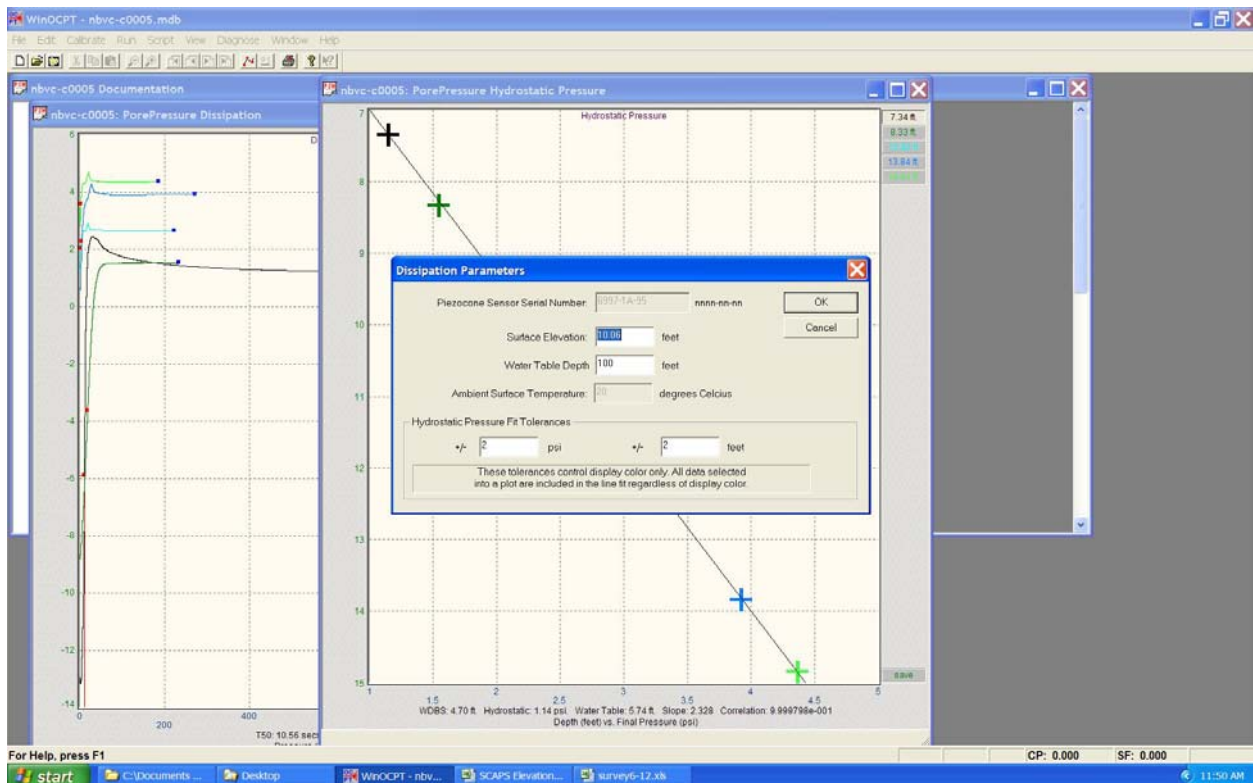
An example layout of strip charts and plots is presented below.



7.6 Exporting Data Files for GMS Model

Before commencing the file export function, edit dissipation values as follows

- From the file menu select “Edit Dissipation Parameters”.
- Enter new surface elevations and press OK.
- Close data file.



The system requires accurate survey data for each push location in order to export data to Groundwater Modeling System. If northing and easting values have not been entered, open each data file and follow the procedures in Section 7.5.

To export the file to GMS:

- Close all data files
- From the FILE menu, select "GMS export".
- Using the dialog box, select the desired files for export using the system tools to navigate to the location of the files.
- Click "OK"
- A box will appear asking the user to select a new export file name and location. Enter the desired name and target location.
- Click "Save"

The GMS Export is now complete. Refer to GMS manual to open the file and process with GMS.

STANDARD OPERATING PROCEDURE

ATTACHMENT 1

DATA COLLECTION SHEET

Transducer specifications

Transducer serial number:

Excitation Voltage:

Pressure Sensitivity:

Temperature Sensitivity:

CALIBRATION MATRIX

	TEMP 1 _____ °C	TEMP 2 _____ °C	TEMP 3 _____ °C	TEMP 4 _____ °C
TEMP OUTPUT ROW (mV output at each Temp)	_____ mV	_____ mV	_____ mV	_____ mV
PRESSURE 1 OUTPUT ROW P1 = _____ PSI	_____ mV	_____ mV	_____ mV	_____ mV
PRESSURE 2 OUTPUT ROW P2 = _____ PSI	_____ mV	_____ mV	_____ mV	_____ mV
PRESSURE 3 OUTPUT ROW P3 = _____ PSI	_____ mV	_____ mV	_____ mV	_____ mV
PRESSURE 4 OUTPUT ROW P4 = _____ PSI	_____ mV	_____ mV	_____ mV	_____ mV
PRESSURE 5 OUTPUT ROW P5 = _____ PSI	_____ mV	_____ mV	_____ mV	_____ mV
PRESSURE 6 OUTPUT ROW P6 = _____ PSI	_____ mV	_____ mV	_____ mV	_____ mV

STANDARD OPERATING PROCEDURE

ATTACHMENT 2

EXAMPLE PIEZOCONE.CAL PIEZOCONE CALIBRATION FILE

The following is a Piezocone calibration table. When a new transducer is used, this table, located in the WinOCPT root directory (piezocone.cal) is updated. In the example below, there are calibration data for three transducers. The table header includes explanation of each field for the temperature/ pressure response curve for each transducer. Once updated with the response data for a new transducer, the file is replaced and linked to the system by the transducer serial number prompted at the start of each push.

High Resolution Pressure Transducer Calibration Tables

// Pressure transducer serial numbers identify the beginning of each section.
// Serial numbers are entered by the user and must match one of these serial
// numbers exactly, including case.

// The number of table data columns (not including the first column) is defined
// by the first value in the temperatures row. Subsequent rows must contain the
// same number of data columns. The order of rows MUST be temperatures, temperature
// sensor output, followed by two or more rows of pressure output values. The delimiter
// between column values can be space, comma or tab (mixtures are allowed). Each
// line must be terminated by CRLF or a single LF. The first value in the temperature
// output row indicates the number of pressure rows.

Barometric Sensitivity: 12.493 mV/mBARA
Barometric Zero Balance: 700 mBARA

S/N: 6997-1A-94

Excitation: 10 VDC

Pressure Sensitivity: 3.017 mV/PSI

Temperature Sensitivity: 3.75 mV/deg. C

4	0 15 25 40	// four data columns; four temperature reading values
6	6420 6470 6502 6570	// six pressure rows; temperature output values (mV)
0	1.31 1.72 1.87 2.35	// pressure; pressure output (mV)
5	16.42 16.83 16.98 17.44	// pressure; pressure output (mV)
10	31.50 31.91 32.06 32.51	// pressure; pressure output (mV)

15	46.57	46.98	47.13	47.57	// pressure; pressure output (mV)
20	61.63	62.02	62.17	62.59	// pressure; pressure output (mV)
25	76.63	77.04	77.18	77.6	// pressure; pressure output (mV)

S/N: 6997-1A-95

Excitation: 12.02 VDC

Pressure Sensitivity: 3.3313 mV/PSI

Temperature Sensitivity: 4.58 mV/deg. C

3	6.3	19.6	39.3		// four data columns; four temperature reading values
6	6783	6860	6934		// six pressure rows; temperature output values (mV)
0	2.9753	2.7899	2.5098		// pressure; pressure output (mV)
5	19.7958	19.4464	19.064		// pressure; pressure output (mV)
10	36.6163	36.1029	35.618		// pressure; pressure output (mV)
15	53.4368	52.7594	52.172		// pressure; pressure output (mV)
20	70.2573	69.4159	68.726		// pressure; pressure output (mV)
25	87.0778	86.0724	85.28		// pressure; pressure output (mV)

S/N: 6997-1A-96

Excitation: 10 VDC

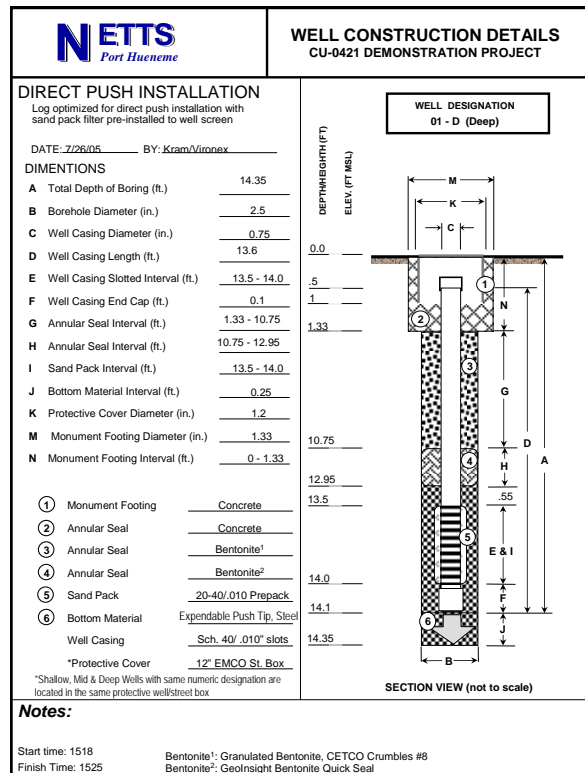
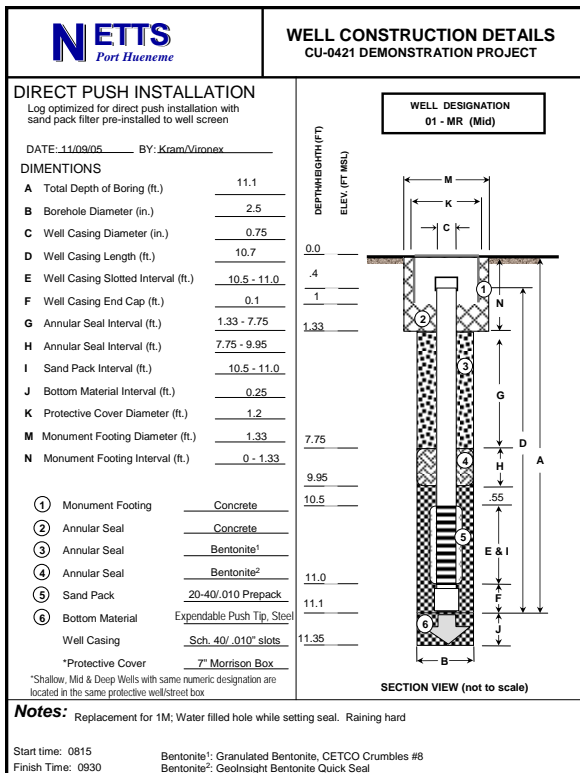
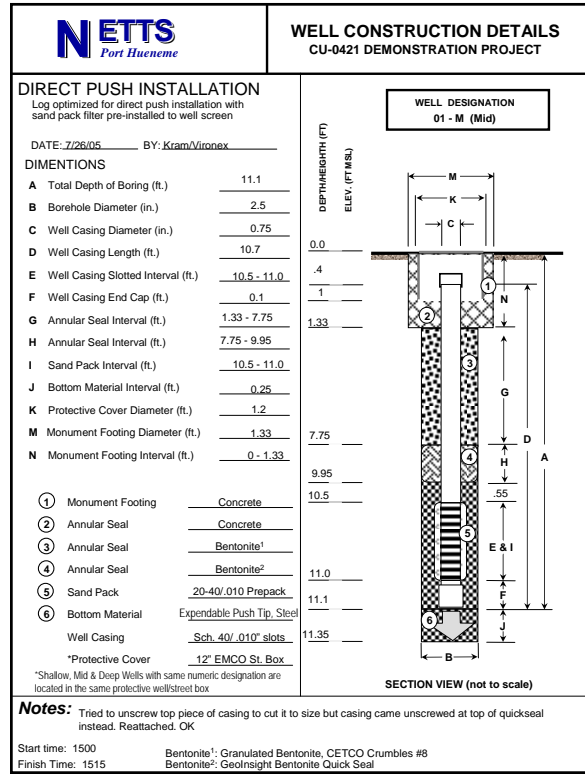
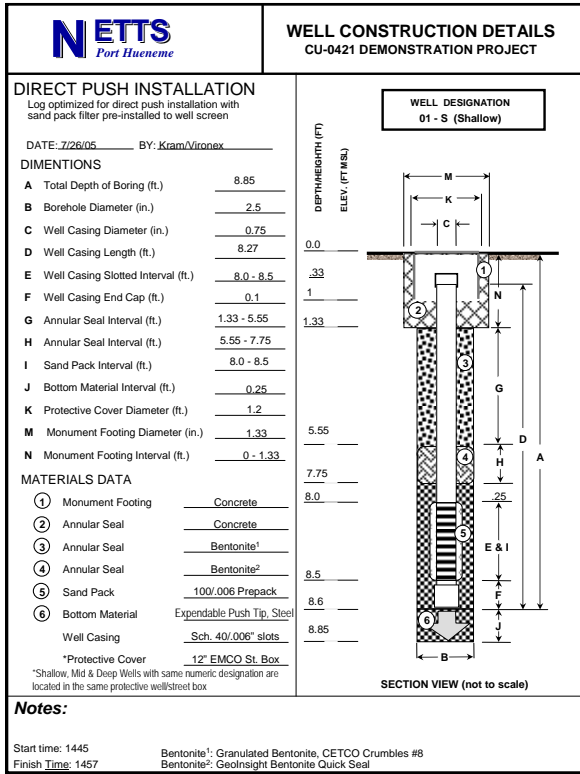
Pressure Sensitivity: 2.998 mV/PSI

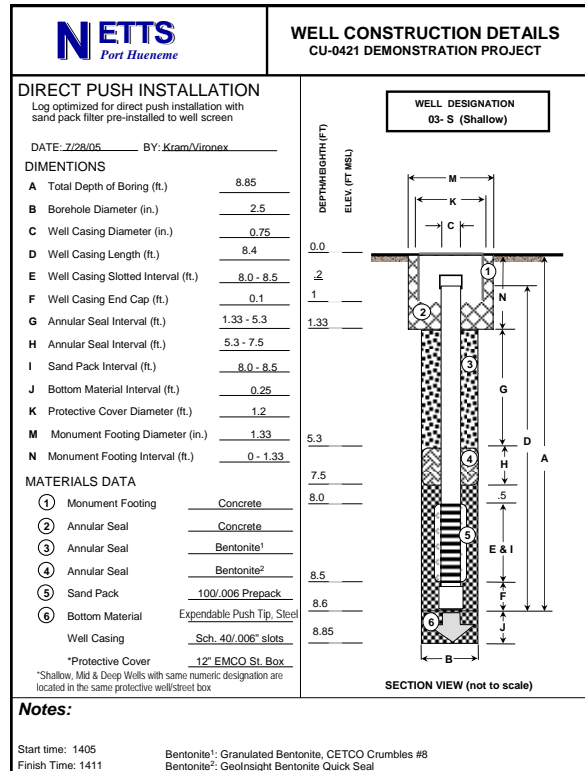
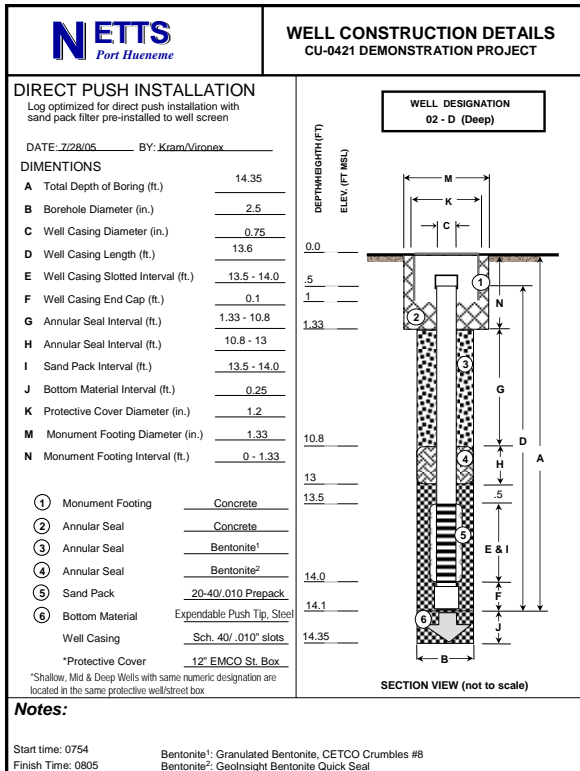
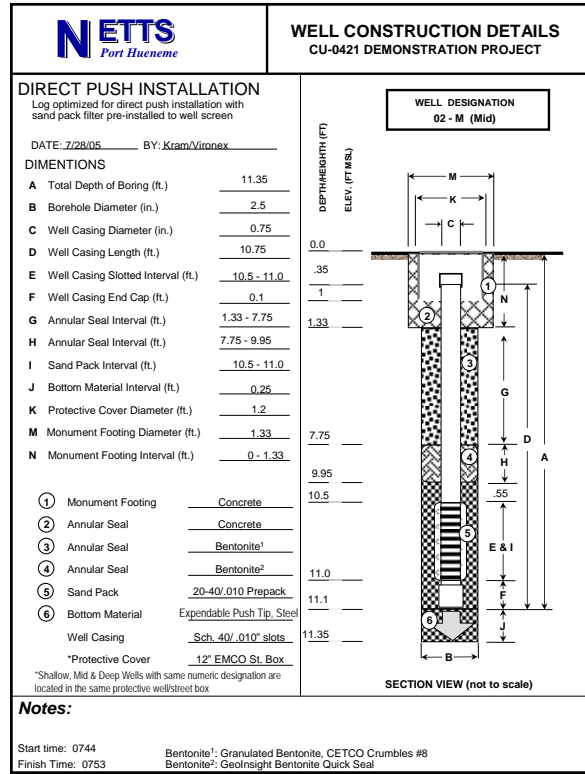
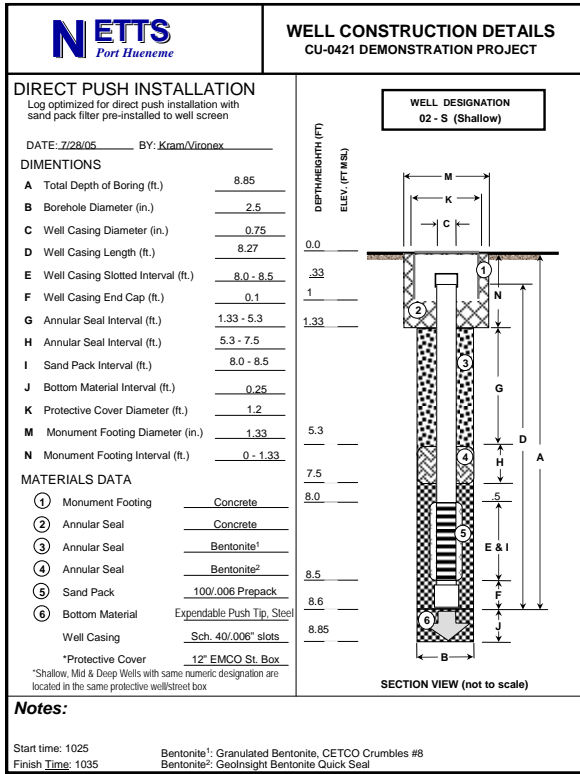
Temperature Sensitivity: 3.975 mV/deg. C

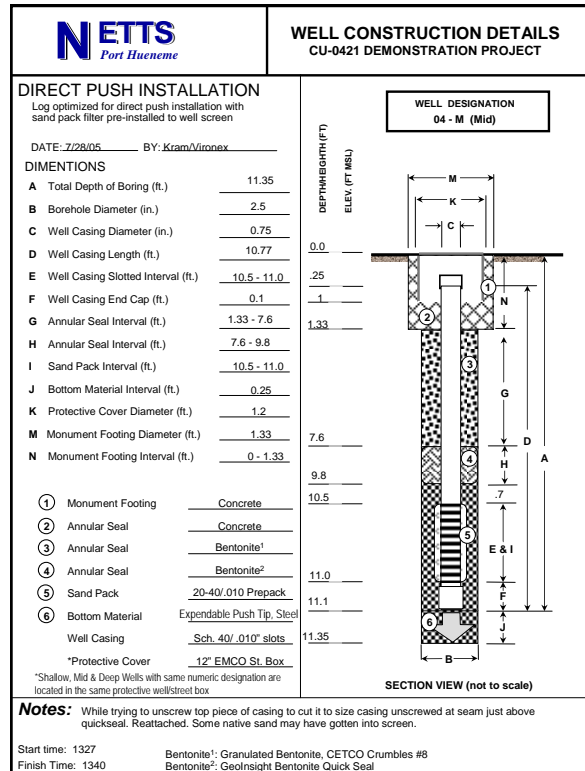
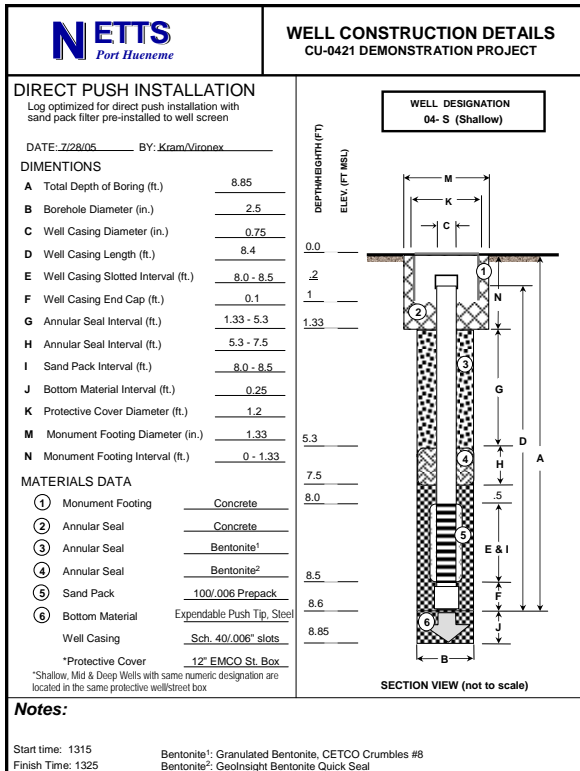
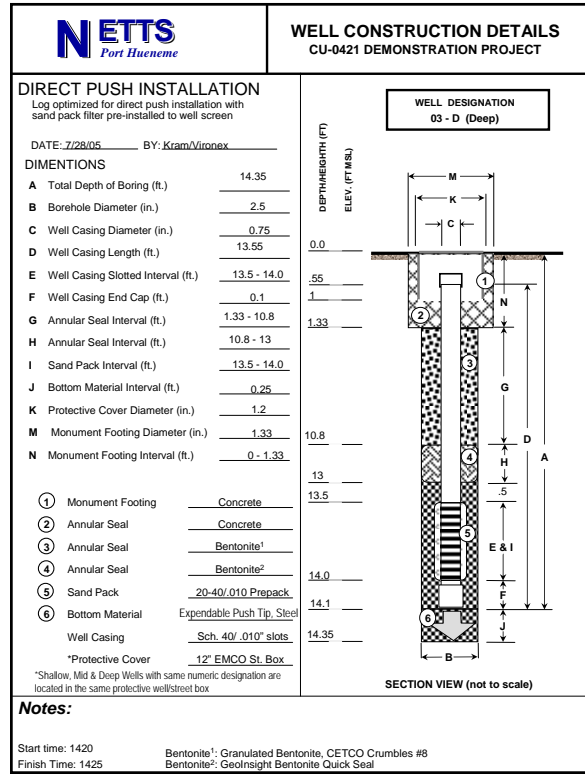
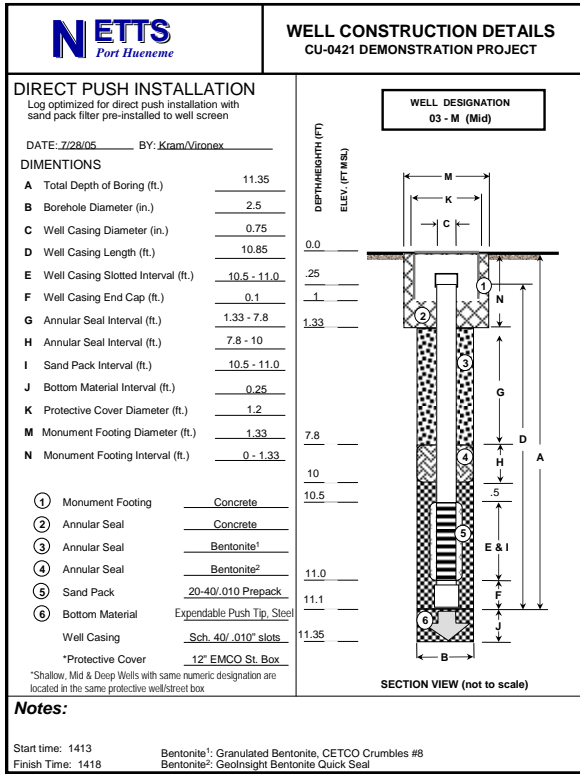
4	0	15	25	40	// four data columns; four temperature reading values
6	6409	6459	6497	6568	// six pressure rows; temperature output values (mV)
0	0.34	0.62	0.66	1.06	// pressure; pressure output (mV)
5	15.34	15.63	15.67	16.08	// pressure; pressure output (mV)
10	30.31	30.62	30.67	31.07	// pressure; pressure output (mV)
15	45.26	45.59	45.64	46.05	// pressure; pressure output (mV)
20	60.2	60.54	60.59	61	// pressure; pressure output (mV)
25	75.1	75.46	75.52	75.93	// pressure; pressure output (mV)

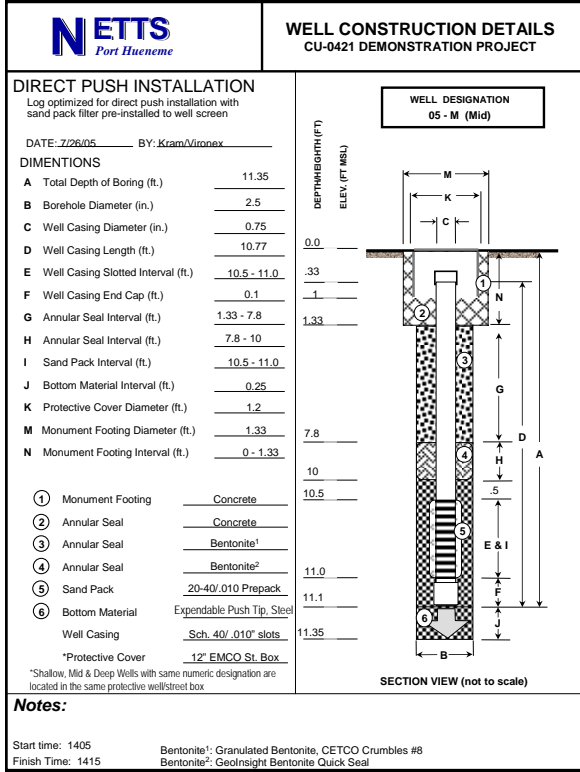
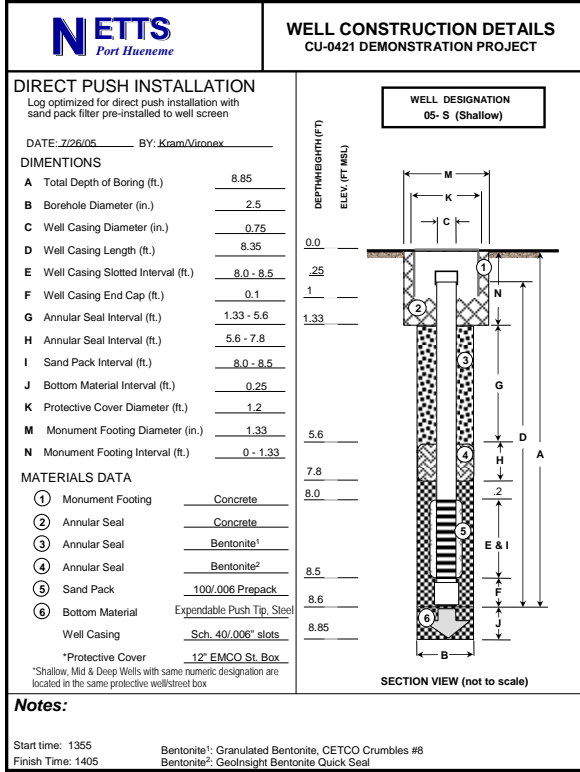
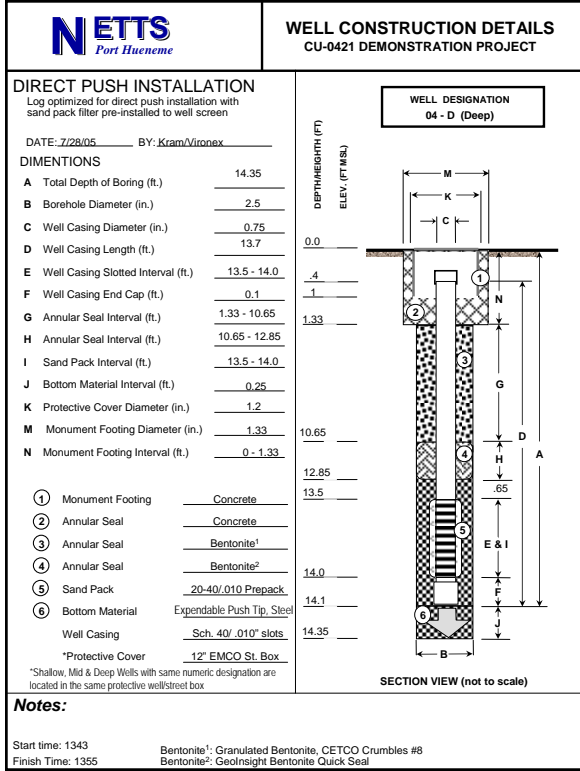
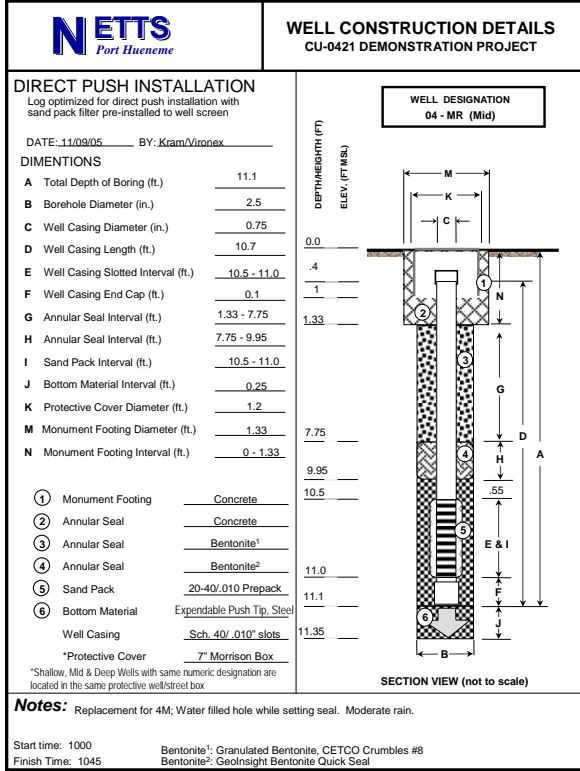
APPENDIX K

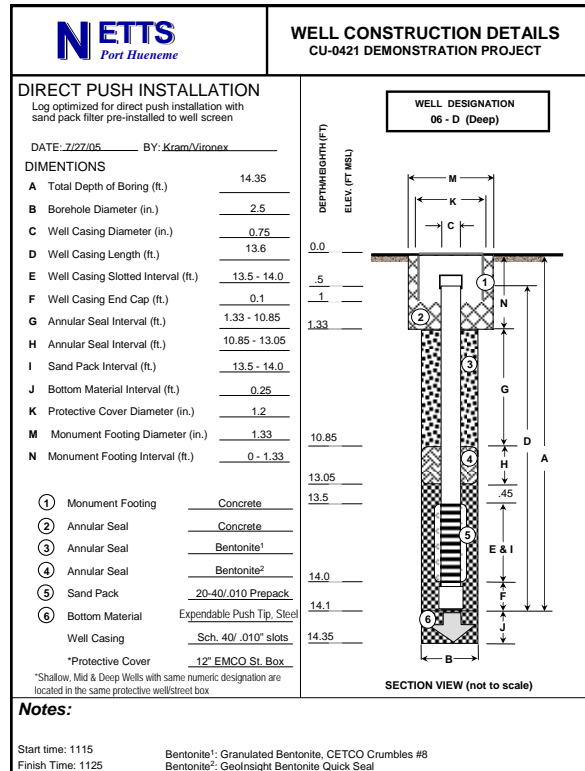
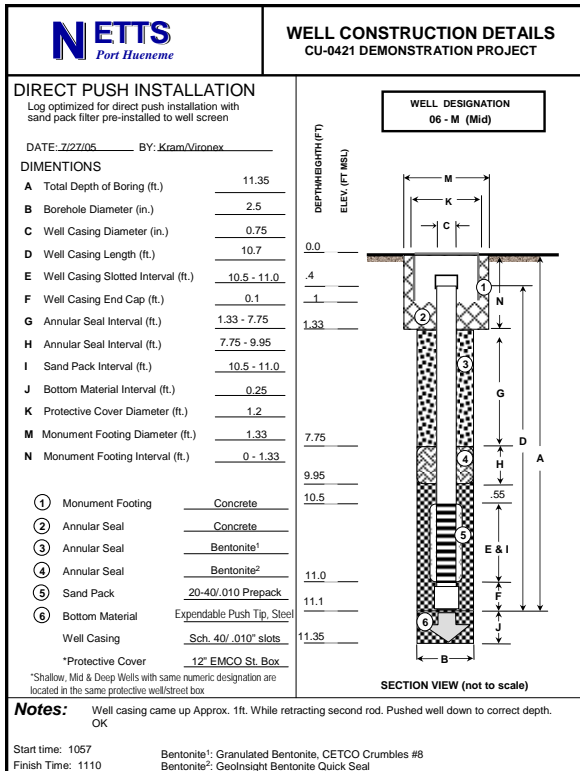
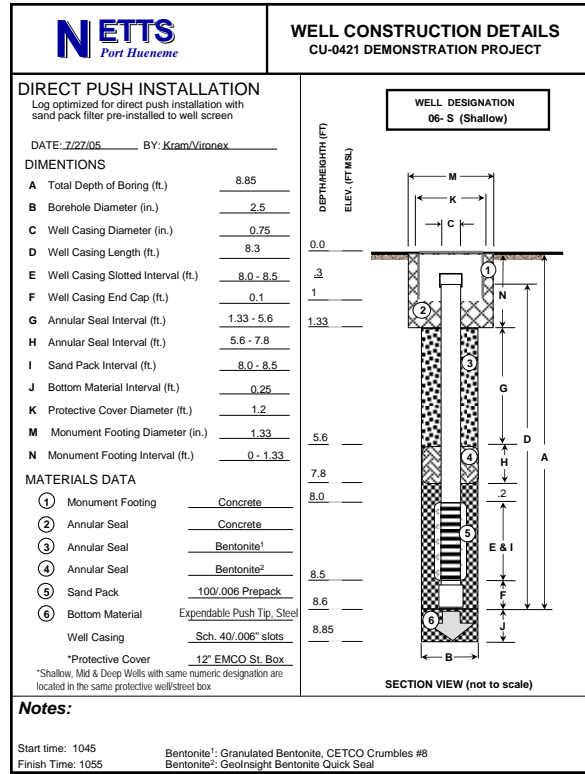
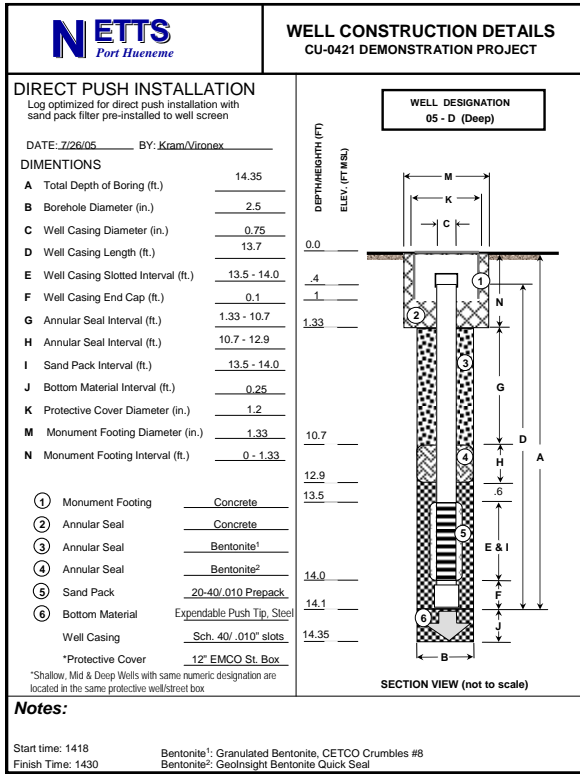
Well Logs

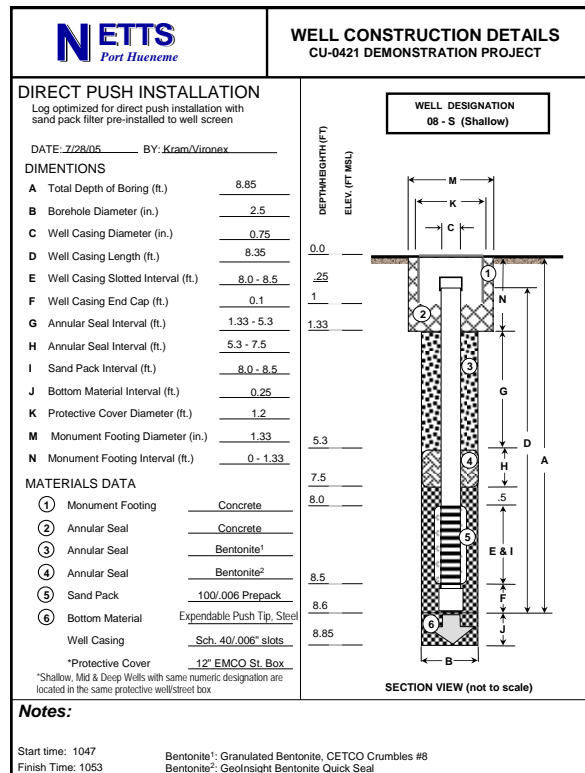
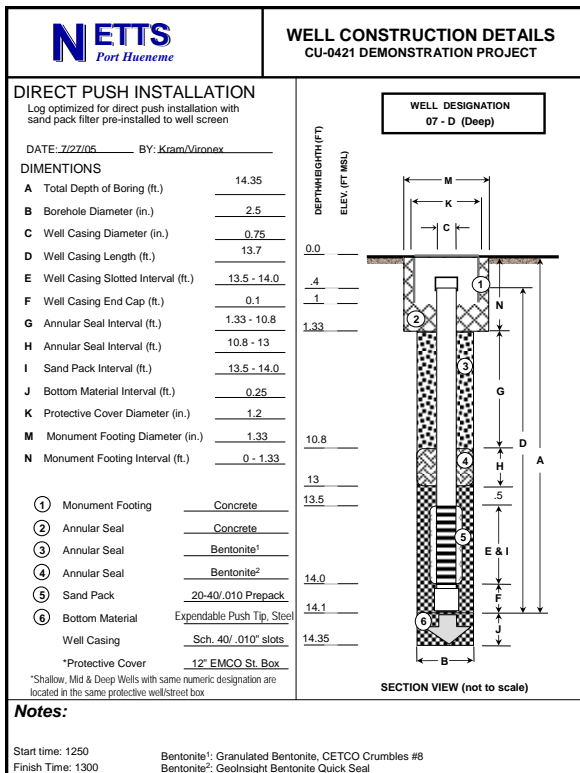
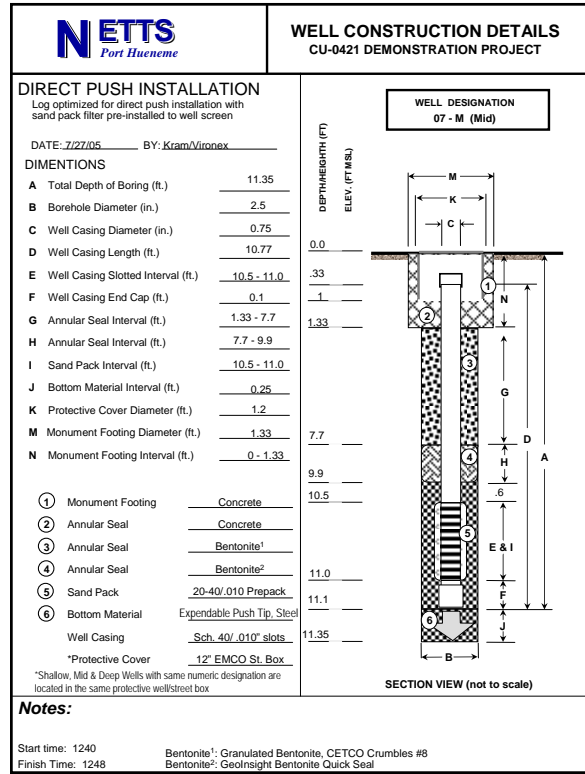
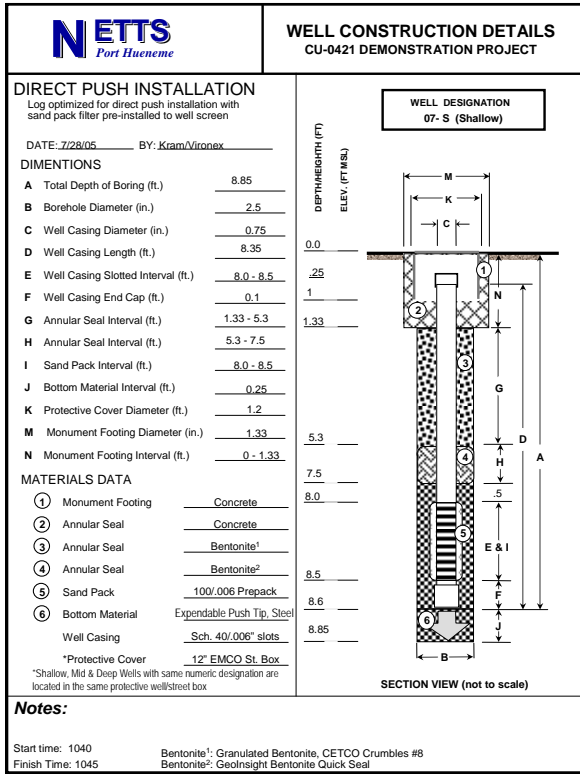


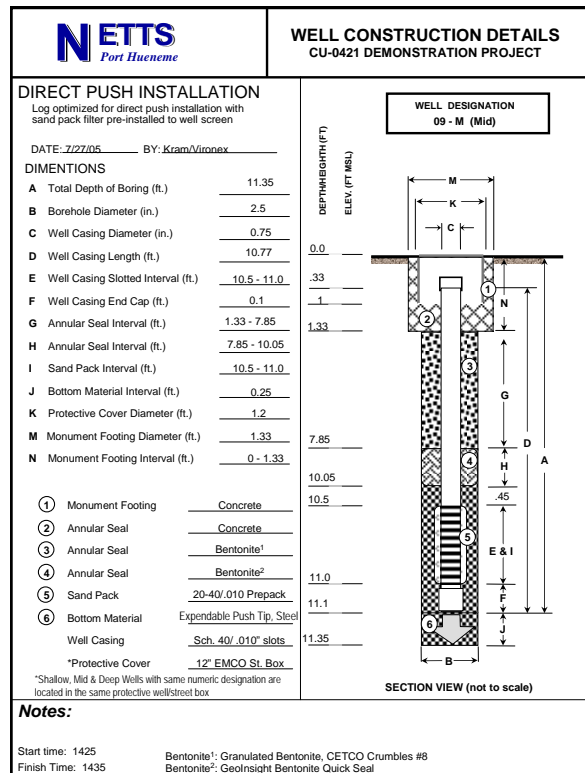
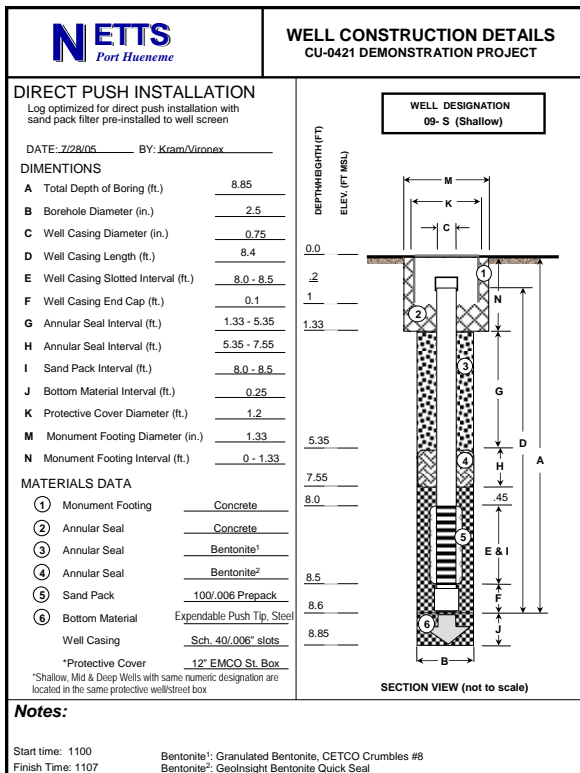
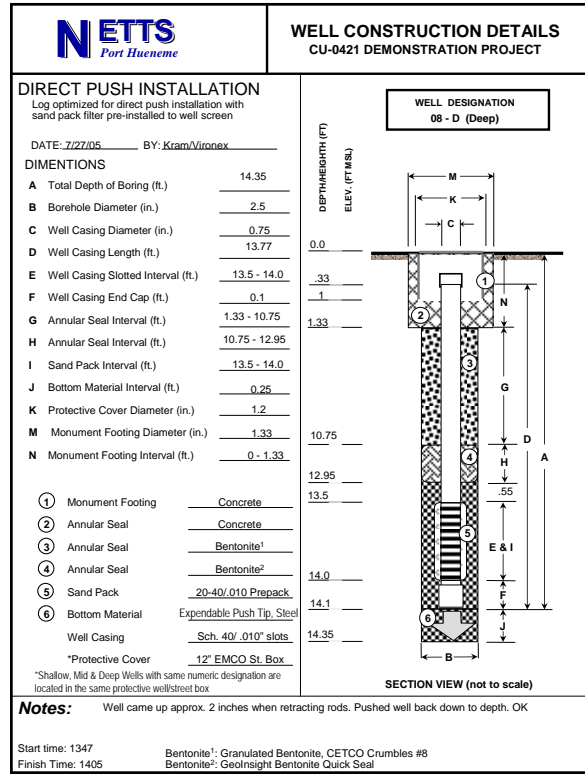
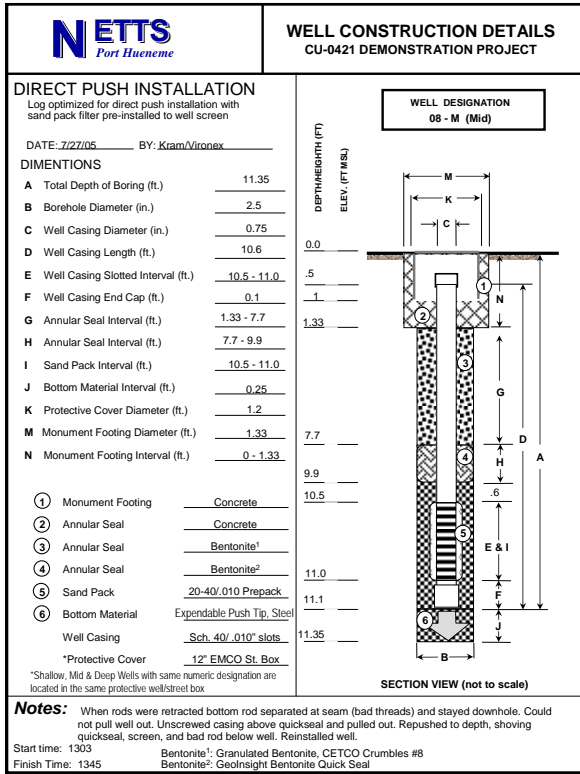


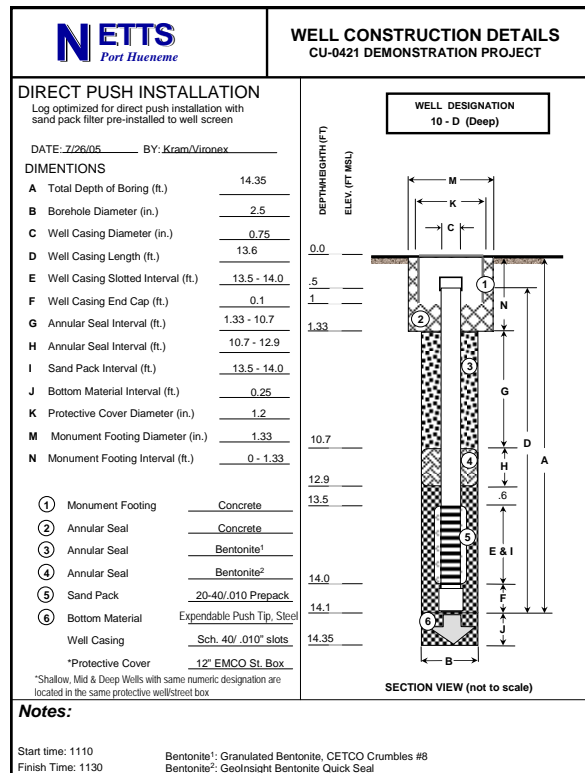
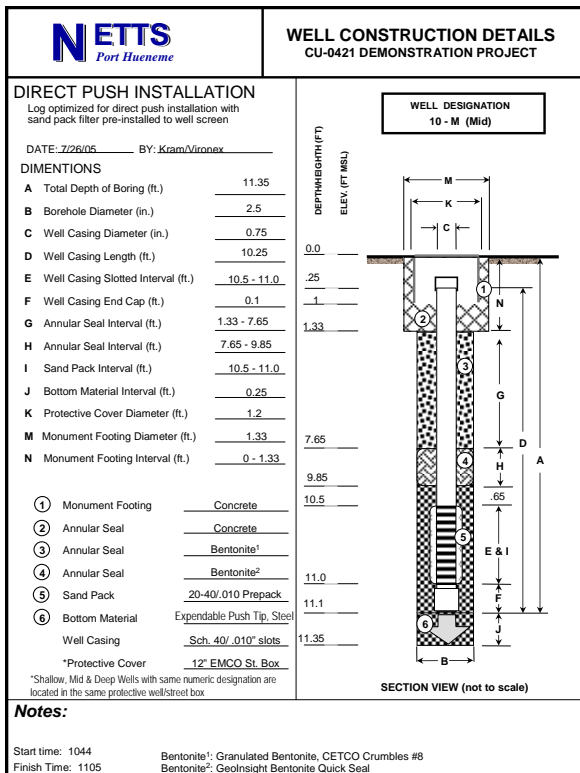
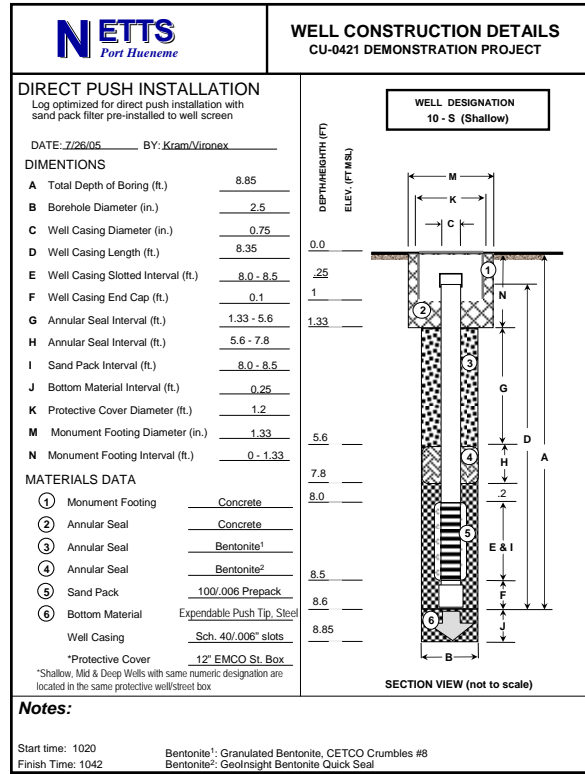
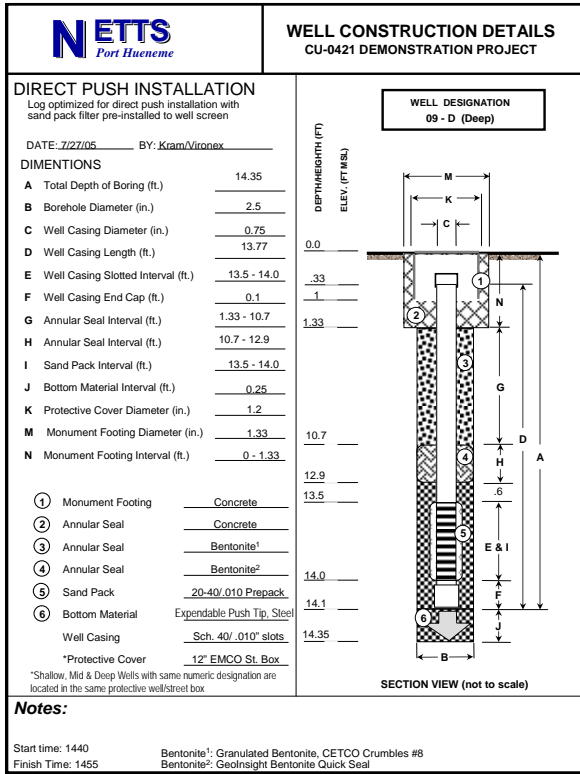


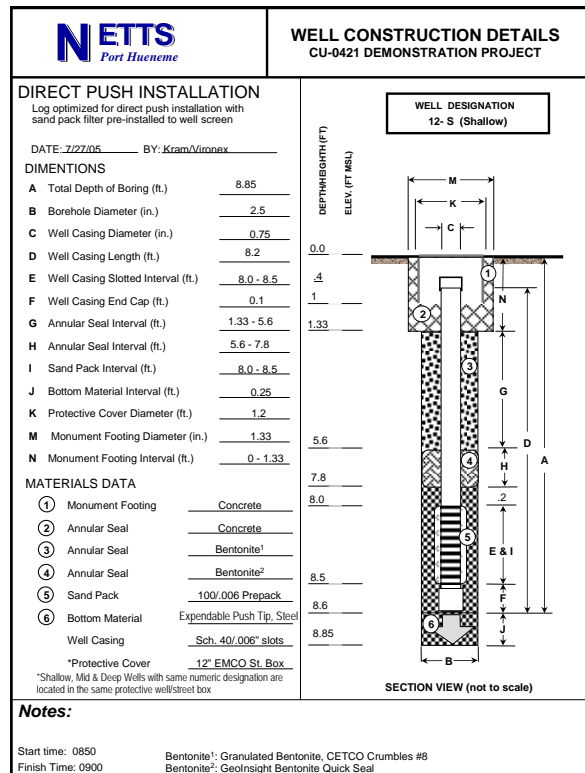
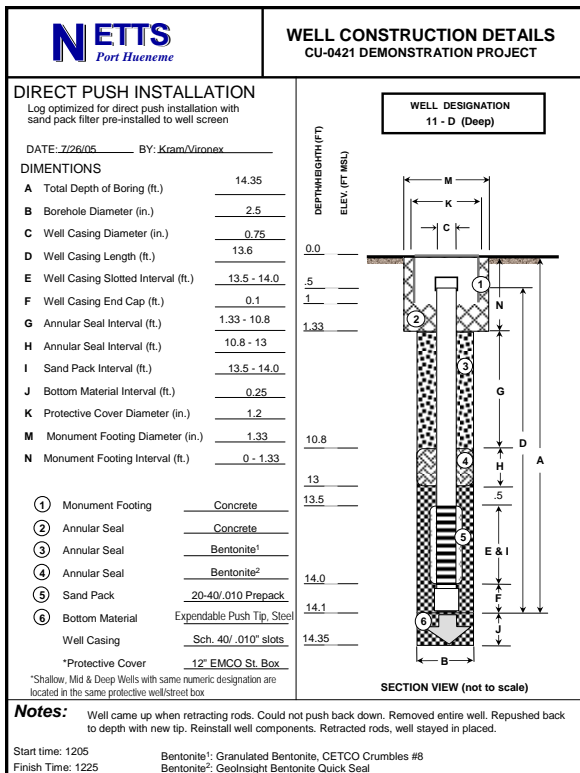
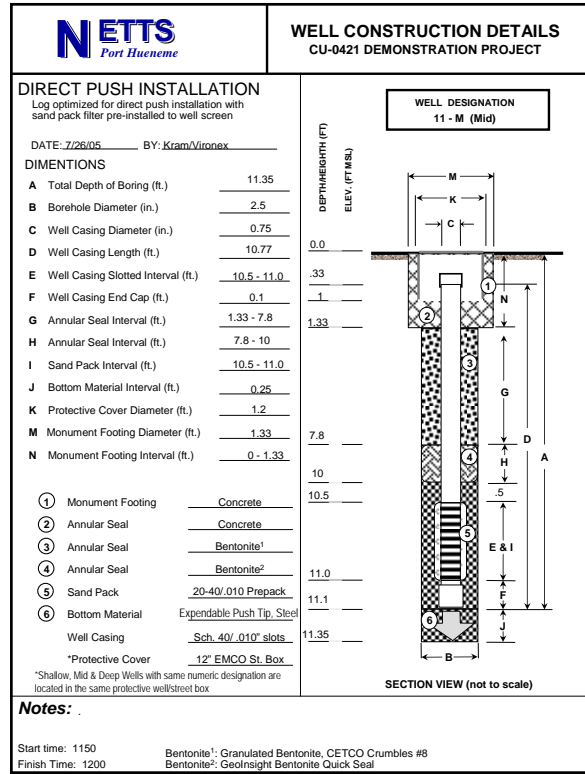
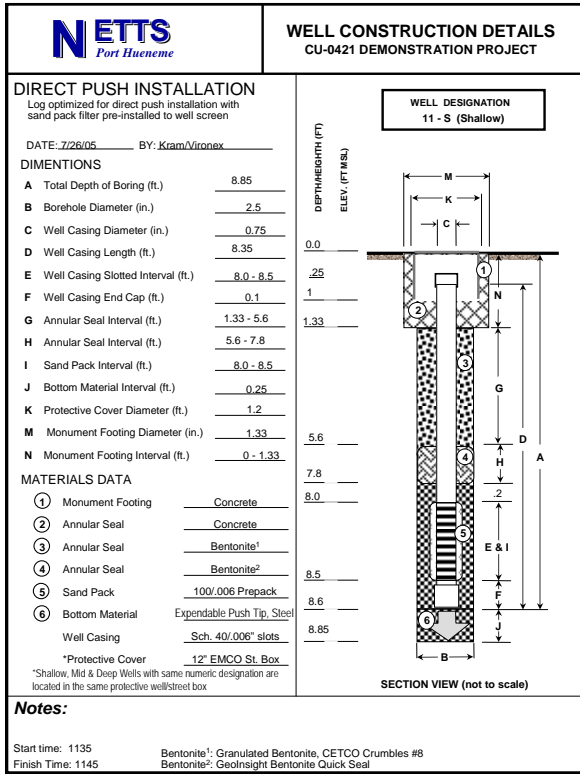


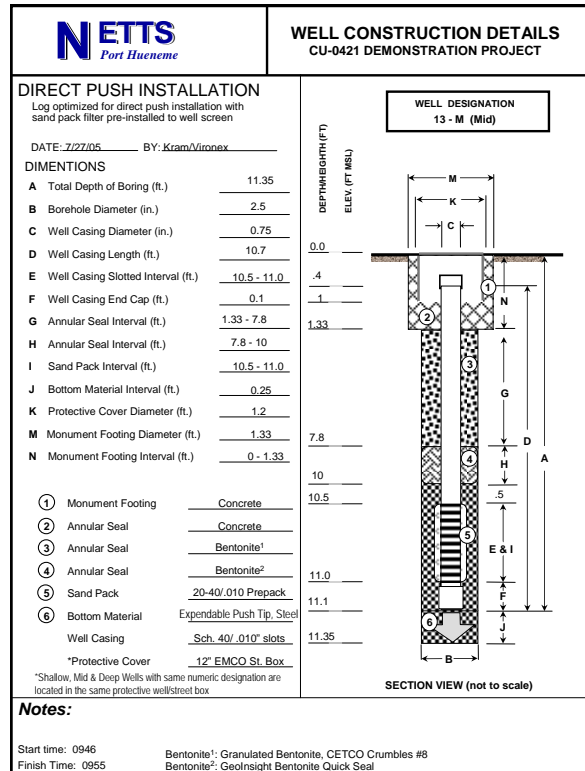
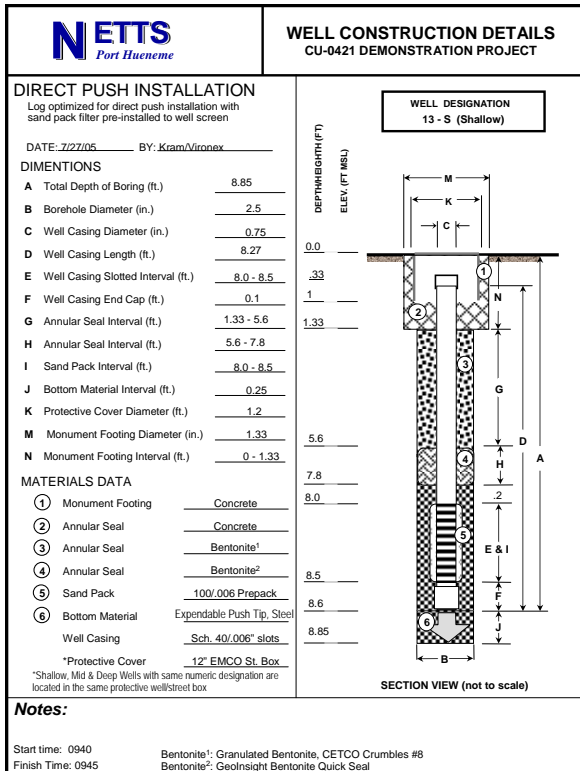
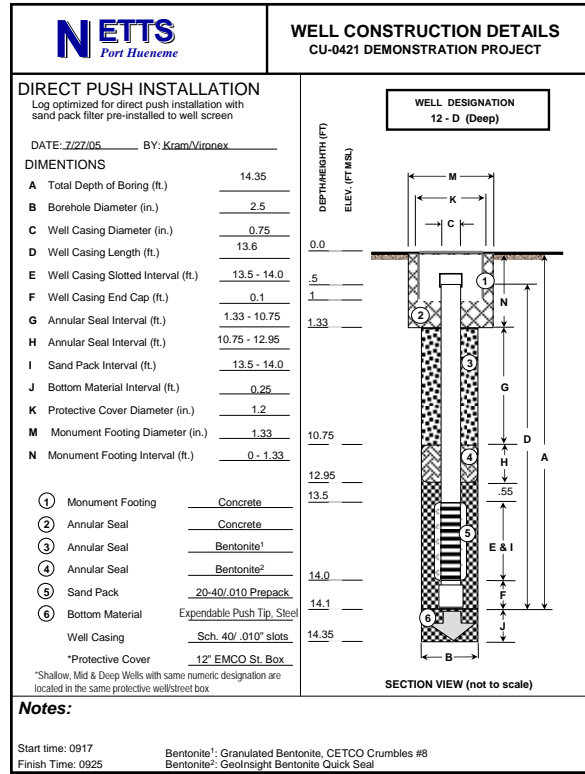
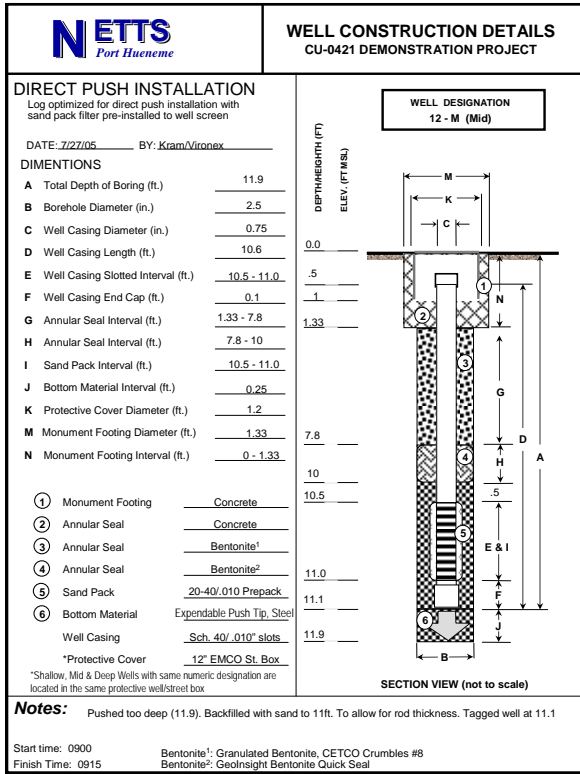


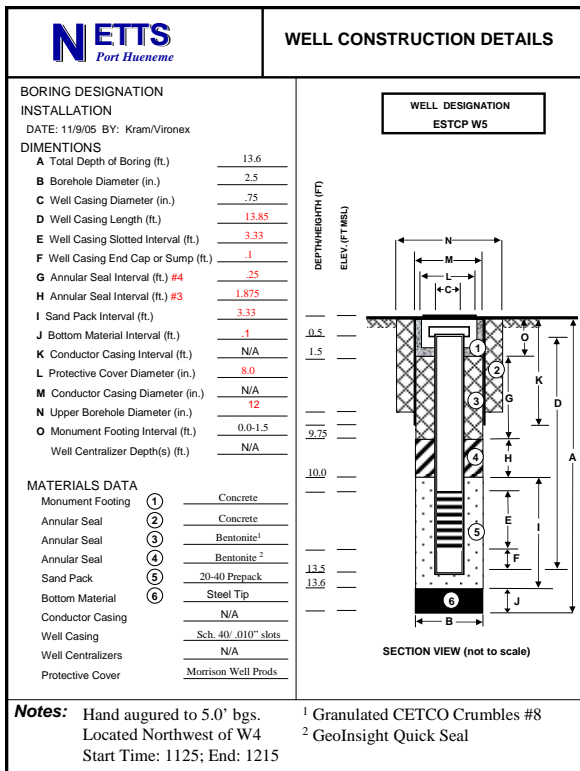
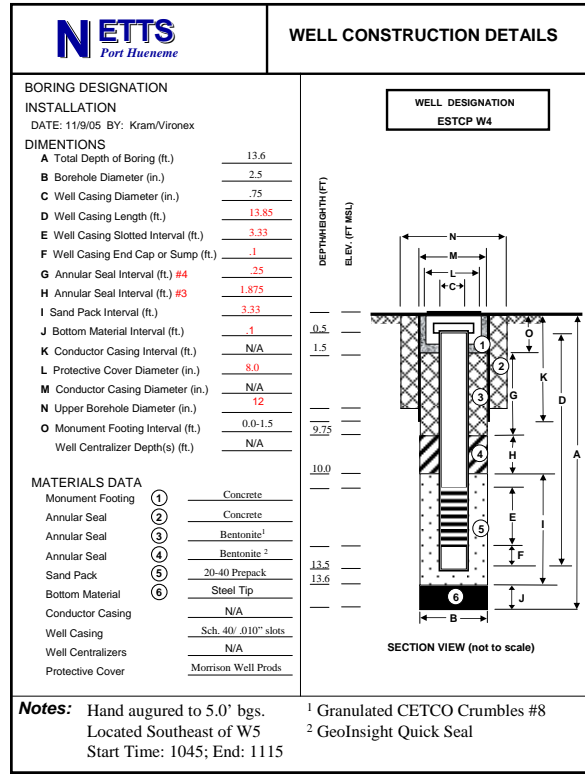
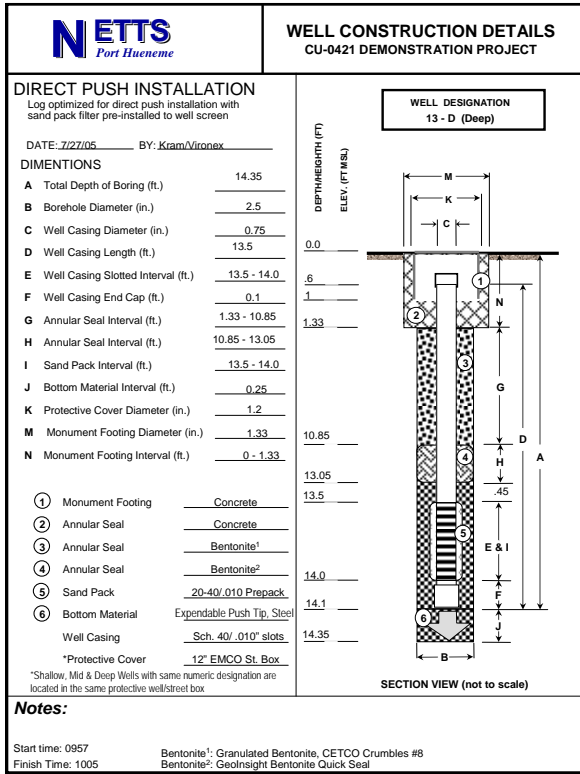












APPENDIX L

High-Resolution Piezocone Push Logs

